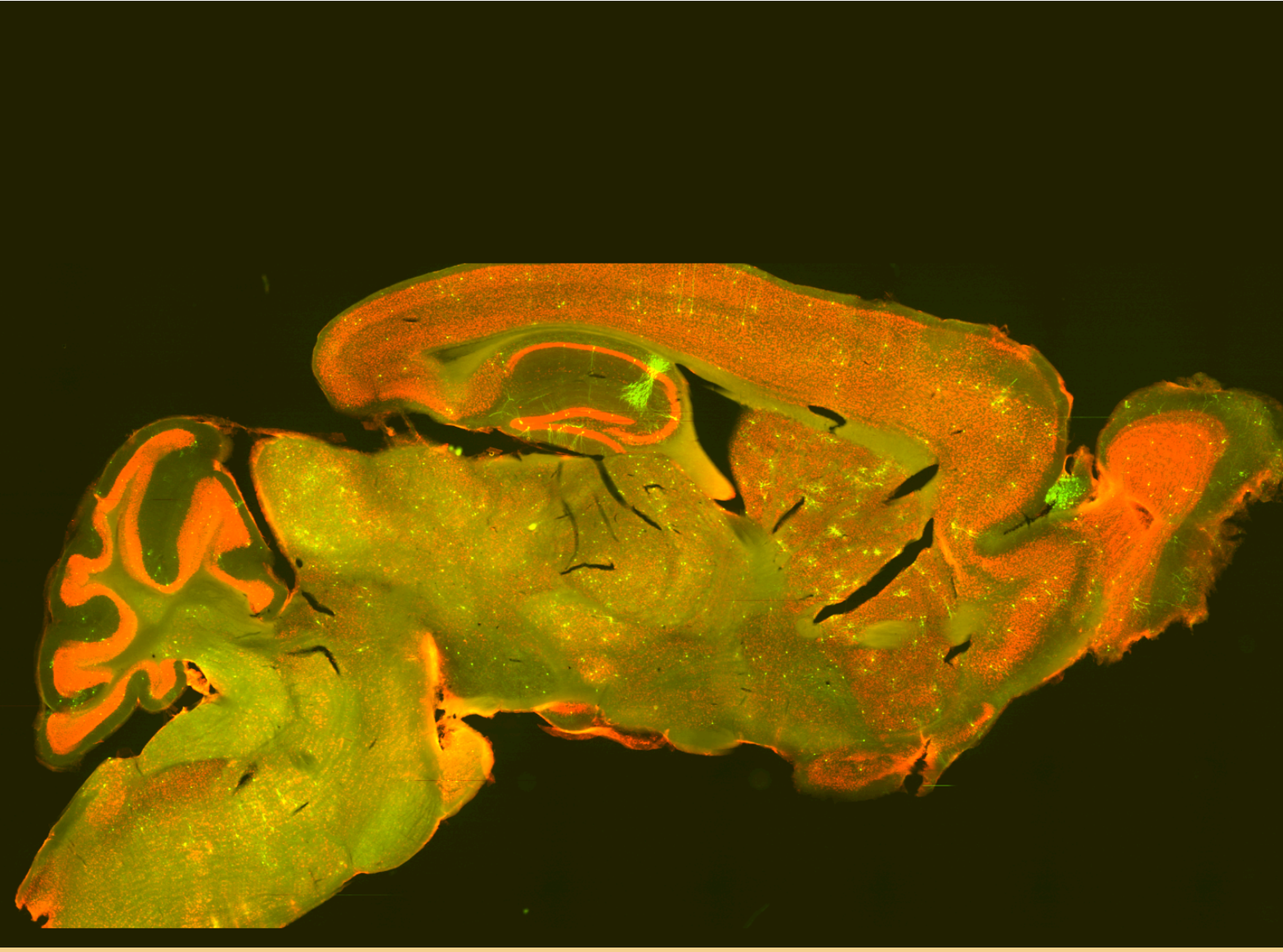

Patrícia Isabel Rodrigues Monteiro

SYNAPTIC AND CIRCUITRY MECHANISMS OF BASAL GANGLIA DYSFUNCTION IN COMPULSIVE AND REPETITIVE BEHAVIOR

Doctoral Thesis in Biosciences with specialization in Neuroscience, under the supervision of Professors Guoping Feng and Carlos Jorge Alves Miranda Bandeira Duarte, and presented to the Department of Life Sciences, Faculty of Science and Technology, University of Coimbra

May 2015

· U C ·

UNIVERSIDADE DE COIMBRA

SYNAPTIC AND CIRCUITRY MECHANISMS OF BASAL GANGLIA DYSFUNCTION IN COMPULSIVE AND REPETITIVE BEHAVIOR

Patrícia Isabel Rodrigues Monteiro

Universidade de Coimbra

2015

• U C •

UNIVERSIDADE DE COIMBRA

Dissertação orientada pelos Professores Guoping Feng e Carlos Jorge Alves Miranda Bandeira Duarte, apresentada ao Departamento de Ciências da Vida da Faculdade de Ciências e Tecnologia da Universidade de Coimbra para prestação de provas de Doutoramento em Biociências, no ramo de especialização de Neurociências.

uc2001020935@student.uc.pt

Cover Illustration: Patrícia Isabel Rodrigues Monteiro
Published in Portugal on April 2015

“Que, quanto mais vos pago, mais vos devo”

Luís Vaz de Camões

Aos meus pais.

To my parents.

Thesis work performed under the supervision of Prof. Guoping Feng, PhD, and under academic advisement from Prof. Carlos Jorge Alves Miranda Bandeira Duarte, PhD, from Center for Neurosciences and Cell Biology, Department of Life Sciences, University of Coimbra (Portugal). Thesis work performed at the Department of Brain and Cognitive Sciences, Massachusetts Institute of Technology (USA) with support from Doctoral Program in Experimental Biology and Biomedicine (PDBEB) organized by the Center for Neuroscience and Cell Biology, Coimbra University (FCT PhD fellowship SFRH/BD/33894/2009).

Financial support to P.Monteiro from the Portuguese Foundation for Science and Technology (FCT PhD fellowship SFRH/BD/33894/2009) and from the Stanley Center for Psychiatric Research at the Broad Institute of MIT and Harvard. Research in the Laboratory of Guoping Feng has been supported by the Poitras Center for Affective Disorders Research at MIT, Stanley Center for Psychiatric Research at Broad Institute of MIT and Harvard, National Institute of Health (NINDS and NIMH), Alfred P. Sloan Foundation, American Heart Association, The Arnold and Mabel Beckman Foundation, The EJLB Foundation, The Esther A. & Joseph Klingenstein Fund, The Hartwell Foundation, March of Dimes Birth Defects Foundation, McKnight Endowment Fund for Neuroscience, Nancy Lurie Marks Family Foundation, Ruth K. Broad Foundation for Biomedical Research, Simons Foundation Autism Research Initiative (SFARI), and The Whitehall Foundation.

The work of this thesis was included in the following publications:

Chapter 1:

Monteiro P. and Feng G. Learning from Animal Models of Obsessive-Compulsive Disorder. *Biol Psychiatry* (*in press*).

Chapter 2:

Monteiro P., McRae R., Zhou Y., Wickersham I.R., and Feng G. Distinct role of parvalbumin interneurons of the dorsomedial striatum in habit formation. (*in preparation*)

Chapter 3:

Mei Y.*, **Monteiro P.*** and Feng G. Adult restoration of Shank3 expression rescues selective autistic-like phenotypes. (*under revision*). *These authors contributed equally to this work.

Chapter 4:

Yang Zhou, Tobias Kaiser*, **Patrícia Monteiro***, Xiangyu Zhang*, Marie. S. Van der Goes, Dongqing Wang, Boaz Barak, Menglong Zeng, Aldo Amaya, Shannon Nguyen, Michael Lewis, Neville Sanjana, Yongdi Zhou, Mingjie Zhang, Feng Zhang, Zhanyan Fu, Guoping Feng. Shank3 mutations associated with ASD and schizophrenia display both shared and distinct defects. (*under revision*) *These authors contributed equally to this work.

Chapter 5:

Burguière E, **Monteiro P**, Feng G, Graybiel AM. Optogenetic stimulation of lateral orbitofronto-striatal pathway suppresses compulsive behaviors. *Science* 2013, 340:1243-1246.

Appendix A:

Burguière E, **Monteiro P**, Mallet L, Feng G, Graybiel AM. Striatal circuits, habits, and implications for obsessive-compulsive disorder. *Curr Opin Neurobiol*. 2014;30C:59-65.

Abstract

Neuropsychiatric disorders encompass a wide range of diseases that manifest as one or many altered behaviors, including but not limited to self-injurious behavior, impaired social-emotional communication and cognitive deficits. Due to the lack of biomarkers and overlapping behavioral symptoms, diagnosis of neuropsychiatric disorders sometimes relies on exclusion of other underlying conditions. Current data from large scale genomic studies, suggests overlapping genes and pathways for different neuropsychiatric disorders. Proteins that play a role in synaptogenesis or excitatory/inhibitory synaptic transmission are implicated as well as cortico-striato-thalamocortical circuits (CSTC).

In recent years striatal dysfunction has been hypothesized in repetitive and stereotyped behaviors associated with neuropsychiatric disorders, such as obsessive compulsive disorder (OCD) and autism spectrum disorders (ASD). Autism spectrum disorders (ASD) are clinically defined by the symptoms of social impairment and repetitive behavior/restricted interests, affecting 1 in 68 children in the United States. OCD (Obsessive Compulsive Disorder) affects 2-3 % of the worldwide population and is characterized by excessive preoccupations (obsessions) associated to specific rituals (compulsions). Approximately 30-40 % ASD patients have comorbidity with OCD, suggesting some degree of overlapping circuitry.

Shank3, one of the most prominent ASD genes that is estimated to contribute to ~1 % of all ASD cases, is enriched at corticostriatal glutamatergic synapses and directly interacts with SAPAP protein-family. At corticostriatal glutamatergic synapses SAPAP3 and SHANK3 proteins show a unique expression pattern, being the only members of their protein-family highly enriched at this location. Deletion of the *Sapap3* gene in mice leads to striking OCD-like behavior and mice with *Shank3* deletion exhibit self-injurious repetitive grooming and social interaction deficits, reminiscent of autistic-like behaviors.

Experimental work described on this thesis deepens our knowledge on the neural (and genetic) basis of compulsive behavior and anxiety, using *Sapap3* and *Shank3*-KO mice as animal models of OCD and ASD-like behaviors. Results suggest that insufficient striatal inhibition might be causing striatum hyperactivity in the *Sapap3*-KO mice and leading to repetitive overgrooming. Parvalbumin interneurons within the striatum are shown to be required for proper habit formation in WT mice, implicating them as key players in determining striatum behavioral output.

Experimental work described on this thesis also takes advantage of a *Shank3* cKI mouse to show that pathological grooming and social interaction deficits can be reversed in adulthood, but not anxiety. This supports the idea that different symptom dimensions might be associated with distinct neural substrates and might be independent of one another. Further experimental work shows that two mutant mice lines carrying exon 21 *Shank3* mutations linked to ASD and schizophrenia, display both shared and distinct defects. This study provides an explanation at the molecular, synaptic, circuit and behavioral level, on how different mutations in the *Shank3* gene may contribute to different symptoms and hence disorders.

Although *Sapap3*- and *Shank3*-KO mice have self-injurious grooming phenotypes that are unique in their biological origins, both genes share an enriched corticostriatal expression. In regards to human pathology, we suggest that a commonly shared pathological behavior, compulsivity, may arise from different causal insults that impact the same brain circuits. Moreover these results illustrate how disruption of scaffolding proteins can affect brain circuitry and are able to provide insightful links to neuropsychiatric disorders.

Key words: Obsessive Compulsive Disorder, Autism Spectrum Disorders, Basal ganglia

Resumo

As doenças neuropsiquiátricas abrangem um largo espectro de distúrbios comportamentais, incluindo auto-flagelação, défices cognitivos, problemas de interacção social e emocional, entre outros. Dada a ausência de biomarcadores concretos e a sobreposição de sintomas comportamentais, o diagnóstico das doenças neuropsiquiátricas é por vezes efectuado por exclusão relativamente a outras causas subjacentes. Estudos genómicos em larga escala revelaram uma sobreposição de genes e vias de sinalização envolvidas em diferentes transtornos neuropsiquiátricos. Proteínas relacionadas com a sinaptogénese ou com a transmissão sináptica excitatória/inibitória, parecem estar implicadas, assim como os circuitos córtico-estriado-tálamo-corticais (CETC).

Hipóteses recentes sugerem que uma disfunção estriatal possa estar na génese de padrões repetitivos e estereotipados de comportamento associados a doenças neuropsiquiátricas, tais como a Perturbação Obsessiva-Compulsiva (POC) e as Perturbações do Espectro Autista (PEA). As PEA afectam uma em cada 68 crianças nos Estados Unidos e são caracterizadas clinicamente por dificuldades ao nível da socialização e a pela existência de interesses repetitivos/estereótipados. A Perturbação Obsessiva-Compulsiva (POC) afecta 2-3 % da população mundial e é caracterizada pela manifestação de preocupações excessivas (obsessões) associadas a rituais específicos (compulsões). Aproximadamente 30-40 % dos doentes com PEA apresentam comorbidade com POC, sugerindo alguma sobreposição ao nível dos circuitos neuronais envolvidos.

O gene *Shank3*, um dos principais candidatos em PEA que contribui possivelmente para ~1 % de todos os casos, encontra-se enriquecido em sinapses cortico-estriatais glutamatérgicas e interage directamente com proteínas da família SAPAP. Ao nível das sinapses glutamatérgicas cortico-estriatais, as proteínas SAPAP3 e SHANK3 apresentam um padrão de expressão único, sendo os únicos membros das respectivas famílias proteicas enriquecidos nesta localização. A delecção do gene *Sapap3* em murganhos resulta em comportamentos semelhantes a POC e a delecção do gene *Shank3* resulta em lesões devido a *grooming* repetitivo e problemas de interacção social, assemelhando-se aos comportamentos observados em PEA.

O trabalho experimental descrito nesta tese aprofunda o conhecimento relacionado com as bases neurais (e genéticas) do comportamento compulsivo e da ansiedade, utilizando murganhos *Sapap3* e *Shank3*-KO como modelos de

comportamento animal semelhante a POC e PEA. Os resultados sugerem que uma insuficiência de inibição estriatal pode causar uma hiperactividade do estriado nos murganhos *Sapap3*-KO, conduzindo a *grooming* excessivo. Demonstra-se que os interneurónios do estriado que expressam parvalbumina são necessários para o estabelecimento de hábitos nos murganhos WT, indicando-os como elementos-chave do perfil comportamental determinado pelo estriado.

No trabalho descrito nesta tese foram também utilizados murganhos *Shank3*-cKI para demonstrar que o *grooming* patológico e problemas de interacção social, mas não a ansiedade, podem ser revertidos no estado adulto. Isto corrobora a hipótese de que diferentes dimensões sintomatológicas podem não só estar associadas com substratos neuronais distintos, como também ser independentes entre si. O trabalho realizado permitiu também observar que duas linhas distintas de murganhos transgénicos, contendo mutações associadas a PEA e esquizofrenia no exão 21 do gene *Shank3,* apresentam défices distintos e outros partilhados entre elas. Este estudo ilustra ao nível molecular, sináptico, bem como ao nível de circuitos neuronais e comportamental, como diferentes mutações no gene *Shank3* podem contribuir para sintomas distintos e perturbações associadas.

Embora os murganhos *Sapap3*- e *Shank3*-KO apresentem um fenótipo de lesões devido a *grooming* repetitivo com origem biológica distinta, ambos os genes partilham um padrão de expressão elevado ao nível cortico-estriatal. Relativamente à patologia humana, propomos que um comportamento patológico em comum possa na verdade emergir de diferentes perturbações afectando os mesmo circuitos neuronais. Estes resultados ilustram também a forma como uma disrupção de proteínas com uma função sináptica pode afectar os circuitos neuronais e ao mesmo tempo promover a descoberta de elos importantes na compreensão de doenças neuropsiquiátricas.

Palavras-chave: Perturbação Obsessiva-Compulsiva, Perturbações do Espectro Autista, Gânglios da base

Acknowledgements

Ao Professor **Carlos Jorge Alves Miranda Bandeira Duarte** por todo o apoio ao longo do doutoramento e disponibilidade incondicional. Muito obrigada.

To Professor **Guoping Feng** for his unconditional support and mentoring (both professionally and personally). Thank you so much Guoping.

À **Fundação para a Ciência e a Tecnologia** pelo apoio financeiro concedido através da bolsa de doutoramento SFRH / BD / 33894 / 2009.

To all the **Fengtastic lab members**, I have learned so much from all of you. Special thanks to **Wenting**, **Qiangge**, **Dongqing**, **Yang**, **Zhanyan**, **Holly** and **Boaz** for teaching and support throughout different stages of this long journey.

Aos amigos do coração:

À **Patrícia**, obrigada por estares sempre presente na minha vida e por "*andares sempre ao meu passo*". Que a vida seja sempre uma caminhada ao teu lado. Obrigada Pat.

Ao **Carlos**. Este doutoramento não teria sido o mesmo sem ti e o teu apoio incondicional. E como um "obrigada" isolado nunca será suficiente para te agradecer, escrevo um "obrigada" imortalizado nesta tese.

À **Susana** por fazeres parte da família que escolhi. Obrigada por me deixares atravessar a rua há 14 anos atrás e entrar na tua vida. Cinco dedos de uma mão.

À **Rita** por seres parte desta família que Coimbra me deu. Por seres sincera, por seres amiga. Longe ou perto, estás sempre no meu coração. Obrigada pelo carinho e apoio incondional.

À **Zé**, por seres a "caixa de chocolates" do *Forrest Gump*. És uma amiga com "A" grande. Obrigada.

Ao **Ruben**, pelas risadas, conversas, cultura cinematográfica e consumo de café. A minha vida sem ti não teria as mesmas cores, obrigada por fazeres parte dela.

Ao **Gonçalo**, por quem tenho um carinho imenso. "Coimbra" e "amizade" serão sempre sinónimos do teu nome. Que a Lia possa um dia encontrar um amigo como tu. Obrigada.

À minha família, por serem a minha raiz primária a partir da qual outras raízes podem brotar:

À minha **tia** que teria muito orgulho em ver este dia. Obrigada por tudo tia, até sempre.

Aos meus **pais**, a quem dedico esta tese e todo o meu amor incondicional. Vocês são o meu exemplo e o meu orgulho. Amo-vos muito.

À minha **irmã,** por seres o meu modelo. Cresci a olhar pra ti e a querer fazer o que tu fazias e ser como tu eras. Ainda continuo assim. Obrigada por me dares a Beatriz e o Guilherme. Espero um dia ser uma mãe como tu.

Ao meu **irmão**, por seres a minha metade e por estares sempre ao meu lado. Sem ti estaria incompleta e sem ti a vida não faria sentido. Tenho muito orgulho em ti. Obrigada por cresceres comigo e seres o meu herói.

Ao **Artur**, por seres todas estas pessoas juntas. És a minha família, amigo e raiz. Obrigada pelo teu apoio e amor incondicional. És o meu porto de abrigo e fazes de mim uma pessoa melhor todos os dias. Sem ti esta tese não teria sido possível. Sem ti, "eu" como sou, não existiria. Obrigada.

CONTENTS

Contents

List of figures

List of tables

List of Abbreviations

A2A	A2A Adenosine receptor
ACh	Acetylcholine
AMPAr	α-amino-3-hydroxy-5-methyl-4-isoxazolepropionic acid receptor
ASD	Autism Spectrum Disorders
BG	Basal Ganglia
CamKII	Calcium/calmodulin-dependent Kinase II
CBT	Cognitive Behavioral Therapy
Cg	Cingulate
ChAT	Choline acetyltransferase
ChR2	Channelrhodopsin
cKI	conditional Knock In
cKO	conditional Knock Out
CPu	Caudate Putamen
D	Dopamine receptor
DA	Dopamine
DARPP32	Dopamine- and cAMP-Regulated Neuronal Phosphoprotein
DBS	Deep Brain Stimulation
DLO	Dorsolateral Orbital
dlPFC	dorsolateral Prefrontal Cortex
DLS	Dorsolateral Striatum
DMS	Dorsomedial Striatum
Dyn	Dynorphin
Enk	Enkephalin
FLEX	Flip-Excision
FSi	Fast Spiking interneurons
GK	Guanylate Kinase
GP	Globus Pallidus
GPCR	G Protein-Coupled Receptors
GPe	external Globus Pallidus
GPi	internal Globus Pallidus
GPm	medial Globus Pallidus
GR	Germline Rescue
IL	Infralimbic
KI	Knock In
KO	Knock Out
LO	Lateral Orbital
lPFC	lateral Prefrontal Cortex
LTS	Low Threshold Spiking interneurons
M	Muscarinic acetylcholine receptor
MAGUK	Membrane-associated Guanylate Kinases
mEPSC	miniature Excitatory Postsynaptic Currents
mGluR	metabotropic Glutamate Receptor
mIPSC	miniature Inhibitory Postsynaptic Currents

MO	Medial Orbital
mPFC	medial Prefrontal Cortex
MSN	Medium Spiny Neuron
NAcc	Nucleus Accumbens
nAChR	nicotinic Acetylcholine Receptor
NLG	Neuroligin
NMDAr	N-methyl D-aspartate receptor
NOS	Nitric Oxide Synthase
NpHR	Halorhodopsin
NPY	Neuropeptide Y
NRXN	Neurexin
OCD	Obsessive Compulsive Disorder
OFC	Orbitofontal Cortex
ON	Overnight
PDZ	PSD-95/Dlg-1/ZO-1
PFC	Prefrontal Cortex
PL	Prelimbic
PMS	Phelan-McDermid Syndrome
PSD	Postsynaptic Density
PV	Parvalbumin
SAPAP	SAP90/PSD-95 associated protein
SH3	Src Homology-3
SHANK	SH3 and Ankyrin repeat-containing protein
SNc	Substantia nigra pars compacta
SNr	Substantia nigra pars reticulata
SOM	Somatostatin
SP	Substance P
SSFO	Stabilized Step Function Opsin
SSRI	Selective Serotonin Re-uptake Inhibitors
STN	Subthalamic Nucleus
TAN	Tonically Active Neurons
TS	Tourette Syndrome
VMS	Ventromedial Striatum
WT	Wild Type

PART I

GENERAL INTRODUCTION

Chapter 1

Basal ganglia functional and dysfunctional circuitry

The basal ganglia are a group of forebrain nuclei that work as a functional unit involved in psychomotor behavior processing. These nuclei are interrelated with the cortex, thalamus and brainstem, and are one of the oldest parts in terms of brain's phylogeny[1]. The basal ganglia (BG) were first illustrated by Andreas Vesalius in his book *De humani corporis fabrica libri septem*[2] in 1543 (Latin for "On the fabric of the human body in seven books"). Despite this representation, no interpretation or relevance was given until few decades later Thomas Willis pioneered the field of BG in his book *Cerebri anatome* (1664). Here he first describes the "corpus striatum" and the basal ganglia as a unique and fascinating neuroanatomical structure:

> *"These bodies, if they should be dissected along the middle, appear marked, with medullar streaks, as it were rays or beams (…) And it is worth observation, that in the whole head besides there is no part found chamferred or streaked after the like manner"* - Thomas Willis, 1664.

Willis also correctly inferred later that the corpus striatum was related to sensorimotor functions and reported the degeneration of this structure in patients who had suffered severe paralyses. Leveraging from his pioneer view, significant knowledge on the neuroanatomical organization of BG was later gathered during 18^{th}-19^{th} century by anatomists such as Félix Vicq-d'Azyr (who identified substantia nigra) and Karl Friedrich Burdach (first to differentiate between caudate nucleus and putamen; identified *globus pallidus* as well as the internal and external capsules)[3]. During 20^{th} century, pioneer studies started reporting associations between basal ganglia lesions and movement disorders[4], leading to a better understanding of the BG system. In 1986, André Parent publishes the first thorough description of the basal ganglia system across different mammalian and non-mammalian vertebrates in his book *Comparative Neurobiology of the Basal Ganglia*[5].

Despite an amazing level of novel neurophysiological, biochemical and genetic understanding about the basal ganglia nowadays, much remains elusive, fascinating contemporary neuroscientists as much as it did 350 years ago.

1.1 Striatum anatomy

Striatum is anatomically divided into a dorsal sensorimotor area and a ventral limbic region. In primates the dorsal area is further subdivided by the internal capsule into caudate nucleus and putamen. The caudate nucleus receives most of its excitatory inputs from orbitofrontal, prefrontal and cingulate cortex areas, whereas putamen receives majority of its cortical inputs from sensorimotor areas[6,7].

In contrast with primates, rodent's striatum is not anatomically divided into caudate and putamen, rather having the appearance of a single structure. Based on behavioral studies, a loose terminology can be adopted to define limbic, associative and motor striatal territories in mice, as well as their respective source of cortical inputs[8,9]. It should be emphasized however, that despite some functional resemblance between mice and primates structures, there are important species-specific limitations and mice often do not fulfill primates' neuroanatomical connectivity criteria[8–13]. Mice orbital cortices seem to have a medial–lateral gradient of connectivity, where MO (medial orbital) projects more medially into striatum compared to LO/DLO (lateral/dorsolateral orbital). Medial prefrontal cortex (comprising PL, IL and Cg) seems organized in a dorsal–ventral gradient of connectivity such that dorsal PL projects to dorsomedial regions of striatum (DMS, associative striatum) and ventral PL projects mainly to ventral striatum (limbic striatum)[13]. These ventromedial striatum regions are considered to be caudate-like in rodents[9,10,14]. Finally, motor cortex projects mainly to rodents' dorsolateral striatum (DLS, a region considered more similar to primates' putamen)[9,10] (Fig.1.1).

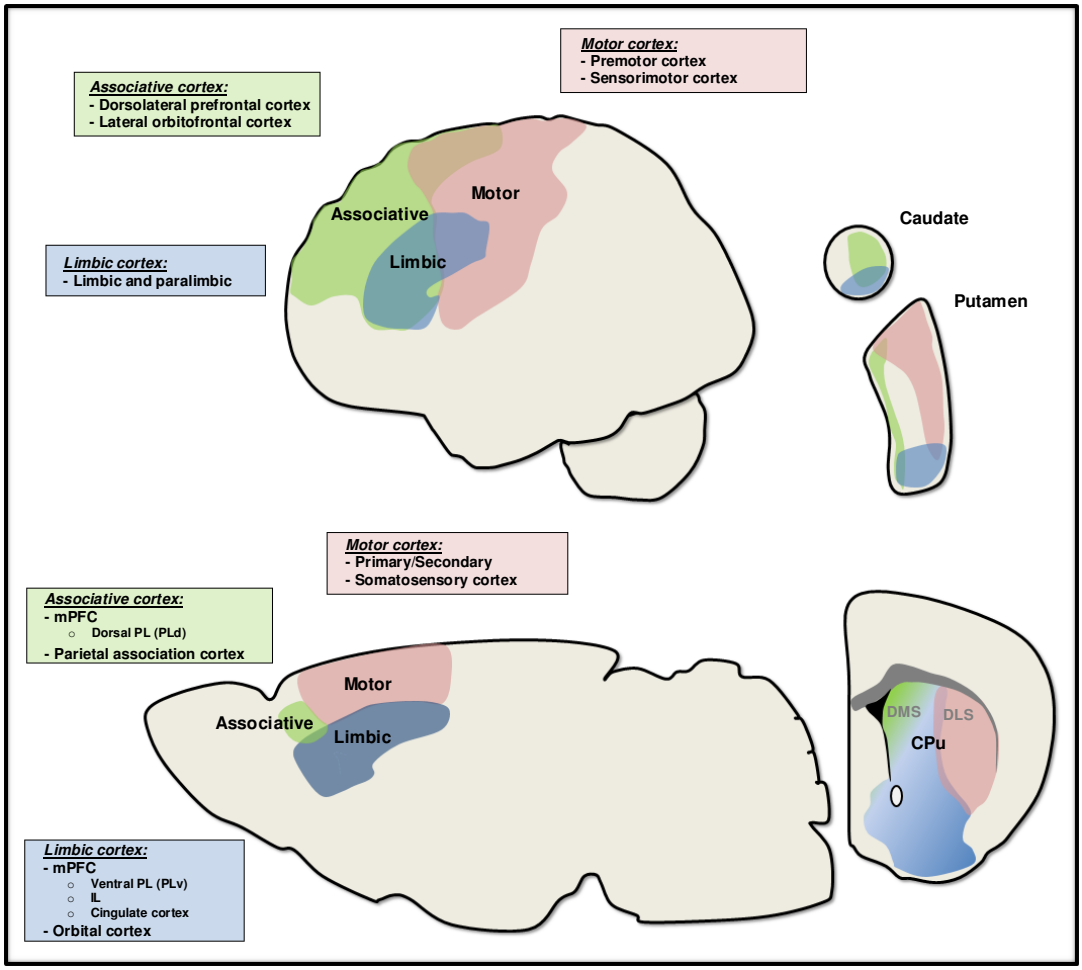

Figure 1.1 | Simplified neuroanatomical model of cortico-striatal circuitry within the human and mouse brain.

Motor: Human motor cortex is represented here by premotor and sensorimotor cortical regions that mainly project to posterolateral putamen[6]. Mouse motor cortex is represented here by somatosensory and motor cortex that mainly project to dorsolateral striatum region[13]. Associative: Human associative cortex represented here by the dorsolateral PFC and lateral OFC, projects to the caudate and anteromedial portion of the putamen[6]. Mouse associative cortex is represented here by dorsal prelimbic and parietal association cortices that mainly project to dorsomedial striatum region[9]. Limbic: Human limbic cortex represented here by the paralimbic and limbic cortices (including entorhinal cortex-area28, perirhinal cortex-area35, medial OFC-area11, anterior cingulate cortex-area24)[6,15], projects to the ventral striatum (ventral region of the caudate nucleus and putamen, including *nucleus accumbens* - NAcc). Mouse limbic cortex is represented here by OFC and PFC (ventral prelimbic, infralimbic and cingulate cortices), that mainly project to ventromedial striatum region (including NAcc)[9,13]. All regions depicted are representative and do not intend to provide specific accurate locations.

In recent years, neurophysiology and behavior studies have suggested that DLS and DMS striatum regions support an important behavioral transition in mice: intentional goal-directed actions (DMS encoded) that after repetition often become habitual automated responses (DLS encoded)[10,14,16–20]. These behavior repertoires can be distinguished based on their sensitivity to outcome expectancy. If behavioral adaptation occurs after obtaining an unexpected outcome, this reflects a goal-directedness response (influenced by consequences). On the other hand, a behavior pattern that persists after defrauded outcome is considered habitual (controlled by antecedent stimuli).

Local modulation of striatum medium spiny neurons (MSNs) is required for successfully engaging or transitioning between the two behavioral patterns[21,22]. Even though several lines of evidence support this distinct functionality between DLS and DMS regions, it is not known exactly how this occurs at cellular level. A dynamic competition is thought to take place between these two striatal regions during habits acquisition. DMS likely guides the expression of behaviors as they are turning into habits, but once this DMS activity drops, DLS-circuits take control over behaviors[23]. Evidence emerged from mice that upon DMS lesion, show tendency for action generalization strategies (habitual responses). Indicating that DLS (sensorimotor striatum) guides behavioral performance when DMS (associative striatum) function is compromised[16].

Similarly to the connectivity pattern observed between cortex and striatum, it is believed that downstream basal ganglia territories (such as *globus pallidus* - GP) are equally well organization into associative, limbic and sensorimotor regions. An important body of evidence for this cognitive, emotional and motor organization of basal ganglia was made clear through some groundbreaking monkey studies[24,25]. Bicuculline injections in limbic region of globus pallidus can induce stereotypies, whereas injections in associative region can lead to attention deficit and/or hyperactivity. Abnormal movements are not observed unless injections occur at GP's sensorimotor region, suggesting a particular role for associative and limbic anatomical territories in the etiology of compulsive behaviors[24].

1.2 Striatal macrocircuitry

Main regions comprising the basal ganglia are the **dorsal striatum** (rodents: caudate-putamen [CPu]; primates: caudate nucleus and putamen), **ventral striatum** (*nucleus accumbens* [NAcc]), **dorsal *pallidum*** (rodents: *globus pallidus* [GP] and medial GP [GPm]; primates: external and internal GP [GPe, GPi]), **ventral *pallidum***, **substantia nigra *pars reticulata*** (SNr), **substantia nigra *pars compacta*** (SNc) and the **subthalamic nucleus** (STN). These structures integrate the various inputs arriving mainly from cortex and thalamus and use this information for psychomotor and cognitive behavioral processing[7].

The entry point to basal ganglia is striatum, which receives numerous cortical converging inputs from the motor, limbic and associative cortices[15,26]. Axons arriving to striatum principal cells (the medium spiny neurons – MSNs) convey information that is passed along through two different pathways - the direct and indirect-pathway - defined on the basis of their axonal target projections:

Direct pathway: axons from striatonigral MSNs leave striatum to directly form inhibitory synapses onto basal ganglia output nuclei (SNr and GPm).

Indirect pathway: inhibitory axons from striatopallidal MSNs target the GP that then forms inhibitory synapses onto the STN. STN cells send excitatory axons that finally target basal ganglia output nuclei (SNr and GPm).

When information reaches basal ganglia output nuclei, SNr and GPm inhibitory neurons send their projections to ventroposterior thalamic motor nuclei, where excitatory neurons project back to cerebral cortex. This circuit is known as cortico-striato-thalamocortical circuit (CSTC) (Fig.1.2A).

In virtual absence of inputs, tonically-active neurons in SNr, GP and GPm would inhibit their downstream target structures (Fig.1.2B). Once direct-pathway activation occurs, striatonigral MSNs directly inhibit SNr and GPm, leading to an excitatory net effect due to thalamic disinhibition (Fig.1.2C). By contrast, indirect-pathway activation leads to SNr and GPm activation (through a direct inhibition of the GP and consequent disinhibition of the STN), resulting in opposite net effects (Fig.1.2D)[27,28].

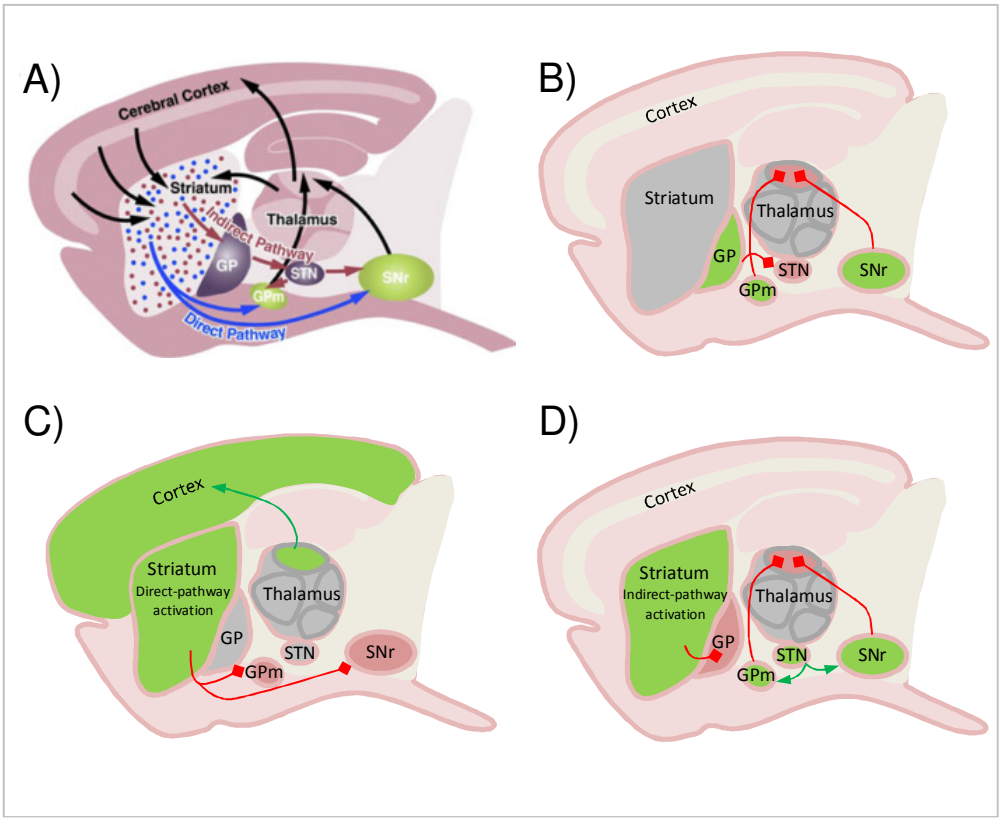

Figure 1.2 | Cortico-striato-thalamocortical circuit (CSTC).

Panel A: Representation of a mouse sagittal brain view with detailed schematic of the cortico-striato-thalamocortical circuit (adapted from Kreitzer and Malenka[28]). Cortical inputs into striatum are relayed forward to BG output nuclei through direct (projects to GPm and SNr) and indirect pathways (projects to GP that in turn projects to STN; STN finally projects to GPm and SNr). BG output nuclei (GPm and SNr) project to ventroposterior thalamic motor nuclei, where excitatory neurons project back to cerebral cortex. Panel B: In virtual absence of inputs, tonically-active neurons in SNr, GP and GPm would inhibit their downstream target structures. Panel C: Upon direct-pathway activation, striatonigral MSNs directly inhibit SNr and GPm, leading to an excitatory net effect in cortex due to thalamic disinhibition. Panel D: Indirect-pathway MSNs inhibit GP. This leads to disinhibition of STN and excitation of BG output nuclei (SNr and GPm) with consequent inhibition of thalamo-cortical excitatory projections.

Another level of complexity in the basal ganglia involves inputs arriving to this circuit through non-corticostriatal routes. Striatum receives numerous excitatory glutamatergic inputs from the thalamus, mainly from the intralaminar thalamic nuclei, but also midline and specific thalamic nuclei[29]. The connectivity between striatum and GP is also important given the fact that this has been proven not to be a “one-way road”. Although striatum strongly projects to GP, 25-30 % GP neurons also project back to striatum, preferentially targeting striatum

GABAergic interneurons that can exert powerful control over MSNs[30–33]. Another very important source of input to BG is composed by cortical and thalamic excitatory axons that directly target the STN. Given STN's prime connectivity to SNr and GPm, this route bypasses the striatum and exerts powerful control over BG output nuclei, being referred to as the hyperdirect pathway[34–36].

Adding to these intrincated GABAergic- and glutamatergic-mediated inputs, other neuromodulatory terminals innervate the basal ganglia nuclei (such as dopamine, acetylcholine, adenosine and nitric oxide inputs) further shaping its physiology and contributing to its great complexity level.

It is worth to mention that striatum MSNs project to substantia nigra *pars reticulata* neurons (SNr) and in turn receive strong dopaminergic inputs from substantia nigra *pars compacta* neurons (SNc). This dopaminergic source can have opposite effects on striatal MSNs physiology, resulting in stimulation of direct-pathway MSNs (acting through their D1 receptors) and reducing activity of indirect-pathway MSNs (due to D2 receptors expression in this group of cells)[27,28]. As a result, increased striatal dopamine levels can inhibit SNr and GP's activity, providing net facilitation to motor regions. Conversely, lack of dopamine input leads to increased SNr and GP's activity, with consequent inhibition of thalamocortical projection neurons[26] (Fig.1.3).

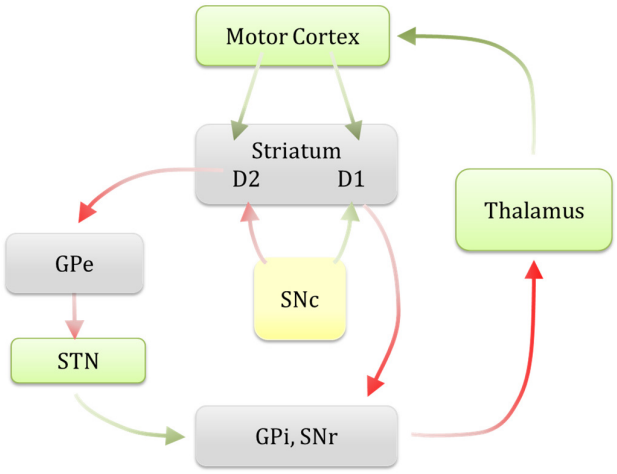

Figure 1.3 | Schematic representation of basal ganglia-thalamocortical circuitry upon dopaminergic striatal activation.

Dopaminergic inputs from substantia nigra *pars compacta* (SNc) neurons stimulate direct-pathway MSNs (acting through their D1 receptors) and reduce indirect-pathway MSNs activity (through D2 receptors). As a result, SNr and GP's activity are inhibited, providing net facilitation to motor regions. Conversely, lack of dopaminergic input leads to

increased SNr and GP's activity, with consequent inhibition of thalamocortical projection neurons. Excitatory connections are depicted in green and inhibitory in red.

BG circuitry dysfunction leads to heterogeneous clinical syndromes (Parkinson´s, Huntington, Hemiballism) that often share a common result: deterioration of motor control. Understanding the neural implementations of motor actions can allow us to break into behavioral malfunctions and correct disease states. Therefore, it is crucial to illuminate the synaptic and circuitry mechanisms of basal ganglia (dys)function and understand how manipulating their output can help us to correct disease states.

1.3 Striatal microcircuitry

An important consideration when discussing basal ganglia neurophysiology is the microcircuitry inside striatum itself (Fig.1.4). GABAergic medium spiny neurons (MSNs) are the major cell type within striatum (>90 %) and can be classified into 2 main subtypes: **striatonigral** (direct-pathway cells; express D1, M1, M4, mGluR1/5; immunoreactive for dynorphin and substanceP) and **striatopallidal** (indirect-pathway cells; express D2, A2A, M1, mGluR1/5; immunoreactive for enkephalin)[28,37]. Besides these spiny projection neurons, striatum contains mainly 3 classes of interneurons: **fast-spiking interneurons** (FS; project to both MSNs but are more likely to target D1-MSNs; express D5, nAChR; immunoreactive for parvalbumin - PV)[37,38], **low-threshold spiking interneurons** (LTS; project to MSNs; express M1, D5, M2; immunoreactive for somatostatin, neuropeptide Y, nitric oxide synthase and calretinin)[28,37,38] and **cholinergic interneurons** (TANs-tonically active neurons; project to MSNs and FS interneurons; express D2, D5, M2, M4; immunoreactive for choline acetyltransferase -ChAT)[28,37,39].

The classical model of basal ganglia motor output function postulates that direct-pathway activation facilitates movement and indirect-pathway activation suppresses movement[26,27,40,41]. Although some recent mouse studies still support this classical idea[42], validity of this model has been called into question through recent data showing concurrent activation of both pathways during action initiation in mice[43]. Accordingly, critical reappraisal is emerging in the field suggesting that indeed these two pathways are not only structurally intertwined but also functionally intertwined and that this intrastriatal connections might be

critical in determining BG output[44]. A possible reuniting explanation would be that activation of both pathways would be important for specific action selection and initiation: direct-pathway cells could be activated to promote a specifically intended motor program, whereas indirect-pathway cells could be concomitantly activated in order to inhibit specifically competing motor programs. In this scenario we could imagine that unspecific overall activation of all indirect-pathway cells would lead to inhibition of all motor programs (bradykinesia); whereas the opposite (overall ablation/silencing of all indirect-pathway cells) would lead to hyperkinesia. Moreover, another recent study has demonstrated that isolated optogenetic activation of each projection pathway can lead to both, excitation and inhibition of SNr neurons[45], regardless of which pathway is being activated. This suggests a cellular response heterogeneity that is far more complex than our classical view of the direct pathway inhibiting SNr and indirect pathway exciting SNr neurons. Despite individual cell firing data, this study did find that at the population level, effective direct pathway-mediated motor initiation correlates with a subpopulation of inhibited SNr neurons. Indirect pathway-mediated motor supression was in turn correlated with excited SNr neurons.

A proper dynamic cooperation between the two pathways thus seems crucial in all the aforementioned studies. Further experimental work will certainly help us to better understand the relevance and functional complexity of the direct and indirect pathways.

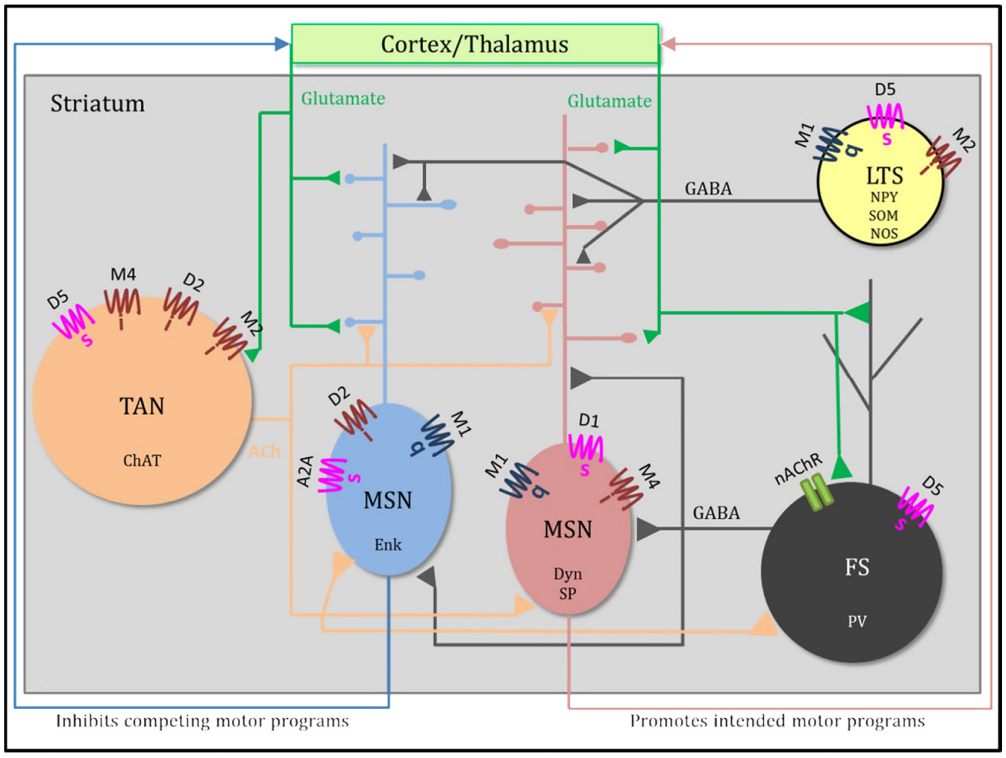

Figure 1.4 | Simplified representation of intrastriatal microcircuitry.

Cortico- and thalamo-striatal excitatory axons target the dendritic spines of MSNs as well as dendritic shafts and soma of striatal interneurons. FS interneurons receive more cortical contacts and are more responsive to cortical inputs than MSNs[46,47]; FS synapse proximally onto both MSN types[48] (with a bias towards D1+MSNs)[38]; FS interneurons also synapse with other FS (but not LTS or TANs)[38]. LTS interneurons send sparse inhibitory projections onto MSNs dendrites[33,38,49]. TANs send inputs to dendritic spines, shafts and soma of MSNs[50] and provide powerful excitatory cholinergic input to FS interneurons[51,52]. D1+MSNs have greater total dendritic length (more primary dendrites)[53] and project to SNr[37] (not represented); this direct-pathway promotes the execution of intended motor programs[43]. D2+MSNs project to GP[37] (not represented); this indirect-pathway may inhibit the execution of competing motor programs[43]. GPCRs (G protein–coupled receptors) are depicted with their associated G-protein: Gs (pink), Gi (brown), Gq (blue). M- muscarinic ACh receptors; nAChR- ionotropic nicotinic ACh receptor; D- dopamine receptors; A2A- A2A adenosine receptor; ChAT- choline acetyltransferase; Enk- enkephalin; SP- substanceP; Dyn- dynorphin; PV- parvalbumin; SOM- somatostatin; NPY- neuropeptide Y; NOS- nitric oxide synthase.

1.4 Postsynaptic density (PSD)

In order to achieve proper neural circuit communication, specialized cell-to-cell contact zones (synapses) are required. During development and throughout life, neurons undergo dynamic processes of synaptic regulation and plasticity. Such dynamic changes occur through alterations in molecular composition of their synapses and by chemical modification of synaptic proteins[54].

Glutamatergic synapses in the central nervous system are characterized by an electron dense thickening underneath the postsynaptic membrane, named the postsynaptic density (PSD). PSD contains hundreds of proteins including **membrane-tethered receptors and channels** (such as N-methyl D-aspartate receptors [NMDARs], metabotropic glutamate receptors [mGluRs] and α-amino-3-hydroxy-5-methyl-4-isoxazolepropionic acid receptors [AMPARs]); **adaptor and scaffolding proteins** (such as post-synaptic density protein 95 [PSD-95], SAPAP and SHANK); **cytoskeletal and cell-adhesion proteins** (such as actin and neuroligin) and **signaling molecules** (such as calcium/calmodulin-dependent kinase II [CamKII]); creating a macromolecular complex that serves a wide range of functions[55]. Prominent PSD proteins such as members of the MAGUK family build up a dense scaffold that serves as interface between clustered membrane-bound receptors, cell adhesion molecules and the actin-cytoskeleton[56]. Identification of this family of proteins and the subsequent chain-link cloning of their associated proteins, extended our comprehension of the molecular composition of the glutamatergic PSD[54].

MAGUK proteins are composed of multiple domains that act as specific sites for protein-protein interactions, such as PDZ (PSD-95/DLG/ZO1) domains, SH3 domains and C-terminal guanylate kinase (GK) domains. The tethering of NMDA receptors to PSD-95 relies on a PDZ domain, portraying the importance of such interactions. Moreover, the C-terminal GK domain of PSD-95 is linked to SAPAP (SAP90/PSD-95 associated protein) family of proteins, which subsequently bind to SHANK (SH3 and ankyrin repeat-containing protein) family of proteins. SHANK family further connects to the actin-cytoskeleton and Homer proteins, which in turn interact with mGluRs. Through this link, PSD-95/SAPAP/SHANK/Homer proteins form a quaternary complex that brings together NMDA- and mGluR- receptor complexes in the postsynaptic specialization, possibly providing a functional link between NMDARs and mGluRs

that facilitates crosstalk between ionotropic and metabotropic glutamate receptors at the PSD (Fig.1.5).

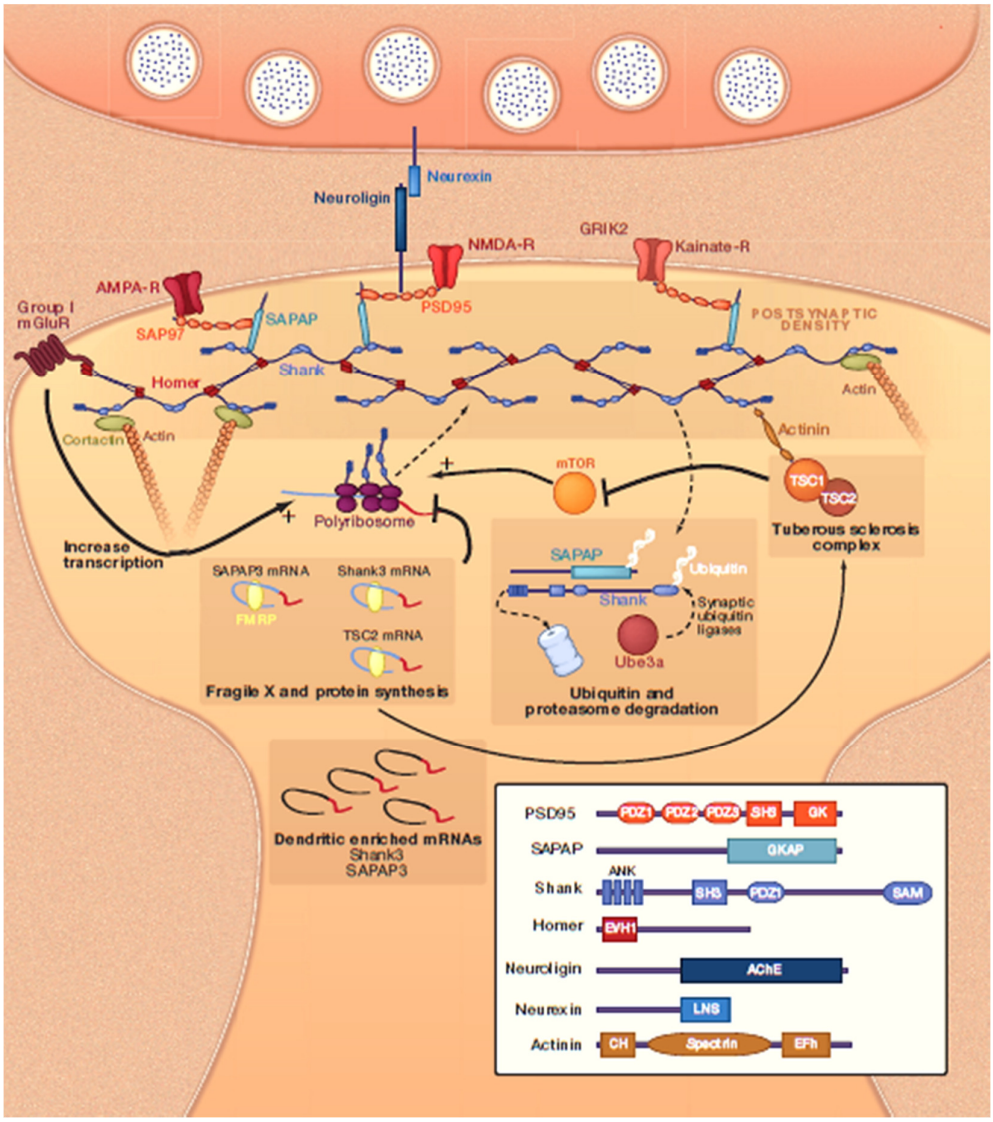

Figure 1.5 | Representation of glutamatergic post-synaptic site (adapted from Peça *et al.*, 2011[57]).

Glutamatergic synapses are characterized by an electron dense thickening underneath the postsynaptic membrane, named the postsynaptic density (PSD). PSD contains hundreds of proteins including receptors (such as NMDA and AMPA); adaptor and scaffolding proteins (PSD95, SAPAP and SHANK); cytoskeletal and cell-adhesion proteins (such as actin and neuroligin) and signaling molecules; creating a well-orchestrated macromolecular complex. Disruption of scaffolding proteins can affect brain circuitry and lead to neuropsychiatric disorders.

At cortical-striatal glutamatergic synapses SAPAP3 and SHANK3 proteins show a unique expression pattern, being the only members of their protein-family

highly enriched at this location. Deletion of the *Sapap3* gene in mice leads to striking OCD-like behavior[58] and mice with simultaneous alpha and beta SHANK3 isoforms deletion exhibit self-injurious repetitive grooming and social interaction deficits, reminiscent of autistic-like behaviors[59]. These studies illustrate how disruption of scaffolding proteins can affect brain circuitry and are able to provide insightful links to neuropsychiatric disorders.

1.5 Obsessive Compulsive Disorder (OCD)

Neuropsychiatric disorders are complex neurological traits that manifest as altered behavioral responses such as self-injurious behavior, hypo or hyperactivity to sensory input, psychomotor dysfunction, impaired social-emotional communication, cognitive deficits, among other symptoms. Due to their volatile nature in terms of assessment, evaluation sometimes relies on exclusion diagnosis, empirical observation of manifested behaviors as well as patients' self-assessment on the phenomenological symptoms.

Obsessive Compulsive Disorder (OCD) has a 2-3 % worldwide prevalence[60,61] and is characterized by excessive preoccupations (obsessions) associated to specific rituals (compulsions) (Table 1.1). Current treatments to alleviate symptoms involve cognitive behavioral therapy (CBT) and SSRIs (selective serotonin re-uptake inhibitors)[62,63]. In more severe cases where patients do not respond to medication and CBT, other interventions have been used such as deep brain stimulation (DBS) of subcortical structures[64–66]. Abnormalities in the glutamatergic system have also been proposed and some NMDA antagonists (namely ketamine and memantine) have been tested as possible therapies[63,67].

Table 1.1 – Diagnostic criteria for OCD according to DSM-5.

	Diagnostic criteria for Obsessive-Compulsive Disorder (DSM-V)
A	Presence of Obsessions, Compulsions or both
	Obsessions: intrusive and unwanted thoughts, urges or impulses that cause anxiety or distress Compulsions: repetitive behaviors performed in response to an obsession and aiming to prevent anxiety or distress
B	Symptoms are time-consuming or cause significant distress/impairment
	E.g. obsessions or compulsions take more than 1H *per* day
C	Symptoms are not attributable to medication or other medical condition
	E.g. symptoms are not attributable to a drug of abuse
D	Symptoms are not better explained by the symptoms of another mental disorder
	E.g. pervasive and intrusive worries about appearance as in body dysmorphic disorder

Previously considered under the spectrum of anxiety disorders, OCD is now categorized with other obsessive compulsive related disorders in the recently revised DSM-5. Re-grouping (together with trichotillomania, body dysmorphic disorder, skin-picking and hoarding disorder) is based on behavioral similarities and common features, namely repetitive behaviors and obsessive preoccupation. Such stratification helps guiding diagnostic criteria and ensures consistency between medical terms, although a more "biologically-valid framework" for mental disorders has been proposed by the US National Institute of Mental Health (NIMH). This new research framework designated Research Domain Criteria (RDoC) tries to emphasize mental disorders as biological disorders that span through specific domains of behavior, emotion, cognition (*e.g.*, social interactions, mood), that can co-occur in a range from normal to extreme. The future goal is to map brain circuits, genetic and cognitive aspects of mental disorders that will help to understand and target the biological basis of these complex behavioral traits. Animal research can contribute to this dimensional approach by providing means to test biological causality. Advancements have been made in several domains of OCD (neurophysiology, behavior and genetics) using animal models of compulsive/repetitive behavior.

1.5.1 Neurophysiology of OCD

One of the most replicated findings in human OCD studies is the involvement of cortico-striatal-thalamo-cortical circuitry (CSTC)[68,69]. Increased activity in the anterior cingulate/caudal medial prefrontal cortex, orbitofrontal cortex (OFC) and caudate region has been reported in OCD by functional imaging studies[70]. Some aspects of executive function as well as evaluation of significance have been implicated with these regions[7], but how can these findings be connected with behavioral manifestations observed in OCD?

One major contribution derived from animal models' research is the possibility of directly manipulating neural circuits and test behavioral outcomes. Among the variety of tools that have recently became available to study neurocircuits, one holds great promise and has sent a bolt of interest across the neuroscience field. Optogenetics is a neuromodulation technique that takes advantage of genetically encoded light-sensors (microbial opsins) to induce activation or silencing of defined neuronal populations in freely-moving animals[71,72]. Specific optogenetic proteins like

channelrhodopsin (ChR2), halorhodopsin (NpHR) or SSFO (stabilized step function opsin), can be used to respectively activate, silence or stabilize membrane potentials in particular neuronal subsets just by shedding specific light wavelengths. Using this strategy, a recent report led by René Hen's group directly tested the CSTC hyperactivity hypothesis in OCD[73]. In their study, authors directly activate orbitofrontal cortex excitatory neurons (MO/VO) that project onto ventromedial striatum region (VMS) using ChR2 in mice. Repeated hyperstimulation during 5 consecutive days progressively led to a surprising increase in repetitive grooming behavior, together with increased cell firing at VMS. Acute stimulation however was not sufficient to induce increased-grooming patterns, suggesting the need for a reinforcing circuitry loop in repetitive OCD-like behaviors.

Another supportive finding for the hyperactivity hypothesis arrives from the *Slitrk5* mouse model. These mice show increased FosB levels (a cellular marker for sustained neuronal activity[74]) specifically at OFC, suggesting hyperactivity of this brain region (matching human functional imaging data). Electrophysiological assessment of this model revealed impaired cortico-striatal transmission (decreased fEPSPs-field excitatory postsynaptic potentials), that can be creating imbalanced basal ganglia activity in the direct *versus* indirect pathway. These results are of particular interest when trying to understand the increased metabolic activity that has been observed in OFC and caudate nucleus of OCD patients[75].

A recent study from Thomas Südhof's lab shows that imbalanced basal ganglia activity can clearly influence the formation of repetitive motor routines[76]. In this particular study the authors show that disinhibition of D1-MSNs in nucleus accumbens/ventral striatum can enhance the formation of repetitive motor routines (increased rotarod learning). This phenotype does not require cerebellum or dorsal striatum, although D1-MSNs in dorsal striatum are important for overall motor coordination. Such studies support the idea that different symptom dimensions might be associated with distinct neural substrates[77]. A proper balance between direct and indirect pathway seems crucial as well as a proper dynamic interaction between different striatal subregions. Repetitive behaviors observed in OCD may arise from brief but repeated bursts of neuronal

activity at specific brain areas, which will hence lead to facilitated activation during subsequent stimulation episodes.

1.5.2 Behavioral studies in animal models of OCD

Behavioral manifestations of OCD usually entail a particular ritual (compulsive act) that is performed in response to a specific thought (obsession). *Repertoire* displayed by individuals can vary but their obsessions/compulsions usually share common themes, ordinary content and are uncontrollable despite individuals' self-awareness[7].

Animal models of neuropsychiatric disorders often exhibit atypical behaviors that resemble human symptomatology (face validity). They may also share biological grounds with human conditions such as a specific gene (construct validity) and successfully respond to the same therapeutic agents prescribed to patients, allowing outcome predictability (predictive validity).

To evaluate OCD-like behaviors in animal models and establish parallels with patients' traits, specific behavioral paradigms have been developed in the last decades to assess multiple components such as anxiety and compulsivity. Patterns of exploratory activity can be evaluated by quantifying time spent in open areas (anxiogenic areas) *versus* time spent in perimeter or protected areas (open field, elevated zero/plus maze tests). Despite the relevance of anxiety assessment, it is important to emphasize that anxiety is an equally relevant trait to other non-OCD spectrums. Similarly it is important to emphasize that OCD itself shares important links with anxiety disorders, although this is not true for all other OC-spectrum disorders[78]. Additional behavioral paradigms focus on compulsive behaviors, considering them as closer translational manifestations of the human condition. Time spent in repetitive tasks such as non-nutritive chewing, grooming or shifting/digging bedding (*e.g.* marble burying test) can be simply observed. Other more complex tests involve learned tasks where presence of compulsive traits can be tested under specific conditioning paradigms (*e.g.* delayed reinforcement task - helps to dissociate impulsive choices from the motor impulsivity observed in OCD) or serial reaction time tasks (time, number and perseverance of choices can distinguish impulsive and compulsive responses)[8,79].

Several animal models exhibit OCD-like behaviors (anxiety, compulsivity) in the aforementioned paradigms and have been useful in underpinning distinct aspects of neurobiological mechanisms related to OCD. The first genetic mouse model presenting face, construct and predictive validity for OCD was published in 2007[58]. These mice lack SAPAP3 a scaffolding protein normally enriched at cortico-striatal glutamatergic synapses. Besides impaired cortico-striatal transmission, these mice display self-injurious grooming and increased anxiety as assessed by the open field, elevated zero maze and dark light emergence tests. Both anxiety and compulsive grooming can be partially alleviated by fluoxetine treatment, conferring great predictive validity to this model. An interesting key finding in these mice is that restoring SAPAP3 expression in the striatum can rescue self-injurious grooming and cortico-striatal transmission, emphasizing striatum's role in compulsive behaviors.

Other interesting finding emerged from the genetic deletion of *Slitrk5* in mice. SLITRK protein family controls neurite outgrowth[80] and deletion of SLITRK5 protein in mice leads to increased anxiety (assessed by elevated plus-maze and open field tests) and compulsivity (increased marble burying behavior and self-injurious grooming)[81]. Chronic fluoxetine treatment can alleviate this phenotype, entailing another example of a promising mouse model for studying and testing OCD-like behavior.

1.5.3 Genetic studies of OCD – insights from patients and animal models

- SLC1A1/EAAC1

Common acts carried out by OCD patients involve actions such as checking (self-doubts on accomplishment of specific tasks and repeated double-checking), washing (unsatisfactory feeling about proper cleaning and urge to repeat washing act) and ordering (organizing/lining up things on a particular order or specific manner). The fact that these themes are not random and occur consistently in patients across distinct socio-cultural backgrounds worldwide, raises the possibility for common genetic basis[82,83]. In fact, twin studies of obsessive-compulsive disorder also support this assumption, being the strongest evidence for genetic contribution in OCD. An extensive review work published by van

Grootheest *et al.*[84] concluded that using dimensional approach for twin studies holds convincing results for OCD symptom's heritability, ranging from 45-65 % in children and 27-47 % in adults (analyzing the data with covariance modeling).

The first genome-wide linkage study for OCD was carried out in 2002 to identify susceptible chromosomal regions for early-onset OCD[85]. The results suggest a link to 9p24 chromosomal region with the closest gene being *SLC1A1* (Solute Carrier Family 1, Member 1) - a glutamate transporter also known as *EAAC1* (excitatory amino acid transporter 1). Since then several linkage studies have supported OCD association with this genomic region but always with nominal evidence (studies support different SNPs association)[86–88]. An *EAAC1*-null mice was first generated and published in 1997 although with minor relevance to OCD-behaviors[89]. As reported by the study, *EAAC1*-null mice develop dicarboxylic aminoaciduria and show reduced spontaneous locomotion in the open field. Later studies report reduced neuronal glutathione levels and age-dependent neurodegeneration in *EAAC1*-null mice (age-dependent cortical thinning and ventricular enlargement). Despite the absence of a strong-OCD phenotype in the *EAAC-1*-null mice, several studies have identified *SLC1A1* as being positively associated with at least some cases of OCD[86,90]. It is plausible that EAAC-1 functional deficits are not well recapitulated in mice or that this gene rather plays a role in a multigenic perspective (by contributing to individual susceptibility together with other factors).

- SAPAP AND SLITRK

Recently a new attempt has been made to search for common SNPs predisposing to OCD. More than 20 research groups have worked together to accomplish the first Genome-Wide Association Study (GWAS) for human OCD[91]. Results from this study suggest the involvement of two SNPs (single nucleotide polymorphisms) located within *DLGAP1* gene that encodes the SAPAP1 protein. Previously, another member from the same family of proteins had been implicated in a genetic mouse model with OCD-like behavior (the *Sapap3/Dlgap3* KO mice), reinforcing the idea that proteins from this family might play a role in OC-related behaviors.

A recent study led by the OCD Collaborative Genetics Association Study (OCGAS)[92] on human genetics of OCD, observed association of a

marker on chromosome 9 near *PTPRD* (although no genome-wide significance was achieved). PTPRD protein seems to play a role in regulating the development of inhibitory synapses through its interaction with SLITRK3. SLITRKS (SLITRK1-6) are a relatively recent discovered family of proteins[80] that have emerged as candidate genes in neuropsychiatric disorders[93]. Human genetic studies have suggested an association link between *SLITRK1* and Tourette syndrome (TS; a neuropsychiatric disorder characterized by motor and vocal tics)[94]. *Slitrk1*-null mice display increased anxiety and noradrenergic abnormalities (consistent with reports of increased norepinephrine levels in cerebrospinal fluid of Tourette's patients[95]). The hypothesis of SLITRK1 involvement in TS and the fact that SLITRKS are highly expressed in mammalian CNS[96], motivated the generation of a *Slitrk5*-KO mouse to search for possible phenotypes. *Slitrk5*-KO mice display OCD-like behaviors and impaired corticostriatal circuitry. Given that both *Slitrk5*- and *Sapap3*-KO mice display impaired corticostriatal transmission and OCD-like behaviors that are responsive to fluoxetine treatment (one of the pharmacological agents used in OCD), it would be interesting to address whether these proteins share common pathways among corticostriatal circuits.

- HOXB8

Another interesting OCD-hypothesis comes from the genetic deletion of the *Hoxb8* gene in mice, suggesting a link between immune system and OCD[97]. This transcription factor is detected in the adult brain, being expressed in bone-marrow derived microglia cells that migrate into brain OFC, cingulate cortex and limbic system as well as other regions, during postnatal period[97,98]. *Hoxb8*-KO mice display self-injurious and cage-mate excessive grooming that can be rescued by bone marrow transplantation from WT mice. Although this link between immune system and OCD might seem puzzling at first, it is recognized that microglia plays a role in regulating neuronal cell death and in modulating neural networks (microglia contacts synapses in an activity-dependent manner and releases cytokines). In fact, a subset of children with OCD can experience worsening of symptoms following a strep infection. One brain region affected in PANDAS (Pediatric Autoimmune Neuropsychiatric Disorders Associated with Streptococcal Infections) is the basal ganglia[99]. Although

brain wide expressed, HOXB8 is predominantly found in adult brainstem, olfactory bulb, cortex and striatum[97,98], being the latest two regions highly implicated in OCD.

Although HOXB8-, SAPAP3- and SLITRK5-KO mice have distinct grooming phenotypes (especially in regards to its biological origin), all proteins share an enriched corticostriatal expression. In regards to human OCD, these mice studies suggest that a similarly shared pathological finding (compulsive behavior) might be a reflection of different subjacent causal insults to the same brain region.

- OTHER GENES

Currently approved treatments to alleviate OCD symptoms involve serotonergic medication among others. Although exact mechanisms are unknown, it is thought that 5-HT_{2C} serotonin receptor agonism might contribute to therapeutic benefits in OCD[100]. Genetic deletion of 5-HT_{2C}-R in mice leads to enhanced sensitivity to induced motor stereotypy and compulsive-like behaviors such as non-nutritive chewing and increased head-dipping[101–104], confirming serotonergic involvement in compulsivity. Contrarily to other OCD models, these mice show less anxiety than WT mice (open field, elevated plus maze, novel object, mirrored chamber) suggesting that compulsivity and anxiety symptoms might be dissociable.

Other useful way to look for candidate genes besides exploratory gene deletion in mice, is genomic sequencing from animals displaying spontaneously-occurring pathological behaviors. Some dog breeds display OCD-like behaviors including incessant tail chasing and relentless paw chewing. Given the fact that dogs' genome is far less complex than human genome, a dog-OCD GWAS study was recently carried for the first time and identified four synaptic genes with major case-only variation (CDH2, CTNNA2, ATXN1, PGCP)[105].

Together these genetic studies seem to point towards CSTC synaptic dysfunction across distinct OCD-animal models (Table 1.2). Although animals can never fully recapitulate human OCD spectrum due to species-specific limitations, they do allow us to precisely study gene-linked phenotypes by limiting some confounds such as genetic background and environmental variability that are inherent to human studies.

Table 1.2– Candidate genes from animal models with OCD-like behaviors.
Genes listed in this table have emerged from sequencing studies or from single gene KO studies that resulted in OCD-like phenotypes.

Candidate genes from animal models of Obsessive-Compulsive Disorder (OCD)					
Gene	**Genetic evidence**	**Behavioral phenotype**	**Neurophysiology**	**Notes**	**References**
HOXB8	-Global Hoxb8-KO mice with relevant phenotype -Conditional-KO (hematopoietic cells) exhibit the global KO mice phenotype	-Self-injurious grooming -Cage mate over-grooming	-Hoxb8 expressed in bone-marrow derived microglia that migrate into brain OFC, cingulate cortex and basal ganglia regions	-Wild-type bone marrow transplantation rescues excessive grooming -KO bone marrow transplantation induces excessive grooming in WT	Chen et al. 2010; Greer and Capecchi 2002
SAPAP3	-Global Sapap3-KO mice with strong phenotype -Two SNPs located in Sapap1 (family member) found in human OCD GWAS study	-Self-injurious grooming -Increased anxiety (open-field, elevated zero maze and dark light emergence) -Deficit in adaptive grooming response during conditioning task	-Sapap3 mainly expressed in neocortex, striatum, hippocampus and thalamus -Impaired cortico-striatal function (reduced fEPSP, mEPSC and AMPA/NMDA ratio; increased silent synapses and eCB-LTD) -Increased spontaneous MSN firing activity in centromedial striatum -Reduced interneuron PV number in centromedial striatum	-Striatum infection using lentivirus-Sapap3 rescues self-injurious grooming and fEPSP -Fluoxetine treatment partially alleviates compulsive grooming and anxiety	Burguière et al. 2013; M. Chen et al. 2011; Stewart et al. 2013; Wan, Feng, and Calakos 2011; Wan et al. 2014; Welch et al. 2007
SLITRK5	-Global Slitrk5-KO mice with strong phenotype	-Self-injurious grooming -Increased anxiety (open-field, elevated plus maze) -Compulsive-like behavior (marble burying test)	-Slitrk5 mainly expressed in neocortex, striatum and hippocampus -Impaired cortico-striatal function (reduced fEPSP) -OFC hyperactivity (increased FosB staining levels) -Decreased striatal volume and decreased MSN dendritic complexity	-Fluoxetine alleviates over-grooming	Shmelkov et al. 2010
SLC1A1 ,EAAC1	-Human OCD genetic studies -EAAC1-null mice show modest phenotype	-Human OCD -EAAC1-KO mice show cognitive and motivational impairment at old age -Reduced spontaneous locomotion in the open field	-SLC1A1 is highly expressed in human cortex, striatum and thalamus	-Age-dependent cortical thinning and ventricular enlargement in EAAC1-null mice -Dicarboxylic aminoaciduria	Aoyama et al. 2006; Peghini, Janzen, and Stoffel 1997; Rothstein et al. 1994; Wu et al. 2012
CDH2	-Dog OCD small GWAS	-Canine OCD (incessant tail chasing, relentless paw chewing)	ND in dogs	-CDH2 KO mice die during early embryonic stages	Pielarski et al. 2013; Radice et al. 1997; Tang et al. 2014
HT2RC	-Global 5-HT_{2C}-R-KO mice show compulsive phenotype	-Non-nutritive chewing -Increased head-dipping -Reduced anxiety (open field, elevated plus maze, novel object, mirrored chamber)	-Decreased corticotrophin hormone release from the extended amygdala in response to anxiogenic stimuli	-Mid-life obesity (due to hyperphagia) -Prone to death from spontaneous seizures -Altered sleep homeostasis	Chou-Green et al. 2003; Heisler et al. 2007

1.6 Autism Spectrum Disorders (ASD)

In recent years striatal dysfunction has been hypothesized in repetitive and stereotyped behaviors associated with neuropsychiatric disorders, such as obsessive compulsive disorder (OCD) and autism spectrum disorders (ASD)[7,75,106]. The word “autism” comes from the Greek words “autos” (“self”) and “ismos” ("action") and autistic patients were first described in 1943 by Kanner[107]:

“*The children of our group have all shown their extreme aloneness from the very beginning of life, not responding to anything that comes to them from the outside world(…) Second our children are able to establish and maintain an excellent, purposeful, and ‘intelligent’ relation to objects that do not threaten to interfere with their aloneness, but are from the start anxiously and tensely impervious to people(…) All of the children’s activities and utterances are governed rigidly and consistently by the powerful desire for aloneness and sameness*” – L. Kanner

Currently 1 in 88 children in the United States[108] is diagnosed with ASD with the prevalence being 4x greater in boys than girls (1 in 54 boys compared to 1 in 252 girls)[109]. Other genetic conditions such as Fragile X mental retardation, tuberous sclerosis and Down's syndrome are often associated with autism. In the previous version of the "Diagnostic and Statistical Manual of Mental Disorders" (DSM-IV), autism spectrum disorders were divided in 5 subgroups: Autistic disorder; Asperger's syndrome; Pervasive developmental disorder-not otherwise specified (PDD-NOS); Rett syndrome and Childhood disintegrative disorder. In the new DSM-V, Rett syndrome is separate from ASDs and the remaining 4 subgroups no longer exist. Instead all patients will now be given unified ASD diagnosis with a specified severity from 1 to 3 (1-least severe; 3-most severe). ASD diagnosis in DMS-V is defined by deficits in social communication and social interaction, associated with narrow stereotyped, repetitive behavioral interests (Table 1.3). Symptoms must be present in early childhood and interfere with individual's daily activities. Currently there is no medication to treat the core features of autism.

Table 1.3 – Diagnostic criteria for Autism-Spectrum Disorder according to DSM-5.

	Diagnostic criteria for Autism-Spectrum Disorder (DSM-V)
A	Persistence of social communication and interaction deficits
	Deficits in social-emotional reciprocity, nonverbal communicative behaviors and age-appropriate peer relationships
B	Narrow, stereotyped, repetitive behavioral interests
	Repetitive motor movements, use of objects or speech; Insistence on sameness; Perseverative interest with abnormal intensity or focus; Hyper- or hyporeactivity to sensory input
C	Symptoms are present in early childhood
	Despite present, symptoms are sometimes not noticed until later social demand
D	Symptoms cause significant distress/impairment
	Impairment in social, occupational or other relevant areas of functioning
E	Symptoms are not better explained by the symptoms of another mental disorder
	Not better explained by intellectual disability or global developmental delay

1.6.1 Neurophysiology of ASD

Although ASD's neurophysiology remains elusive, social behavior processing seems involved. Diminished gaze fixation has been reported in autistic patients as well as failure in developing age-appropriate peer relationships[110]. Many brain areas have been indicated as part of the "social brain", including the medial prefrontal cortex (mPFC), amygdala,

anterior insula, anterior cingulate cortex (ACC), inferior frontal gyrus (IFG) and the superior temporal sulcus (STS)[111]. Higher order executive functions such as decision making and behavioral planning are associated with frontal lobes, whereas amygdala plays a role in emotional processing, anxiety and memory associations.

Hypoactivation of fusiform gyrus has been reported in autistic patients along with amygdalar hyperactivation in response to faces[112]. In 2004 a study reported larger left and right amygdala volumes in male children with autism, but not in adolescents[113], suggesting amygdala involvement in the early neurobiology of ASD.

One recent emerging theory proposes a social motivation deficit in ASD rather than a social cognition core deficit[114]. According to this idea, lack of social motivation might be a primary deficit in autism and therefore affect the development of social cognition. At the biological level, motivation processing involves regions such as the amygdala, ventral striatum and ventromedial PFC. Dysfunction at orbitofrontal-striatum-amygdala circuit has been suggested in ASD[115], although it is unclear whether this abnormal reward processing is restricted to social stimuli or encompasses a more generalized deficit in stimulus-reward associations.

Oxytocin is a neuromodulator released by the pituitary gland, important for human social behavior[116]. Recent studies in mice have shown that social reward requires coordinated activity of oxytocin and serotonin in nucleus accumbens[117], as well as dopamine modulation[118]. Given the hypothesis that autistic patients might have a motivational impairment to engage in reciprocal social interaction, recent studies have looked into oxytocin in ASD[119,120]. Whether or not these neuromodulators (or any others) can play a role in ASD neurobiology will certainly be addressed in future studies.

Adding to social interaction deficits, perseverative and stereotyped behaviors are present in ASD and have been correlated with frontostriatal and basal ganglia dysfunction[121–124]. Approximately 30-40 % ASD patients have comorbidity with OCD, suggesting some degree of overlapping circuitry between these disorders[125]. An MRI study from Sears *et al.*[126] found increased caudate volume in autistic patients and a significant correlation between this parameter and ritualistic/repetitive behaviors. Earlier Siegel *et al.*[127] had reported reduced glucose metabolism in left posterior putamen, implicating basal ganglia dysfunction. Recently

Mostofsky *et al.*[128] reported that abnormalities in basal ganglia shape can predict social and communication dysfunctions as well as impaired motor skills in ASD boys.

In line with this clinical data, several research studies have shown that SHANK3 deletion (a protein highly enriched in striatum) leads to ASD-like behaviors in mice[59,129–133]. Severe social interaction deficits are observed together with repetitive self-injurious grooming upon PDZ-targeted *Shank3* disruption (Δex13-16)[59]. Like the *Sapap3*-KO mice (OCD-model)[58], *Shank3*-Δex13-16 mice have biochemical and electrophysiological corticostriatal deficits, suggesting a shared CSTC circuitry dysfunction between these repetitive/compulsive behaviors.

1.6.2 Genetic studies of ASD – insights from patients and animal models

The biggest evidence for genetic contribution in ASD comes from twin studies where results show 31 % concordance rates for dizygotic twins and 88 % for monozygotic twins[134]. ASDs are clinically heterogeneous, with symptoms severity ranging from mild social deficits with normal cognitive abilities to severe mental impairment and absence of language skills. Evidence points towards involvement of different genetic variations (chromosomal rearrangements, *de novo* copy-number variants and coding-sequence variants) that have been associated also with different genes[135,136]. Despite this heterogeneity many of the implicated genes encode synaptic proteins that play important roles in development or functioning of brain circuits (*Shank3*, *Neuroligin-3*, *Neuroligin-4* and *Neurexin-1*)[137,138]. This evidence suggests that ASDs are etiologically heterogeneous (possibly involving polygenic, monogenic and environmental factors) but synaptic dysfunction might well be a common underlying mechanism for a defined ASD subset.

- NEUREXIN AND NEUROLIGINS

Neuroligins (NLGNs) are cell adhesion molecules that play an important role in synaptic function and maintenance[139]. Neuroligins localize at the postsynaptic membrane and make trans-synaptic links with neurexins (NRXNs). Mammalian genomes typically encode 4 neuroligins,

with the human genome encoding NLGN3 and NLGN4 in the X chromosome and another NLGN5 gene in the Y chromosome. NLGN1 is exclusively localized at excitatory synapses, NLGN2 at inhibitory synapses and NLGN3 is probably present in both[139]. Several mutations in NRXN1, NLGN3 and NLGN4 have been found in patients with autism (NRXN1: 7 point mutations, 2 distinct translocations and 4 different large-scale deletions; NLGN3: a single mutation [Arg451Cys] and a 33kb deletion; NLGN4: 2 frameshifts, 5 missense mutations, 3 internal deletions and 5 large deletions in chromosome X including *NLGN4* locus)[139,140]. Three mouse models carrying these ASD patient's mutations have been generated: *Nlgn3*-KO[141], NLGN3 R451C mutant[141] and *Nlgn4*-KO mouse[142]. All show traits of ASD-like behaviors, although distinct between each line (detailed behavioral description below in 1.6.3). Overall these studies support dysfunction of synaptic proteins as a potential mechanism underlying a subset of ASDs, potentially with overlapping defects to those caused by *Shank3* mutations.

- SHANK3

SHANK3 (SH3 and multiple ankyrin repeat domains 3; also known as ProSAP2) is a scaffolding protein of the PSD that is enriched at corticostriatal glutamatergic synapses[59,143]. Its gene has multiple intragenic promoters (probably 6)[144] and several alternative splicing exons (exons 10-12, exon 18, exon 21 and exon 22)[144], resulting in a wide variety of transcripts (Fig1.6). Its full length structure contains 5 domains for protein-protein interactions: Ank (ankyrin repeats), SH3 (Src homology domain), PDZ (PSD95/Dlg/ZO-1 domain), Pro (proline-rich region) and SAM (sterile alpha motif). N-terminal Ank domain interacts with Sharpin[145] and likely binds cytoskeleton through α-fodrin interaction[146]; SH3 domain is followed by PDZ domain that interacts with GKAP/SAPAP[147]; Proline-rich domain binds to Homer[148,149] and Cortactin proteins[147]; C-terminal SAM domain of SHANK is known to self-associate[147,150] and is required for the localization of SHANK2 and SHANK3 to the PSD[151].

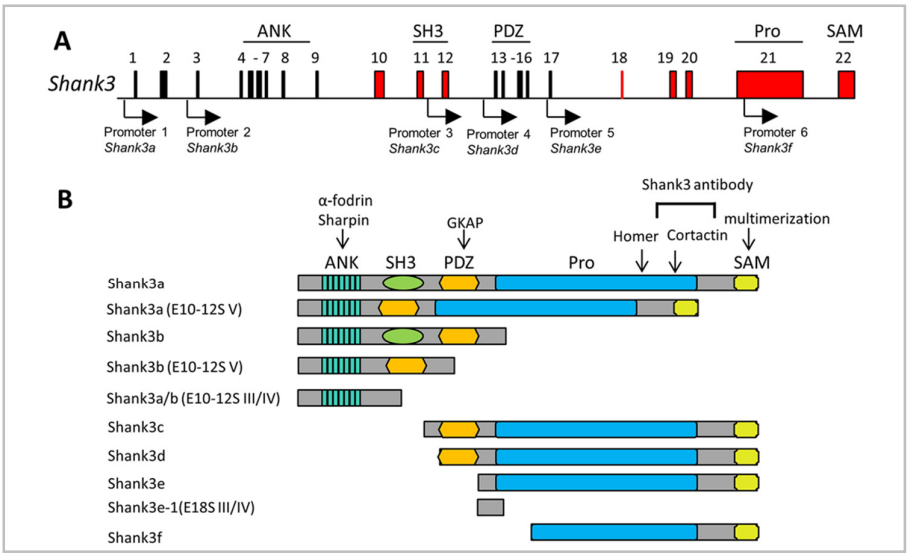

Figure 1.6 | Diverse *Shank3* isoforms result from intragenic promoters and alternative splicing (adapted from Wang *et al.*, 2014[144]).

(A) Multiple promoters of the *Shank3* gene. Mouse *Shank3* has 22 coding exons as illustrated. The alternatively spliced exons are highlighted in red. The positions of intragenic promoters are shown as black arrows. Protein domains encoded by exons are labeled above the gene structure. (B) The predicted SHANK3 protein isoforms were deduced from the combination of intragenic promoters and alternative splicing of mRNAs described above and *in silico* analysis. The binding positions of several well-known PSD proteins are shown by arrows. The epitope position for the SHANK3 antibody used in this study is also indicated[144].

Phelan-McDermid syndrome (PMS, 22q13.3 deletion) is an autism spectrum disorder characterized by autistic-like behaviors, hypotonia, and delayed/absent speech[152]. Genomic rearrangements in PMS patients range from deletions, ring chromosomes, interstitial deletions to unbalanced translocations[153,154]. *Shank3* is one of the genes deleted in PMS and its disruption is thought to cause the core neurodevelopmental and behavior deficits. Individuals carrying a ring chromosome 22 with intact *Shank3* gene are phenotypically normal, supporting the idea that core symptoms are due to *Shank3* haploinsufficiency[152]. Genetic screens have identified microdeletions, coding mutations and *Shank3* breakpoints in ASD patients not diagnosed with PMS (Table 1.3)[155–158]. A recent study indicates that *Shank3* mutations correlate with more severe cognitive deficits in patients (compared to *Shank1* and *2* mutations) and contribute to ~1 % of all ASD cases[154]. This suggests *Shank3* mutation/disruption as

a potential monogenic cause for autism-spectrum disorder that should be considered for mutation screening in clinical practice.

Table 1.4 – Genotype/Phenotype correlations of human *SHANK3* mutations (extracted from Yong-hui Jiang and Michael D. Ehlers, 2013[159]).

Genetic Defect		No. of Case	SHANK3 Isoforms Affected	Other Genes Disrupted	ASD-Related Diagnosis	Intellectual Disability (ID)	Other Clinical Features
22q13.3 deletion (including SHANK3) (0.1-10Mb)		>1000	All isoforms disrupted	From 2-30 other genes	ASD diagnosis in >75% of cases	>95% cases with developmental delay, moderate to severe ID, absent speech, or severe speech delay	Hypotonia, seizure, motor development delay, facial dysmorphism, increased pain threshold, bipolar disorder, mild congenital anomaly
Microdeletion of SHANK3		3	All isoforms disrupted	None or / ACR	ASD	Speech delay and mild ID	Hyperactivity, hypospadias, behavioral issues, seizure/regression
Intragenic deletion							
Deletion size	Exons/domain deleted						
38 kb	exon 1–9 ANK	1	SHANK3a/b	none	Not mentioned	Moderate ID, profound delay in language acquisition	Microcephaly, astigmatism
74 kb	exon 1–17 ANK/ SH3/PDZ	1	SHANK3a-e	none	Not evaluated	Profound ID	Mild congenital anomalies
44 kb	Exon 19–23 Homer binding/SAM	1	SHANK3f	ACR	ASD	Moderate ID/hyperactivity disorder	Short stature, facial dysmorphism, astigmatism
27 kb	exon 20–23 Homer binding/ SAM	1	SHANK3f	ACR[a]	Classical autism	Not mentioned	ADHD, no facial dysmorphism
17 kb	Exon 23 SAM	1	SHANK3f	ACR	No ASD by CARS and ABC	Mild ID, severe delay in language acquisition	Mild facial dysmorphism, mild motor delay
Point mutation/Small deletion							
Mutation	Exon/protein domain	1					
c.601-1G > A	ANK	1	SHANK3a-b	None	No ASD	Mild ID, severe language impairment	
p.Q312R[b]	Exon 8 ANK	1	SHANK3a-b	None	ASD by ADI-R and ADOS	language delay	Abnormal EEG but no seizures; has self-injurious behavior
p.A447fs[c]	Exon 11 SH3	1	SHANK3a-c	None	Borderline score for ASD evaluation	Language delay	No facial dysmorphism
p.G440_P446 del	Exon 11 SH3	1	SHANK3a-c	None	ASD	Severe ID	Delayed psychomotor development
c.1820-4G > A	PDZ	1	SHANK3a-d	None	Asperger's syndrome	Normal speech and some behavioral problems	Facial dysmorphism/ mild congenital anomaly
p.R656H[d]	Exon 16 PDZ	1	SHANK3a-d	None	ASD	Mild ID, development delay	
c.2265+1 del G		1	SHANK3a-e	None	ASD	Not mentioned	
p.R1117X	Exon 21 Homer binding	1	SHANK3f	None	No evidence for ASD	Mild to moderate ID	Schizophrenia, hyperactivity/no facial dysmorphism
p.A1227fs	Exon 21 Homer-binding	1	SHANK3f	None	ASD	Severe ID and impaired speech	
p.E1311fs	Exon 21 Homer-binding	1	SHANK3f	None	PDD-NOS	Severe ID and absent speech	Seizure, facial dysmorphism, motor development delay

The information in the table is extracted from following reports: Boccuto et al., 2013; Bonaglia et al., 2011; Dhar et al., 2010; Durand et al., 2007; Gauthier et al., 2009, 2010; Moessner et al., 2007; Phelan, 2007; Sarasua et al., 2011; Waga et al., 2011; Wilson et al., 2003; Wong et al., 1997). ACR, Acrosin, a sperm specific proteinase which has no known function in brain; ABC, autism behavioral checklist; ADHD, attention deficit-hyperactivity disorder; ADI-R, autism diagnosis interview-revised; ADOS, autism diagnosis observation scale; CARS, child autism rating scale; Del, deletion; EEG,, electroencephalography; ID, intellectual disability; PDD-NOS, pervasive developmental disorder-otherwise not specified.

[a]Proband has a chromosome 9p24.3 copy number gain that is inherited from mother and considered a benign variant.

[b]Parents are first cousins.

[c]The variant is inherited from father who has learning disability and attention deficit disorder.

[d]Variant is also found in healthy and normal father.

Genetically engineered mice carrying *Shank3* mutations have extended our understanding of SHANK3 protein function and have further supported its association with ASD (Fig1.7) [59,129,130,132]. So far 6 mouse lines carrying different *Shank3* deletions causing frame shifts have been generated: Δex4-9^{Buxbaum} (Ank domain)[130], Δex4-9^{Jiang} (Ank domain)[129], Δex4-7^{Peça} (Ank domain)[59], Δex11 (SH3 domain)[131], Δex13-16 (PDZ domain)[59], and Δex21 (Pro domain).

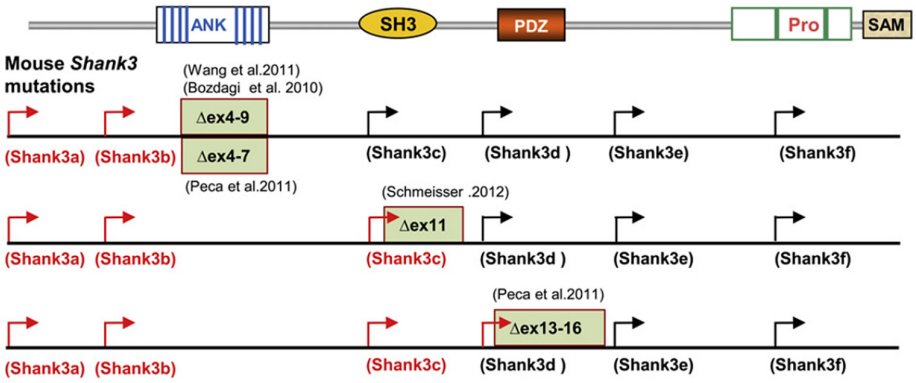

Figure 1.7 | Targeted mutations in *Shank3* Gene in Mice (adapted from Yong-hui Jiang and Michael D. Ehlers, 2013[159]).
Positions of targeted mutations in five different lines of *Shank3* mutant mice are shown. The transcripts from promoters upstream of deleted exons are predicted to be truncated or disrupted (red arrows) and the transcripts from promoter downstream of deleted exons are predicted to be intact in each mutant line of mice (black arrows)[159].

Despite the heterogeneity of transcripts that might be putatively intact or disrupted in these different mouse lines, all show deficient synaptic function, repetitive routines and impaired social behaviors (although all parameters are affected to a different extent in each line; detailed description below in 1.6.3). An interesting observation is that disruption of *Shank3a* to *Shank3c* leads to increased repetitive grooming phenotype. Given that this phenotype is absent in *Shank3a* and *Shank3b* KO mice (and excluding variables as genetic background and environmental factors), it could be inferred that *Shank3c* is probably implicated in the development of increased self-grooming behavior. More importantly all *Shank3*-KO mice support the idea that distinct *Shank3* mutations might underlie a defined subset of ASDs and contribute to the myriad of phenotypes (genotype/phenotype correlation).

1.6.3 Behavioral studies in animal models of ASD

Animal models of ASD (SHANK3, NLGN3 and NLGN4 mutant mice) have demonstrated remarkable face and construct validity. They carry genetic mutations reported in patients and display behavior phenotypes that closely resemble those described in human ASDs. Since there is no current medication to treat autism core features, predictive validity remains to be tested.

Nlgn4-KO mice show deficits in reciprocal social interaction and have reduced ultrasonic vocalizations[142]. Other two neuroligin mutant mice were previously generated in 2007 focusing on the *Nlgn3* gene[141]. A knockin was generated carrying the *Nlgn3* R451C substitution found in two Swedish male siblings[160] (one diagnosed with typical autism and one with Asperger's syndrome) and simultaneously a *Nlgn3*-KO was also generated to search for common phenotypes between this line and the described knockin mutation. R451C mice have increased cortical inhibitory transmission, impaired social interaction but enhanced spatial learning. Surprisingly, *Nlgn3*-KO did not cause any of these changes, suggesting that R451C mutations represents a gain of function. More recently another study compared both mouse lines and focused on common behavioral changes among these two *Nlgn3* ASD-associated mutations. Given that no social interaction deficits were previously found in *Nlgn3*-KO, this recent study focused on another ASD core symptom - repetitive and stereotyped movements. Using rotarod motor learning as a proxy for acquired repetitive behaviors, the authors found that *Nlgn3*-KO and R451C mutant mice share enhanced formation of repetitive motor routines[76]. Opposite to previously reported enhanced inhibitory synaptic transmission seen in the cortex, these mice have reduced D1-inhibition in ventral striatum. This D1-pathway imbalance enhances rotarod learning, emphasizing striatum's role in the genesis of repetitive motor routines. Other important finding from this study is that Nlgn3 manipulations (in ventral striatum), both in adulthood and developmentally, lead to the same phenotype regardless of age. This suggests that even neurodevelopmental disorders (early onset such as ASDs) might be amenable to adult interventions (at least those caused by the *Nlgn3* gene).

Striking ASD-like behaviors have also been observed in animal models carrying *Shank3* gene mutations. Among the different mouse lines generated so far[59,129–133], 5 out of 6 lines have impaired social interaction and 5 out of 6 display repetitive behaviors, strongly supporting *Shank3* as an ASD-candidate gene. Other behavioral parameters such as USV calls (ultrasonic vocalizations) and learning and memory, have been evaluated in some of these mutant lines, holding distinct results that might be associated to specific domain disruptions in each line (Table 1.5).

Table 1.5 – Molecular, biochemical, synaptic, and behavioral phenotypes of *Shank3* mutant mice (extracted from Yong-hui Jiang and Michael D. Ehlers, 2013[159]).

Reference	Bozdagi et al., 2010; Yang et al., 2012	Wang et al., 2011	Peça et al., 2011	Peça et al., 2011	Schmeisser et al., 2012
Exons/domain targeted	Exons 4–9^{B}/ANK repeat (Δex4–9^{B})	Exons 4–9^{I}/ANK repeat (Δex4–9^{I})	Exons 4–7/ANK repeat (Δex4–7)	Exons 13–16/PDZ (Δex13–16)	Exon 11/SH3 (Δex11)
Strain/background	Bruce4 C57BL/6 ES cell and maintain on C57BL/6	129SvEv ES cell backcrossing to C57BL/6J for more than 6 generations	129SvR1 ES cell and backcrossing to C57BL/6J for one generation	129 SvR1 ES cells and backcrossing to C57BL/6J for more than 1 generations	129SvR1 ES cell and backcrossing to C57BL/6 for more than 10 generations
Age of mouse	Biochemistry: 3 months Morphology: 3 months Electrophysiology:3 months Behaviors: P21 days to 16 weeks	Biochemistry: 3–4 months Morphology: P1 neuron culture and 1–3 months Electrophysiology: 4–6 weeks. Behaviors: 3–8 months	Biochemistry: not stated Electrophysiology: 6–7 weeks Behaviors: 5–6 weeks	Biochemistry: not stated Morphology: 5 weeks Electrophysiology: 5–7 weeks Behaviors: 5–6 weeks	Biochemical: P25 and P70 days Morphology: adult Electrophysiology: N/A Behaviors: N/A
Transcripts not disrupted	*Shank3c,d,e, f*	*Shank3c,d,e,f*	*Shank3c,d,e,f*	*Shank3e, f*	*Shank3d, e, f*
Genotype of mice analyzed	Heterozygous/homozygous	Homozygous	Homozygous	Homozygous	Homozygous
Altered synaptic proteins	Reduction of GluA1	Reduction of GKAP, Homer1b/c, GluA1, GluN2A	N/A	Reduction of SAPAP3/GKAP3, Homer1, PSD-93, GluA2, GluN2A, GluN2B	Increased GluN2B and Shank2
Brain and synaptic morphology	**CA1 Hippocampus** Activity-dependent spine remodeling was affected,	**CA1 Hippocampus** Longer dendritic spines. Decreased spine density. No change in length and thickness of PSD.	N/A	**Striatum** Increase in striatal volume, dendritic length, and surface area. Decreased spine density, length, and thickness of PSD.	**CA1 hippocampus** No defect identified.
Synaptic physiology	**CA1 Hippocampus** Reduced AMPAR-mediated basal transmission. Decreased mEPSC amplitude. Increased mEPSC frequency. Decrease in paired-pulse ratio. Reduced LTP. No change in NMDAR- or mGluR-mediated LTD.	**CA1 Hippocampus** No change in basal synaptic transmission. No change in amplitude or frequency of mEPSCs or mIPSCs. No change in paired-pulse ratio, I/O, fiber volley. Reduced LTP.	**Striatum** Slight reduction in corticostriatal synaptic transmission.	**CA1 Hippocampus** No change in field recordings of population spikes, paired-pulse ratio, mEPSC frequency and amplitude. **Striatum** No change in paired-pulse ratio. Reduced field population spikes. Reduced mEPSC frequency and amplitude.	N/A
Social behaviors	Reduced social sniffing by males in male-female interactions, mild social impairment in reciprocal interactions in juveniles. Normal three chamber test for adult mice.	Reduced interest in novel mice in nonsocial versus novel social pairing in three chamber test, females performed better than males. Decreased bidirectional social interactions in dyadic test.	Normal initiation of social interaction. Perturbed recognition of social novelty during three chamber test.	Perturbed recognition of social novelty during three chamber test. Decreased reciprocal interactions in dyadic test. Decreased frequency of nose-to-nose interaction. Decreased anogenital sniffing.	N/A
USV calls	Reduced calls observed in some cohorts of adult mice during social interaction but no difference in newborn pups.	Males made more calls, while females made fewer calls. Altered frequency, complexity, and duration of calls.	Not mentioned	N/A	N/A
Repetitive behaviors	Increased self-grooming. Inflexible behavior in reversal of water maze observed in some cohorts.	Increased head pokes in hole-board test, increased self-grooming. Stereotypic object manipulation in novel object test.	No increase in self-injurious grooming.	Self-injurious grooming, causing skin lesions.	Self-injurious grooming, causing skin lesions.
Learning and memory	Impaired novel object recognition. Normal Morris water maze, normal fear conditioning.	Impaired in acquisition and reversal in Morris water maze. Impaired short- and long-term memory	N/A	No difference observed in Morris water maze.	N/A
Schizophrenia-related behaviors	Normal sensory gating and startle reflex.	No difference in PPI. Not hyperactive in the open field.	N/A	N/A	N/A

AMPA, α-amino-3-hydroxy-5-methyl-4-isoxazolepropionic acid; LTP, long-term potentiation; LTD, long-term depression; NMDA, N-methyl-D-asparate; mEPSC, miniature excitatory postsynaptic current; mIPSC, miniature inhibitory postsynaptic current; mGluR5, metabotropic glutamate receptor 5; N/A, not analyzed; I/O, input/output; PPI, prepulse inhibition; USV, ultrasonic vocalization.

Overall what these behavioral studies do support is that synaptic impairment might cause the core symptoms of autism. Particularly striatum dysfunction might underlie repetitive behaviors observed not only between different ASD-mouse models (*Nlgn3*-KO, NLGN3 R451C mutant, *Shank3*Δex4-9^{Buxbaum}, *Shank3*Δex4-9^{Jiang}, *Shank3*Δex11, *Shank3*Δex13-16 and *Shank3*Δex21) but also seen across several OCD-mouse models (*Sapap3*-, *Slitrk5*- and *Hoxb8*-KO mice).

PART II

EXPERIMENTAL WORK

Chapter 2

Distinct role of parvalbumin interneurons of the dorsomedial striatum in habit formation

2.1 Summary

Rodent striatum displays a dorsolateral-to-ventromedial topographical organization. Within the dorsal region, medial and lateral striatum territories (DMS and DLS) support distinct behavioral outcomes. DMS encodes goal-directed actions that upon repetition often become habits (encoded by DLS). At cellular level, it is not clear how this transition of activity from DMS to DLS takes place. Parvalbumin interneurons (PV) provide important striatal inhibition but their role in striatum-mediated habit formation is unknown. Using retrograde viral mapping we show that parvalbumin interneurons in DMS receive unique mPFC inputs and have distinct electrophysiological signature from parvalbumin interneuron in DLS region. Using TeLC (tetanus toxin light chain) in a *cre* dependent manner, we locally silence this PV population and show that PV-inhibitory activity in DMS is required for habit formation in mice.

2.2 Background

Proper psychomotor behavior processing such as motor control, procedural learning and behavioral switching requires basal ganglia circuits[1,3,9,10]. Striatum is a major basal ganglia input station and dysfunction to this region has been related to OCD and ASD, thickening the list of previously known striatum-related disorders such as Parkinson and Huntington's disease[37]. Anatomically, the striatum has a dorsal sensorimotor area and a ventral limbic region. Recent neurophysiology and behavior studies have suggested a further subdivision of the dorsal area into dorso-lateral (DLS) and dorso-medial (DMS) striatum. These rodent regions respectively resemble primate's putamen and caudate regions[13,161,162] and seem to differentially support two behavioral strategies: intentional goal-directed actions (DMS mediated) that after repetition often become habitual automated responses (DLS mediated)[10,14,16–20]. Simultaneous recordings in DLS and DMS during initial task learning and extended training, show increasing firing rates during early training in both regions. However extended training reveals markedly opposed patterns. DMS activity gradually wanes to naïve levels, whereas DLS activity further increases with training[23,163,164]. This data together with previous lesions studies[16,19,165] suggests a model where strengthening of DLS activity together with decline of DMS activity is required for habits formation. In a scenario where DMS activity is prematurely

suppressed (such as excitotoxic lesions), DLS activity is uncovered and habits immediately emerge early in training. Previous studies have shown that local modulation of striatum medium-spiny neurons (MSNs) is required for successfully engaging or transitioning between these two behavioral strategies[21,22]. Even though several lines of evidence support this distinct functionality between DLS and DMS regions, it is not known what neuronal correlates are responsible at the cellular level.

Parvalbumin interneurons (PVs) can act as powerful circuit-modulators[47,166,167], posing as ideal candidates for regulating striatal output. Here we provide electrophysiological and histological evidence for dichotomous PV populations between DLS and DMS regions. In line with previous reports[168,169], we observed that larger-elaborate PV cells cluster along the lateral striatum in contrast to a smaller-simple PV population in DMS region. Taking advantage of parvalbumin-*cre* transgenic mice, we have performed retrograde monosynaptic tracing and whole-cell recordings to show that parvalbumin interneurons located in dorsomedial striatum are intrinsically more excitable and receive unique mPFC inputs. By locally silencing this population in a cre dependent manner (AAV-FLEX-TeLC; tetanus toxin light chain), we found that PV-inhibitory activity in DMS is required for habit formation in mice but not goal-directed learning. Underpinning neuronal substrates that control purposeful versus habitual actions is crucial to understand striatum dysfunction in a broad range of complex neuropsychiatric disorders.

2.3 Results

2.3.1 Pvalb$^{tm1(cre)Arbr}$:ROSA26-*stop^{flox}-tdTomato* mice label striatal parvalbumin interneurons

Parvalbumin interneurons represent a very small percentage of all striatal neurons (~1 %) but provide robust feedforward inhibition that shapes the firing activity of MSNs[38,170]. A larger elaborate PV population can be observed in dorsolateral striatum contrasting to a smaller-simple PV population in the dorsomedial area (Fig.2.1). To allow identification and electrophysiological recordings from these two populations we started by crossing Pvalb$^{tm1(cre)Arbr}$ with ROSA26-*stop^{flox}-tdTomato* mice to drive *tdTomato* expression under the control of endogeneous parvalbumin promoter. To confirm whether PV cells can be correctly labeled by this strategy we performed slice immunostaining with known

striatal markers. Faithful colocalization is observed between *tdTomato* native signal and parvalbumin staining, but no other striatal markers (DARPP32, SOM, ChAT), indicating a correct reporting strategy (Fig.2.2).

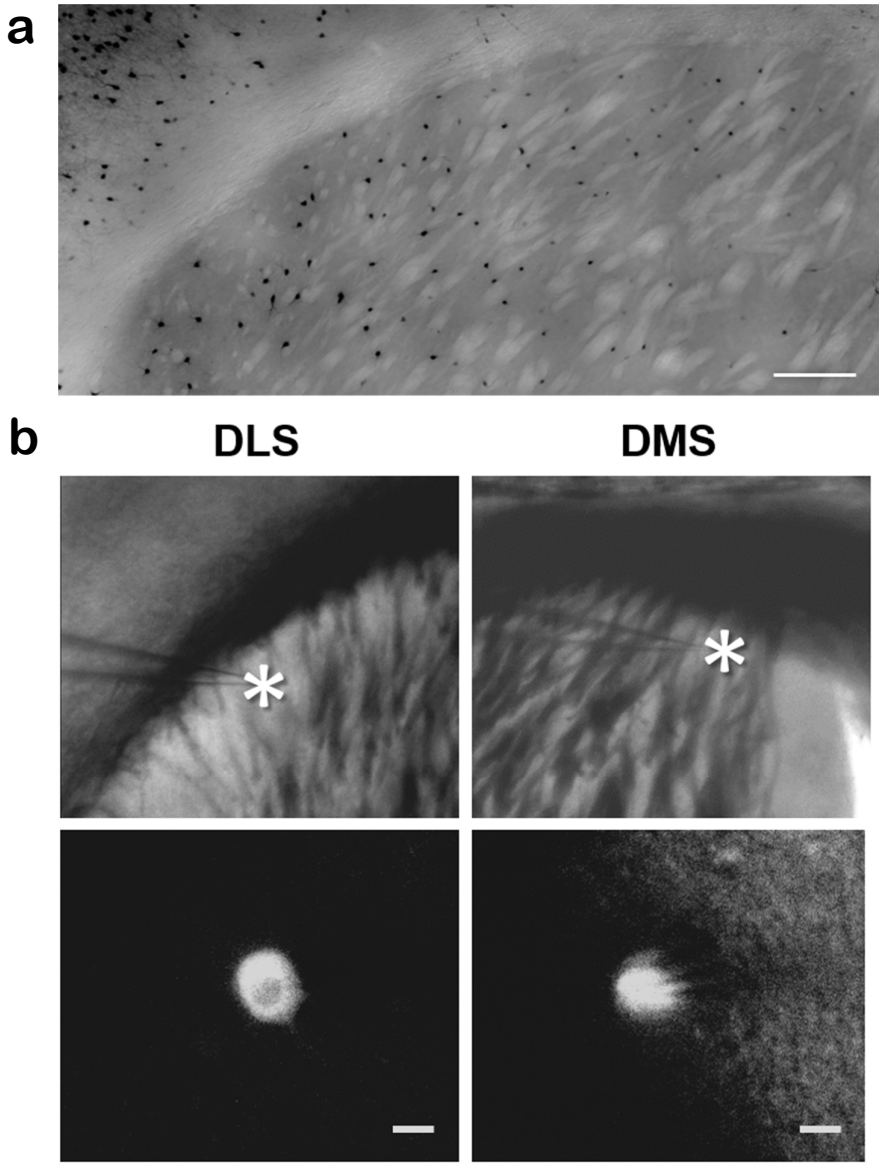

Figure 2.1 | Larger elaborate PV population in DLS and smaller simple PV population in DMS.

a, Parvalbumin immunostaining shows a larger elaborate PV population in dorsolateral striatum contrasting to a smaller-simple PV population in the dorsomedial region. **b**, Infrared differential interference contrast (IR-DIC) image of DLS and DMS regions targeted for electrophysiology recordings (top) and fluorescent images of recorded tdTomato-positive cells in DLS and DMS (bottom). Scale bar a= 200 µm, b= 10 µm.

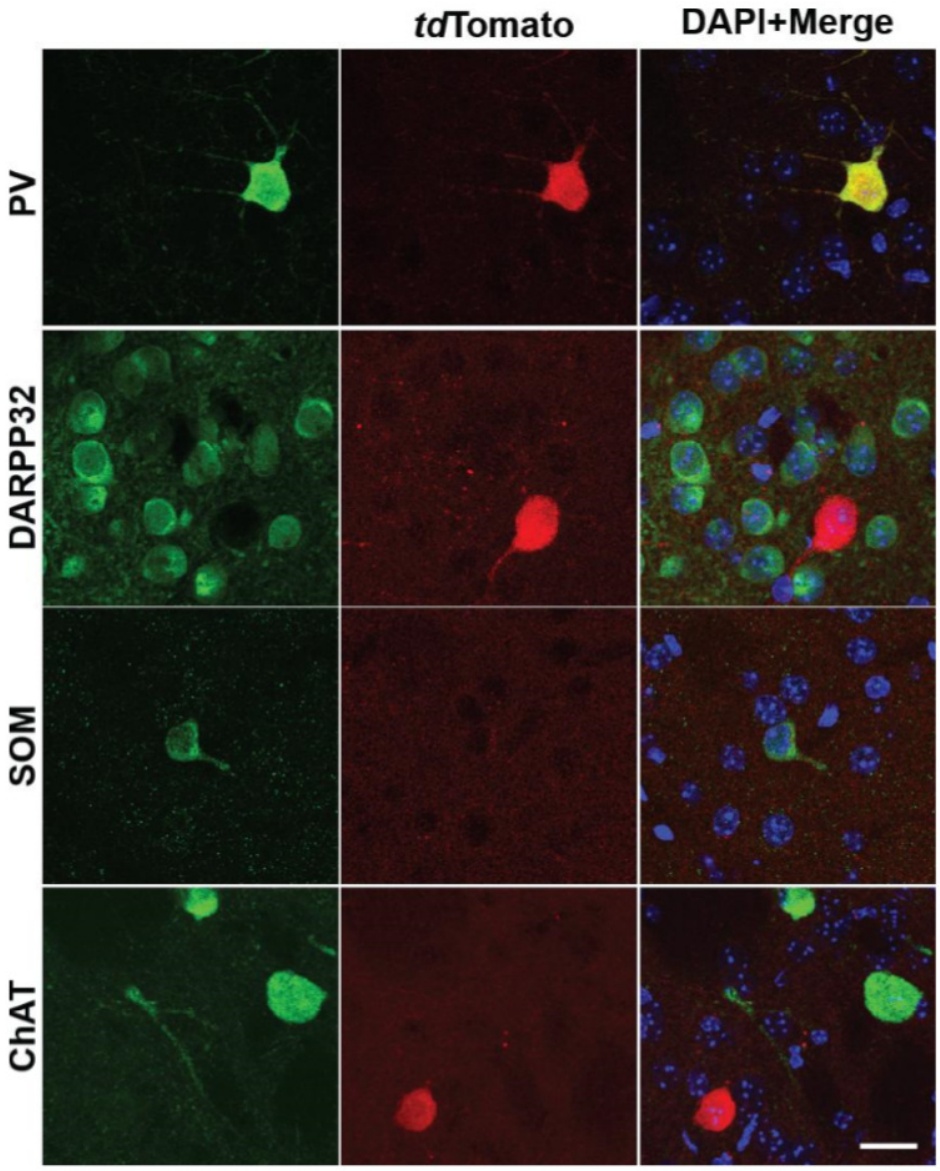

Figure 2.2 | Pvalb$^{tm1(cre)Arbr}$:ROSA26-*stop*^{flox}-*tdTomato* mice express tdTomato fluorescence in striatal parvalbumin interneurons.

Fluorescence images of histological sections show colocalization of native tdTomato expression with endogenous PV immunoreactivity, but not DARPP32, SOM or ChAT (scale bar= 20 µm).

2.3.2 Striatal PV interneurons have different intrinsic excitability in medial and lateral territories

We performed whole-cell intrasomatic current injection in striatal *tdTomato*-positive PV cells to study passive and active membrane properties. PVs located in DMS show higher intrinsic excitability, as represented by their left-shifted I-V curve (Fig.2.3A). Input resistance obtained through extrapolation from the I-V plot as well as direct measurement through a -150 pA hyperpolarizing current step, shows significantly higher value for DMS-PVs than DLS-PVs (Fig.2.3B) (DMS-PV median= 42 MΩ, n= 25; DLS-PV median= 28 MΩ, n= 25; ***p<0.001). In addition, significantly higher membrane resistance was observed for the DMS population (Fig.2.3B) (DMS-PV median= 104 MΩ, n= 25; DLS-PV median= 69 MΩ, n= 25; **p<0.01). Active membrane properties also show that DMS-PV interneurons are more excitable, displaying a left-shifted I-F curve (Fig.2.3C). Action potential triggering (rheobase) also requires less current injection compared to DLS-PV population (DMS-PV median= 450 pA, DLS-PV median= 550 pA, ***p<0.001) (Fig.2.3C right panel; Fig.2.4). This hyperexcitable profile could also reflect a smaller membrane surface area, as suggested by the staining data showing a smaller-simple PV population in DMS (Fig.2.1). We thus measured whole-cell capacitance and confirmed smaller values for the DMS-PV population (Fig.2.4). Notably resting membrane potential (DMS-PV= -86 mV, DLS-PV= -85 mV; NS) and spike threshold (DMS-PV median= -40 mV, DLS-PV median= -41 mV, NS) were not different between the two populations and hence do not seem to contribute for the observed excitability differences (Fig.2.4).

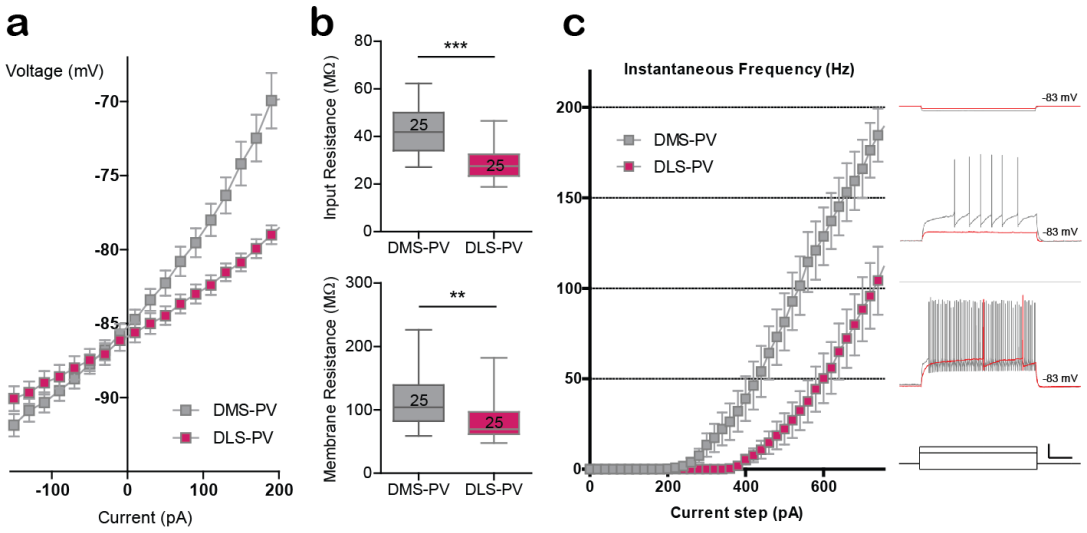

Figure 2.3 | PV interneurons in DMS and DLS regions have different intrinsic excitability.

Increased intrinsic excitability for DMS-PVs is shown by their left-shifted IV curve (**a**) and higher input and membrane resistance values (**b**). **c,** IF-plot and representative current injection steps for the two striatal PV populations demonstrate intrinsic hyperexcitability in dorsomedial PV population compared to dorsolateral PVs. **P<0.01; ***P<0.001; unpaired t-test (DMS n= 25 PV, DLS n= 25 PV cells).

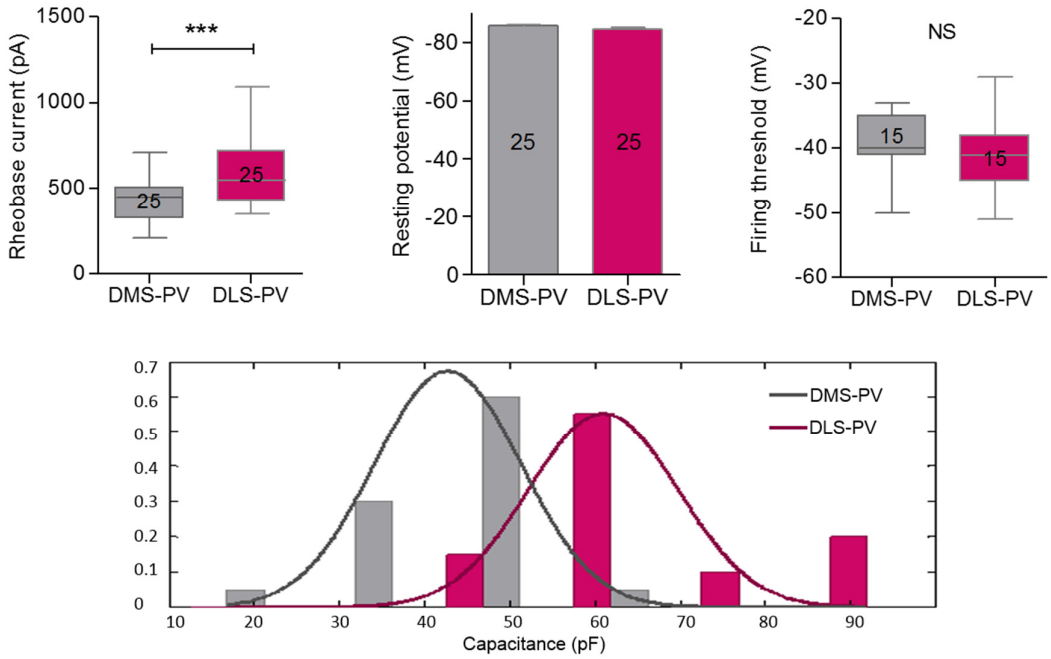

Figure 2.4 | Lower rheobase and smaller capacitance values indicate that DMS-PVs are intrinsically more excitablity than DLS-PVs.

Top panel, DMS-PVs display lower rheobase values (left panel; n= 25 cells). No differences were found in resting membrane potential (middle panel; n= 25 cells) or firing threshold (right panel; n= 15 cells) between the two PV populations (***p<0.001, unpaired t-test); Lower panel, Whole-cell capacitance histogram with Gaussian curve fit indicates smaller membrane surface area in dorsomedial PV cells (DMS-PV normal distribution mean= 43 pF; DLS-PV normal distribution mean= 61 pF; ***p<0.001, two-sample Kolmogrov-Smirnov test, n= 20 cells per group).

2.3.3 Parvalbumin interneurons receive higher mEPSC and lower mIPSC frequency in dorsomedial striatum

To address excitatory and inhibitory transmission in these lateral and medial interneurons, synaptic physiology recordings were obtained from the two populations in the same slices. Increased mEPSC frequency was observed for DMS-PV cells with no changes in amplitude (DLS-PV= 15.49 Hz ±1.3, peak= 13.08 ±0.8 pA; DMS-PV= 22.31 Hz ±1.8, peak= 15.25 pA ±0.8) (Fig.2.5). Decreased mIPSC frequency with higher amplitude was observed in DMS-PVs (DLS-PV= 8.2 Hz ±0.8, peak= 24.42 pA ±1.4; DMS-PV= 5.7 Hz ±0.5, peak= 29.66 pA ±2.0; n= 16 cells) (Fig.2.5). These results show that parvalbumin

interneurons display synaptic connectivity differences along lateral and medial striatum axis. This data together with the dichotomous electrophysiological membrane properties observed, suggests the existence of two discrete parvalbumin interneuron populations that can potentially be a substrate for differential targeting by upstream circuitry.

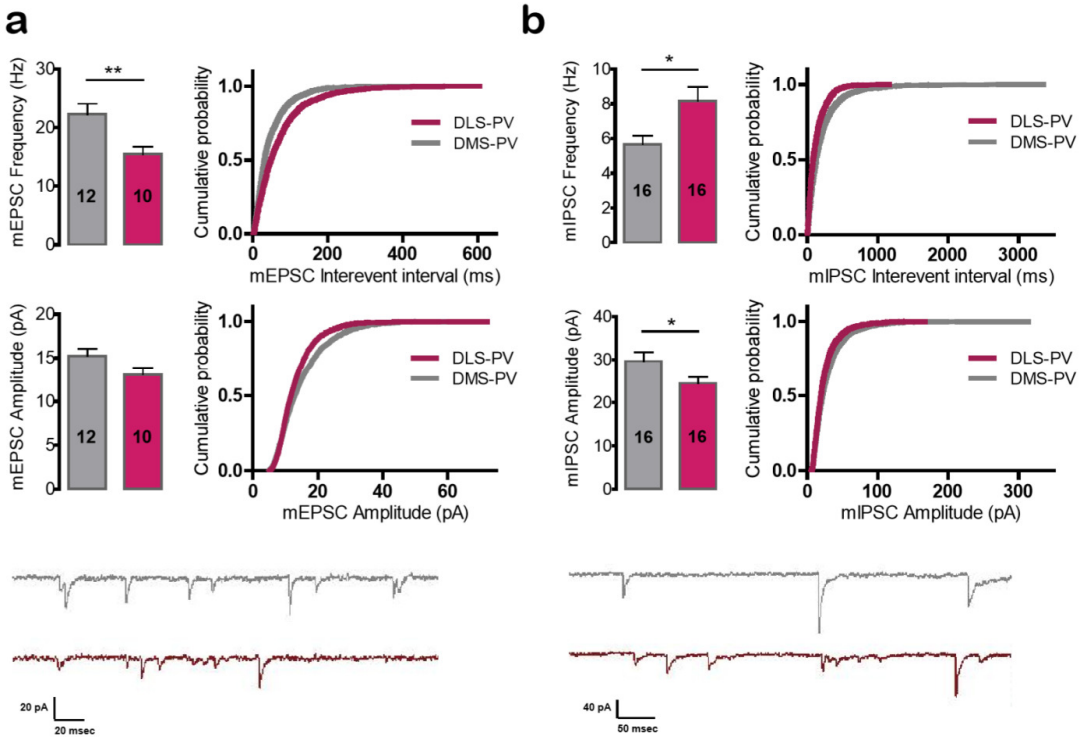

Figure 2.5 | Increased mEPSC frequency and decreased mIPSC frequency in DMS-PV interneurons.

a, Summary bar graphs (DMS n= 12 PV, DLS n= 10 PV cells) and cumulative probability curves (200 events *per* cell) show significantly increased mEPSC frequency in DMS-PV cells with no difference in amplitude. **b,** Summary bar graphs (n= 16 PV cells) and cumulative probability curves (140 events *per* cell) show that DMS-PV cells have reduced mIPSC frequency; amplitude however is increased. Example traces are shown at the bottom for both panels (top grey traces= DMS-PV; bottom red traces= DLS-PV). *P<0.05; **P<0.01; unpaired t-test; data presented as means ±s.e.m.

2.3.4 Mapping inputs to striatal parvalbumin cells using rabies-virus monosynaptic tracing reveals unique mPFC projections to DMS-PV interneurons

Corticostriatal connectivity criteria has been classically used to distinguish dorsal and ventral striatum areas (sensorimotor *versus* limbic-innervated territories). Within dorsal striatum, topographical cortical innervation has also been used to further define lateral and medial territories (sensorimotor *versus* higher associational cortex-innervated territories)[13]. However, at the cellular level, it is not known whether striatal interneurons obey to a corticostriatal topographical organization. To address this question we used modified rabies-virus to perform *in vivo cre*-dependent monosynaptic retrograde tracing of the inputs that innervate striatal PV cells. A conditional helper virus (AAV-synP-DIO-sTpEpB) was injected into lateral or medial striatum territories in PV-*cre* mice (Pvalbtm1(cre)Arbr) and followed by injection of modified rabies virus 2weeks later (EnvA-ΔG-RFP-rabies). Post-hoc analysis of brain sections revealed that parvalbumin interneurons in dorsomedial striatum receive afferent innervation from mPFC region (Fig.2.6). This connectivity pattern was not observed for parvalbumin interneurons located in dorsolateral striatum region (Fig.2.6). Both populations seem to integrate inputs from thalamus and GP regions (data not shown).

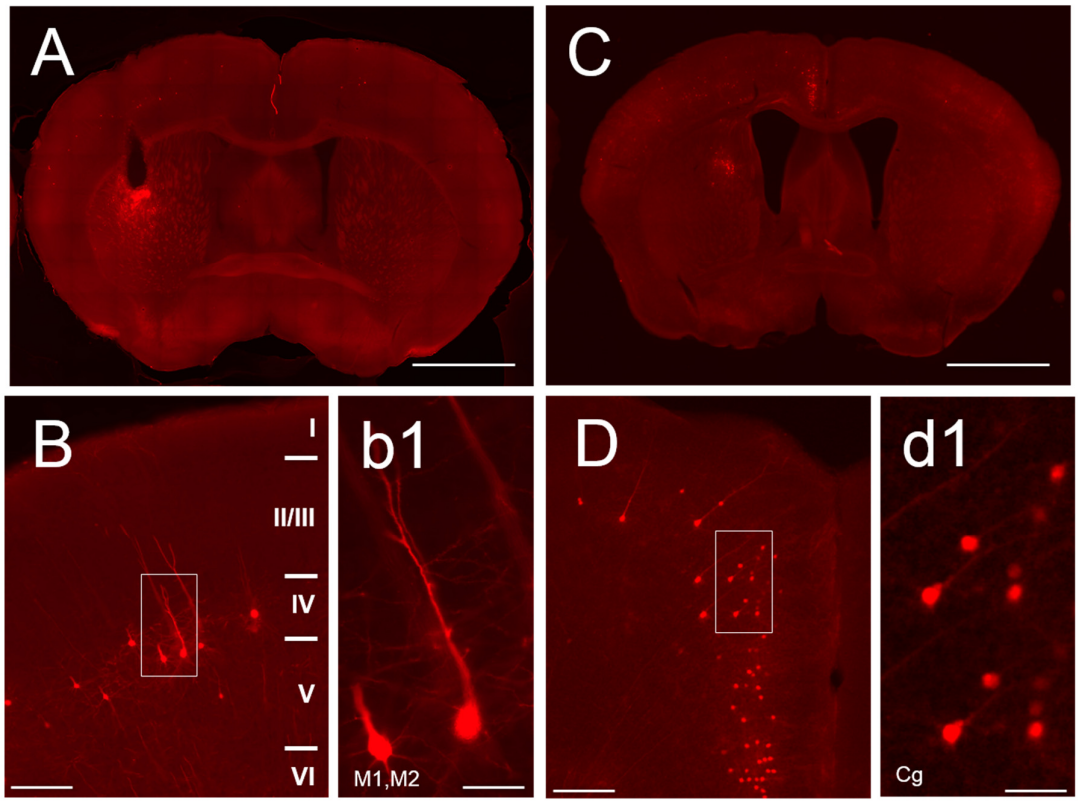

Figure 2.6 | Cre-dependent monosynaptic retrograde tracing from striatum parvalbumin interneurons.

Panels showing rabies-labeled neuronal subtypes in various brain regions due to retrograde monosynaptic spreading from PV–cre striatum infected cells. **a,b**, DLS-PV cells receive inputs from sensorimotor cortex but not mPFC. **c,d**, DMS-PV cells receive dense inputs from mPFC region. A,C= scale 2 mm; B,D= scale 200 µm; b1,d1= scale 50 µm.

2.3.5 Conditional expression of TeLC in striatal parvalbumin-interneurons efficiently reduces inhibitory transmission onto MSNs

To directly test whether parvalbumin interneurons in DMS region can play a role in striatum-mediated behaviors, we ought to locally silence DMS-PV interneurons *in vivo*. Previous pharmacological manipulation of parvalbumin interneurons in the opposite region (DLS), showed that lack of DLS-PV inhibiton can cause dyskinesias[171]. To silence DMS-PV interneurons without affecting their action-potential firing, we used tetanus toxin light chain (TeLC) that is known to cleave VAMP2 and block neurotransmitter release at the synaptic terminal[172–174]. To achieve cell-type silencing using this strategy, we generated a viral vector containing the TeLC inverted sequence in a flip-excision (FLEX) cassette[175]. Injection of FLEX-TeLC into PV-*cre* mice (Pvalbtm1(cre)Arbr) allows for restricted expression of TeLC in parvalbumin interneurons and further prevents reorientation of the remaining Lox sites. This strategy can hence conditionally suppress synaptic release from infected parvalbumin interneurons. To test this, PV-*cre* mice were bilaterally injected with AAV-FLEX-eYFP (control condition) or AAV-FLEX-TeLC-eYFP (test condition) into DMS region (Fig.2.7). We then performed patch-clamp in striatal brain slices to record sIPSCs from neighboring MSNs. Significant reduction of sIPSC frequency was observed in TeLC condition compared to eYFP control (eYFP= 3.0Hz ±0.5, peak= 36 pA, n= 6 cells; TeLC= 0.8 Hz ±0.15, peak= 35 pA; n= 8 cells), confirming a successful reduction of inhibitory synaptic transmission (Fig.2.7).

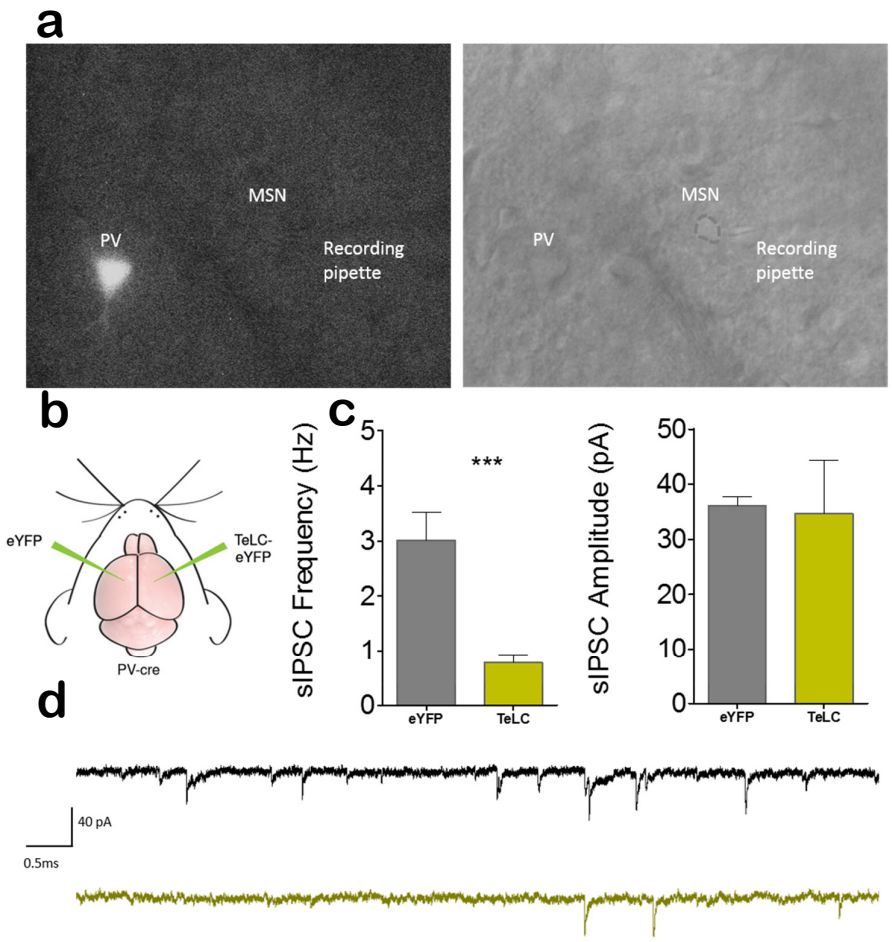

Figure 2.7 | Conditional expression of TeLC in striatal parvalbumin-interneurons efficiently reduces synaptic inhibitory transmission onto MSNs.

a, Targeted sIPSC recording from a medium spiny neuron (MSN) located in the vicinity of an eYFP labeled PV interneuron. **b,** Cartoon illustrating the strategy used for testing the efficiency of tetanus toxin; For this experiment, PV-cre mice were injected in one hemisphere with *cre*-dependent-AAV-eYFP and *cre*-dependent-AAV-TeLC-eYFP on the other hemisphere. sIPSCs where later recorded from the same animal for the two viral conditions. **c**, Reduced sIPSC frequency in TeLC-eYFP condition compared to eYFP condition, with no significant changes in amplitude. **d,** Inset of sIPSC traces recorded from eYFP (top black trace) and TeLC-eYFP (bottom green trace) conditions. ***P<0.001, unpaired t-test (n= 6MSNS for eYFP, n= 8MSNs for TeLC); data presented as means ±s.e.m.

2.3.6 Parvalbumin-inhibitory activity in DMS is required for habit learning, but not goal-directed learning

To test whether local silencing PV-DMS interneurons influences striatum-dependent behavior, we probed mice in a self-operant conditioning paradigm that requires striatum function[10,14,20,115,176]. Two-weeks after bilateral injections (eYFP *versus* TeLC), mice were trained under two different training schedules (random interval [RI] and random ratio [RR]) that respectively promote habitual *versus* goal-directed responses[10,176]. Briefly, mice were food restricted and trained to lever-press for obtaining food pellets. Two different schedules of reinforcement were used: a progressive random-ratio schedule that consisted in 3 days of continuous reinforcement (CRF; 1lever press= 1pellet; fixed ratio 1), 2 days of random ratio 10 (RR10) and 4 days of random ratio 20 (RR20); or a progressive random-interval schedule that consisted in 3 days of continuous reinforcement (CRF; 1lever press= 1pellet; fixed ratio 1), 2 days of random interval 30s (RI30) and 4 days of random interval 60s (RI60). After that period, a selective satiety devaluation test (pre-feeding) was performed to address their lever pressing behavior between valued and devaluated conditions (mice were pre-fed with either regular home cage mouse chow or the pellets earned during lever-pressing). RR training schedule was used to promote goal-directed performance that should result in reduced lever pressing on the devalued condition. Both mice groups (eYFP and TeLC) trained under RR reinforcement schedule showed increasing lever-pressing rates across training days ($F_{8,144}$= 110.24, p<0.0001) (Fig.2.8A) and both readily reduced their lever pressing upon devaluation test (eYFP p= 0.0003; TeLC p= 0.008) (Fig.2.8C). There was no effect of group on lever pressing ($F_{1,144}$= 0.97, p= 0.38) or interaction between training and group ($F_{8,144}$= 1.65, p= 0.08) (Fig.2.8A). The rate of reinforcements *per* minute changed throughout training ($F_{8,144}$= 4.26, p= 0.0001) with no significant difference between groups ($F_{1,144}$= 0.39, p= 0.54), or interaction between training and groups ($F_{8,144}$= 1.28, p= 0.26) (Fig.2.8B). This indicates that a reduction in dorsomedial PV-mediated inhibition does not seem to affect goal-directed responses. Both mice groups (eYFP and TeLC) showed no obvious signs of neurological deficits and behaved similarly in open-field and elevated zero maze tests, suggesting that locomotion and anxiety levels were unaffected (Fig.2.9). However when RI training schedule was used to promote habitual responses, TeLC mice failed to develop lever-pressing habit upon devaluation test (eYFP p= 0.07; TeLC p= 0.0054) (Fig.2.8F). Once again both mice groups (eYFP control

and TeLC) showed increasing lever-pressing rates across training days ($F_{8,456}$= 150.31, p<0.0001) with no effect of group on lever pressing ($F_{1,456}$= 0.78, p= 0.38) or interaction between training and group ($F_{8,456}$= 0.69, p= 0.7) (Fig.2.8D). The rate of reinforcements *per* minute changed throughout training ($F_{8,456}$= 22.19, p<0.0001) with no significant difference between groups ($F_{1,456}$= 0.42, p= 0.52), or interaction between training and groups ($F_{8,456}$= 0.35, p= 0.95) (Fig.2.8E). This result suggests that inhibitory activity from parvalbumin interneurons in dorsomedial striatum is required for normal habit formation in mice.

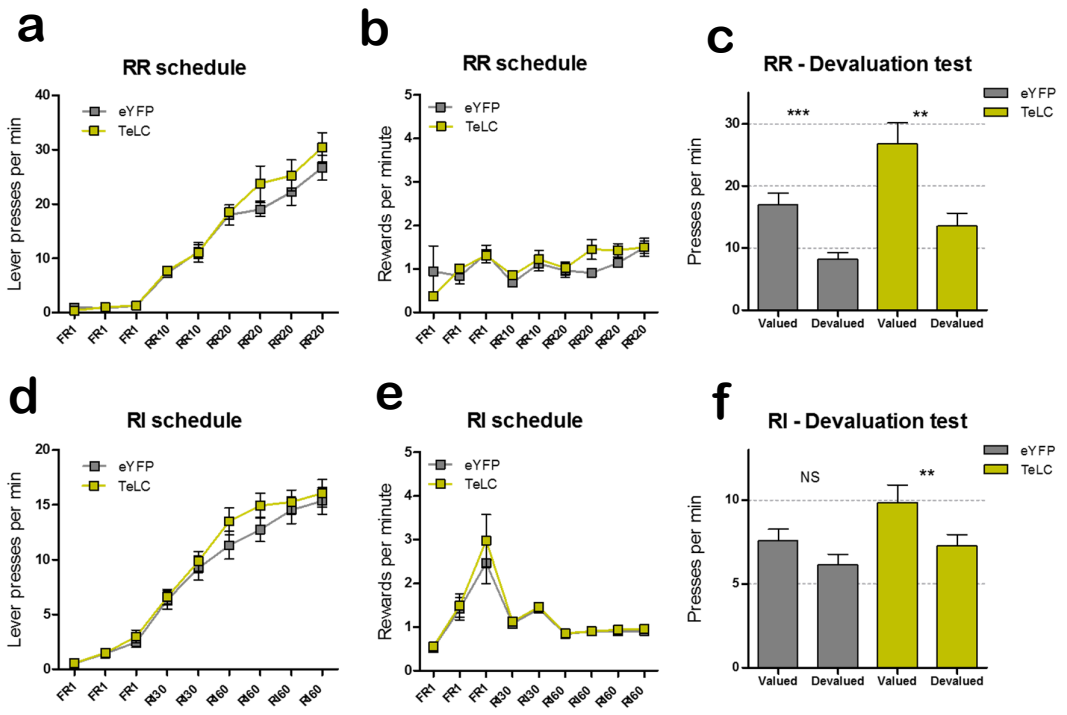

Figure 2.8 | Parvalbumin-inhibitory activity in DMS is required for habit learning but not goal-directed response.

a, Average lever-presses per minute across training days (RR schedule). **b,** Average rate of reinforcements throughout RR schedule training. **c,** Lever pressing in valued and devalued states shows goal-directed response in both mice groups. **d,** Average lever-presses per minute across training days (RI schedule). **e,** Average rate of reinforcements throughout RI schedule training. **f,** Lever pressing in valued and devalued states shows habitual response in control mice and goal-directedness in TeLC mice. Repeated-measures 2-way ANOVA in a, b, d, e with Bonferroni post-hoc test; Paired t-tests for c and f. Error bars indicate s.e.m. **P<0.01, ***P<0.001.

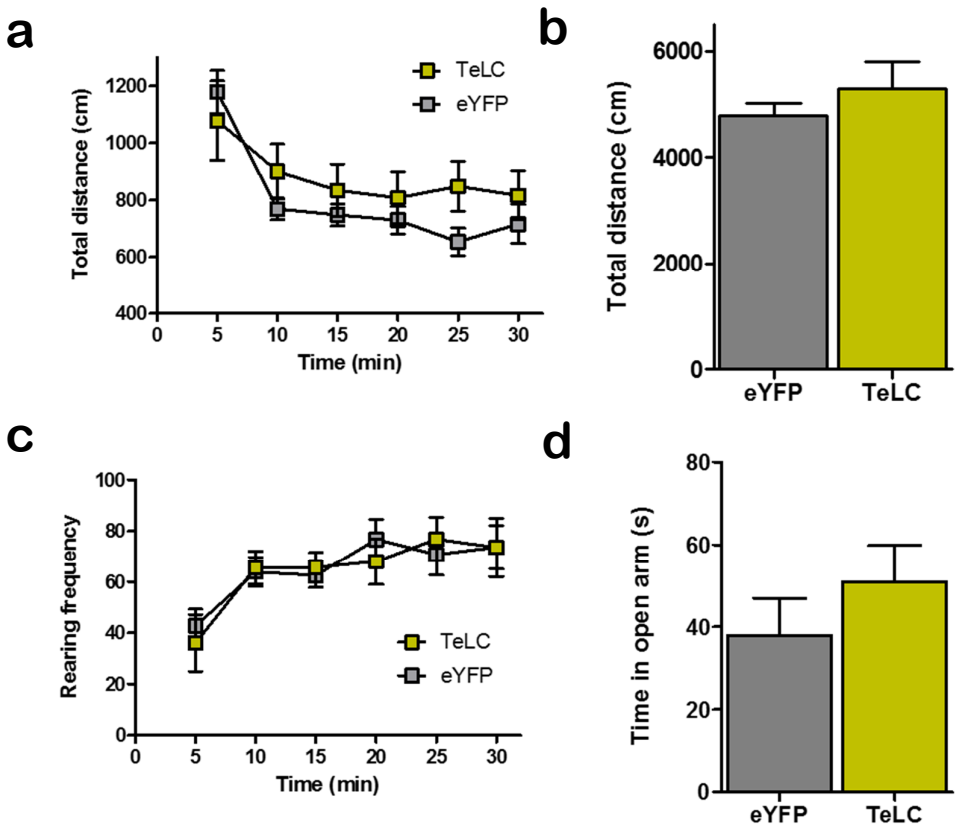

Figure 2.9 | Silencing DMS-PVs does not induce changes in anxiety or locomotion. **a**,**b**, Open field results show no difference in total distance between TeLC and eYFP groups. **c**, Rearing frequency in the open field shows no difference between TeLC and eYFP groups. **d**, Both mice groups spend similar time exploring the open arm, indicating again comparable levels of anxiety. Two-way repeated measures ANOVA with Bonferroni post hoc test for a and c; Two-tailed unpaired t-test for b and d; All data presented as means ± s.e.m. (n= 10 eYFP and n= 10 TeLC mice).

2.4 Discussion

Here we characterize for the first time the physiology of striatal parvalbumin interneurons in DLS versus DMS territories and provide evidence for dichotomous populations between these regions. Whole-cell recordings revealed that parvalbumin interneurons in dorsomedial striatum are intrinsically more excitable. Given the important role of DMS during initial learning[14,177], one could imagine that having a more responsive PV population in this region would confer greater advantage. In a scenario where an unexpected outcome occurs and behavioral flexibility is required (such as during early training), having a more responsive PV population could quickly inhibit local MSNs and stop an ongoing behavior program, promoting behavioral flexibility. On the other hand, once a task has been extensively repeated and a specific behavioral strategy has proven to be effective, it should be preserved and not easily changeable (habitual behavior; DLS mediated). In this case, stronger inputs (and repeated inputs perhaps) would be needed to activate the less excitable DLS-PV inhibitory cells and stop an ongoing habitual response (less sensitive to outcome changes). Second, the finding that mPFC inputs target parvalbumin cells in DMS region (but not DLS) comes to suggest that these discrete PV populations in lateral and medial territories are part of different corticostriatal networks and may contribute to the parallel/competing roles of DLS and DMS in controlling behavior. The results obtained from our behavioral testing indeed suggest that PVs in DMS are required for habit formation but not goal-directed responses. Given previous findings that DMS activation is seen early during training (and required for goal directedness), one could imagine that inhibition provided by PVs at that stage of training, might not be too relevant. However with extended training, DMS activity tends to decrease and habits start to emerge. It is then tempting to speculate that PV cells might be providing an important inhibitory contribution by helping to wan DMS activity at that point. By artificially silencing DMS-PVs in this study, we speculate that DMS activity period is being abnormally extended during training and impairing the formation of habits. This finding can bring tremendous implications for human studies where exaggerated habitual routines are hard to extinguish (maybe due to lowered MSN activity in DMS [“caudate”]; or abnormally high DLS [“putamen”] MSN activity). Interestingly OCD symptomatology has been reported after lesion in the left caudate nucleus[178]; although caudate hypermetabolism has also been reported in OCD[179]. One exciting possibility is the

differential involvement of cell populations that lead to opposite striatal output (striatal excitation or inhibiton). Clarifying the neural correlates responsible for the mechanisms of habit formation can allow us to create a better model of striatal function and help to manipulate behavioral phenotypes.

2.5 Methods

Experimental animals: PV-cre mice and ROSA26-*stop*^{flox}-*tdTomato* cKI mice have been previously described[180,181]. Specific primers were designed in this study to distinguish PV-cre heterozygous from homozygous mice:

Primer 5'-GCTCAGAGCCTCCATTCCCT-3'

Primer 5'-GCTCAGAGCCTCCATTCCCT-3'

Primer 5'-CAGCCTCTGTTCCACATACACTTC-3'

ROSA26-stopflox-tdTomato+/+ mice were crossed with PV-cre mice to generate PV-cre+/-:ROSA26-stopflox-tdTomato+/+ mice for electrophysiology recordings. PV-cre mice were also crossed with C57BL6 mice to generate PV-cre+/- mice for injections and behavioral testing. Animals were housed on controlled environment (12h light/dark cycles, 24h temperature and humidity monitoring), 2-5 mice per cage and *ad libitum* water. *Ad libitum* food was generally provided, except during operant conditioning training. Post-surgery mice were individually housed after surgery. All animals were blinded before behavioral testing. All experimental procedures were reviewed and approved by the MIT Committee on Animal Care (CAC).

Slice preparation: Acute striatal slices were prepared from 5-6-week-old PV-cre+/-:ROSA26-*stop*^{flox}-*tdTomato*+/+. Animals were anesthetized by avertin intraperitoneal injection (tribromoethanol, 20 mg/ml, 0.5 mg/g body weight) and transcardially perfused with cutting NMDG-based aCSF (mM): 92 N-methyl-D-glucamine (NMDG), 2.5 KCl, 1.20 NaH_2PO_4, 30 $NaHCO_3$, 20 HEPES, 25 glucose, 2 thiourea, 5 Na-ascorbate, 3 Na-pyruvate, 0.5 $CaCl_2.2H_2O$, 10 $MgSO_4.7H_2O$ (~300 mOsm, 7.2-7.4 pH). Following decapitation, brain was removed and coronal brain slices (300 µm) prepared using a Vibratome 1000 Plus (Leica Microsystems, USA). Slices were recovered in cutting solution at 32–34℃ for 10-15 minutes and transferred to room-temperature carbogenated regular aCSF(mM): 119 NaCl, 2.5 KCl, 1.2 NaH_2PO_4, 24 $NaHCO_3$, 12.5 glucose, 2 $MgSO_4.7H_2O$, 2 $CaCl_2.2H_2O$ (~300 mOsm, 7.2-7.4 pH). All slices were allowed to recover at least ≥1h prior to whole-cell recordings.

Electrophysiology recordings: Slices were transferred to the recording chamber (RC-27L, Warner Instruments) and constantly perfused with carbogenated regular aCSF at 30±2℃, ~2 ml/minute rate. Borosilicate glass

microelectrodes (King Precision Glass) were pulled on a P-97 horizontal puller (Sutter Instruments) and backfilled either with KGlu, CsCl or CsGlu internal (KGlu mM: 145 K-Gluconate, 10 HEPES, 1 EGTA, 2 MgATP, 0.3 NaGTP and 2 $MgCl_2$; pH adjusted to 7.3 with KOH and osmolarity adjusted to ~300 mOsm with sucrose. CsGlu mM: 110 CsOH, 110 D-Gluconic acid, 15 KCl, 4 NaCl, 5 TEA-Cl, 20 HEPES, 0.2 EGTA, 5 Lidocaine N-ethyl chloride, 4 MgATP, 0.3 NaGTP; pH adjusted to 7.3 with KOH and osmolarity adjusted to ~300 mOsm with K_2SO_4. CsCl mM: 103 CsCl, 12 CsOH, 12 Methanesulfonic acid, 5 TEA-Cl, 10 HEPES, 0.5 EGTA, 5 Lidocaine N-ethyl chloride, 4 MgATP, 0.3 NaGTP, 10 Phosphocreatine, 4 NaCl; pH adjusted to 7.3 with KOH and osmolarity adjusted to ~300 mOsm with K_2SO_4), presenting a typical resistance around 2-4 MΩ. Slices were visualized under IR-DIC (infrared-differential interference contrast) using a BX-51WI microscope (Olympus) and recordings were obtained after seal rupture and internal equilibrium from visually identified tdTomato-positive cells. Picrotoxin 100 uM and TTX 1 uM were added for mEPSC experiments and AP-V 50 uM, NBQX 10 uM and TTX 1 uM were added for mIPSC experiments (all drugs from Tocris). Data was acquired using a MultiClamp 700B amplifier and a Digidata 1440A. Signals were filtered at 1-2 KHz and digitized at 10 KHz. For current-clamp recordings, bridge balance was adjusted and pipette capacitance neutralized. Series resistance compensation (<20 MΩ) was performed in voltage-clamping mode. Theoretical liquid junction potential was estimated to be around –11 mV and not corrected-for.

Antibodies: Mouse anti-parvalbumin antibody (PV235, 1:5000 dilution) from Swant; mouse anti-DARPP32 (611520, 1:1000) from BD Biosciences; rabbit anti-Somatostatin (AB5494, 1:200) from Milllipore; and goat anti-ChAT antibody (AB144P, 1:500 dilution) from Millipore.

IHC and confocal imaging: Mice were anesthetized by isofluorone inhalation and transcardially perfused with PBS solution followed by 4 % PFA (paraformadehyde) fixative solution. Brains were kept in 4 % PFA overnight at 4 ℃, then transferred to PBS and sectioned at 50 microns. Sections were washed 3x in PBS and permeabilized for 5 minutes using a PBS solution containing 10 % MeOH, 3 % H_2O_2, and 0.5 % $NaBH_2$, except for ChAT immunostaining. Slices were again washed 3x PBS and incubated in 1.2 % Triton-X 100 for 15 minutes, followed by another 3x PBS wash. Blocking was then performed for 1h in PBS containing 2 % BSA and 0.2 % Triton-X. Primary antibodies were incubated

overnight at 4°C for detection of the respective antigens. Next day sections were washed 3x PBS, followed by 2-4 h incubation with secondary antibody (species-specific Alexa488-conjugated antibody, 1:1500, Invitrogen) at room temperature. Lastly, sections were washed 3x PBS, stained for DAPI, mounted in ProlongGold (Invitrogen) and imaged using a confocal microscope.

Statistical Analyses: All statistical analyses were performed using Prism (GraphPad Software) and MATLAB Software (MathWorks). Mean and median results are graphically displayed with respective SEMs and whisker bars showing general distribution. Data sets were analyzed for significance using either student's t-test or two-way repeated ANOVA measures with post-hoc Bonferroni test, using $p<0.05$ as significance threshold. Further details on particular statistical analyses can be found on the respective results section.

Surgeries and viruses: 6-8 weeks old mice were anesthetized with isoflurane, placed on a stereotactic frame and viral injections performed using a Nanoject device. For TeLC/eYFP experiments we bilaterally injected mice in 2 coordinates per hemisphere: ML+-1.4, AP+1.18, 2.5 and ML+-2.0, AP+0.5, 2.4 from bregma (~0.1 µl virus *per* site). Mice were used for behavioral experiments 2 weeks after recovery. pGEMTEZ-TeTxLC plasmid was a gift from Ron Yu and was PCR-amplified and inserted into AAV-hSyn-FLEX. AAV-hSyn-FLEX-P2A-eYFP-WPRE-PolyA and AAV-hSyn-FLEX-TeLC-P2A-eYFP-WPRE-PolyA plasmids were then packaged in AAV2/8 (~2e+13 vg/ml) by Virovek (California).

For monosynaptic tracing experiments we injected ~0.1 µl AAV-synP-DIO-sTpEpB at DLS or DMS (bregma coordinates: DLS ML+2.75, AP+0.5, 2.0; DMS ML+2.0, AP+0.5, 2.3). 2-3 weeks later we injected 0.1 µl RVΔG-RFP(EnvA) at the same bregma location. Mice were sacrificed 7days later to observe expression pattern. AAV-synP-DIO-sTpEpB and RVΔG-RFP(EnvA) where generated by MIT Genetic Neuroengineering Group (Massachusetts Institute of Technology)[182].

Open Field: Automated Omnitech Digiscan apparatus (AccuScan Instruments) was used to assess spontaneous locomotion by total distance traveled in the open field apparatus. Anxiety was assessed by rearing activity. The first 30 minutes were evaluated for all parameters. Two-way ANOVA with Bonferroni post-test was used to test statistical significance.

Zero Maze: Animals were habituated for at least one hour before testing. An elevated zero maze apparatus was indirectly illuminated at 60 lux and the animal was introduced into the closed arm and allowed to freely explore the maze for 5 minutes. A blinded observer performed data analysis using automated tracking software Noldus Ethovision. Anxiety-like behavior was assessed by the time spent in the open arm during the 5-min interval.

Operant chambers: Eight Med Associates operant chambers (21.6 cm long x 17.8 cm wide and 12.7 cm high) with sound-attenuating walls, two retractable levers, one food magazine and a 3 W 24 V house light on the opposite wall, were used for operant conditioning. Operant chambers and levers used (left or right lever) were counterbalanced across groups. Bio-Serv 14 mg pellets were used as reward during operant conditioning. Med Associates behavioral software (Med-PC) was used and behavioral programs for conditioned reinforcement (CRF), extinction test, random interval schedules (RI30 and RI60) and random ratio schedules (RR10 and RR20) were gently provided by Dr. Henry Yin (Duke University, USA) and Dr. Rui Costa (Champalimaud Center for the Unknown, Portugal). Each training session begins by lever insertion and house light illumination. At the completion of each session, house light is turned off and the lever retracted.

Operant training: 3 days prior to training, animals were gradually food-restricted (~2 g mouse chow *per* day) and maintained at approximately 85 % of their *ad libitum* body weight throughout the entire experiment. Mice were initially trained on a continuous reinforcement schedule during 3 consecutive days (CRF; 1lever press= 1pellet; fixed ratio 1). The session would end after 60 minutes or if 50 reward pellets were earned. After CRF training completion, different mice started training under RR or RI reinforcement schedule. To generate goal-directed behavior, mice were trained using a random ratio schedule (RR)[176,183]. Training started with 2 consecutive days of random ratio 10 (RR10), followed by 4 consecutive days of random ratio 20 (RR20). To generate habitual behavior, mice were trained using a random interval schedule[176,183,184]. Training started with 2 consecutive days of random interval 30 s (RI30) and 4 consecutive days of random interval 60 s (RI60). Two-way ANOVA repeated measures was used to evaluate differences between groups.

Devaluation test: After the training period (3 days CRF + 2 days RR10/RI30 + 4 days RR20/RI60), a selective satiety devaluation test was performed on the next 2 days. On each day, mice were given 1H *ad libitum* access to either mouse chow (home cage food; valued condition; minimum food consumption= 0.4 g) or the pellets earned during lever-pressing (devalued condition; minimum food consumption= 0.4 g). Immediately after the feeding session, mice were tested for training lever presses during 5 minutes (with no pellets earned). Valued and devalued conditions were counterbalanced across groups, being tested either on devaluation day 1 or day 2. If there is a behavioral adaptation after obtaining an unexpected outcome, this reflects a goal-directedness response and lever presses should decrease in devalued condition (influenced by consequences). On the other hand, a behavior pattern that persists after a defrauded outcome is considered habitual and lever presses number should not decrease in devalued condition (controlled by antecedent stimuli). Group comparisons were performed using paired t-test between valued and devalued conditions.

Chapter 3

Adult Restoration of *Shank3* Expression Rescues Selective Autistic-like Phenotypes

3.1 Summary

Autism and autism spectrum disorders (ASD) are clinically defined by the symptoms of social impairment and repetitive behavior/restricted interests, affecting 1 in 68 children in the United States[185]. Because patients with ASD typically display symptoms before the age of three, the ASDs are classically categorized as developmental disorders[186]. One of the key questions in autism research is whether the pathology is reversible in adults. Previous work on mouse models with ASD-linked genes including Mecp2 and Syngap1 have provided opposing results upon adult gene rescue[187,188]. This suggests that different genes involved in ASD have distinct developmental properties. Here we investigate the developmental requirement of *Shank3*, one of the most prominent ASD genes that is estimated to contribute to ~1 % of all ASD cases[154–156,189,190]. SHANK3 is a master postsynaptic scaffold protein that regulates synaptic development, function and plasticity by orchestrating the assembly of postsynaptic density (PSD) macromolecular signaling complex[157,191–193]. Disruptions of the *Shank3* gene in mouse models have resulted in synaptic dysfunction and autistic-like phenotypes including anxiety, social interaction deficits, and repetitive/stereotyped behavior[59,129,130,132]. Here we have generated a novel *Shank3* conditional knock-in mouse model and used it to demonstrate that re-expression of the *Shank3* gene in adult leads to improvements in selective ASD-related phenotypes. We provide synaptic, circuit, and behavioral evidence that certain phenotypes including social interaction deficit and repetitive grooming behavior can be significantly rescued in adulthood while anxiety and motor coordination deficit cannot be recovered. These results suggest that plasticity for certain neural circuits persist into adulthood in the diseased brain, and that the underlying mechanisms for different autistic-like phenotypes have distinct properties.

3.2 Background

The SHANK3 protein contains five protein-protein interaction domains including N-terminal ankyrin repeats, SH3 domain, PDZ domain, proline-rich region, and a C-terminal SAM domain. Through the PDZ domain, it binds to SAPAP to form the PSD-95-SAPAP-SHANK complex. This assembly of proteins acts as a scaffold at the excitatory synapse, coordinating the recruitment and

interactions of many postsynaptic signaling molecules[143,194]. Previous work shows that *Shank3* germline deletion disrupts the protein composition at the postsynaptic density (PSD), reduces neurotransmission efficiency and leads to autistic-like behavior[59,129,130,132].

To address whether adult reversal of this ASD-like phenotype is possible, we adopted a genetic method that allows for inducible *Shank3* expression by Cre recombinase. Because *Shank3* duplication is linked to ADHD and bipolar disorder, and *Shank3* overexpression in mice leads to manic-like phenotypes and abnormal synaptic function[156,157,195], it is critical to maintain tight regulation of *Shank3* expression within its physiological concentrations to avoid potential confounds. Other targeting methods including inducible transgene expression and viral delivery do not provide such precise control[196,197]. Thus, we generated a novel *Shank3* conditional knock-in mouse by using the Cre-dependent genetic switch (FLEx) strategy[175], which enables the conditional manipulation of the *Shank3* gene at its endogenous genetic locus. To our knowledge this is the first engineered conditional mouse model of autism using FLEx strategy in vivo.

3.3 Results

3.3.1 *Shank3*$^{fx/fx}$ mice have disrupted SHANK3 expression, corticostriatal and behavior deficits

We genetically targeted the PDZ domain, which includes exons 13 to 16, due to its presence in all major isoforms of SHANK3 and its role in assembling the multiprotein scaffold complex in the PSD. In addition, our previously reported *Shank3*B knockout mice, which show significant synaptic dysfunction and autistic-like behaviors, were also generated by disrupting the PDZ domain[59]. We inverted and flanked exons 13-16 with two staggered pairs of inward-facing non-matching Lox sites (Fig. 3.1A). The introduction of Cre recombinase will catalyze the re-orientation of the inverted and double floxed exons 13-16, allowing correct gene transcription. Further inversion of the re-oriented exons will be prevented by the incompatibility of the remaining Lox sites, which are LoxP and Lox2722 (Fig. 3.1A, Fig. 3.2). In the absence of Cre, the *Shank3*fx/fx mice function as SHANK3 knockout (KO), and result in the deletion of most major isoforms of SHANK3 including the putative alpha, beta, and gamma bands (Fig. 3.1B). Similar to behavioral abnormalities previously reported on SHANK3 knockout mice[59,129,130,132], these *Shank3*fx/fx mice show significant deficits in exploratory

behavior (Fig. 3.1C), anxiety (Fig. 3.1E), motor deficits (Fig. 3.1D), and display open wound lesions which suggest repetitive/stereotyped grooming behavior[59,198]. In addition, they show impaired cortico-striatal transmission in the dorsal striatum (Fig. 3.1F-G), consistent with our previous findings in *Shank3*B knockout mice. These physiological and behavioral deficits indicated that our novel *Shank3*fx/fx mice recapitulate autistic-like phenotypes, enabling us to investigate the possibility of reversing these phenotypes in adulthood.

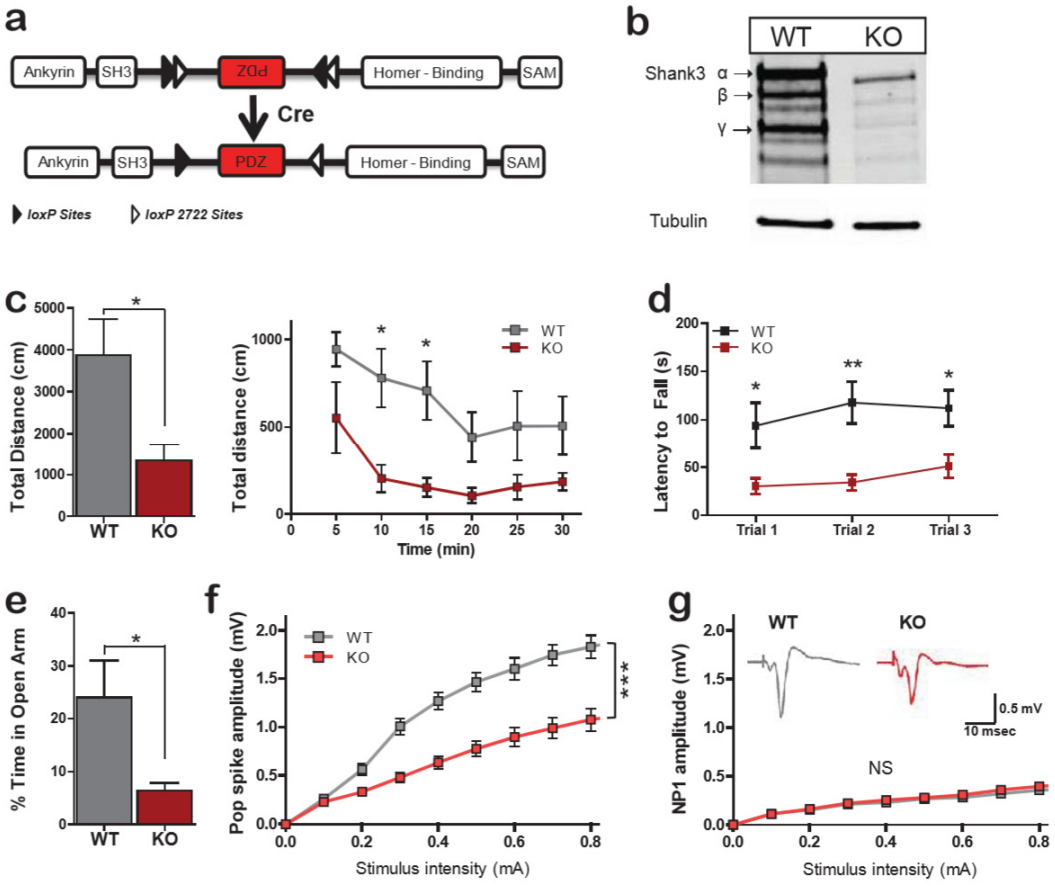

Figure 3.1 | *Shank3*fx/fx mice have disrupted SHANK3 expression, corticostriatal and behavior deficits.

a, Schematic domain structure of SHANK3 protein, with FLExed PDZ domain inverted; flanked domain can be re-oriented in presence of Cre recombinase. **b**, Western blot showing SHANK3 expression in PSD preparation from striatum (3 µg total protein per lane), for wildtype (WT) and *Shank3*fx/fx (KO) mice. **c**, *Shank3*fx/fx mice show decreased total distance traveled in the open field test compared to WT. **d**, KO mice show impaired motor coordination in rotarod test. **e**, *Shank3*fx/fx mice spend less time at the open arm in elevated zero maze test. **f**, *Shank3*fx/fx mice show inefficient cortico-striatal transmission as measured by decreased pop spike amplitude in extracellular field recordings. **g**, Normal relationship of stimulation intensity to the negative peak 1 amplitude (NP1; action potential component) suggesting unaltered presynaptic function; insets show representative field traces from *Shank3*fx/fx and WT mice. *P< 0.05, **P<0.01, ***P< 0.001; All data presented as means ± s.e.m. (all behavior data from n= 6 WT and n= 7 KO mice); two-tailed t-test for c (left panel) and e; two-way repeated measures ANOVA with Bonferroni post hoc test for c (right panel), d, f and g (electrophysiology data from n= 9 slices; 3 mice per genotype).

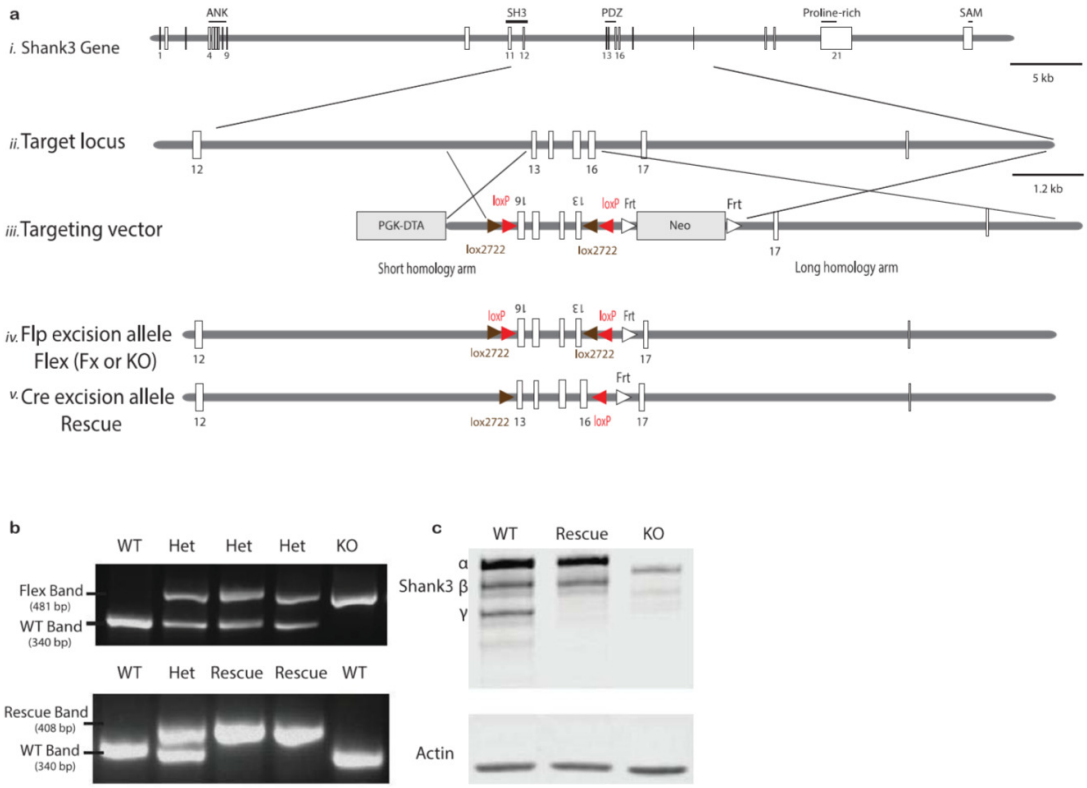

Figure 3.2 | Generation of *Shank3*CKI mouse.

ai-ii, Schematic of the *Shank3* gene and the target locus (image drawn to scale). **a**iii, Targeted Exons 13-16. **a**iv, Neo-cassette excision via breeding with a germline Flp-expressing mouse. **a**v, Exons 13-16 re-inversion via breeding with Cre-expressing mouse. **b**, PCR genotyping showing the bands for Fx, Rescue, and WT. **c**, Western blot showing almost complete rescue of *Shank3* expression upon Cre recombination, with exception of putative *Shank3*γ isoform. This is likely due to disruption of a putative intronic promoter by the introduction of the LoxP sites.

3.3.2 Rescue of PSD proteins and cortico-striatal transmission

To achieve temporal control of *Shank3* expression, we crossed the *Shank3*fx/fx mice to an inducible CAGGS-CreER mouse line (CAGGS comprises a CMV enhancer and chicken-actin promoter[199,200] that activates global Cre function upon tamoxifen treatment (Fig. 3.4). When the *Shank3*fx/fx:CreER+/- mice reach 2-4.5 months, we use oral gavage to deliver 5 consecutive daily doses of tamoxifen followed by a 2-week hiatus and then another 5 consecutive

daily doses of tamoxifen to ensure complete Cre-mediated re-orientation of exons 13-16 (Fig. 3.3A). All experiments post-feeding were performed on the following three groups: *Shank3*+/+:CreER+/- treated with tamoxifen (WT), *Shank3*fx/fx:CreER+/- treated with tamoxifen (TM), and *Shank3*fx/fx:CreER+/- treated with corn oil vehicle (KO). Synaptosomal preparations show that tamoxifen treatment of *Shank3*fx/fx:CreER+/- mice restores the expression of major SHANK3 isoforms to the wildtype level at synapses (Fig. 3.3B).

Previous reports indicated that *Shank3* deletion in vivo significantly decreases the concentration of multiple PSD scaffold proteins and receptor subunits[59]. However, it is unknown whether re-expressing *Shank3* after development can rescue the recruitment of various proteins to the synapse and improve synaptic transmission. Because SHANK3 is the only SHANK protein family member highly enriched in the striatum, a region strongly implicated in repetitive behavior[58], biochemical and synaptic characterizations were carried out on striatal neurons.

We found that in the tamoxifen rescue condition, the synaptic concentrations of scaffold proteins SAPAP3 and Homer1b/c are significantly increased compared to those in the KO, reaching the level of WT controls (Fig. 3.3C). Similarly, there is also significant rescue in the level of receptor subunits of NMDAR and AMPAR including NR2A, NR2B, and GluA2, with no significant difference between the tamoxifen rescue condition and the WT controls (Fig. 3.3C). This molecular rescue at the synaptic level shows for the first time that restoring *Shank3* expression in the adult brain can efficiently recruit major scaffolding and signaling proteins to the synapse and assemble the PSD protein network even after the developmental period.

Due to the encouraging synaptic molecular repair after adult *Shank3* expression, we investigated whether there were parallel changes at the functional level. We prepared acute brain slices from tamoxifen treated adult mice and controls to simultaneously test their cortico-striatal evoked transmission. As expected, *Shank3*fx/fx:CreER+/- (KO) mice treated with corn oil show significantly reduced field population spikes. However, the reduced field responses *Shank3*fx/fx:CreER+/- mice treated with tamoxifen are rescued to WT levels (Fig. 3.3D-F). These results suggest that the impaired cortico-striatal circuitry in KO mice can be reversed by restoring *Shank3* expression in adulthood, in parallel with restored PSD molecular composition. Interestingly, the KO mice also have reduced mEPSC frequency that is not rescued in the tamoxifen condition,

suggesting that other compensation mechanisms might be taking place to properly restore the levels of cortico-striatal synaptic transmission (Fig. 3.5).

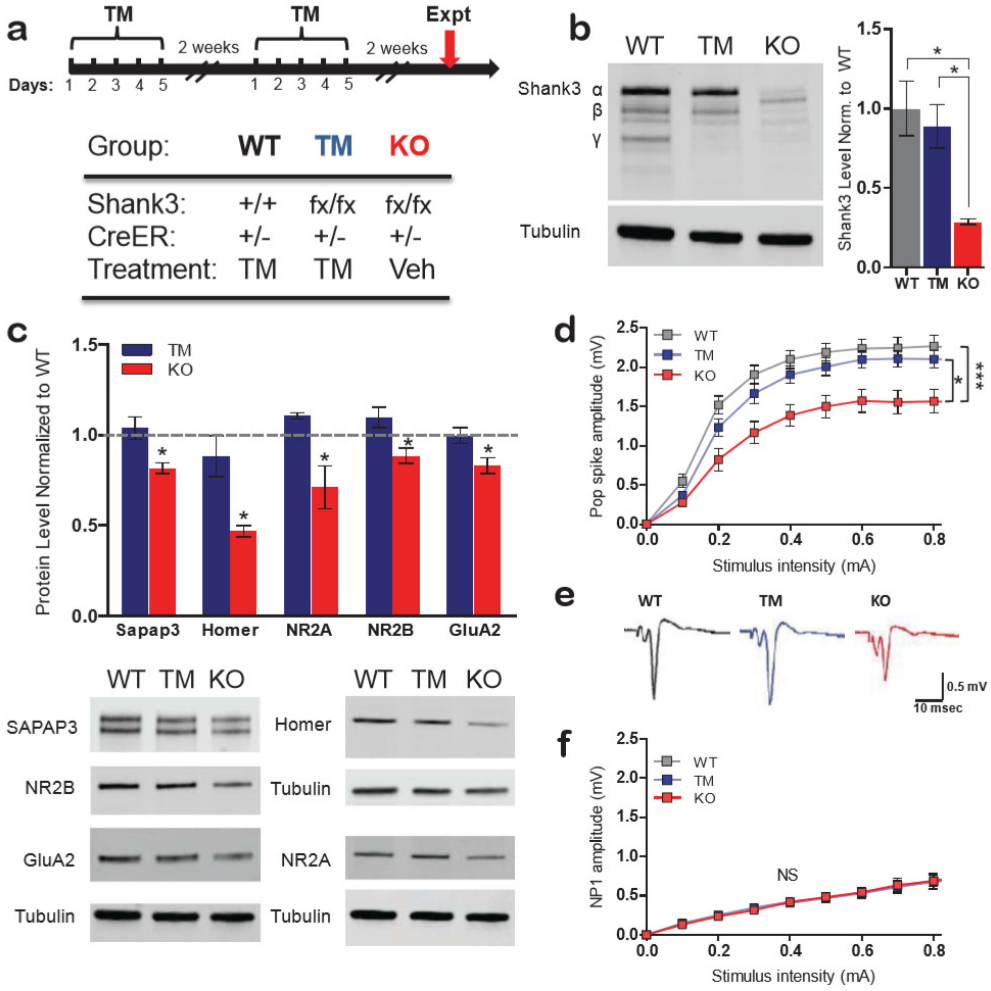

Figure 3.3 | Rescue of PSD proteins and cortico-striatal transmission.

a, Feeding scheme and mouse genotype for all groups oral gavaged. **b**, Western blot from striatal synaptosome preparation after tamoxifen feeding shows restoration of most SHANK3 isoforms. **c**, Western blot analysis of synaptosomal fractions from striatal tissue after feeding scheme; PSD proteins are significantly increased in TM group compared to KO; No difference between the TM and WT controls; 10 µg of protein per lane with tubulin as loading control and normalized to wildtype levels. **d**, Rescued cortico-striatal field response in KO mice fed with tamoxifen compared to controls. **e**, Representative field traces for WT mice fed with tamoxifen and KO mice fed with tamoxifen (TM) or corn oil (KO). **f**, Indistinguishable relationship of stimulation intensity to the NP1 amplitude per group suggests unaltered presynaptic function. *P< 0.05, **P<0.01, ***P< 0.001; Student's two-tailed t-test for b and c (n= 3 WT, n= 4 TM, n= 3 KO; each sample

represents combined striatal tissue from 2 mice); Two-way repeated measures ANOVA, with Bonferroni post hoc test for d and f (n= 12 slices from 4 WT, n= 12 slices from 4 TM and n= 12 slices from 4 KO mice). All data presented as means ± s.e.m.

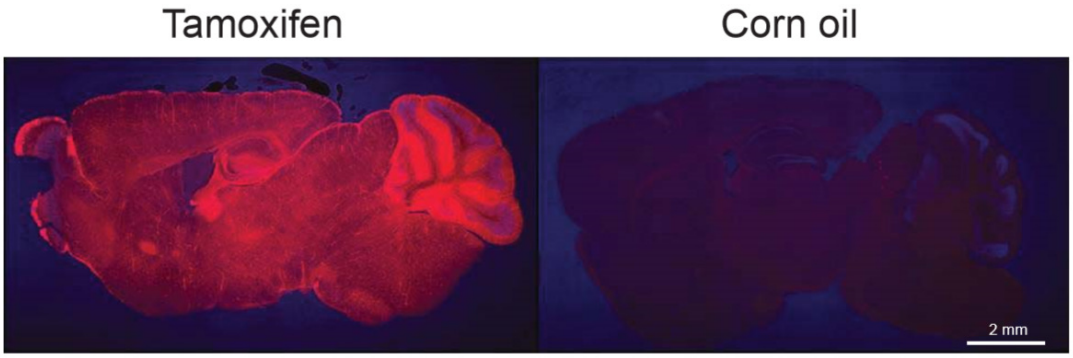

Figure 3.4 | Tamoxifen-inducible Cre strategy leads to broad reporter expression. Sagital sections from pCAGGS-CreER+/-:Rosa-*stop*^{flox}-*tdTomato*+/- mice after feeding with tamoxifen (left panel) or corn oil (right panel). Results show specific induction of tdTomato reporter expression upon tamoxifen-induced Cre expression but not in the absence of Cre (corn oil feeding); pCAGGS promoter consists of the CMV early enhancer with chicken β-actin promoter.

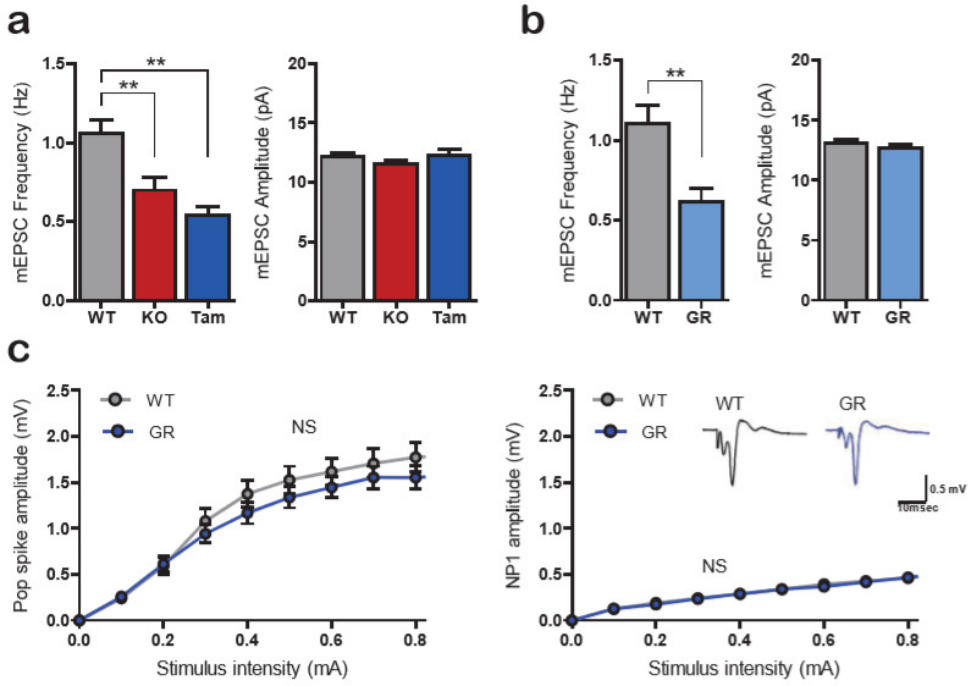

Figure 3.5 | Rescued cortico-striatal transmission but not miniature excitatory post-synaptic currents in *Shank3*fx/fx rescued mice.

a, Reduced mEPSC frequency in KO and TM mice compared to WT, with no changes in peak current amplitude. **b**, Reduced mEPSC frequency in germline rescued (GR) mice compared to WT, with no changes in peak current amplitude. **c**, Normal cortical-striatal pop spike amplitude and NP1 in genetically rescued GR mice (insets show representative field traces). Data in b suggests that reduced mEPSC frequency observed in the TM condition (a) is not due to adult rescue age-limitation but probably rather due to incomplete rescue of all *Shank3* isoforms (namely γ) as seen for the western blot in Figure 3.2 (panel c). This fact did not affect mice behavior (main text Fig.3.7); *Shank3* GR mice appear normal, display no lesions and have normal cortico-striatal transmission (panel c). **p<0.01; two-tailed t-test for a,b (for a: n= 23 MSNs from 4WT, n= 19 MSNs from 3KO and n= 23 MSNs from 3TM; for b: n= 21 MSNs from 3WT, n= 21 from 3GR); Two-way repeated measures ANOVA, with Bonferroni post hoc test for c (n= 11 slices from 3 mice per group); all data presented as means ±s.e.m.

3.3.3 Adult *Shank3* expression rescues grooming-induced lesions and social interaction

To assess the impact of *Shank3* re-expression in adulthood on behavior, we performed a battery of behavioral assays. Since one of the defining features of autism is the impairment in social interaction, we used a modified three-chamber assay to probe voluntary social interaction in the test mice[59,132,201]. After habituating to the three-chamber box, the test mice were given a choice of either interacting with a novel object or a novel mouse. We measured the duration and frequency of close interaction between the test mouse and its target of interest to determine the level of social preference. We found that while WT mice (*Shank3*+/+:CreER+/- treated with tamoxifen) demonstrated strong preference for the novel mouse over the novel object, KO mice (*Shank3*fx/fx:CreER+/- treated with corn oil) displayed no preference for either the object or the novel mouse (Fig. 3.6 A-C). This result is consistent with previous reports indicating that *Shank3* deletion leads to social interaction deficits in mice[59,129,130,132]. Interestingly, we found that in the same cohorts, TM mice (*Shank3*fx/fx:CreER+/- treated with tamoxifen) behave similarly to their WT controls in that they show strong preference for the novel mouse in both duration and frequency of interaction (Fig. 3.6 A-C).

During tamoxifen treatment, we noticed that some *Shank3*fx/fx:CreER+/- mice that initially developed lesions began to heal and regrow their lost fur (Fig. 3.6D), suggesting that stereotyped/excessive grooming phenotype may be reversible in the *Shank3*fx/fx mice. Thus, we videotaped WT (*Shank3*+/+:CreER+/- treated with tamoxifen), TM (*Shank3*fx/fx:CreER+/- treated with tamoxifen), and KO (*Shank3*fx/fx:CreER+/- treated with corn oil) mice after treatment, and quantified their grooming time. The results indicate that while there is significant increase in the percentage of time spent grooming in the knockout mice treated with corn oil compared to WT mice, knockout mice treated with tamoxifen exhibit significantly reduced grooming time and there is no significant difference in grooming time between the rescue condition and the WT controls (Fig. 3.6 E-F). These data show that similar to social interaction deficit, repetitive grooming behavior can also be rescued in adulthood.

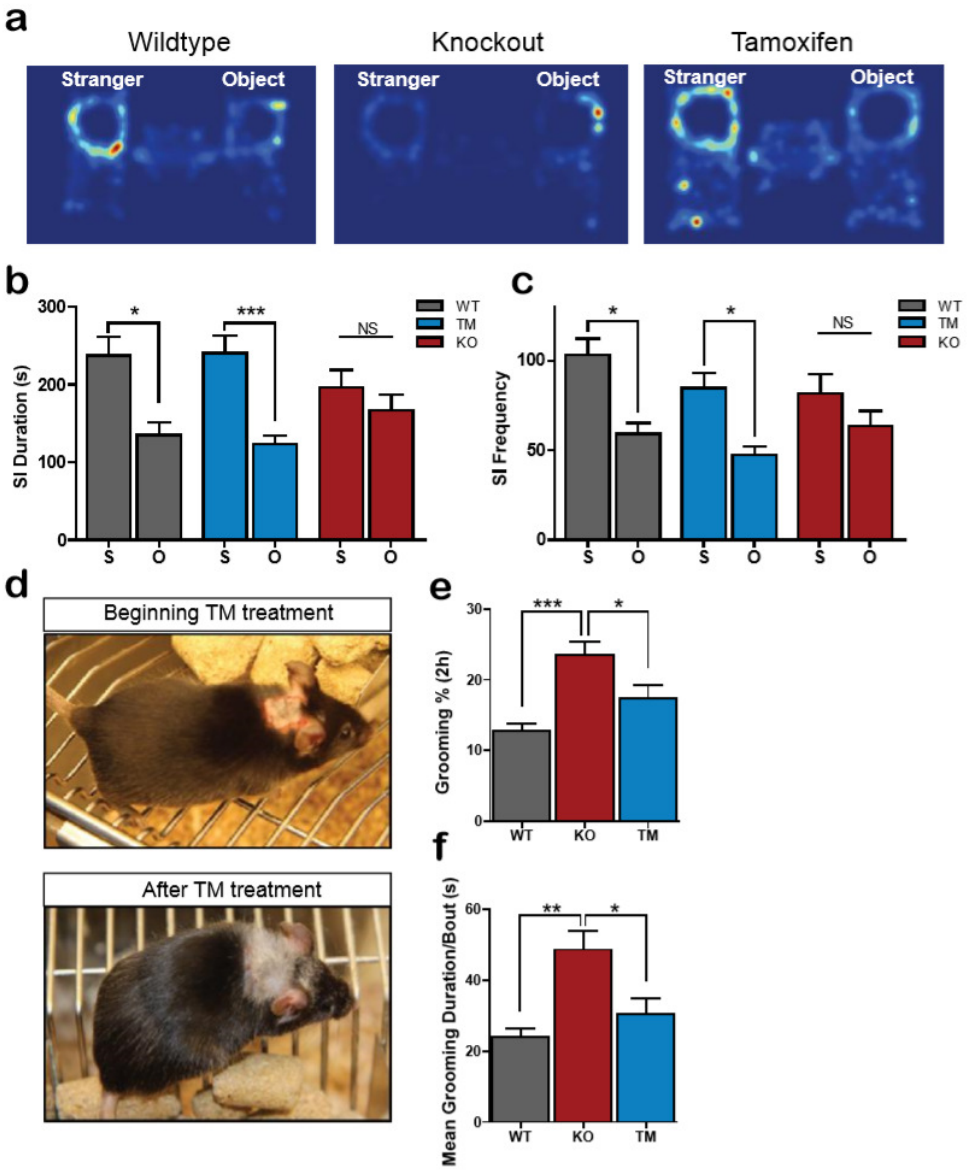

Figure 3.6 | Adult *Shank3* expression rescues grooming-induced lesions and social interaction.

a, Representative heat map analysis from the social interaction test for all groups (1WT, 1TM and 1KO); **b**,**c**, KO mice (red bars) showed no preferential interaction between a stranger mouse and an inanimate object, as assessed by interaction duration and frequency; this behavior is rescued after tamoxifen treatment, with TM group (blue bars) showing preference for social interaction (stranger); the same social preference is observed in WT mice (grey bars). **d**, *Shank3*fx/fx mouse showing pronounced neck lesion at the beginning of tamoxifen feeding and picture of the same mouse showing lesion healing and regrown fur after tamoxifen feeding scheme. **e**,**f**, Significantly reduced repetitive grooming behavior (both in terms of total time spent grooming and mean

grooming duration per bout) in KO mice after tamoxifen feeding. *P<0.05, **P<0.01, ***P<0.001; all data presented as means ± s.e.m; Two-way repeated measures ANOVA with Bonferroni post hoc test for all data (b,c: n= 22 WT, n= 30 TM and n= 30 KO;; e,f: n= 9 WT, n= 9 TM and n= 12 KO mice).

3.3.4 Restoring *Shank3* expression in adulthood does not rescue anxiety and rotarod deficits

Motivated by these findings, we ran a battery of other behavior tests to assess the extent of the rescue. In contrast to the social interaction and grooming results, adult *Shank3* re-expression has minimal impact on anxiety-like behavior and motor coordination deficit. In the open field test, TM (*Shank3*fx/fx:CreER+/- treated with tamoxifen) mice showed no significant difference from the KO mice (*Shank3*fx/fx:CreER+/- treated with corn oil) in exploratory behavior (Fig. 3.7A) and anxiety-like behavior including rearing time and rearing frequency (Fig. 3.7C). This result was further corroborated by our observations from the elevated zero maze (Fig. 3.7B). In addition, we found no significant recovery in motor coordination deficit after re-expressing *Shank3* in adulthood (Fig. 3.7D). To address whether the lack of rescue in these phenotypes is indeed due to post-developmental gene expression, we crossed *Shank3*fx/fx mice to a transgenic line that expresses Cre under the β-actin promoter, enabling germline rescue of *Shank3* expression. The germline rescue (GR) mice show no significant differences in exploratory behavior (Fig. 3.7E), anxiety (Fig. 3.7 F-G), and motor coordination (Fig. 3.7H) from their wildtype littermates, indicating that, unlike in adulthood, restoring *Shank3* expression at the germ cell stage can restore all behavioral phenotypes. This selective rescue of social interaction and grooming together with the lack of rescue in anxiety and motor coordination deficit suggest the existence of different critical periods for the establishment of various behavioral phenotypes.

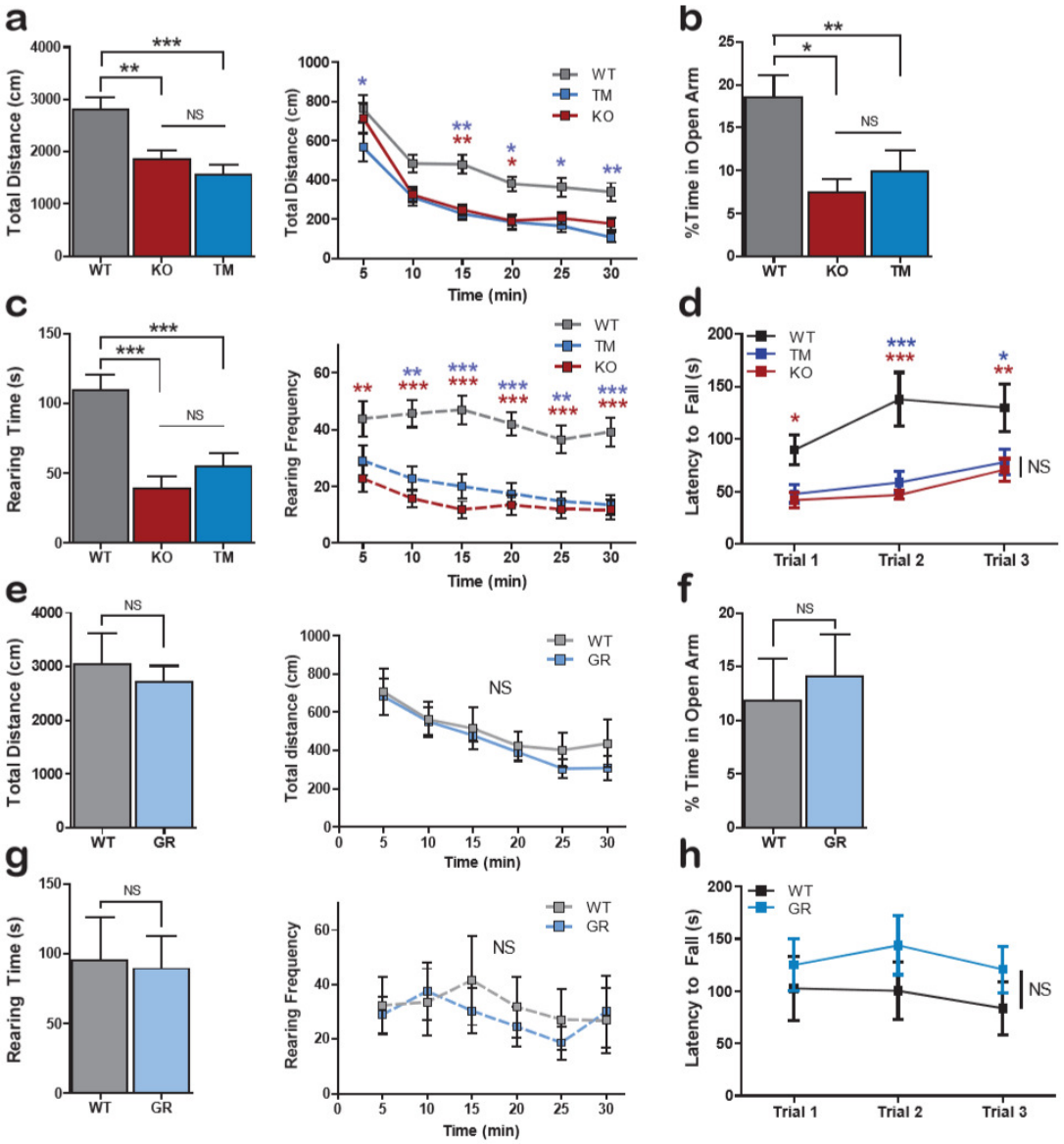

Figure 3.7 | Restoring *Shank3* expression in adulthood does not rescue anxiety and rotarod deficits.

a, Open field results indicate that tamoxifen feeding in adults does not rescue total locomotion in the *Shank3*fx/fx mice. **b**, *Shank3*fx/fx mice spend less time exploring the open arm; this behavior is also not rescued in the tamoxifen group compared to the control groups. **c**, Other parameters from open field test including rearing time and rearing frequency show that anxiogenic behavior is not rescued after tamoxifen feeding. **d**, Motor coordination measurement from rotarod is not rescued in adult *Shank3*fx/fx mice. **e**-**h**, Germline rescued *Shank3*fx/fx mice show that all previous parameters for open field, elevated zero maze and rotarod tests can be rescued if *Shank3* expression is restored at germ cell stage; results indicate the existence of a critical period such that

adult expression of *Shank3* cannot rescue these behaviors. *P < 0.05, **P<0.01, ***P < 0.001; One way ANOVA for a (left panel), b, and c (left panel); Two-tailed t-test for e (left panel) f and g (left panel); Two-way repeated measures ANOVA with Bonferroni post hoc test for a (right panel), c (right panel), d, e (right panel), g (right panel) and h; All data presented as means ± s.e.m. (a-c: n= 18 WT, n= 25 TM and n= 27 KO; d: n= 13 WT, n= 19 TM and n= 21 KO; e-h: n= 10 WT and n= 8 GR mice).

3.4 Discussion

Although *Shank3* disruption has been shown to cause ASD-associated phenotypes in human patients and mouse models, it has never been shown whether *Shank3* restoration can lead to neural functional and/or behavioral improvements during adulthood. In this study, we demonstrate selective phenotypic rescue at the synaptic, circuit, and behavioral levels when *Shank3* expression is efficiently induced in adult mice. We showed that the PSD protein composition and cortico-striatal neurotransmission can be restored. This indicates that adult expression of *Shank3* in the synapse is sufficient to recruit its key interaction partners at synapses, restoring the normal concentrations of neurotransmitter receptors at the PSD. At the behavioral level, our results indicate selective phenotype rescue in social interaction and repetitive behavior, but not anxiety and motor coordination deficits. These data suggest that different mechanisms/brain circuits with distinct critical periods may underlie the reversibility of these complex behaviors. Indeed, a previous study involving timed serotonin receptor gene expression concluded that anxious behaviors in mice cannot be rescued in adulthood possibly due to permanent changes in brain circuitry[202]. Our approach for adult rescue of *Shank3* knockout supports the conclusion that specific biochemical, functional and behavioral aspects can be reversed in adulthood. These fundamental changes may have great translational implications and give rise to significant improvements in selective autistic-like behavioral phenotypes.

3.5 Methods

Generation of *Shank3*CKI: The *Shank3*fx/fx targeting vector was designed by inverting the PDZ domain (exons 13 to 16) and flanking it with the FLEx cassette, which is composed of one pair of LoxP sites staggered with one pair of Lox2722 sites. *Shank3*fx/fx conditional knock-in mice were generated by homologous recombination in R1 embryonic stem cells and implanting the correctly targeted cells in C57 blastocysts using standard procedures. Correct locus insertion of the targeting construct into the genomic DNA was determined by PCR genotyping using two primers End_F (5'-GGCAGACTCCACACAGTTCCTG-3') and LoxR (5'-GTATCCTATACGAAGTTATTCCGGGTCGAC-3'). Subsequent mouse genotyping was determined by PCR of mouse tail or ear DNA using three primers. For the wildtype (WT) allele, primer FuncF2 (5'-CGTTTGACACACATAAGCACC-3') and primer FuncFlipR4 (5'-CTCCACCTAGCTGAATTTCCC-3') were used to produce a band of 340 bp. For the knockout (Fx) allele, primer FuncF2 (5'-CGTTTGACACACATAAGCACC-3') and primer Gen_Flx_R1 (5'-GCTGACATCACATTGCTGCC-3') were used to produce a band of 481 bp. For the rescue allele, primer FuncF2 (5'-CGTTTGACACACATAAGCACC-3') and primer FuncFlipR4 (5'-CTCCACCTAGCTGAATTTCCC-3') were used to produce a band of 408 bp.

Chimeric males were crossed to C57BL/6J females from Jackson Labs. The F1 hybrids were crossed with C57BL/6J β-Actin Flp to remove the Neomycin cassette. All progeny were bred onto the pure C57BL/6J (Jackson Labs) for at least two generations before being bred onto a mixed background with 129S1/SvImJ (Jackson Labs). Heterozygotes were initially bred with heterozygotes to produce experimental animals. All germline *Shank3*fx/fx (KO) and germline rescue (GR) mice along with their respective wildtype littermates were produced by breeding heterozygotes with heterozygotes. For the adult *Shank3* rescue experiments, the *Shank3* conditional knock-in line was crossed with CAGGS-CreER. In order to produce enough animals for all necessary experiments, breeding strategy was switched to heterozygotes crossed with homozygotes and homozygotes crossed with homozygotes for all conditions (*Shank3*fx/+:CreER+/- bred with *Shank3*fx/fx:CreER-/-; *Shank3*fx/fx: CreER+/- bred with *Shank3*fx/fx:CreER-/-; *Shank3*+/+ :CreER+/- bred with *Shank3*+/+:CreER-/-; *Shank3*+/-:CreER+/- bred with *Shank3*+/+:CreER-/-). It

should be noted that all animals in the rescue condition were produced from the same litters as the animals in the knockout condition.

Animals were housed by genotype at a constant 23℃ in a 12 h light/dark cycle (lights on at 07:00, lights dark at 19:00) with ad libitum food and water. Rescue treatment i.e. tamoxifen feeding was initiated on mice at 2-4.5 months. All electrophysiological and behavioral experiments were done 6 weeks after treatment in adult mice with the experimenter being blinded to the genotypes. Only age-matched male mice were used for behavioral assays. All experimental procedures were inspected and approved by the MIT Committee on Animal Care.

Open Field: An automated Omnitech Digiscan apparatus (AccuScan Instruments) was used to assess spontaneous locomotion as previously described[58]. Anxiety-like behaviors were assessed by the following parameters: time spent rearing and frequency of rearing. Locomotion was evaluated by the total distance traveled. The first 30 minutes were evaluated for all parameters. Statistical analysis was done using one-way ANOVA with Bonferroni multiple comparison tests.

Zero Maze: An elevated zero maze was illuminated such that the open arm was lit by 60 lux, and the dark arm was lit by 10-20 lux. Animals were habituated with 10-20 lux for at least one hour before test. The animal was introduced into the closed arm and allowed to freely explore the maze for 5 minutes, which was videotaped. An observer blinded to the genotype performed analysis using an automated tracking software Noldus Ethovision. Anxiety-like behavior was assessed by the percentage of time spent by the animal in the open arm during the 5 minutes interval. Statistical analysis was done using one-way ANOVA with Bonferroni multiple comparison tests.

Rotarod: Animals were placed on a rotarod apparatus (Med Associates) that accelerates 4-40 rpm for 5 minutes. Each animal was tested for three trials with 60 minutes between trials in a single day. All trials were videotaped. Latency to fall was manually analyzed for each trial by a blinded observer on Noldus Observer. The change in the latency to fall over the course of three trails indicates the quality of motor coordination. Statistical analysis was done using two-way repeated measures ANOVA with Bonferroni post-hoc tests.

Grooming: Animals were individually placed into a novel cage and allowed to habituate. Grooming behavior was videotaped for 2 hours from 19:00 to 21:00h with red light (2 lux). An observer blinded to the genotype manually quantified grooming behavior using Noldus Observer. All instances of face-wiping, scratching/rubbing of head and ears, and full-body grooming were counted as grooming behavior. Statistical analysis was done using one-way ANOVA with Bonferroni multiple comparison tests.

Social Interaction: A modified version of the three-chamber social interaction assay was used as previously described[59,132,201]. Only age-matched males were used for all tests. S129 males were used as stranger mice and were habituated to the test chamber for 3 sessions (20 minutes each) one or two days prior to the behavioral assay. On the day of the test, both test and stranger animals were habituated to the test room for at least one hour before the start of the assay. The left and right chamber of the three-chamber apparatus were both lit by 4-6 lux during the test session. Each test animal was first placed into the center chamber with open access to both the left and right chamber, each of which contained an empty wired cup placed upside down. This allowed the animal to habituate to not only the social apparatus, but also the cups that will eventually contain the stranger mice. After 15 minutes of habituation, the test animal was moved back to the center chamber briefly before the next session. During the social phase, an age-matched stranger mouse was placed randomly into one of the two side chambers while a novel object was placed into the other side chamber. The test animal was allowed to freely explore the social apparatus and demonstrate whether it prefers to interact with the novel object or the novel mouse. This social phase was also 15 minutes. The placement of the stranger mouse and the object was alternated between test mice to eliminate any confounds due to chamber bias. Time spent by the test animal in close proximity (~5 cm) to the cup containing either the stranger or the object was calculated. Analysis was done by an observer blinded to the genotype on Noldus Ethovision. One-way ANOVA with Bonferroni post hoc test was used for statistical analysis.

Tamoxifen Preparation and Feeding: After comparisons of different methods of induction, oral gavage was used because it induces much more efficient and widespread recombination than intraperitoneal injections[203]. Tamoxifen (Sigma #T5648) was dissolved in corn oil at 20 mg/ml through vortexing. Freshly prepared tamoxifen was protected from light by aluminum foil

and kept for 2-3 days at room temperature. Animal feeding needles from Harvard Apparatus (cat #52-4025) were used for oral gavage. To avoid toxicity of tamoxifen, the following dosages were used:

Mice at 17-21 g body weight were fed 5 mg/day

Mice at 22-25 g body weight were fed 6 mg/day

Mice at 26-29 g body weight were fed 7 mg/day

Mice at 30-35 g body weight were fed 8 mg/day

The animals were fed for 5 consecutive days followed by two weeks of rest. Then the animals were fed for 5 more consecutive days followed by another two weeks of rest. Corn oil was fed as a control. The mice fed with tamoxifen and mice fed with corn oil were housed separately to avoid contamination.

Western Blot: PSD and synaptosomal fractions of the striatum were prepared as previously described[58]. Purified fractions were separated on SDS-PAGE and quantified using Odyssey Licor. β-Actin and Tubulin were used as loading controls. Specific primary antibody for SAPAP3 was prepared as previously described[58]. Commercial antibodies used include SHANK3 (Santa Cruz), GluR2 (Abcam), NR2A (Millipore), NR2B (Millipore), Homer (Chemicon), B-actin (Sigma), Tubulin (Sigma). Statistical analysis was done using two-tailed students' t-tests.

Electrophysiology slice preparation: Acute striatal slices were prepared from 3-6 months old mice. For extracellular field recordings, slices were prepared from a daily group of mice containing all the 3 genotypes/treatments on randomized order. For whole-cell patch clamp, slices were prepared from a single animal per day. All slice preparations and recordings were performed with experimenter blinded to the genotypes. Animals were anesthetized by avertin intraperitoneal injection (tribromoethanol, 20 mg/ml, 0.5 mg/g body weight) and transcardially perfused with cutting NMDG-based aCSF solution (mM): 92 N-methyl-D-glucamine (NMDG), 2.5 KCl, 1.20 NaH_2PO_4, 30 $NaHCO_3$, 20 HEPES, 25 glucose, 2 thiourea, 5 Na-ascorbate, 3 Na-pyruvate, 0.5 $CaCl_2.2H_2O$, 10 $MgSO_4.7H_2O$ (~300 mOsm, 7.2-7.4 pH). Following decapitation, brains were removed for coronal sectioning (300 µm) using a Vibratome 1000 Plus, Leica Microsystems, USA. Slices were then recovered in cutting solution at 32–34°C for 10-15 minutes and transferred to room-temperature carbogenated regular aCSF(mM): 119 NaCl, 2.5 KCl, 1.2 NaH_2PO_4, 24 $NaHCO_3$, 12.5 glucose, 2

$MgSO_4.7H_2O$, 2 $CaCl_2.2H_2O$ (~300 mOsm, 7.2-7.4 pH). Slices were allowed to recover at least ≥1h prior to all recordings.

Extracellular field recordings: Slices were transferred into a recording chamber (RC-27L, Warner Instruments) and constantly perfused at RT with carbogenated regular aCSF at a rate of approximately 2 ml/minute. Borosilicate glass recording microelectrodes (King Precision Glass) were pulled on a P-97 horizontal puller (Sutter Instruments) and backfilled with 2 M NaCl. Slices were visualized under IR-DIC (infrared-differential interference contrast) using a BX-51WI microscope (Olympus) and stimulated by a platinum iridium concentric bipolar electrode (CBAPC75, FHC) that was placed in the dorsolateral striatum at the inner border of corpus callosum. Recording electrode was placed ~400 µm away from stimulating electrode and field population-spike was evoked by a 0.1 ms stimulation step (Isoflex, AMPI) delivered at 0.05 Hz frequency. Input-output functions were generated through consecutive rounds from 0.1-1.0 mA in 0.1 mA increments (triplicate measurements per stimulation intensity). Three components were resolved in the recording traces: stimulation artifact, negative peak 1 (NP1, presynaptic fiber volley) and field population spike. Amplitude for each component was determined by the average peak amplitude from the triplicated measurements per stimulation intensity. Data was amplified using a MultiClamp 700B and sampled at 10 KHz using a Digidata 1440A acquisition system. Analysis was performed blinded to genotype using pCLAMP 10 software (Axon Instruments/Molecular Devices).

Whole-cell patch-clamp: Slices were transferred into a recording chamber (RC-27L, Warner Instruments) and constantly perfused at RT with carbogenated regular aCSF at a rate of approximately 2 ml/minute. Borosilicate glass recording microelectrodes (King Precision Glass) were pulled on a P-97 horizontal puller (Sutter Instruments) and backfilled with CsGlu (mM: 110 CsOH, 110 D-Gluconic acid, 15 KCl, 4 NaCl, 5 TEA-Cl, 20 HEPES, 0.2 EGTA, 5 Lidocaine N-ethyl chloride, 4 MgATP, 0.3 NaGTP). Internal pH was adjusted to ~7.3 with KOH and osmolarity adjusted to ~300 mOsm with K_2SO_4, giving a typical internal resistance around 3-5 MΩ. MSNs were visually identified based on their shape, size and location under IR-DIC (infrared-differential interference contrast), using a BX-51WI microscope (Olympus). After seal rupture and internal equilibrium (5 minutes to allow proper dialysis of Cs+ internal), cells were recorded with series-resistance values <20 MΩ. Voltage clamp traces were recorded with theoretical

liquid junction potential not corrected-for and cells were held at -70 mV in the presence of 100 µM PTX (picrotoxin, Tocris) and 1 µM TTX (tetrodotoxin, Tocris). Signals were filtered at 1 KHz, digitized at 10 KHz and data acquired using a MultiClamp 700B amplifier and a Digidata 1440A. All analysis was performed blinded to the genotype using pCLAMP10 (Axon Instruments, Molecular Devices) and Minianalysis software (Synaptosoft Inc, USA) with a detection threshold set at 5x root mean square (RMS) noise and manually checked for detection accuracy.

Statistical Analyses (ephys): All electrophysiology statistical analyses were performed using Prism (GraphPad Software). Results are graphically displayed with respective SEMs and data sets were analyzed for significance using either unpaired student's two-tailed t-test or by two-way repeated ANOVA measures with post-hoc Bonferroni test, using $p<0.05$ as significance threshold. Further details on particular statistical analyses can be found on the respective figures/results section for each data set.

Chapter 4

Shank3 mutations associated with ASD and schizophrenia display both shared and distinct defects

4.1 Summary

Dysfunctions in frontostriatal brain circuits have been implicated in neuropsychiatric disorders, including those characterized by the presence of repetitive behaviors. Genetic studies have revealed a significant overlap of risk genes among major psychiatric disorders. However, it is not clear how different mutations of the same gene could causally contribute to the manifestation of different diseases. Here we characterized two lines of mutant mice with *Shank3* mutations linked to ASD and schizophrenia. We found that only mutant mice with the ASD-linked InsG3680 mutation manifest defective synaptic transmission before weaning age, coinciding with the early onset of ASD symptoms. At the same time, only mice carrying the schizophrenia-linked R1117X mutation show profound synaptic defects in prefrontal cortex. We also found differential *Shank3* mRNA stability and Shank1/2 upregulation in these two lines. Furthermore, the two mutant lines show both common and distinct behavioral abnormalities. Together, these data provide an explanation, at molecular, synaptic, circuit and behavioral levels, on how distinct mutations of the *Shank3* gene may causally and mechanistically contribute to different disorders.

4.2 Background

Although schizophrenia and autism are two distinct disorders (DSM-5), it has long been proposed that they share some common pathology and symptoms[204]. Currently, the etiologies of schizophrenia and autism are largely unknown[205–209], but recent human genetic studies highlight the contribution of genetic risk factors to both disorders[210–212]. In particular, mutations of a group of genes linked to synaptic development, function and plasticity were frequently identified from patients diagnosed with either schizophrenia or autism[213–216], suggesting that genetic mutations leading to dysregulation of synaptic transmission play critical roles in the pathophysiology of both schizophrenia and autism[212,217–219]. Interestingly, recent genetic studies further revealed significant overlaps of risk genes across major psychiatric disorders including schizophrenia, bipolar disorder, major depressive disorder and autism[220].

Furthermore, large scale exome sequencing of autism spectrum disorder (ASD) and schizophrenia patient DNA samples has identified many of the same

genes in both disorders, suggesting that different mutations of the same gene can cause/contribute to different disorders[221–224].

One such example is the *Shank3* gene. *Shank3* is a member of the Shank family of proteins (Shank1-3)[147,194]. Members of Shank family share five main domain regions: N-terminal ankyrin repeats, SH3 domain, PDZ domain, proline-rich region, and a C-terminal SAM domain[143]. Through these functional domains, Shank interacts with many PSD proteins. Most notably, Shank binds to SAPAP which in turn binds to PSD95 to form the PSD95/SAPAP/Shank postsynaptic complex[225,226]. Together, these three groups of multi-domain proteins are proposed to form a key scaffold, orchestrating the assembly of the macromolecular postsynaptic signaling complex at glutamatergic synapses. This complex has been shown to play an important role in targeting, anchoring, and dynamically regulating synaptic localization of neurotransmitter receptors and signaling molecules[227]. Shank is also connected to the mGluR pathway through its binding to Homer[228]. In addition, given its link to actin-binding proteins, Shank has been shown to regulate spine development[229–231]. Together with recent studies of ASD-linked *Shank3* mutations in cultured neurons[232,233], these evidences strongly suggest that Shank proteins play key roles in synaptic development and function[149,150,234,235].

Deletion of *Shank3* has been shown to be the cause of core neurodevelopmental and neurobehavioral deficits in Phelan-McDermid syndrome (PMS), an autism spectrum disorder that shows intellectual disability, autistic behaviors, hypotonia, and impaired development of speech and language[236–240]. Mutation of *Shank3* gene in autistic patients was initially discovered by Durand and colleagues, in which they identified a number of de novo mutations including a guanine nucleotide insertion in exon 21 of *Shank3* gene from two subjects diagnosed with ASD. Insertion of this guanine nucleotide at the position 3680 of *Shank3* cDNA results in a frameshift and a premature stop codon[157]. Subsequent genetic screens also identified a variety of mutations in the *Shank3* gene including microdeletion, nonsense mutation, and recurrent breakpoint in ASD patients not diagnosed with PMS[155–157]. These data implicate *Shank3* gene disruption/mutation as a monogenic cause of ASD. In supporting these genetic findings, studies of *Shank3* mutant mice from our laboratory and others revealed various degrees of synaptic dysfunction and autistic-like behaviors[59,129,130]. In addition, duplication of the *Shank3* gene was found from patients diagnosed with bipolar disorders and mice with *Shank3* overexpression exhibit synaptic dysfunction and manic-like phenotypes[195]. These genetic evidence further

support the critical involvement of *Shank3* mutation, deletion and duplication in the development of neuropsychiatric disorders[222].

Interestingly, a non-sense mutation of *Shank3* changing an arginine to stop codon was identified from three brothers diagnosed with schizophrenia between ages 16-21 without showing obvious autistic features during their childhood[241]. This is very intriguing considering the differences in core symptoms and clinical onset time between schizophrenia and autism. Understanding the mechanisms by which different mutations in the same gene lead to different disorders will likely shed light on unique neural mechanisms of these disorders. We therefore created two mutant mouse lines; one harbors the ASD patient-linked single guanine nucleotide (G) insertion at cDNA position 3680 leading to a frameshift and downstream stop codon (InsG3680 mutation), and the other contains the schizophrenia patient-linked point mutation changing arginine 1117 to a stop codon (R1117X mutation). We performed systematic comparison between the two mutant lines at molecular, cellular, synaptic and behavioral levels and found both distinct and shared defects in these two mutant models. In particular, we found that mutant mice with the ASD-linked InsG3680 mutation, but not with the schizophrenia-linked R1117X mutation, manifest defective synaptic transmission before weaning age, coinciding with early onset of ASD symptoms. On the other hand, mice with R1117X mutation, but not with InsG3680 mutation, show synaptic defects in prefrontal cortex, consistent with clinical findings implicating prefrontal cortex defects in schizophrenia patients. Biochemical studies also revealed differential defects in postsynaptic signaling complexes and in compensatory mechanisms in these two mutant lines. Behaviorally, both lines of mutant mice exhibit anxiety-like behavior and social interaction deficits. However, InsG3680 mutant mice show stronger repetitive/compulsive grooming behavior whereas R1117X mutant mice show stronger dominance/aggressive behavior. Together with supporting molecular and biochemical data, our study provides a potentially mechanistic explanation on how distinct mutations of the *Shank3* gene may contribute to different disorders.

4.3 Results

4.3.1 Distinct effects of InsG3680 and R1117X mutations on SHANK3 protein and mRNA

Both InsG3680 and R1117X mutations are in exon 21 and only 325 nucleotides apart (Figure 4.1A). For the ASD-linked InsG3680 mutation, we inserted a guanine nucleotide (G) at the nucleotide position 3680 of cDNA sequence to introduce the G insertion mutation (InsG3680) as described in the original finding (Durand *et al*., 2007). The G insertion at 3680 of *Shank3* causes a frameshift and a stop codon immediately after the G insertion (Figure 4.1A,B). For R1117X mutation, we changed arginine (R) codon "CGG" to stop codon "TGA" to introduce the "R" to "X" mutation at the amino acid position 1117 as described in the finding from schizophrenia patients[241] (Figure 4.1A). Targeted R1 ES cells were confirmed by sequencing the PCR product to verify the successful introducing of mutations at desired sites (Figure 4.1B) and then injected into blastocysts derived from C57 BL/6J mice as previously described[59]. We built up a C57 B6/S129 Sv mixed background mice population for all experiments performed in this study unless otherwise specified (Experimental procedures). Both homozygous InsG3680 and R1117X *Shank3* mutant mice are viable and fertile.

The predicted sizes of truncated protein are 135 kDa for InsG3680 mutation and 122 kDa for R1117X mutation, respectively. To examine whether such truncated SHANK3 proteins exist in the brain, we prepared postsynaptic density (PSD) fractions from striatum tissue and probed with antibodies recognizing epitopes located at either N terminus (located upstream of both mutations) or C terminus of SHANK3 protein (located downstream of both mutations; see Supplemental Table S4.1). When probed with the C terminus antibody, no signals above 75 kDa were detected in striatal PSD preparations from either homozygous InsG3680 mutant mice (InsG3680+/+) or R1117X mutant mice (R1117X+/+) (Figure 4.1C and 4.1D). This is consistent with the fact that the C-terminus antibody recognizes epitopes between amino acids 1431-1590 of SHANK3, which are beyond premature stop codons caused by InsG3680 and R1117X mutations. In contrast, when probed with an antibody raised against the N terminus of SHANK3 (Neuromab 367/62), we detected truncated SHANK3 bands in striatal PSD preparations from the R1117X mutant mice with the major band matching the predicted 122 kDa expressed in HEK293 cells (Figure 4.1D).

However, no clear signals were detected in striatal PSD preparations from InsG3680 mutant mice (Figure 4.1C). Similar results were obtained in PSD preparations from cortex of R1117X and InsG3680 mutant mice using N-terminus and C-terminus antibodies (Fig 4.2). Together, our results reveal that R1117X and InsG3680 mutations have distinct effects on SHANK3 protein expression.

Since non-sense mutations could lead to reduced mRNA levels through non-sense mediated decay (NMD) of abnormal mRNAs[242], we next examined Shank3 mRNA levels in the striatum of InsG3680 and R1117X mutant mice by quantitative real-time PCR. Due to the extensive alternative splicing of multiple coding exons in the *Shank3* gene[129], we designed four pairs of primers probing different coding regions to minimize the potential detection bias caused by alternative splicing. We consistently observed dramatically reduced levels of Shank3 mRNA from striatum tissue of InsG3680+/+ mice with all four pairs of probes (Figure 4.1E-H). Interestingly, striatal tissues from R1117X+/+ mice showed significantly higher levels of Shank3 mRNA than that from InsG3680+/+ mice (Figure 4.1E-H). These results suggest that Shank3 mRNAs with R1117X mutation are more stable than mRNAs with InsG3680 mutation, consistent with our result that truncated SHANK3 proteins are present in R1117X+/+ mice. Together, our data suggest that ASD-linked InsG3680 mutation resulted in almost a complete loss of SHANK3 protein, which is consistent with full deletion of *Shank3* gene identified from most Phelan-McDermid Syndrome patients[153,240]. In contrast, schizophrenia-linked R1117X mutation results in the generation of truncated SHANK3 protein which could potentially be either partially functional or act in dominant-negative form.

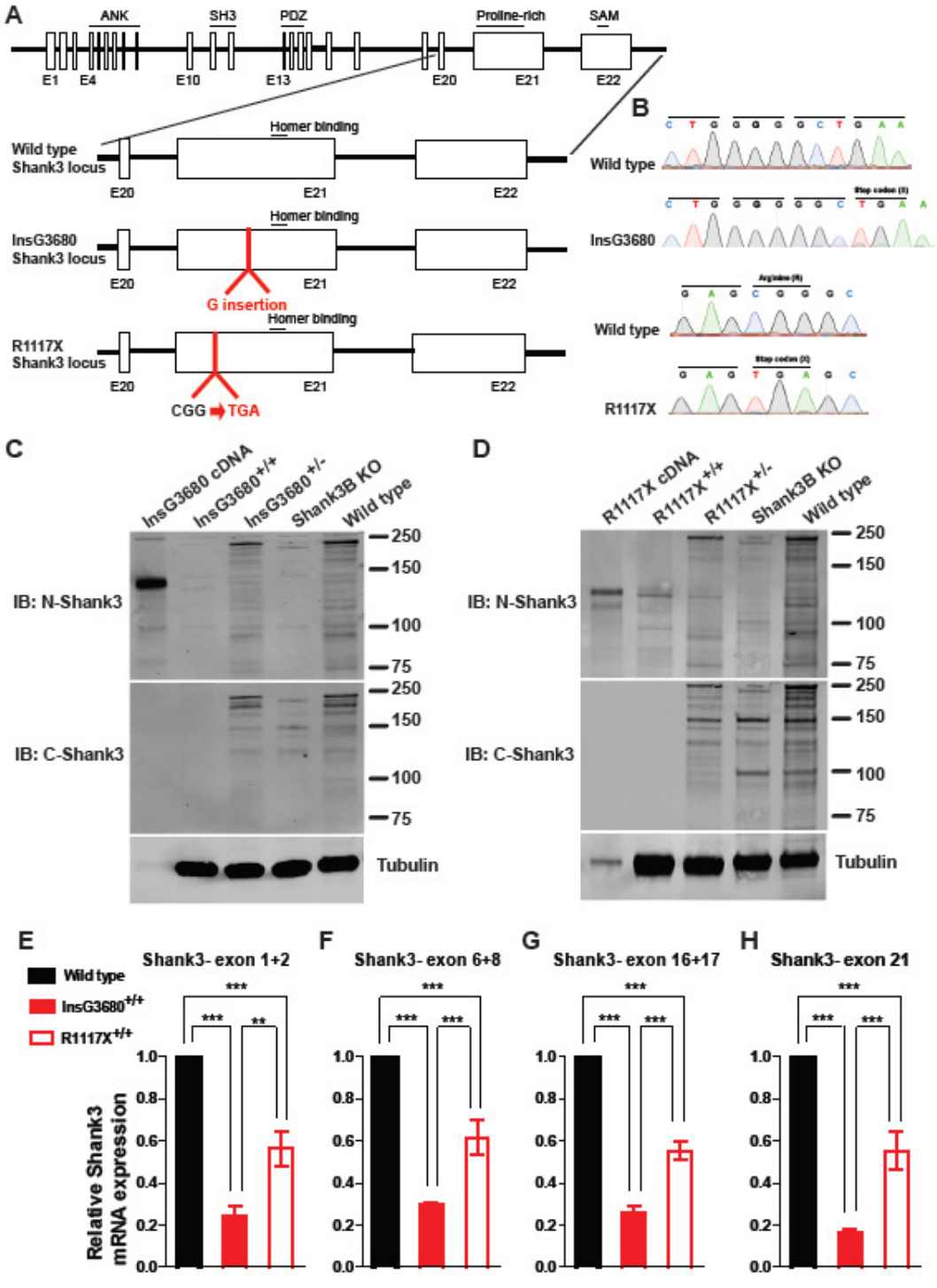

Figure 4.1 | Genetically engineered mice with InsG3680 or R1117X *Shank3* mutation differentially express SHANK3 **protein and mRNA.**

(A) Schematic diagram for wild type *Shank3*, InsG3680 and R1117X targeted *Shank3* alleles. Gene structure of wild type mouse *Shank3* gene and magnified panels on the structure between exon 20 and exon 22 are shown below. Top: wild type *Shank3*;

middle: Autism-associated InsG3680 *Shank3* mutation with an insertion of "guanine" nucleotide at position 3680; bottom: schizophrenia-associated R1117X *Shank3* mutation changing the "CGG" codon for arginine to a "TGA" stop codon. **(B)** Representative sequencing chromatograms of wild type and InsG3680 mutated alleles; wild type and R1117X mutated alleles showing the point mutations. **(C)** Representative western blots using striatal PSD fractions prepared from wild type, *Shank3*B KO mice, InsG3680+/- mice, InsG3680+/+ mice; lysate from HEK239 cells expressing cDNA plasmid encoding the InsG3680 mutated *Shank3*. Note that neither the antibody against the N- nor C-terminus detected SHANK3 protein in InsG3680+/+ mice**. (D)** Representative western blots using striatal PSD fractions prepared from wild type, Shank3B KO mice, R1117X+/- mice, R1117X++ mice; lysate from HEK239 cells expressing cDNA plasmid encoding the R1117X mutated *Shank3*. Note that SHANK3 protein expression is almost abolished except for a prominent truncated isoform in the R1117X+/+ line that is detected with the antibody against the N-terminus. **(E-H)** The relative level of Shank3 mRNA in striatum is different between the two lines as quantified by primers amplifying exon 1 to 2, exon 6 to 8, 16 to 17 and partial exon 21 before both *Shank3* mutation sites. Data are normalized to Gapdh mRNA and presented as mean ± SEM. ** $P < 0.01$, *** $P < 0.001$; one-way ANOVA with Bonferroni post hoc test, WT mice (n= 5), R1117X+/+ mice (n= 5) and InsG3680+/+ mice (n= 5).

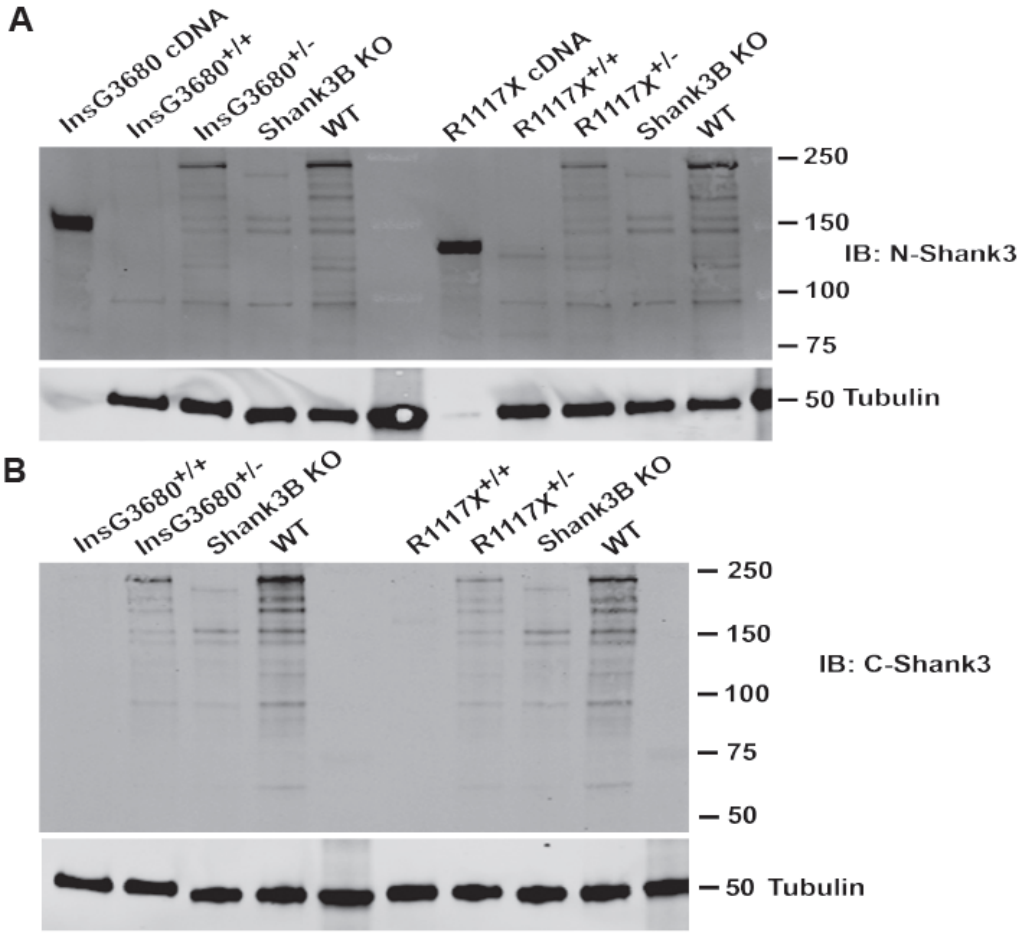

Figure 4.2 | InsG3680 and R1117X *Shank3* mutations differentially affect SHANK3 **proteins in the cortex.**

A and **B**) Representative western blots using cortical PSD fractions prepared from wild type, *Shank3*B KO mice, R1117X+/- mice, R1117X+/+ mice, InsG3680+/- mice, InsG3680+/+ mice; lysate from HEK239 cells expressing cDNA plasmid encoding the Myc-tagged R1117X mutated *Shank3* and Myc tagged InsG3680 mutated *Shank3*. Blots were probed with antibodies against the N-terminus and C-terminus of *Shank3*. Note the presence of truncated SHANK3 proteins in R1117X+/+ mice.

4.3.2 InsG3680 but not R1117X mutants exhibit early synaptic defects

Since ASD patients with *Shank3* mutations are usually diagnosed before the age of 3, whereas the schizophrenia patients carrying the R1117X mutation were diagnosed between ages 16-21, we wondered whether these two mutated

mice exhibit any differential defects at early developmental stages. We firstly examined strength of evoked synaptic transmission at cortico-striatal synapses by performing field recordings in dorsolateral striatum from acute brain slices at postnatal day 14 (P14). We found that InsG3680G+/+ mice have reduced corticostriatal transmission at postnatal day 14 (P14). Two-way ANOVA showed a main effect of genotype ($F(1,176)= 7.92$, $p= 0.0101$) and Bonferroni post hoc tests revealed significant difference between fields at stimulus 0.2-0.4mA (Figure 4.3 A,B). In contrast, no difference was found between R1117X+/+ mice and their wild type littermate controls (Figure 4.3 D,E). Presynaptic function seems unaffected, as indicated by the relationship of stimulation intensity to amplitude of the negative peak 1 (NP1; no difference between wild type, InsG3680+/+ and R1117X+/+ mutations) (Figure 4.3 C,F). We further measured the ratio of evoked AMPA to NMDA current by whole-cell patch clamping recordings of dorsolateral striatal medium spiny neurons (MSNs). Consistent with the pop spike results, we found significant reduction of AMPA/NMDA ratio in InsG3680+/+ mice (Figure 4.3 G) but not in R1117X+/+ mice (Figure 4.3 H). However, no change of miniature EPSCs frequency was detected from both mutants as compared to their wild type (Fig 4.4). These results suggest an increased number of silent synapses in InsG3680+/+ mice. Interestingly, we observed a small increase of mEPSC amplitude in InsG3680+/+ mutation only (Fig 4.4), suggesting potential compensatory effects from remaining functional synapses. Together, these data indicate that mice with ASD-linked InsG3680 mutation, but not with schizophrenia-linked R1117X mutation, show defective synaptic transmission at early postnatal age.

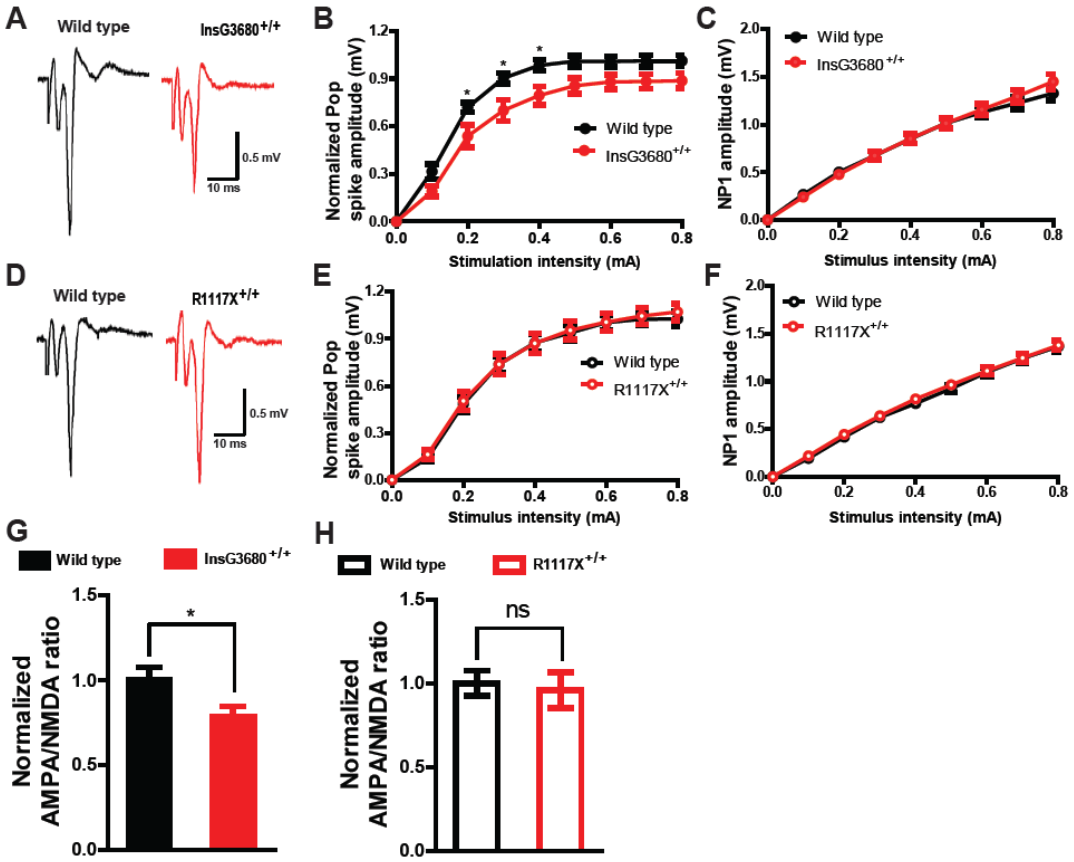

Figure 4.3 | InsG3680 but not R1117X mice display impaired striatal synaptic transmission at P14.

A and **D**) Representative cortico-striatal pop spike traces recorded from mice with indicated genotype. **B** and **C**) Cortical-striatal input-output curve show reduced pop spike responses in InsG3680+/+ mice compared to wild type littermates. NP1 amplitude is similar between the genotypes, suggesting presynaptic input is not different. **E** and **F**) Cortical-striatal input-output curve show similar pop spike responses and NP1 amplitude between R1117X+/+ mice and their wild type littermates. In (B, C, E and F) Data are presented as mean ± SEM. * $P < 0.05$; two-way ANOVA repeated measures with Bonferroni post hoc test. n= 12 slices from 4 pairs of littermates for each genotype. **(G and H)** AMPA/NMDA current ratio is reduced in InsG3680+/+ mice, but not R1117X+/+ mice, compared to their wild type littermates. * $P < 0.05$; two tail t-test. In (G), n= 18 neurons for WT; n= 19 neurons for InsG3680+/+ from 3 pairs of littermates; In (H), n= 16 neurons for WT; n= 15 neurons for R1117X+/+ from 3 pairs of littermates.

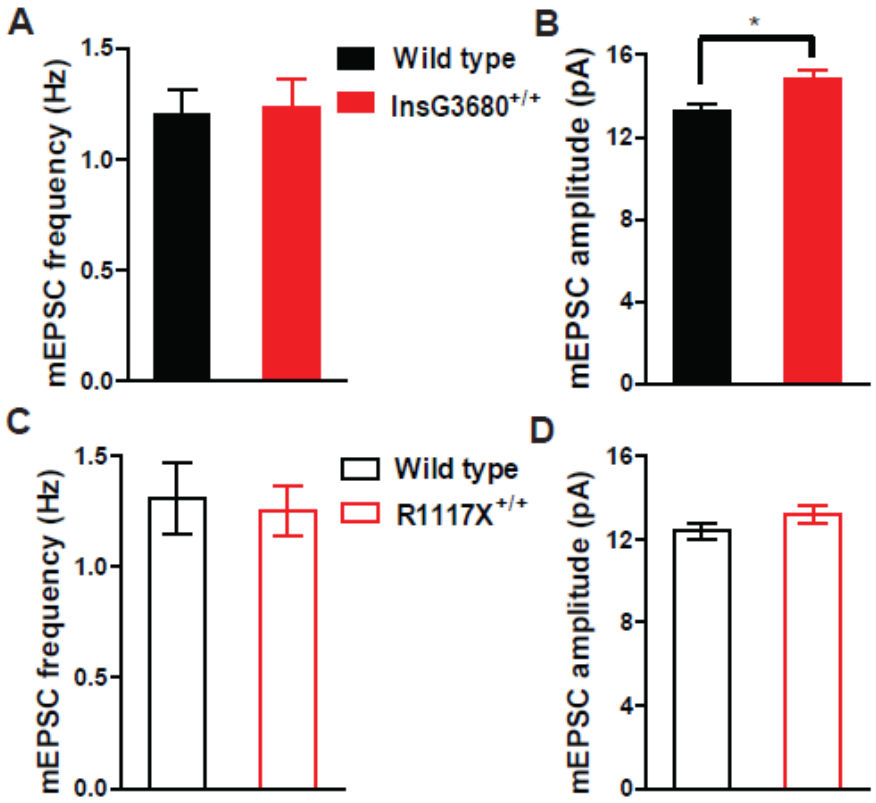

Figure 4.4 | Miniature EPSC recordings from R1117X and InsG3680 mutants at P14. **A** and **B**) mEPSC amplitude, but not frequency, of striatal MSNs is increased in InsG3680+/+ mice compared to their wild type littermates. n= 29 neurons for WT; n= 29 neurons for InsG3680+/+ from three pairs of littermate mice. **C** and **D**) No significant difference in mEPSC frequency and amplitude of striatal MSNs between R1117X+/+ mice and their wild type littermates. n= 30 neurons for WT; n= 31 neurons for R1117X+/+ from three pairs of littermate mice. In (A-D) Data are presented as mean ± SEM. * $P < 0.05$; two-tailed student t-test.

4.3.3 Reduced striatal synaptic transmission in both adult mutant lines

Although *Shank3* is expressed in many brain regions including striatum, cortex, hippocampus and cerebellum, it is the only member of the Shank family that is enriched in striatum. Our previous studies of young adult homozygous *Shank3*B knockout mice revealed significant synaptic defects in MSNs of the striatum including reduced pop spike responses by field recordings and reduced frequency and amplitude of miniature excitatory postsynaptic current (mEPSC) by

whole cell recordings[59]. Here we compared the effects of InsG3680 and R1117X mutations on striatal synaptic function using electrophysiological recording on acutely isolated brain slices. We first measured the cortico-striatal pop spike responses in dorsal lateral striatum by stimulating the inner border of corpus callosum. We found both InsG3680 and R1117X homozygous but not heterozygous mice showed reduced pop spike responses (Figure 4.5 A,B,D,E). No differences of presynaptic function were observed among all genotypes as indicated by similar NP1 response among genotypes (Figure 4.5 C and 4.5 F).

We further measured the AMPA receptor-mediated mEPSCs by performing whole-cell patch clamping recordings on dorsolateral striatal MSNs. We found that MSNs of both InsG3680 homozygous and heterozygous mice showed significant reduction of mEPSC frequency with homozygous mice only reach 45 % level of WT controls (2.79 ± 0.22 for wild type vs 1.26 ± 0.16 for InsG3680+/+; Figure 4.5 G,H). This reduction of mEPSC frequency was also observed in R1117X homozygous mice which reach 65 % level of WT controls (2.82 ± 0.24 for wild type vs 1.81 ± 0.21 for R1117X+/+; Figure 4.5 J,K). There is also a small but statistically significant reduction of mEPSC amplitude in MSNs from InsG3680+/+ and R1117X+/+ homozygous as well as R1117X+/- mice (Figure 4.5 I and L). Together, these results suggest that both InsG3680 and R1117X mutations cause significant synaptic dysfunction in the striatum, and InsG3680+/+ mutant mice may have more profound deficits in striatal synaptic transmission than R1117X+/+ mutant mice.

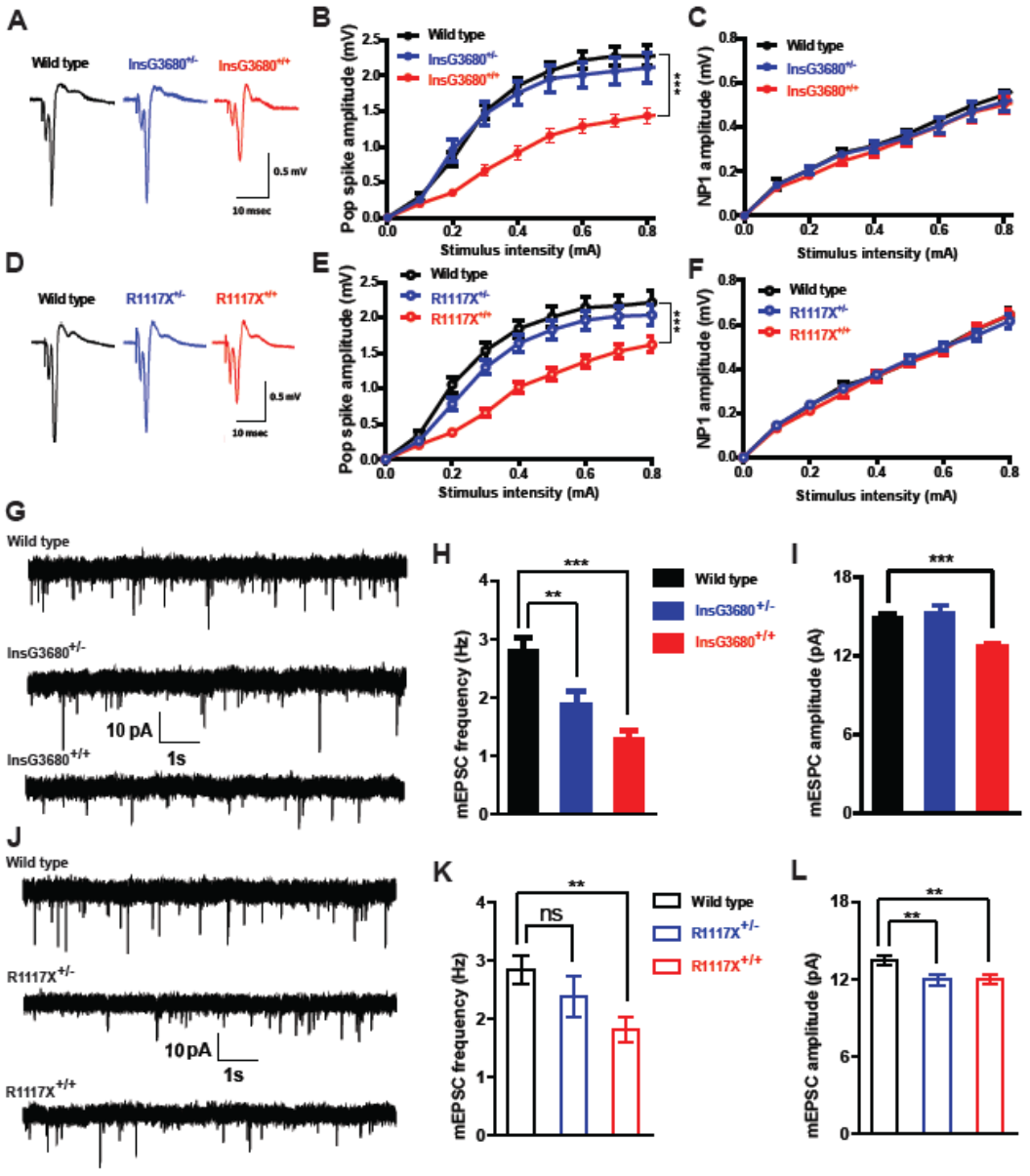

Figure 4.5 | Striatal synaptic transmission is reduced in adult R1117X and InsG3680 mutant mice.

A and **D**) Representative cortical-striatal pop spike traces from mice with indicated genotype. **B** and **E**) Reduced striatal pop spike amplitude in both InsG3680+/+ and R1117X+/+ mice. **C** and **F**) No difference of NP1 amplitude among genotypes. In (B, C, E and F) Data are presented as mean ± SEM. *** $P < 0.001$; two-way ANOVA repeated measures with Bonferroni post hoc test. n= 12 slices per genotype from 4 pairs of mice. **G** and **J**) Typical AMPA receptor mediated mEPSC traces recorded from MSNs with indicated genotype. **H** and **I**) mEPSC frequency of MSNs is reduced in both homozygous and heterozygous InsG3680 mutant mice compared to wild type littermates. mEPSC

amplitude is also reduced in heterozygous InsG3680 mutant mice. n= 26 neurons for WT; n= 24 neurons for InsG3680+/-; n= 21 neurons for InsG3680+/+ from three pairs of mice. **K** and **L**) mEPSC frequency of MSNs is reduced in homozygous R1117X mutant mice compared to wild type littermates. mEPSC amplitude is reduced in both homozygous and heterozygous R1117X mutant mice. n= 23 neurons for WT; n= 24 neurons for R1117X+/-; n= 26 neurons for R1117X+/+ from three pairs of mice. In (H, I, K, L), Data are presented as mean ± SEM. * P < 0.05, ** P < 0.01, *** P < 0.001; two-tailed t-test.

4.3.4 Distinct alteration of synaptic transmission in prefrontal cortex of R1117X mutant mice

Although pathological mechanisms of schizophrenia are still not known, numerous patient studies have implicated the dysfunction of prefrontal cortex (PFC), in particular dorsolateral prefrontal cortex (dlPFC) as an important pathogenic source in patients[12,206,243]. Medial prefrontal cortex (mPFC) in rodents have been found to execute some equivalent functions of primate dlPFC at a rudimentary level[244], such as working memory, decision making and social interaction[245–247]. We measured synaptic transmission in deep layer pyramidal neurons from prelimbic sub-region of the mPFC in acutely prepared coronal brain slices. We found significant reduction of mEPSC frequency in pyramidal neurons of mPFC in both R1117X+/- and R1117X+/+ mutant mice (Figure 4.6 A and B). In addition, we observed a significant reduction of mEPSC amplitude in R1117X+/+ mice (Figure 4.6 C). In contrast, no significant differences of either frequency or amplitude of mEPSC were found in InsG3680+/- or InsG3680+/+ mutant mice when compared to WT controls (Figure 4.6 D-F), although there is a trend of reduction in mEPSC frequency in InsG3680+/+ mutant mice. These results indicate that R1117X mutation, but not InsG3680 mutation, cause profound deficit of synaptic transmission in mPFC.

One of the pathological findings in postmortem brains of schizophrenia patients is the reduction of spine density of layer 3 pyramidal neurons in the prefrontal cortex[248]. To examine whether a similar defect exist in the two lines of *Shank3* mutant mice, we used Golgi staining to measure the spine density of layer 2/3 pyramidal neurons in the frontal association area. We found a significant reduction of spine density in both R1117X heterozygous and homozygous mutant

mice (Figure 4.6 G and I). We also found a significant reduction of spine density in InsG3680 homozygous but not heterozygous mutant mice (Figure 4.6 H and J).

All three SHANK family members are highly homologous and expressed in the cortex[59,143,249,250]. It has also been reported that SHANK3 was up-regulated in SHANK2 knockout mice[131]. Thus, it is possible that SHANK1 and 2 may be up-regulated in SHANK3 mutants to compensate for the loss of SHANK3. To explore this possibility, we quantified the expression level of Shank1 and Shank2 mRNA in the cortex of InsG3680+/+ and R1117X+/+ mutant mice. We found both Shank1 and Shank2 mRNAs were significantly up-regulated in InsG3680+/+ but not R1117X+/+ mutant mice (Figure 4.6 K and L), suggesting the two mutations have differential effects on *Shank1* and *Shank2* mRNA up-regulation. Furthermore, we did not observe up-regulation of Shank1 or Shank2 mRNA in the striatum of either mutant line (Fig 4.7). Together, these results suggest that selective up-regulation of *Shank1* and *Shank2* in the cortex of InsG3680+/+ mutant mice may partially compensate for the loss of *Shank3*, and thus alleviating synaptic defects in mPFC of InsG3680+/+ mutant mice.

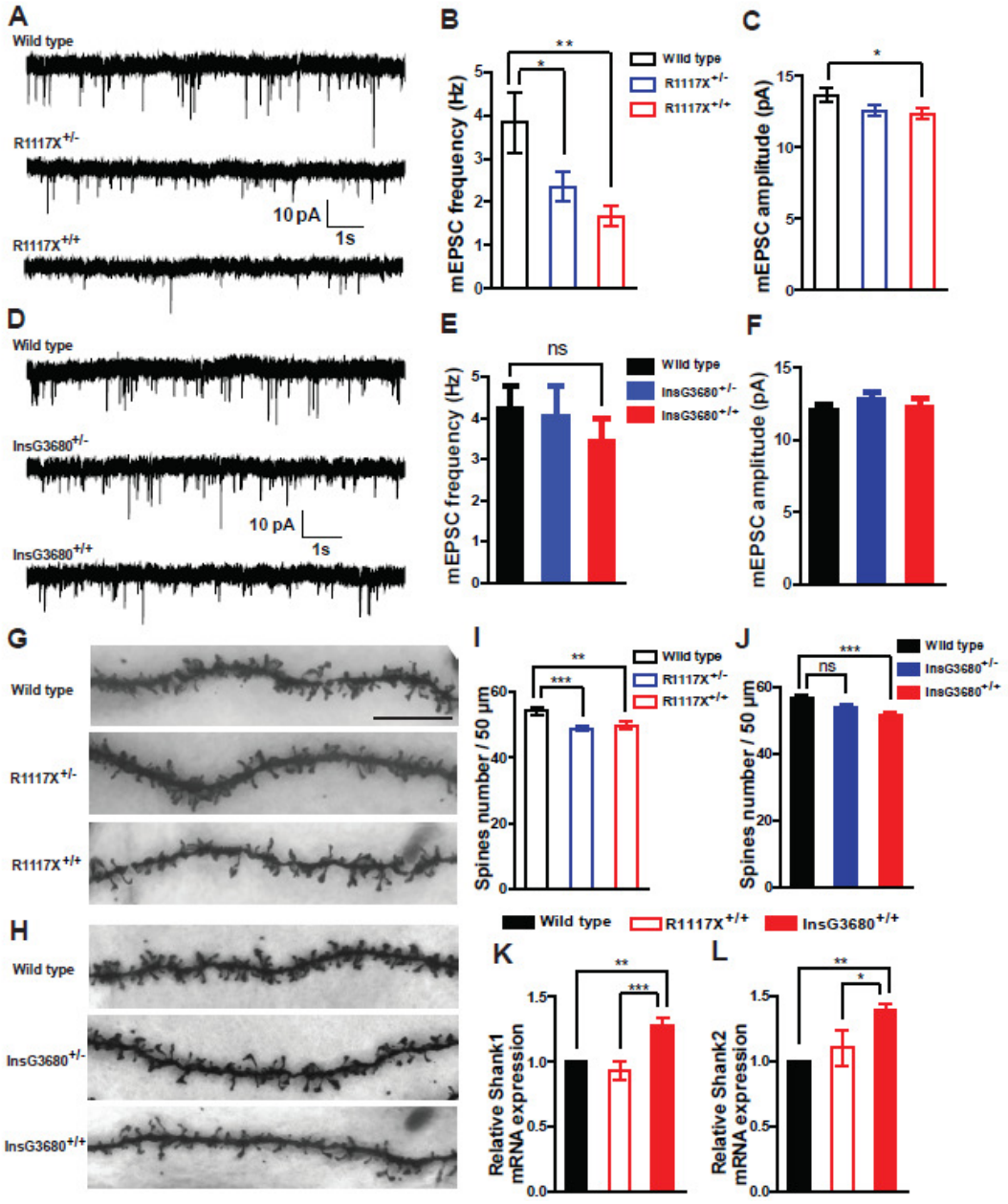

Figure 4.6 | Profound cortical synaptic defects manifest in mice carrying the schizophrenia-associated R1117X mutation.

A-**C**) Typical AMPA receptor mediated mEPSC recordings in the prefrontal cortex and statistical results for R1117X mice. n= 13 neurons for WT; n= 20 neurons for R1117X+/-; n= 18 neurons for R1117X+/+ from three pairs of mice. Note the highly significant reduction in mEPSC frequency in heterozygous and homozygous mice and a modest reduction in amplitude. **D**-**F**) Typical AMPA receptor mediated mEPSC recordings in the prefrontal cortex and statistical results for InsG3680 cohort. n= 18 neurons for WT; n= 16 neurons for InsG3680+/-; n= 17 neurons for InsG3680+/+ from three pairs of mice. Both

heterozygous and homozygous mice display comparable miniature events to wild type mice. In (B, C, E and F) Data are presented as mean ± SEM. * P < 0.05, ** P < 0.01; two-tailed t-test. (G and H) Representative confocal images of secondary dendrites of pyramidal neurons from frontal association area of mice with indicated genotypes (scale bar: 10 µm). (I and J) Quantification of spine number from neurons with indicated genotypes from three littermate pairs indicates reduced spine numbers in R1117X+/-, R1117X+/+ and InsG3680+/+ mice. (K and L) mRNAs of *Shank3* homologues *Shank1* and *Shank2* are up-regulated in cortical tissue from InsG3680 compared to wild type mice. Data are normalized to Gapdh mRNA, and presented as mean ± SEM. WT mice (n= 5), R1117X+/+ mice (n= 5) and InsG3680+/+ mice (n= 5). In (I, J, K and L) * P < 0.05, ** P < 0.01, ** P < 0.001; one-way ANOVA with Bonferroni post hoc test.

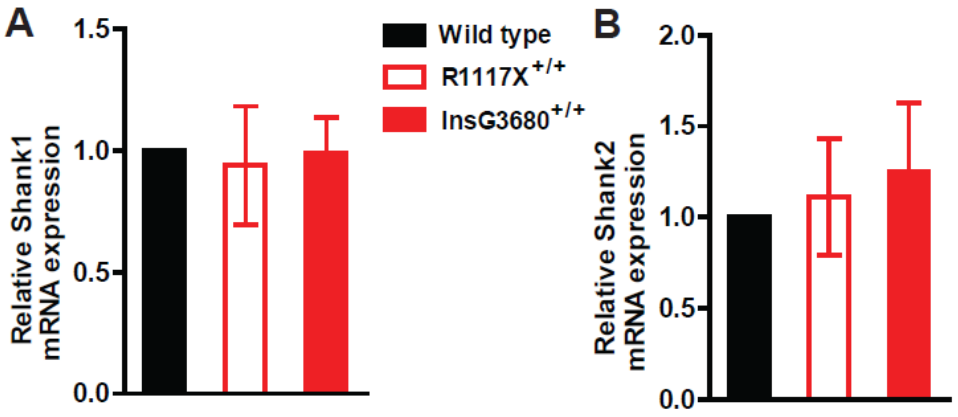

Figure 4.7 | No upregulation of Shank1 and Shank2 mRNA in the striatum.

A and **B**) Relative level of Shank1 and Shank2 mRNA in striatum from indicated genotypes. Data are normalized to Gapdh mRNA, and presented as mean ± SEM. WT mice (n= 5), R1117X+/+ mice (n= 5) and InsG3680+/+ mice (n= 5); one-way ANOVA with Bonferroni post hoc test.

4.3.5 Alteration of PSD composition in R1117X and InsG3680 mutant mice

Shank family proteins, together with PSD95 family proteins and SAPAP family proteins, form the PSD95-SAPAP-Shank scaffolding complex at the excitatory postsynaptic site[147,194,228]. This complex has been proposed to play important roles in the trafficking, assembly and anchoring of signaling proteins to the PSD as well as regulating the dynamic plasticity of PSD[251,252]. Our previous studies showed that several scaffolding proteins and glutamate receptor subunits were reduced in the striatal PSD of *Shank3*B knockout mice[59]. Here we examined levels of several scaffolding and signaling proteins as well as glutamate receptor subunits in the synaptic membrane fraction (SPM) of InsG3680+/+ and R1117X+/+ mutant mice. SPM containing enriched synaptic proteins were purified in parallel from age and gender matched animals and probed with antibodies detecting scaffolds and receptors of PSD proteins (Experimental procedure and Supplemental Table 4.1). In SPM preparation from striatal tissue, we found that Homer1b/c is dramatically reduced in both InsG3680+/+ and R1117X+/+ mutant mice (~14 % of WT; Figure 4.5A and B). This is consistent with the fact that Homer binding domain is located downstream of the premature stop codons caused by InsG3680 and R1117X mutation[228,253]. SynGAP1, NR1 and NR2B are also significantly reduced in both mutant mice (Figure 4.8 A-C).

Interestingly, we found statistically significant reduction of SAPAP3, NR2A, GluR2 and mGluR5 in InsG3680+/+ but not R1117X+/+ mutant mice (Figure 4.8 A-C). Conversely, we found PSD95 reduction only in R1117X mutant mice (Figure 4.8 A, B). These data are consistent with our electrophysiological results showing striatal synaptic defects in both mutant lines that are more severe in InsG3680+/+ mutant mice than in R1117X+/+ mutant mice.

We also examined alterations of PSD protein composition in the cortex. We found that Homer1b/c, PSD 95 and PSD 93 were significantly reduced in both InsG3680+/+ and R1117X+/+ mutant mice as compared to WT controls (Figure 4.8 D and E). Interestingly, the level of Homer1b/c reduction is more dramatic in R1117X+/+ mutant mice than in InsG3680+/+ mice (Figure 4.8 E). In addition, we observed significant reduction of NR1 and its close interacting partner SynGAP1 only in the R1117X+/+ mutant mice (Figure 4.8 D-F), in line with previous findings using postmortem cortex tissue from schizophrenia patients[254,255]. Together, our biochemistry results are consistent with our electrophysiological findings that indicate more severe cortical synaptic defects in R1117X mice than in InsG3680 mutant mice.

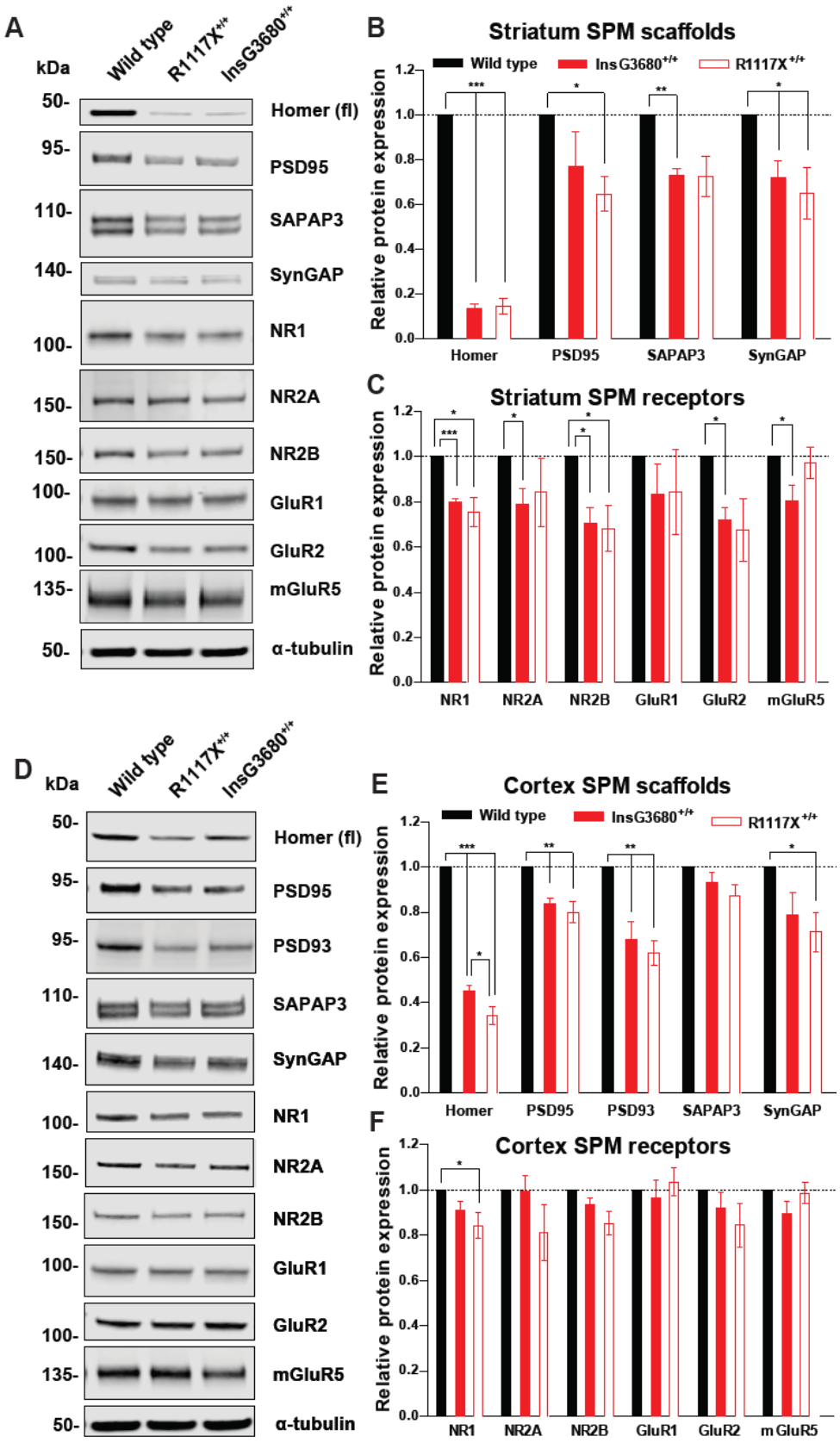
A
kDa
Wild type
R1117X+/+
InsG3680+/+
50-
Homer (fl)
95-
PSD95
110-
SAPAP3
140-
SynGAP
100-
NR1
150-
NR2A
150-
NR2B
100-
GluR1
100-
GluR2
135-
mGluR5
50-
α-tubulin
B
Striatum SPM scaffolds
Wild type
InsG3680+/+
R1117X+/+
Relative protein expression
Homer
PSD95
SAPAP3
SynGAP
C
Striatum SPM receptors
NR1
NR2A
NR2B
GluR1
GluR2
mGluR5
D
kDa
Wild type
R1117X+/+
InsG3680+/+
50-
Homer (fl)
95-
PSD95
95-
PSD93
110-
SAPAP3
140-
SynGAP
100-
NR1
150-
NR2A
150-
NR2B
100-
GluR1
100-
GluR2
135-
mGluR5
50-
α-tubulin
E
Cortex SPM scaffolds
Wild type
InsG3680+/+
R1117X+/+
Relative protein expression
Homer
PSD95
PSD93
SAPAP3
SynGAP
F
Cortex SPM receptors
NR1
NR2A
NR2B
GluR1
GluR2
mGluR5

Figure 4.8 | InsG3680 and R1117X mutant mice display common and distinct disruptions of post-synaptic signaling complexes.

(A) Representative blots for proteins detected by specific antibodies in the striatal SPM fraction from wild type, InsG3680+/+ and R1117X+/+ mice. (B and C) Quantification of relative levels of proteins as normalized to tubulin protein expression from striatal SPM. (n= 4-6 samples per protein per genotype, each n being pooled tissue from three mice). (D) Representative blots for proteins detected by specific antibodies in the cortical SPM fraction from wild type, InsG3680+/+ and R1117X+/+ mice. (E and F) Quantification of relative levels of proteins as normalized to tubulin protein expression from cortex SPM. (n= 4-11 samples per protein per genotype, each n being pooled tissue from two mice). In (B, C, E and F) Data are presented as mean ± SEM. * $P < 0.05$, ** $P < 0.01$, ** $P < 0.001$; one sample t-test.

4.3.6 InsG3680 and R1117X mutant mice show both common and distinct behavioral phenotypes

Previous studies of various *Shank3* knockout mice revealed ASD-related behavioral phenotypes including anxiety, repetitive/compulsive behavior and social interaction deficits[59,129,133]. As described above, our molecular and electrophysiological studies of InsG3680 and R1117X mutant mice showed that they have both shared and distinct synaptic defects. We next tested whether these synaptic defects are accompanied by behavioral changes. We first tested their explorative behavior in an open field arena. We found that both R1117X+/+ and InsG3680+/+ mice explored the arena (total distance) much less compared to WT controls (Figure 4.9 A and B). In addition, InsG3680+/- mice also showed significantly reduced exploration (Figure 4.9 A). We next evaluated anxiety-like behavior using elevated zero maze test. Consistent with reduced explorative behavior, we found both R1117X+/+ and InsG3680+/+ mice spent much less time in the open arms as compared to their wild type littermates (Figure 4.9 C and D). In addition, heterozygous mutants from both lines also spent less time in the open arms as compared to their wild type littermates (Figure 4.9 C and D). These results strongly suggest both R1117X and InsG3680G mutant mice exhibit increased levels of anxiety.

Since impaired social interaction is one of the core features of ASD patients and social withdraw is a characteristic negative symptom in schizophrenia patients[205,207], we tested social interactions of R1117X and

InsG3680 mutant mice with slightly modified standard three chamber social interaction paradigm[201,256]. We counterbalanced the object side (O) and social side (S1) for each mouse, no side preference in specific chamber was observed for any genotypes in the habituation stage in the absence of object and mice (Fig 4.11). As expected, wild type mice showed significant preference for strange mouse (S1) to a novel object (O) (Figure 4.9 E). However, both InsG3680 and R1117X homozygous mutant mice showed no significant preference for other mice compared to novel object side (Figure 4.9 E and F). Interesting, heterozygous R1117X mutant mice, but not heterozygous InG3680 mutant mice, also displayed social interaction deficits (Figure 4.9 E and F). Similarly, in social novelty test, both homozygous and heterozygous R1117X mutant mice exhibited deficits while only homozygous InsG3680 mutant mice showed the defect (Figure 4.9 G and H). Together, these results demonstrated that both InsG3680 mutation and R1117X mutation lead to social interaction deficits, similar to *Shank3* mutant mice with deletion of the ankyrin repeats or PDZ domain[59,129].

Repetitive behavior/restricted interest is another key feature of ASD. Several mouse models of psychiatric disorders including ASD, OCD and Tourette syndrome show repetitive grooming phenotypes and some of them develop skin lesions due to overgrowing[58,59,76,98,198]. These repetitive/compulsive-like behaviors have been strongly linked to cortico-striatal-thalamo-cortical circuitry dysfunction[58,59,73,76,81,257,258(appendix)]. In our breeding colony, we found that 28.1 % of InsG3680 homozygous mutant mice develop skin lesions at the age between four to six months (Figure. 4.10 A), a similar rate to our previous finding in *Shank3*B knockout mice[59]. In contrast, only, 8.7 % R1117X+/+ homozygous mutant mice developed skin lesions at the same age. No skin lesions were found in R1117X+/-, InsG3680+/- and wild type groups. We next quantified the percentage of time R1117X and InsG3680 mice spending on grooming during a two-hour session. We found that InsG3680+/+ mice spend twice as much time on grooming when compared to their WT littermates (Figure 4.10 B). In contrast, R1117X+/+ mice did not show statistically significant increase in grooming time compared to their WT littermates (Figure 4.10 C), although a trend of increase was observed. These results suggest that only InsG3680+/+ mice show robust repetitive/compulsive grooming behavior. This is consistent with our molecular and electrophysiological results indicating more severe disruption of striatal synaptic function in InsG3680 mutant mice.

In our R1117X+/- x WT mating cages, we frequently observed partial or complete facial hair loss of WT mice without any lesions, suggesting

allogrooming/barbering by R1117X+/- mice (Figure 4.10 D). We confirmed that loss of whisker and facial hair was caused by allogrooming by a cage mate instead of self-grooming by separating the mating pairs with the phenotype. We observed nearly full regrowth of facial hairs after weeks of single housing. Furthermore, pairing the recovered animals with their original cagemates induced robust loss of whisker and facial hair again within two weeks (data not shown). This allogrooming/barbering phenotype also happened in R1117X+/- x R1117X+/- mating cages, in which one of the R1117X+/- mice and/or offspring would lose their facial hairs. We observed allogrooming/barbering in 48 % mating cages with R1117X+/- mice. In contrast, we only observed allogrooming/barbering phenotype in 14 % mating cages with InsG3680+/- mice. These results suggest that R1117X and InsG3680 mutations have differential effects on the expression of social dominance/aggression phenotype.

Previous studies in rodents have implicated the impairment of PFC function in social dominance and aggression[245]. Our electrophysiological findings from mPFC indicated that both R1117X+/- and R1117X+/+ have profound deficits of synaptic transmission. To further evaluate the social dominance/aggression phenotype, we performed standard tube test (Figure 4.10 E) between wild type versus heterozygous and wild type versus homozygous mice in two mutant lines. When the two stranger mice meet in the middle of the tube, the dominant/aggressive mouse will advance and drive the other mouse out of the tube[245]. We found both R1117X+/+ and R1117X+/- mice show much higher probability of winning the matches when tested with their wild type opponents (Figure 4.10 F). We also observed a significantly increased winning percentage in InsG3680+/+ but not in InsG3680+/- mice against their wild type opponents (Figure 4.10 G). These results are consistent with our electrophysiological and morphological findings in the prefrontal cortex showing synaptic deficits in both heterozygous and homozygous mice with R1117X mutation but only in homozygous mice with InsG3680 mutation.

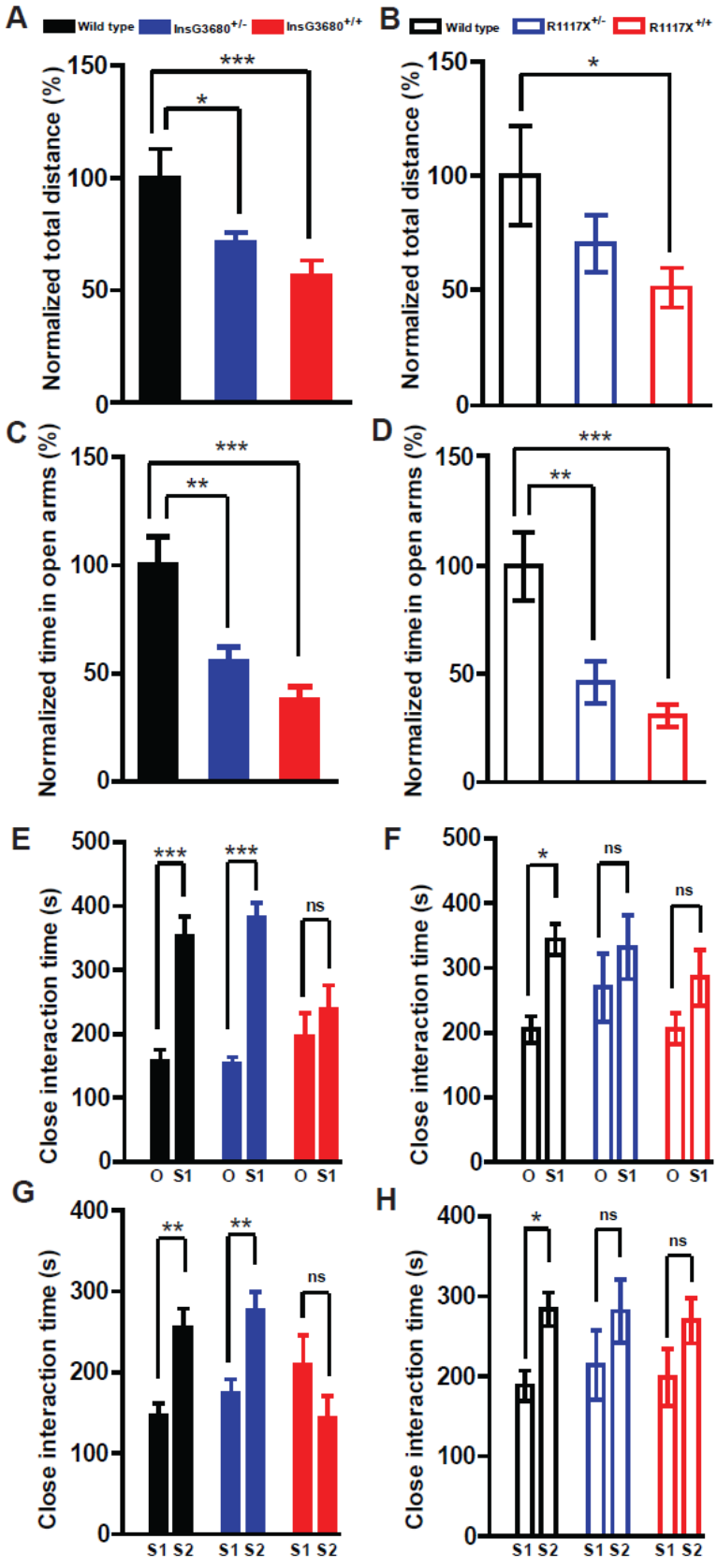
A
Wild type
InsG3680+/-
InsG3680+/+
Normalized total distance (%)
150
100
50
0
***
*
B
Wild type
R1117X+/-
R1117X+/+
Normalized total distance (%)
*
C
Normalized time in open arms (%)
***
**
D
Normalized time in open arms (%)
***
**
E
Close interaction time (s)
500
400
300
200
100
0
***
***
ns
O S1 O S1 O S1
F
Close interaction time (s)
*
ns
ns
O S1 O S1 O S1
G
Close interaction time (s)
400
300
200
100
0
**
**
ns
S1 S2 S1 S2 S1 S2
H
Close interaction time (s)
*
ns
ns
S1 S2 S1 S2 S1 S2

Figure 4.9 | InsG3680 and R1117X mutant mice display anxiety behavior and social interaction deficits.

A and **B**) Total distance travelled in the open field test as normalized to wild type littermates. **C** and **D**) Time spend in the open arms in the elevated zero maze test as normalized to wild type littermates. In the InsG3680 cohort, n= 17 mice for wild type; n= 19 mice for InsG3680+/-; n= 18 mice for InsG3680+/+ group. In the R1117X cohort, n= 15 mice for wild type, n= 15 mice for R1117X+/-; n= 15 mice for R1117X+/+. **E** and **F**) Time spend on close interaction with an object (O) vs stranger mice (S1) in the phase II social interaction test. (G and H) Time spend on close interaction with a familiar mouse (S1) vs stranger mouse (S2) in the phase III social interaction test. In the InsG3680 cohort, n= 17 mice for wild type; n= 19 mice for InsG3680+/-; n= 18 mice for InsG3680+/+ group; in the R1117X cohort, n= 23 for wild type, n= 25 for R1117X+/-; n = 24 for R1117X+/+ group; In all the panels, data are presented as mean ± SEM, * $P < 0.05$, ** $P < 0.01$, *** $P < 0.001$; one-way ANOVA with Bonferroni post hoc test.

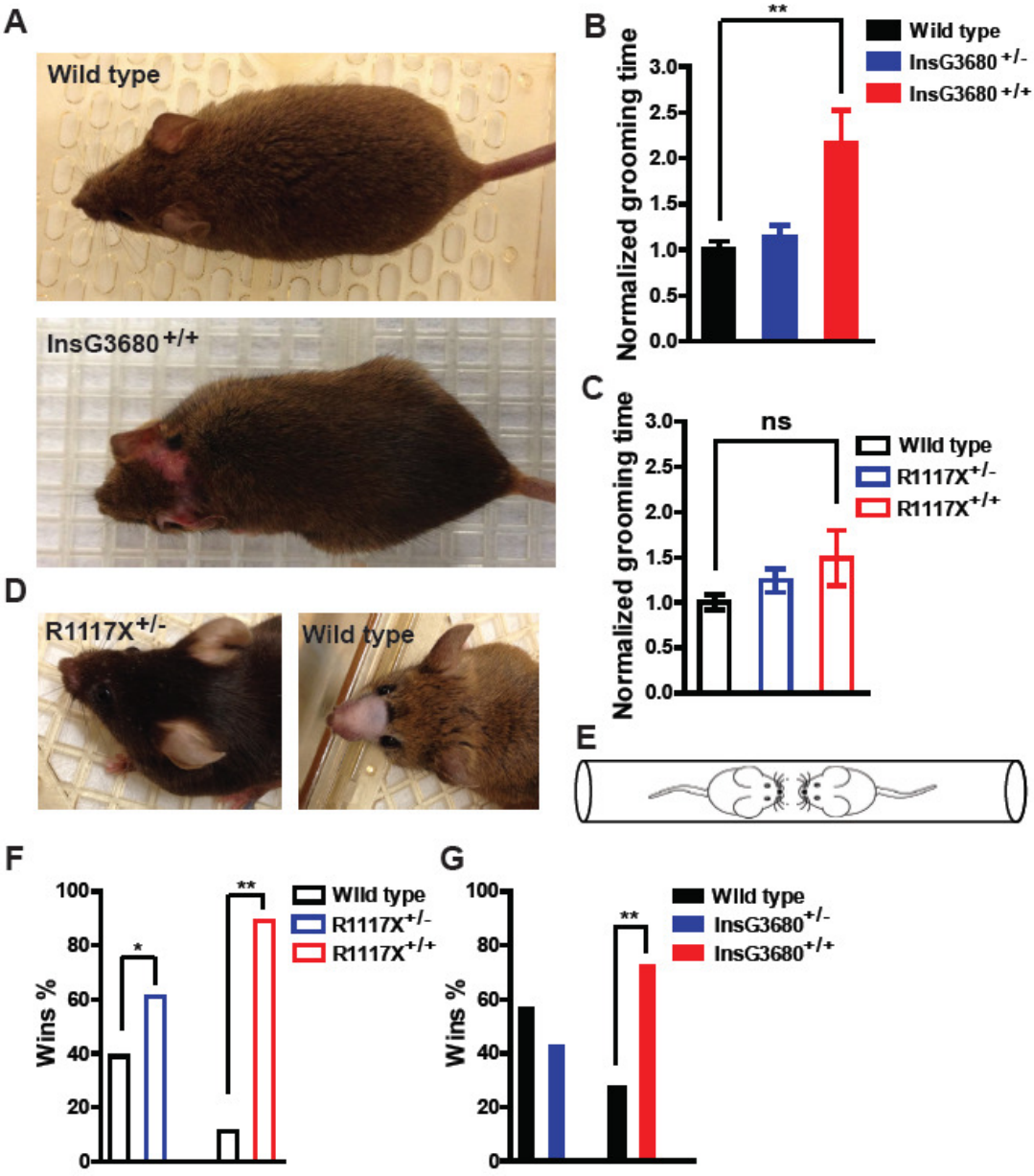

Figure 4.10 | InsG3680 mice show more profound repetitive self-grooming, whereas R1117X mice display allogrooming and aggressive behavior.

A) Representative pictures from an adult wild type and an InsG3680+/+ mouse that developed a lesion in the head/neck area. **B** and **C**) Time spend on grooming during 2 h videotaping of indicated genotypes as normalized to their wild type littermates. In the InsG3680 cohort, n= 9 mice for wild type; n= 9 mice for InsG3680+/-; n= 10 mice from InsG3680+/+ group. In the R1117X cohort, n= 9 mice for wild type, n= 9 mice for R1117X+/-; n= 9 mice for R1117X+/+. Data are presented as mean ± SEM. ** $P < 0.01$; one-way ANOVA with Bonferroni post hoc test. **D**) Representative pictures of an R1117X+/- mouse with intact facial hair and a wild type mouse shaved by its cage mate

as an indication for dominant/aggressive behavior. **E**) Diagram of tube test task between two unfamiliar mice with different genotypes. **F** and **G**) Percentage of wins in test pairs between indicated genotypes, 11/18 (61 %) of R1117X+/- vs WT; 16/18 (89 %) of R1117X+/+ vs WT; 6/14 (43 %) of InsG3680+/- vs WT; 8/11 (73 %) of InsG3680+/+ vs WT. Note that both R1117X+/- and R1117X+/+ mice perform significantly above chance level. One-sample chi-squared test was used to determine the significant difference. * indicate significantly different from an expected chance (50:50 win-lose outcome).

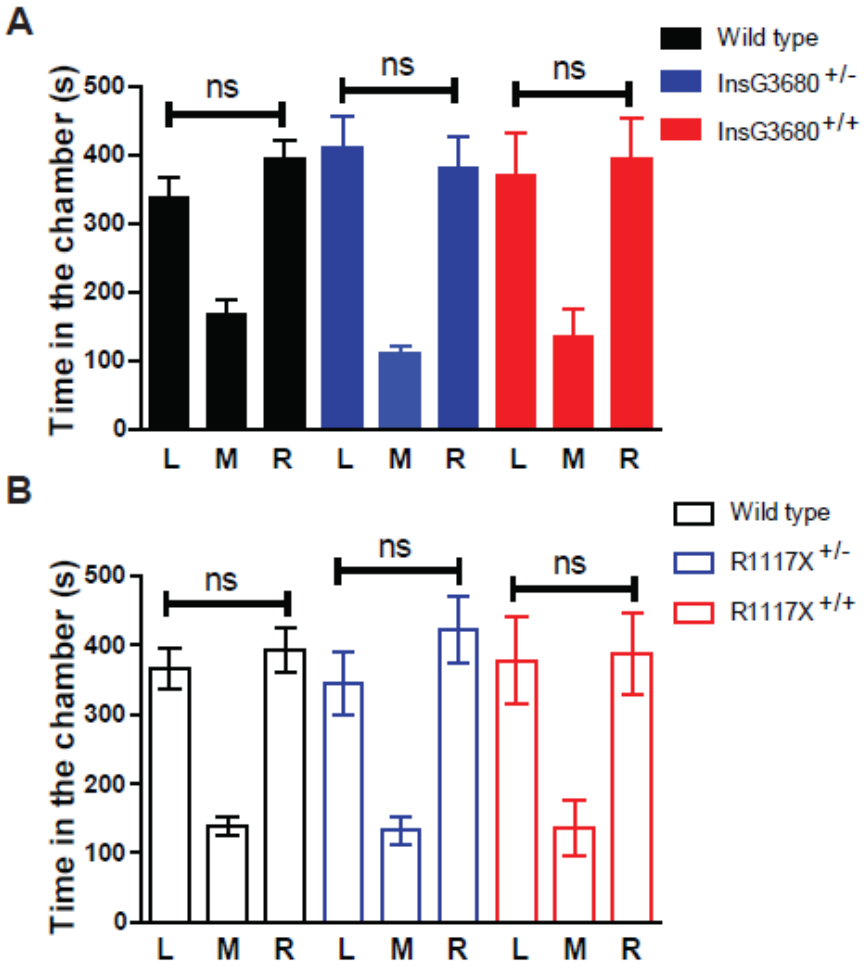

Figure 4.11 | No chamber preference during the habituation phase of social interaction test.

A and **B**) Time spend inside each chamber, left (L); middle (M); right (R). In the InsG3680 cohort, n= 17 mice for WT; n= 19 mice for InsG3680+/-; n= 18 mice for InsG3680+/+ group; in the R1117X cohort, n= 23 for WT; n= 25 for R1117X+/-; n= 24 for R1117X+/+ group. Data are presented as mean ± SEM; one-way ANOVA with Bonferroni post hoc test.

4.4 Discussion

Although schizophrenia and autism are two distinct disorders based on phenomenological diagnosis (DSM-5), it has long been recognized that they share some common features and comorbidity[204,259]. This is particularly true between child onset schizophrenia and autism[260,261]. For example, in a recent study, out of 46 schizophrenia patients with normal intelligence, about 50 % met the diagnostic criteria of ASD[262]. Recent human genetic studies have provided strong biological support for these clinical findings. GWAS, CNV and exome sequencing have all identified many of the same genes in both disorders[220,263]. One such group of shared risk genes encodes proteins important for synaptic development, function and plasticity[212,214,217,222]. Despite strong clinical and genetic evidences, however, it is not clear how different mutations of the same gene may contribute to different disorders. In this study, we generated new mouse models that harbor the highly penetrant *Shank3* mutations found in ASD and schizophrenia patients. Our study revealed both distinct and shared defects in the two lines of mutant mice at molecular, synaptic, circuit and behavioral levels. Our results may provide, for the first time, some neurobiological insights on how different mutations in the *Shank3* gene may lead to mutation-specific defects and relevant behavior abnormalities.

Early developmental defects in mice with ASD-associated mutation

One of the interesting findings is that mice with ASD-associated InsG3680 mutation exhibit earlier synaptic defects as compared with SCZ-associated R1117X mutation. We found a reduction of population spike responses and AMPA/NMDA ratio in P14 InsG3680+/+ mutant mice, indicating defects in evoked synaptic transmission. The lack of obvious presynaptic defects suggests that there are fewer functional synapses in these mutant mice. Interestingly, we found a surprising increase of mEPSC amplitude in striatal MSNs of P14 InsG3680+/+ mutant mice, suggesting a potential compensatory mechanisms by the remaining functional synapses. On the other hand, no defects were identified in SCZ-associated R1117X mutant mice at P14. These early onset deficits of synaptic transmission observed in InsG3680 homozygous mice may provide a cellular mechanism for understanding the fact that ASD patients with *Shank3* mutations have much earlier onset time than SCZ patients with *Shank3* mutations.

SHANK3 expression dramatically increases in neonatal mouse brain and reaches peak level around three weeks postnatally, a period of time with massive synapse formation and maturation, consistent with its role in synaptic development and function. Our data shows that InsG3680 mutation leads to dramatically reduced level of mRNA and almost a complete loss of SHANK3 proteins, whereas R1117X mutation retains a significant amount of truncated SHANK3 protein. SHANK3 proteins contain multiple protein-interacting domains including ankyrin repeats, PDZ domain, SH3 domain, Homer interacting motif and SAM domain[143,225]. As a scaffolding protein, SHANK3 is likely to form multiple signaling complexes through these protein-interacting domains, probably with developmental stage and cell type specificity[139]. R1117X mutation would lead to a truncated protein without the Homer-interacting motif and SAM domain. Our data suggest that this truncated SHANK3 protein is, at least partially, functional in MSNs at early postnatal period. However, this is not the case in the adult cortex since we see dramatic synaptic and behavioral defects in adult R1117X mutant mice (see discussion below). These unique features of mutation-specific effects may provide some explanation on genetic overlaps of risk genes in various psychiatric disorders.

Distinct prefrontal cortex defects in R1117X mutant mice

Currently, the pathological mechanisms underlying schizophrenia are not well understood. However, clinical studies from human patients have implicated the dysfunction of prefrontal cortex (PFC), in particular dorsolateral prefrontal cortex (dlPFC), as an important cause of deficits in working memory, executive function and social impairment[12,206,243]. In addition, postmortem studies have revealed reduced numbers of dendritic spines in pyramidal neurons of dlPFC region from schizophrenia patients[248]. Rodents do not have an anatomically distinct dlPFC[8]. However, electrophysiological and behavioral studies suggest that medial prefrontal cortex (mPFC) in rodents may perform some equivalent functions of primate dlPFC at a rudimentary level[244], such as working memory, decision making and social interaction. Consistent with these findings, our study revealed profound synaptic transmission defects in mPFC of mice with SCZ-associated R1117X mutation, but not with ASD-associated InsG3680 mutation, indicating that these two mutations affect distinct circuits.

Since all three members of the Shank family genes are expressed in the cortex[59,194,249,250], it is possible that they may have functional redundancy to compensate the loss of other members. Very interestingly, we found that

upregulation of *Shank1* and *Shank2* happens only in the cortex of InsG3680 mutants but not in R1117X mutants. The upregulation of *Shank1* and *2* in the cortex of InsG3680 mutants may compensate for the loss of *Shank3* and thus alleviate synaptic defects. In addition, the truncated SHANK3 protein resulted from R1117X mutation may have a dominant-negative effect presumably by preventing full length Shank1 and/or Shank2 assembling into the postsynaptic signaling complex, further mitigating the potential compensation by Shank1 and Shank2 normally expressed in the cortex of R1117X mutants. Interestingly, Shank1 and Shank2 are normally not highly expressed in the striatum[59] and we did not observe up-regulation of Shank1 and Shank2 in the striatum of either mutant line. Thus up-regulation and compensation by Shank1 and Shank2 is not only mutation-specific, but also cell type/brain region-specific, adding another layer of complexity to the study of neurobiological mechanisms underlying genetic overlapping of psychiatric disorders.

Molecular changes in the PSD

Consistent with its role as a postsynaptic scaffolding protein demonstrated by previous studies[251,252], our analysis of the two new lines of *Shank3* mutants revealed many changes in the postsynaptic signaling complex. Most strikingly, we observed about 85 % reduction of Homer1b/c in striatal synaptic membrane preparations from both mutant lines when compared to wild type mice. This is consistent with the fact that both mutations would lead to truncated SHANK3 missing the Homer binding domain and indicates that synaptic localization of Homer1b/c largely depends on Shank. Previous studies of *Shank3* mutant mice with the PDZ domain deletion only showed a mild reduction of Homer1b/c, further supporting this notion[59]. Although Homer has been shown to directly interact with mGluR5[228], we only found a slight reduction of mGluR5 in the striatum of InsG3680 mutants and there is no change of mGluR5 level in R1117X mutants, strongly suggesting that synaptic localization of mGluR5 does not depend on its interaction with Homer1b/c.

Similar to electrophysiological findings, biochemical analysis of synapses also revealed mutation-specific and brain region-specific changes in addition to common defects. In the striatum, we found reduced levels of SAPAP3, NR2A, GluR2 and mGluR5 only in InsG3680 mutant and reduced PSD95 only in R1117X mutants, suggesting InsG3680 mutation leads to more disruption of postsynaptic signaling complex than R1117X mutation does in the striatum. In contrast, in the cortex, we found reduction of SynGAP1 and NR1 only in R1117X

mutants and no InsG3680-specific changes were observed, consistent with our finding of significant synaptic transmission defects found in R1117X mutants but not InsG3680 mutants in the prefrontal cortex.

Commonality and differences in behavioral phenotypes

Multiple *Shank3* knockout mice targeting different regions of the protein including ankyrin repeats and PDZ domain have been generated. These mutant mice show various degree of behavioral phenotypes relevant to ASD including anxiety, repetitive/compulsive behavior and social interaction deficits[59,129,133]. Consistent with these findings, mice with ASD-associated InsG3680 mutation showed anxiety-like behaviors, repetitive grooming leading to skin lesions and social deficits. Interestingly, mice with SCZ-associated R1117X mutation also show anxiety-like behavior and social deficits, suggesting there are common cellular and circuit defects shared by these two mutants.

One of the most common phenotypes in mouse models with mutations of ASD risk genes is the repetitive behavior and previous studies have strongly linked repetitive/compulsive behaviors to defects in cortico-striatal-thalamo-cortical (CSTC) circuits[58,59,76,81,258(appendix)]. Similar to our reported *Shank3*B knockout mice, the repetitive/compulsive grooming behavior in InsG3680 mutant mice are very robust. R1117X mutant mice do not show significant repetitive grooming behavior, although both mutant lines show striatal molecular and synaptic defects. There are several possible explanations of this phenotypic difference. First, both our electrophysiological and biochemical results suggest that striatal synaptic defects are more severe in InsG3680 mutants than in R1117X mutants which may partially contribute the behavioral difference. Second, striatum is only one part of the CSTC circuit and differential defects in other parts of the brain, such as cortex, may significantly affect the behavioral output. Third, recent studies have begun to reveal specific changes in subcircuits/microcircuits of the CSTC that may underlie repetitive behaviors and the two mutations may differentially affect these sub-circuits/micro-circuits. Further studies will be needed to identify the exact mechanisms.

A behavioral phenotype predominantly found in R1117X mutants is the social dominance and aggression behavior in heterozygous mice. In their home cage, they show strong social dominance by barbering/facial hair removal of cage mates. This happened much more often in R1117X mutant mice (48 % of mating cages) than in InsG3680 mutant mice (14 % of the cages). In the tube test of pairs of stranger mice for dominance/aggression, R1117X heterozygous mice

showed significant dominant/aggressive behavior over wild type mice while InsG3680 heterozygous mice did not show this behavior. Although the exact mechanisms/circuits involved in dominance/aggression behavior in mice are still not well understood, recent studies have provided evidence implicating mPFC, hypothalamus, and amygdala in social dominance and aggression[264,265]. Our studies demonstrated significant synaptic transmission defects in the mPFC of R1117X, but not InsG3680 mutant mice. Our biochemical studies also revealed more molecular disruptions of the synaptic signaling complex in the cortex with R1117X mutation than with InsG3680 mutation. These correlative data may provide partial explanation for the difference in social dominance/aggression behavior between these two mutant lines.

Previous studies in mice have demonstrated that two different mutations of the Mecp2 gene in Rett Syndrome patients differentially affect the function of a key domain in Mecp2 and result in different severity of phenotypes similar to disease progression and symptoms observed in patients with these two mutations[266]. Although it is difficult to directly correlate mouse behaviors with patient symptoms and diagnosis, our study at least provides neurobiological evidences and mechanisms that the two *Shank3* mutations associated with ASD and SCZ cause both common and distinct defects at molecular, synaptic and behavioral levels. More broadly, we demonstrated that different mutations of the same gene may elicit neurobiological changes at different developmental stages, brain regions and cell types through a variety of potential mechanisms including differential mRNA stability, differential regulation of compensatory gene expression and different degrees of signaling complex disruption.

4.5 Methods

Animal work statement: All animal related work was performed under the guidelines of Division of Comparative Medicine (DCM), with protocol (# 0513-044-16 of Feng laboratory and #1012-102-15 of Lewis laboratory) approved by Committee for Animal Care (CAC) of Massachusetts Institute of Technology, and was consistent with the Guide for Care and Use of Laboratory Animals, National Research Council 1996 (institutional animal welfare assurance no. A-3125-01). Only aged-matched male mice were used for all behavioral experiments, all other tests included age-matched males and females in proportional contribution across groups.

Generation and breeding of mutant mice: R1117X and InsG3680 *Shank3* mutant mice were generated by homologous recombination in R1 mouse ES cells and implanted in C57 blastocysts using standard procedures. R1117X and InsG3680 *Shank3* targeting vectors were constructed and introduced separately into R1 ES cells to replace the corresponding wild type allele. Homology arms with about 800 bp of size on both sides were designed to flank the desired point mutation, a pair of TALE nuclease plasmids were also designed as previously described[267] to facilitate the recombination efficiency through co-electroporation into ES cells together with targeting vector. The neo cassette was removed after targeting. High percentage chimeric mice were backcrossed with C57BL/6J (Jackson laboratory) to establish germline transmission followed by backcrossing with C57 BL/6J for five to six generations. Genotypes were determined by PCR of mouse tail DNA using the following primer pairs and gave rise to a band of 400 base pairs for wild type allele and 478 for R1117X mutation allele:

Primer F (5'-ATCTGCCATCCCTACAACCCTCC-3');

Primer R (5'-TCTCTCCGAGCAGGCACTGGAATCC-3').

For InsG3680, the following primer pairs were applied and generated a band of 407 base pairs for wild type allele and 486 for InsG3680 mutation:

Primer F (5'-TGCAAACCCGAGACTCTGAGAGAGG -3');

Primer R (5'-AGCGAATACCAGCTCTGGCTCCTCC -3').

To build the colony with C57 B6/S129 Sv mixed genetic background, we crossed the F5 heterozygous mutants with S129 Sv wild type mice (Jackson laboratory) to generate the founder population, and then set up heterozygous x heterozygous brother-sister mating between these founders to generate offspring with

C57B6/S129Sv mixed genetic background for all the experiments in this study. Animals were housed at a constant temperature of 23 ºC with a 12 hours light/dark cycle with free access to food and water. Mice were housed 4–5 by genotype per cage with the exception of the animals individually housed for grooming assay.

Behavioral studies: All behavioral studies were carried out and analyzed with experimenter blinded to genotype. For all assays, mice were habituated in the test facility for 1 hour prior to starting the task. Each cohort of mice were used for maximally three behavioral tests with at least five days' break between tasks.

Grooming behavior test: Adult male mice about 5 month-old were used for analysis of grooming behavior. Animals were individually housed for 2 weeks before video tapping for 2 hours under red light illumination between 7:00-9:00 pm. Grooming behaviors were manually coded and analyzed using Noldus Observer software, so that the total duration that an animal spent on grooming in the 2 hours segment was determined and normalized to its mobile time. Grooming included all sequences of face-wiping, scratching/rubbing of head and ears, and full-body grooming.

Open field: Spontaneous locomotor activity was assessed as total distance travelled (m) over 60 minutes in an automated Omnitech Digiscan apparatus (AccuScan Instruments) as described previously[59]. Activity was quantified over a 60 minute period by a computer operated detecting system.

Elevated zero maze test: The elevated zero maze consists of a circular platform that is equally divided into four quadrants. The zero maze was indirectly illuminated at 60 lux on the open arms and 10 lux on the closed arms. Testing started with an animal being placed into a closed arm of the maze. Behavior was video-taped for 5 minutes and then scored by a trained observer using Noldus Observer software. Anxiety-like behavior was interpreted based upon the percentage of time that mice spent in the open arms. The animals used in the elevated zero maze test were previously tested in the open field assay with one-week's break.

Three-chamber social test: Sociability and social novelty test were performed as previously described[59,201] with minor modifications. Briefly, 3

months-old male mice were used across all cohorts. Both stranger 1 and stranger 2 were wild type male S129 Sv males (Jackson laboratory) with matched age and body weight to test mice. Stranger mice were habituated by placing them inside an inverted wire cup for 30 minutes, two sessions per day for three consecutive days before experiments. Each stranger mouse was used maximally two times per day. Test mice were habituated to the facility environment for 1 hour before the start of behavioral tasks. The social test apparatus was made of a clear plexiglass box (65 (L) x 44 (W) x 30 (H) cm) with removable floor and partitions dividing the box into left, center, and right chambers. Center chamber (21 cm x 22 cm) is half the width of left (21 cm x 44 cm) and right chamber (21 cm x 44 cm). These three chambers were interconnected with 5 cm openings between each chamber which can be closed or opened manually with a lever operated door. The inverted wire cups to contain the stranger mice were cylindrical, 10 cm in height, a bottom diameter of 10 cm with the metal bars spaced 0.8 cm apart. A weighted cup was placed on top of the inverted wire cups to prevent the test mice from climbing onto the wire cup. Each wire cup was used only one time per day then followed by extensive clean with 75 % ethanol and water at the end of the test day. During the habituation phase, an empty wire cup was placed into left and right chamber, and the test mouse was placed into the middle chamber and allowed to explore for 15 minutes, with the doors into both side chambers open. During the sociability test phase, the test mouse was firstly gently introduced to the middle chamber with the doors to both side chambers closed, and an unfamiliar mouse (S1) was placed under the inverted wire cup in one of the side-chambers and a toy object (O) was placed under the inverted wire cup placed on the opposite side chamber. The location of the stranger mouse and object was counterbalanced between test trials to exclude side preference. The experimenter then lifted up the doorways to both side chambers simultaneously, and the test mouse was allowed to explore all three chambers for 15 minutes. During the social novelty test phase, the test mouse was again gently introduced into the middle chamber with the doors to both side chambers closed. Then a novel mouse (S2) was placed under the inverted wire cup, replacing the toy object (O) in one of the side-chambers. The experimenter then lifted up the doorways to both side chambers simultaneously, and the test mouse was allowed to explore all three chambers for an additional 15 minutes. Time spent in close proximity to the stranger mice or toy object was analyzed using the Noldus Ethovison software. The animals used in the social interaction test were previously tested in the zero maze assay with one-week's break.

Tube test: The tube test assay was performed as previously described[245,268]. We used transparent plexiglass tubes with 30 cm length and 3 cm inner diameter. This narrow space is just sufficient for an adult mouse (4-5 month-old) to walk through without being able to reverse its body direction. Mice were habituated to walk through the tube two sessions per day for four consecutive days before testing. On the day of testing, two unfamiliar mice with different genotypes were firstly met in the middle of the tube then released at opposite ends of the plexiglass tube simultaneously. The mouse that completely retreated firstly from the tube within first 6 minutes of the test was defined as the loser, and the other as the winner. In very rare cases, when no mice retreated within 6 minutes, the tests were repeated. The same pair of mice was matched again on the same test day with mice entry sides counterbalanced. The tubes were cleaned with 75 % ethanol between trials. A chi-square analysis was applied to determine the significance of test score between mice when compared with an outcome expected by chance (i.e. a 50:50 win–lose outcome).

Slice preparation for adult mice: Acute brain slices were prepared from 8-weeks-old mice as described previously[59]. Slices were prepared from a pair of mice consists of one wild type, one heterozygous and one homozygous with the same solution and procedure each day. Mice were deeply anesthetized by intra-peritoneal injection of avertin solution (20 mg/ml, 0.5 mg/g body weight) and then transcardially perfused with 25 ml of carbogenated (95 % O2, 5 % CO2) ice cold cutting artificial cerebrospinal fluid (aCSF) with the composition (in mM): 105 NMDG, 105 HCl, 2.5 KCl, 1.2 NaH_2PO_4, 26 $NaHCO_3$, 25 Glucose, 10 $MgSO_4$, 0.5 CaCl2, 1 L-Ascorbic Acid, 3 Sodium Pyruvate, 2 Thiourea (pH 7.4, with osmolarity of 300-310 mOsm). The brains were rapidly removed and placed in ice-cold and oxygenated cutting solution. Coronal slices (300 µm) were sliced using Leica VT1200S (Leica Microsystems) and then transferred to recovery chamber at 32 ºC with carbogenated cutting aCSF solution for 12 minutes, followed by transferring to holding chamber containing aCSF that contained (mM): 119 NaCl, 2.3 KCl, 1.0 NaH_2PO_4, 26 $NaHCO_3$, 11 Glucose, 1.3 $MgSO_4$, 2.5 $CaCl_2$ (pH was adjusted to 7.4 with HCl, with osmolarity of 300-310 mOsm) at room temperature. Slices were allowed to recover for one more hour in holding chamber before recording and used for experiment typically between 2~6 hours after slicing.

Slice preparation for juvenile mice: Acute brain slices from juvenile mice were prepared as described previously[269]. Briefly, a pair of wild type and homozygous mice from the same litter at postnatal day 14 were deeply anesthetized and rapidly decapitated. Dissected brain were placed into carbogenated (95 % O2, 5 % CO2) ice cold cutting artificial cerebrospinal fluid (aCSF) with the composition (in mM) 194 sucrose, 30 NaCl, 4.5 KCl, 1.2 NaH_2PO_4, 26 $NaHCO_3$, 10 glucose, 0.2 $CaCl_2$, 8 $MgSO_4$ (pH 7.4, 350 mOsm). Coronal slices (300 µm) were sliced in the same cutting aCSF using Leica VT1200S (Leica Microsystems) and then transferred into a recovery chamber containing carbogenated normal aCSF of the composition (in mM): 119 NaCl, 2.3 KCl, 1 NaH_2PO_4, 26 $NaHCO_3$, 11 glucose, 2.5 $CaCl_2$, 1.3 $MgSO_4$ (pH 7.3, 300–310 mOsm) for 15 minutes at 32 ºC before moving to the holding chamber at room temperature. Slices were allowed to recover for one more hour in holding chamber before recording and used for recording typically between 2~6 hours after preparation.

Cortico-striatal extracellular field recording: Recording of population spike in dorsal later striatum was performed as described[58,59]. Slice was placed into recording chamber (Warner Instruments) and constantly perfused with oxygenated aCSF at room temperature at a speed of 2.0 ml/minute. A platinum iridium concentric bipolar electrode (FHC) was positioned on the inner border of the corpus callosum between the cortex and dorsolateral striatum to stimulate the predominant cortical input to dorsolateral striatal region. A borosilicate glass recording electrodes filled with 2 M NaCl was placed onto the dorsolateral striatal region approximately 400 µm away from the stimulating electrode. Cortico-striatal field population spikes were elicited by delivery step depolarization (0.15 ms duration with 0.5 mA intensity at a frequency of 0.1 Hz). Stable baseline response of pop spike for at least of 5 minutes from individual slice was ensured before moving to input-output assay. Input-output curves were determined for both the negative peak 1 (NP1; presynaptic fiber volley) and pop spike amplitude by delivery three consecutive stimulation from 0 to 1 mA with 0.1 mA increments. Recordings were performed at room temperature and data were sampled using pCLAMP 10 software (Molecular Devices).

Whole cell patch clamp recording: Slice was placed into recording chamber (Warner Instruments) and constantly perfused with oxygenated aCSF at room temperature at a speed of 2.0 ml/minute. MSNs were visually identified

with a microscope equipped with IR-DIC optics (BX-51WI, Olympus) by location, shape and other electrophysiological parameters. Recording pipettes with resistance about 3~4 MΩ were pulled with pipette puller (P-97, Sutter Instruments) using capillary glass (King Precision Glass, type 8250). Pipettes were filled with internal solution containing (in mM): 107 $CsMeSO_3$, 10 CsCl, 3.7 NaCl, 5 TEA-Cl, 20 HEPES, 0.2 EGTA, 5 lidocaine N-ethyl chloride, 4 ATP magnesium salt, and 0.3 GTP sodium salt (pH 7.3, osmolarity 300~305 mOsm). Series resistance between 10 to 15 MΩ was constantly monitored. Multiclamp 700B amplifier (Molecular Devices) and digidata 1440A were used to acquire whole cell signals. Signals were sampled at 10 kHz and filtered at 2 kHz. AMPA receptor–mediated mEPSCs were collected at least 5 minutes after forming a stable whole cell patch clamping, recordings were performed by holding the MSN at -70 mV and perfused with aCSF supplied with 50 µM DL- APV (Abcam), picrotoxin (100 µM) (Tocris) and 1 µM TTX (Tocris). The mEPSCs data were analyzed with Mini Analysis program (Synaptosoft). Recording of AMPA/NMDA current ratio were performed and data were analyzed as described previously[269]. A platinum iridium concentric bipolar electrode (FHC) was positioned on the inner border of the corpus callosum between the cortex and dorsolateral striatum to stimulate the predominant cortical input to dorsolateral striatal region. After forming a stable whole cell recording for at least 5 minutes, stimulus intensity was adjusted to a value that could evoke an AMPA receptor mediated response between 200 to 300 pA when holding at -70 mV. Recording were performed in the presence of picrotoxin (100 µM) and D-serine (1 µM). Each evoked response was repeated for 15 times with an inter-stimulus interval of 20 s for all MSNs recorded. AMPA/NMDA ratio is calculated by the ratio of the peak of EPSC at -70 mV to the value of the EPSC at +40 mV at 60 ms following stimulation.

SPM and PSD preparation from mouse brain: Striatal and cortical tissue was obtained from two months old mice, experiments were performed as described previously[59]. Briefly, mice were decapitated after an isofluorane overdose and the head was shock-frozen in liquid nitrogen for four seconds. Cortical (bregma 1.4 to -0.46 mm) and striatal (bregma 1.4 to -0.46 mm) regions were micro-dissected and snap-frozen on dry ice. Tissue from two mice for cortex samples or three mice for striatum samples was pooled to generate one sample (one n, approximately 200 mg brain tissue total). All the buffers and solution used for the SPM and PSD preparation were supplied with proetease inhibitor (PI, cOmplete protease inhibitors from Roche). The pooled tissue was homogenized

in 3 ml ice-cold buffer (4 mM HEPES pH 7.4, 0.32 M sucrose) using a 5 ml, tissue grinder (Wheaton# 358005) and power homogenizer at 900 rpm for 30-40 strokes. Homogenates were centrifuged for 15 minutes at 900 g at 4 ℃. Supernatants were centrifuged again for 15 minutes at 900 g at 4 ℃. Next, supernatants were centrifuged for 15 minutes at 18,000 g at 4 ℃ to obtain the crude synaptosomal fraction. This pellet was washed with 3 ml ice-cold buffer (4 mM HEPES pH 7.4, 0.32 M sucrose with PI) and centrifuged for 15 minutes at 18,000 g at 4 ℃. The washed pellet was dissolved in 3 ml hypo-osmotic buffer (4 mM HEPES pH 7.4). Using the tissue grinder, 8 strokes were manually applied. Then the hypo-osmotic synaptosomal fraction was rotated for 1 h at 4 ℃. Hypo-osmotic synaptosomal fractions were centrifuged for 20 minutes at 26,500 g at 4 ℃ and the pellets were snap frozen on dry ice. The pellets were supplemented with 300-400 µl buffer (50 mM HEPES pH 7.4, 2 mM EDTA) and dissolved via sonication (4℃, 10 % power, 30 % ON, 70 % OFF, 30 s, Omni-Ruptor 250). Using the bicinchoninic acid protein assay (Thermo Scientific Pierce), protein concentrations were measured for each sample. To prepare the PSD fraction, pellets of synaptosomal fractions were dissolved in 0.1 ml ice-cold buffer (4 mM HEPES pH 7.4, 0.32 M sucrose) and placed on top of the sucrose gradient 0.8 M/1.0 M/1.2 M (27 %, 34 %, 41 %) in a Beckman ultracentrifuge tube (347356) with 500 ul/layer. Purification was performed by ultracentrifugation use swing bucket rotor TLS-55 at 117,257 g (42,000 rpm) for 2 hours at 4 ºC. Enriched PSD fraction was harvested using 1 ml insulin-syringe with needle to punch a hole on the side around the interface between layer of 1.0 M and 1.2 M. About 400-600 ul of fraction was extracted and diluted to 0.32 M sucrose by adding 2.5x volume of HEPES buffer. Dissolved pellets were further spinned at 128,405 g for 30 minutes (55,000 rpm in TLA100.3). Pellet was resuspended after centrifuge with 1 ml of HEPES buffer (50 mM HEPES pH 7.4, 2 mM EDTA) followed by adding Triton X-100 to 0.5 % (52.6 ul Triton X-100 10 %). Mix thoroughly and rotate at 4 ºC for 15 minutes then spin at 32.000 g for 20 minutes (28.000 rpm with TLA-100.3 rotor). And 1 ml ice-cold HEPES-C/ea into the pellet (PSD-1T), then add 0.5 % Triton X-100 (52.6 ul Triton X-100 10 %). Mix thoroughly and rotate at 4 ºC for 15 minutes. Centrifuge again at 200.000g (65.000 rpm TLA-100.3) for 20 minutes to obtain PSD-2T pellet. Recover PSD-2T in 100 ul of HEPES buffer (50 mM HEPES pH 7.4, 2 mM EDTA). Add 14.24 ul 20 % SDS and 43.94 ul 9M Urea. Brief sonication with 10 % power and 3 pulses (30 % ON-70 % OFF) to dissolve the pellets. Aliquot the PSD fraction and store at -80 ºC before protein quantification and western blotting assays.

Western blotting and quantification: The dissolved samples were mixed with 400 µl 2x Laemmli sample buffer (Bio-Rad). 400 µl of the mixture were kept without boiling and 400 µl were boiled for 5 minutes at 95 °C. Sample volumes corresponding to 25 µg protein amount per lane were loaded onto 4-15 % gradient Mini-PROTEAN TGX gels (Bio-Rad) and ran for 3 hours at 50 V. The proteins were then transferred onto Whatman Protran nitrocellulose membranes (0.2 µm pore size, BA83, Sigma-Aldrich) using a tank blot system (Mini Trans-Blot Cell, Bio-Rad) for 120 minutes at 100 V at 4 °C. The membranes were blocked for 1 hour with the respective blocking buffer (supplementary table 1) that did not contain any Tween-20. Subsequently, the membranes were incubated with primary antibodies diluted in blocking buffer (supplementary table 1) for 12 hours at 4 °C. Following primary antibody incubation, the membranes were washed three times for 5 minutes per wash using TBST buffer (0.05 % Tween-20). Then, the secondary antibodies goat-anti-mouse IRDye680 (Li-COR Biosciences), donkey-anti-rabbit IRDye 800CW (Li-COR Biosciences) or goat-anti-rat IRDye 800CW (Li-COR Biosciences) diluted in 1:1 TBST (0.05 % Tween-20): Odyssey Blocking Buffer (Li-COR Biosciences) were incubated with the membrane for 2 hours at room temperature. Following three rounds of washing with TBST, the membranes were scanned using an Odyssey CLx infrared imaging system (Li-COR Biosciences). Specific bands were then quantified with the contrast-independent, automatic background subtraction rectangular ROI tool of the built-in Software Image Studio 3.1 (Li-COR Biosciences) and normalized to an alpha-tubulin loading control for each lane and each blot. The values obtained for the mutation genotypes were then normalized to the wild-type expression. Statistical significance was tested for using the one-sample t-test for normalized values by asking whether the measured value differs significantly from the hypothetical value 1.0 (wild-type levels).

Golgi staining and spine counting: Golgi staining and spine counting was performed as described previously[131]. Three littermate pairs of male mice at two-month old from both R1117X and InsG3680 cohort were used for spine counting. Golgi staining of mouse brain was carried out according to the standard user manual (FD Rapid GolgiStain™ Kit). Briefly, dissected adult mouse brains were firstly immersed into impregnation solution (solution A+B) for 14 days in the dark, followed by incubating in solution C for 3 days before slicing. To prepare slices for imaging, coronal slices were prepared at 100 µm thickness using vibratome. Z-

stack confocal images were taken using an Olympus FluoView 1000 laser scanning confocal microscope. To quantify the spine density, images of at least ten neurons at the layer II/III of frontal association area for each mouse brain were taken with only one branch per neuron. Slices were imaged and the density of spines were counted by an experimenter blind to the genotype of the mice.

RNA isolation and Q-PCR assay: Tissue was obtained from age-and gender-matched brains of wild type, R1117X+/+ and InsG3680+/+ mice. Briefly, adult mice were decapitated after an isofluorane overdose and the head was shock-frozen in liquid nitrogen for four seconds. Cortical (bregma 1.4 to -0.46 mm) and striatal (bregma 1.4 to -0.46 mm) regions were micro-dissected and snap-frozen on dry ice. Quantitative PCR was performed as described previously (Wang *et al*., 2014). Total RNA was extracted using the RNeasy mini kit (QIAGEN) following the standard user manual. Equivalent amount of total mRNAs were reversely transcripted to cDNAs with iScript cDNA Synthesis Kit (Bio-Rad). Quantitative real-time PCR (q-PCR) was carried out using the iQ5 real-time PCR detection system (Bio-Rad) with the iQ SYBR Green Super mix kit (Bio-Rad) following the guidance of manufacturer's manual. The primers used in this study are listed below:

Shank3 Exon 1 RT forward: 5'-CCGGACCTGCAACAAACGA-3'
Shank3 Exon 2 RT reverse: 5'-GCGCGTCTTGAAGGCTATGAT-3'
Shank3 Exon 6 RT forward: 5'-GTTGCGAGCTGCTTCTCCAT-3'
Shank3 Exon 8 RT reverse: 5'-GCGCAACTCTCCTGGTTGTA-3'
Shank3 Exon 16 RT forward: 5'-GGTTGGACACAAGCAAGTGG-3'
Shank3 Exon 17 RT reverse: 5'-CAGCCGTCATGGACTTGGAC-3'
Shank3 Exon 21 RT forward: 5'-CGGAAGCTTTGCACGAGAAC-3'
Shank3 Exon 21 RT reverse: 5'-CTCATCAATGGAGCGGGAGG-3'
Shank1 RT forward: 5'-CCGCTACAAGACCCGAGTCTA-3'
Shank1 RT reverse: 5'-CCTGAATCTGAGTCGTGGTAGTT-3'
Shank2 RT forward: 5'-AGAGGCCCCAGCTTATTCCAA-3'
Shank2 RT reverse: 5'-CAGGGGTATAGCTTCCAAGGC-3'
Gapdh RT forward: 5'-AAATGGTGAAGGTCGGTGTG-3'
Gapdh RT reverse: 5'-GCATTGCTGACAATCTTGAG-3'

Data Analysis: All behavioral and electrophysiological measurement were performed and analyzed with experimenter blinded to genotype. All comparisons between groups were collected from littermate animals with experiments

performed at the same time. All results were presented as mean ± SEM and were analyzed statistically using Student's t-test, one-way or two-way analysis of variance with proper post-hoc test as specified in legend of each figure (GraphPad Prism). * indicates $P < 0.05$; ** indicates $P < 0.01$; *** indicates $P < 0.001$.

Chapter 5

Optogenetic Stimulation of Lateral Orbitofronto-Striatal Pathway Suppresses Compulsive Behaviors

5.1 Summary

Dysfunctions in frontostriatal brain circuits have been implicated in neuropsychiatric disorders, including those characterized by the presence of repetitive behaviors. We developed an optogenetic approach to block repetitive, compulsive behavior in a mouse model in which deletion of the synaptic scaffolding gene, *Sapap3*, results in excessive grooming. With a delay-conditioning task, we identified in the mutants a selective deficit in behavioral response inhibition and found this to be associated with defective down-regulation of striatal projection neuron activity. Focused optogenetic stimulation of the lateral orbitofrontal cortex and its terminals in the striatum restored the behavioral response inhibition, restored the defective down-regulation, and compensated for impaired fast-spiking neuron striatal microcircuits. These findings raise promising potential for the design of targeted therapy for disorders involving excessive repetitive behavior.

5.2 Background

Repetitive behaviors are cardinal features of a number of neuropsychiatric conditions[95,124]. Single behaviors and ritualistic sequences of behavior can be repeated compulsively to the point of seriously interfering with daily functioning[270]. Attempts to find efficacious therapies for such conditions have been challenging[271,272]. Neuroimaging studies have identified abnormalities in cortico-basal ganglia circuits, particularly those involving the orbitofrontal cortex, implicated in the expression of repetitive, compulsive, and impulsive behaviors[273,274]. Disabling the lateral part of the orbitofrontal cortex (lOFC) reduces response inhibition and increases impulsive choice, and this deficit in response inhibition is likely related to abnormalities in orbitofrontal interactions with the striatum and associated basal ganglia circuits[7,273,275,276]. We targeted this orbito-fronto-striatal system to examine its function and to develop an optogenetic, therapeutic approach to treat compulsive behavior. As a model, we focused on the compulsive behavioral responses exhibited by *Sapap3* mutant mice[58,277], which exhibit spontaneous, repetitive facial overgrooming and anxiety, behaviors that could be considered analogous to pathological repetitive behaviors in obsessive-compulsive disorder–spectrum disorders[278].

5.3 Results

5.3.1 *Sapap3* mutant mice exhibit a deficit in adaptive grooming response during conditioning task

We first asked whether, as is thought to be the case in some human conditions, repetitive behavior in the *Sapap3* mutants could be triggered as an excessive reaction to a neutral stimulus that has been associated with a natural behavioral response. We designed a conditioning paradigm in which a neutral stimulus (a water drop applied to the forehead) provoked a grooming response that could be clearly identified, which allowed us to pair a tone with the water drop in a delay-conditioning paradigm (Fig.5.1, A and B, and Fig.5.2)[279]. The behavior of the *Sapap3* mutant mice and their wild-type littermates diverged sharply during the course of conditioning. Early on, both mutants (n= 7) and littermate controls (n= 7) readily became conditioned, grooming when the conditioning tone was played (Fig.5.1, C and D). Later in training, the wild types began to inhibit this early grooming to the tone onset and to respond immediately after the water-drop release. The *Sapap3* mutants, by contrast, having once acquired the conditioned responses, kept responding to the tones with short-latency grooming, even in probe trials lacking water-drop delivery (Fig.5.1, C to F; Figs. 5.3 and 5.4; and table S5.1). This emergence of excessive short-latency responses was not accompanied by increased general grooming behavior or by hypersensitivity to the tone (Figs. 5.5 and 5.6 and supplementary text). The *Sapap3* mutant mice thus expressed an acquired maladaptive behavior characterized by defective inhibition of their conditioned responses to the originally neutral tone stimuli.

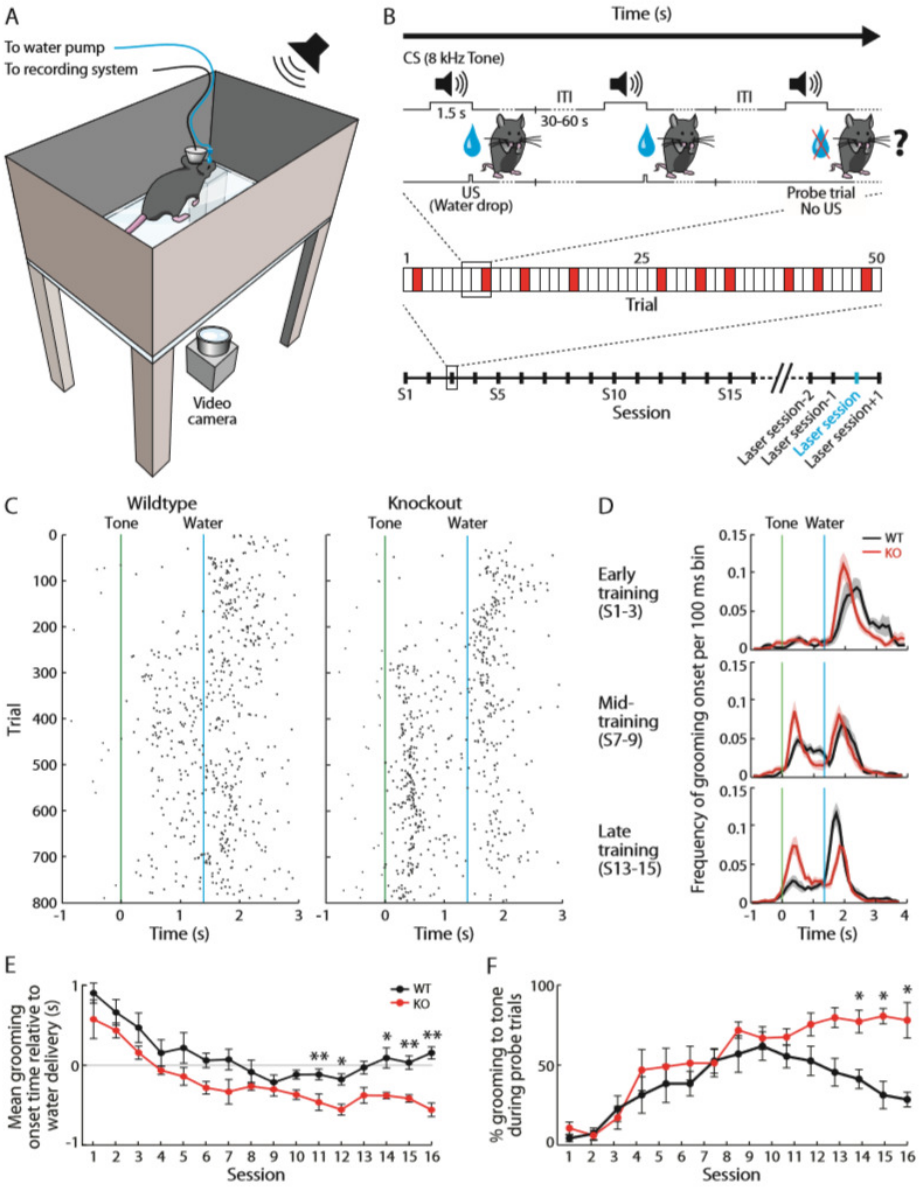

Figure 5.1 | *Sapap3* mutant mice exhibit a deficit in adaptive grooming response during conditioning task.

A) Grooming chamber. **B**) Timelines. (Top) Three successive trials (two standard, one probe). (Middle) Session with 40 normal trials (white) and 10 randomly inserted probe trials (red). (Bottom) Full experiment (14). **C**) Raster plots of grooming onsets (800 normal trials, 16 sessions), one mouse of each genotype. **D**) Grooming onset distribution in wild types (WT) (n= 5) and knockout mutants (KO) (n= 5) in early, middle, and late training phases. Shading, SEM. **E**) Mean grooming onset times [n= 5 mice/genotype; y axis zero, water drop; genotype effect, $P<0.05$, repeated measures analysis of variance (ANOVA)]. **F**) Grooming to tone, probe trials (day-genotype interaction, $P<0.01$, repeated measures ANOVA). (E) and (F) Error bars show SEM.

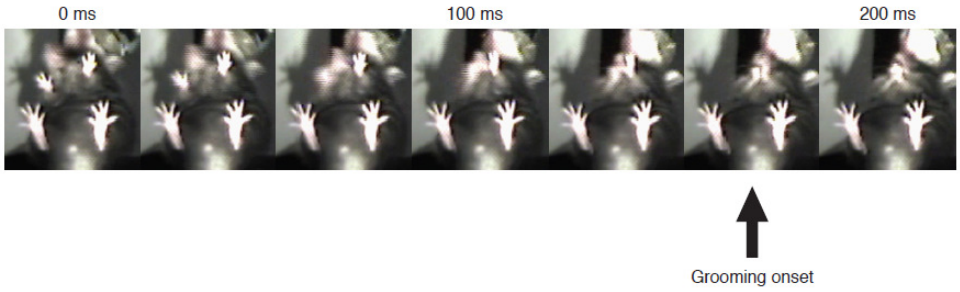

Figure 5.2 | Successive snapshots from video recording over 200 ms (30-Hz sampling rate) during performance of the conditioning task.

The grooming onset was defined as the time when both front paws contacted the forehead.

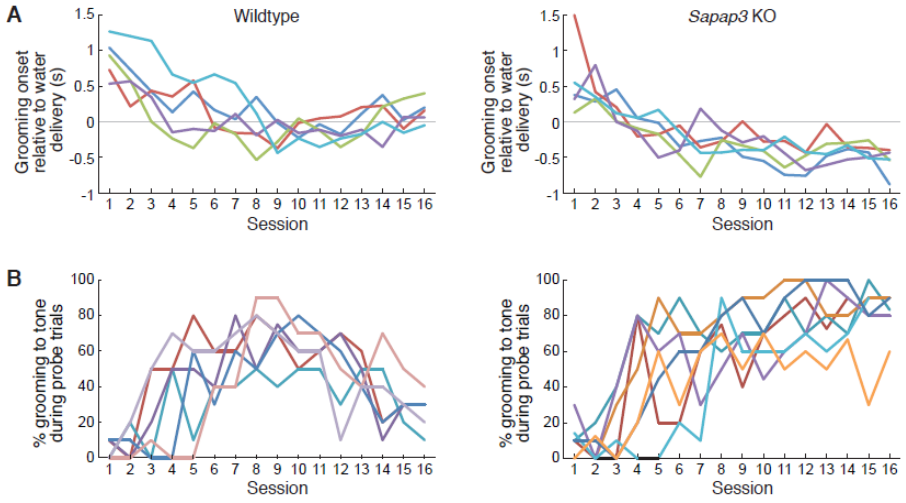

Figure 5.3 | Behavior of individual wildtype (left) and *Sapap3* mutant (right) mice.

A) Grooming onset times relative to water-drop delivery (y-axis zero-point). **B**) Percentage of trials in which the animals groomed in response to the tone during the probe trials.

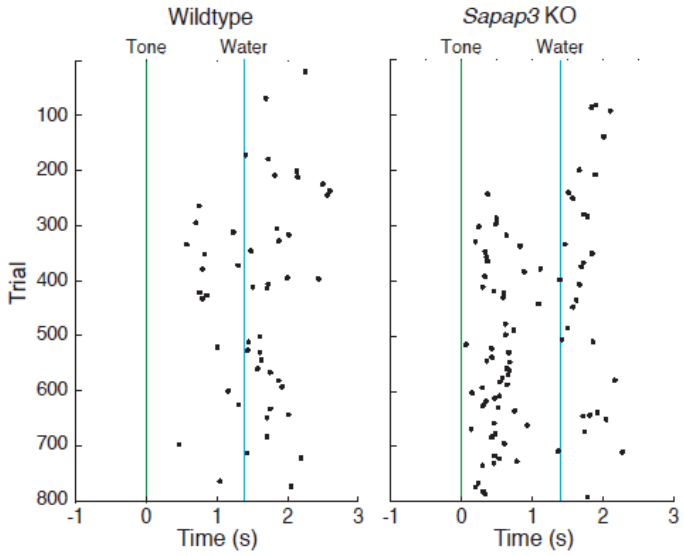

Figure 5.4 | Examples of grooming behavior by a wildtype mouse and a *Sapap3* mutant mouse during probe trials.

Raster plots of grooming onset times in 160 probe trials (16 sessions) for a wildtype mouse (left) and a *Sapap3* mutant mouse (right). Early in training, both mice exhibited almost no grooming to the tone. Later in training, the wildtype mice performed conditioned grooming responses and eventually inhibited grooming responses to the tone. By contrast, the *Sapap3* mutant mouse continued to groom in response to the tone, despite the fact that this grooming during the tone-water interval was ineffective in removing the not-yet-presented water.

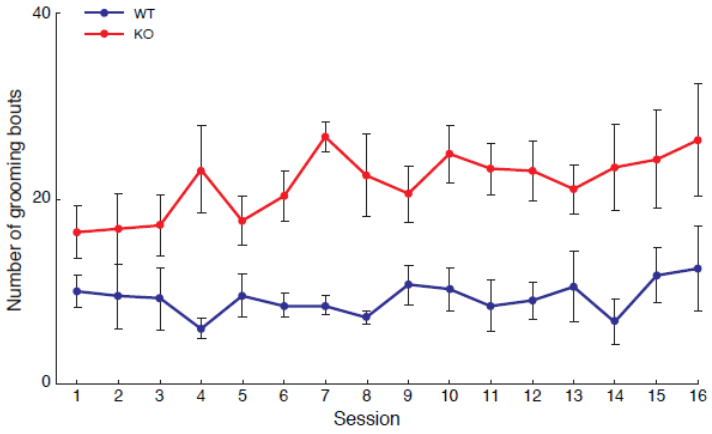

Figure 5.5 | Grooming during intertrial intervals over 15 days of training.

Sapap3 mutant mice (KO, n= 5) showed a significantly higher number of grooming bouts than wildtypes (WT, n= 5) during the intertrial intervals, as expected. However, their

relative amounts of grooming did not change significantly over the course of the 15 days of training ($P > 0.05$, repeated measures ANOVA). Error bars indicate SEM.

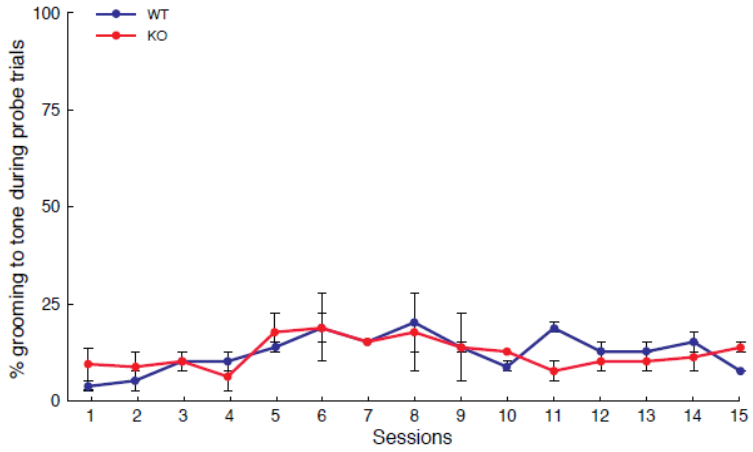

Figure 5.6 | Percentage of grooming responses in probe trials during a control protocol in which the tone and water-drop delivery were not systematically paired. During this protocol, which had variable tone-water intervals, no conditioned grooming in response to the tone was observed over 15 days of training in either wildtype (WT, n= 2) or *Sapap3* mutant (KO, n= 2) mice. This result indicates that a consistent contingency between tone and water-drop events was necessary to provoke grooming in response to the tone, as neither control nor *Sapap3* mutant mice developed compulsive grooming with prolonged exposure to the unpaired tone. Error bars indicate SEM.

5.3.2 Dynamic learning-related changes in lOFC and striatal ensemble activity differ in wild-type and *Sapap3* mutant mice

Learning theories of human compulsive behavior suggest that repetitive behaviors can result from malfunction of a learning process that leads to loss of the ability to repress sensorimotor associations[270,280,281]. To identify the neuronal basis of such a deficit, we recorded spike and local field potential (LFP) activity simultaneously with tetrodes in the lOFC and centromedial striatum as the mice acquired and then performed the task (Fig. 5.8)[279]. The baseline raw firing rates of putative pyramidal cells in the lOFC were similar in mutants (n= 7) and wild types (n= 7) throughout training, but the baseline firing rates of putative medium spiny neurons (MSNs) in the striatum were significantly elevated in the *Sapap3* mutants (Fig.5.7, A and E). During the early stages of training, subpopulations of pyramidal neurons in the lOFC in both genotypes exhibited a significant increase of activity between the tone and water events (Fig.5.7 B, Fig. 5.9 A, and table S5.2)[279]. These lOFC responses remained similar throughout training; activity after the tone became progressively sustained up to the time of water-drop delivery (Fig.5.7, B to D).By contrast, striatal task-related MSN activity patterns diverged markedly during training for the mutant and wild-type mice (Fig.5.7, F to H, and Fig. 5.9 B)[279]. Early on, MSNs in both genotypes exhibited a phasic increase in response to the tone; but the slope of this increase steadily declined in the wild types but did not in the *Sapap3* mutants (Fig.5.7 H). This tuning of MSN activity in the wild types occurred as their grooming onset times shifted toward the time of water-drop delivery (Fig. 5.10). The lack of such learning-related MSN tuning in the mutants could have reflected increased excitation or decreased inhibition of activity after the tone (see supplementary text). We considered one powerful source of MSN inhibition, deriving from fast-spiking striatal interneurons (FSIs), which mediate fast feed-forward inhibition of MSNs in response to cortical activation[282] and largely correspond to parvalbumin (PV)–containing interneurons. In cell counts of PV-immunostained sections, we found significantly fewer PV-positive striatal neurons in the mutants than in the wild types (n= 8 mice per genotype, chi-square test, $P < 0.05$) (Fig. 5.11)[279]. This result suggested that a defect in intrastriatal inhibition could contribute to the *Sapap3* mutant phenotype but did not identify the source of the abnormality.

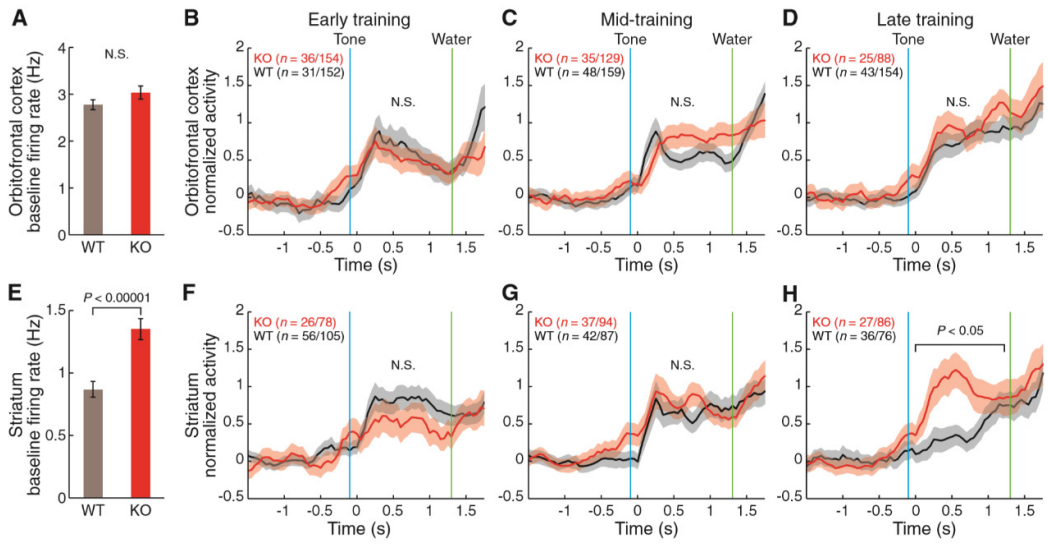

Figure 5.7 | Dynamic learning-related changes in lOFC and striatal ensemble activity differ in wild-type and *Sapap3* mutant mice.

Average base- line firing rates of lOFC (**A**) and striatal (**E**) units. Average activity of lOFC (**B** to **D**) and striatal (**F** to **H**) units classified as task-responsive (*i.e.*, firing preferentially between tone and water events relative to base- line activity). Mean z-scores normalized for each neuron relative to baseline activity for wild-type (WT) (n= 7) and *Sapap3* mutant (KO) (n= 7) mice during training. Above, ratios of task-responsive units to total units per genotype. Shading, SEM.

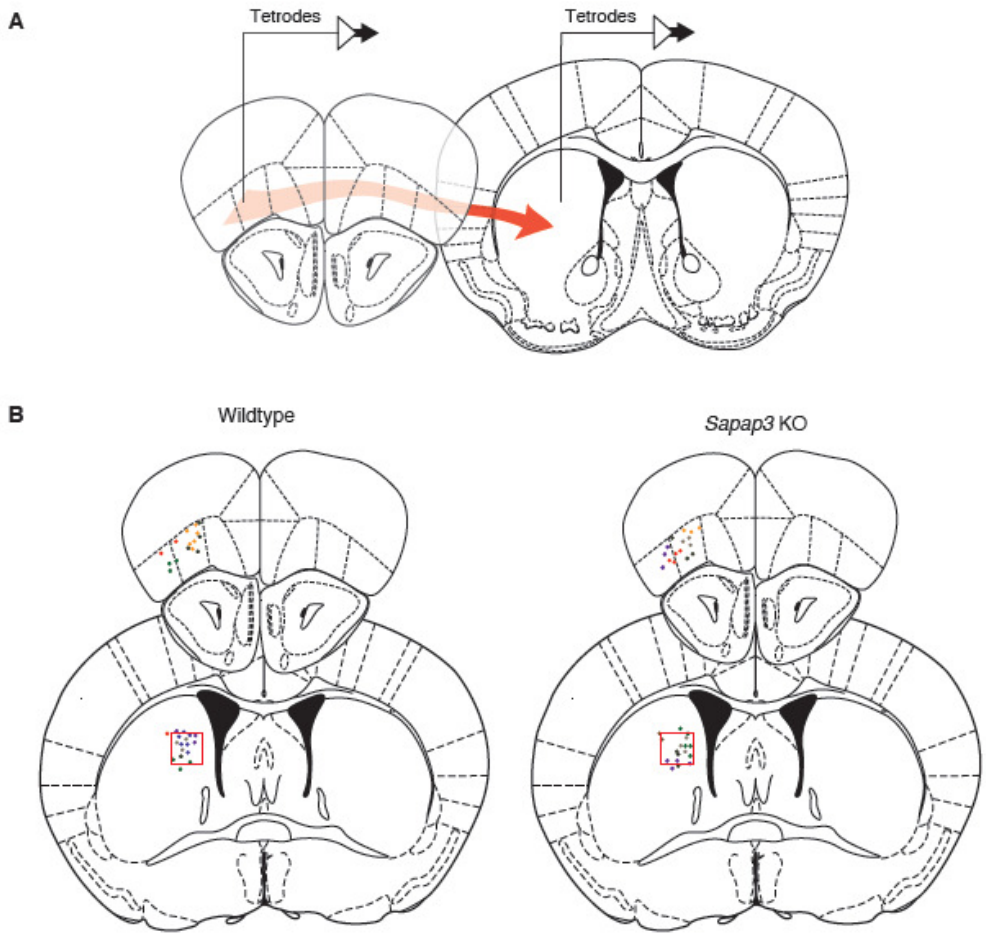

Figure 5.8 | Tetrode recording sites and region of PV-positive neuron counting.
A) Schematic drawing of the protocol for simultaneous tetrode recordings in the lOFC and striatum. **B**) Location of tetrode tips identified by electrolytic marking lesions (colored dots) and, overelaid, the region in which the numbers of PV-positive cells were counted in the anatomical experiments (red rectangles) in wildtype (left) and *Sapap3* mutant (right) mice. Recording sites for individual mice are shown in different colors.

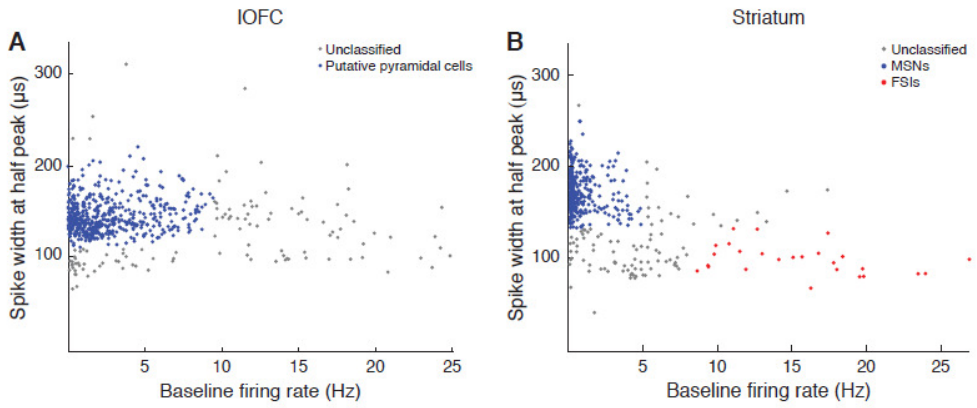

Figure 5.9 | Scatter plots illustrating spike characteristics of all units recorded in the lOFC (left) and sriatum (right) of wildtype and *Sapap3* mutant mice.

Each unit is represented as a dot plotted for average baseline firing rate (x-axis) and average spike width at half-peak amplitude (y-axis). For lOFC units, putative pramidal cells are shown in blue. For striatal units, putative MSNs and FSIs are shown in blue and red, respectively. Gray dots represent units that did not meet criteria for these classifications.

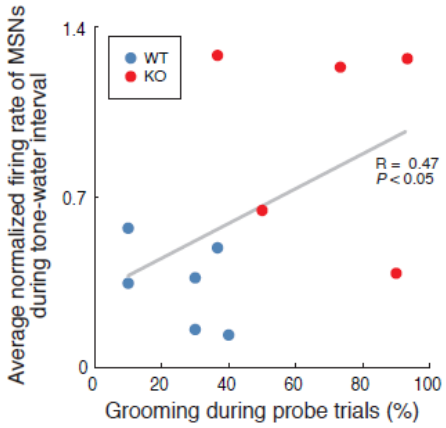

Figure 5.10 | Correlation between probability of grooming behavior and average normalized firing rate of task-related MSNs.

Correlation (R= 0.47, P < 0.05) between probability of grooming behavior (x-axis) and average normalized firing rate of task-related MSNs during the period from tone onset and water-drop delivery (y-axis) at the end of the training. Each dot represents one animal (blue: wildtype, red: *Sapap3* mutant).

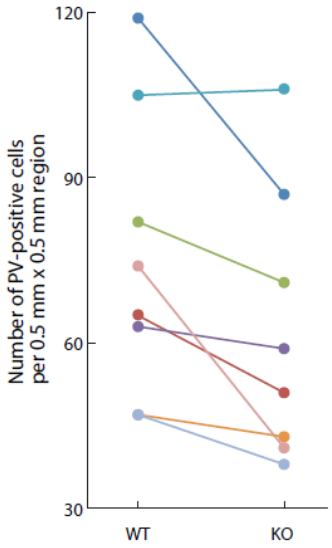

Figure 5.11 | Counts of PV-positive neurons in the centromedial striatum.
Counts of PV-positive neurons in the centromedial striatum in the wildtype mice (WT, n= 8) and *Sapap3* mutant mice (KO, n= 8). Each colored line represents one matched pair of mice with brain sections stained at the same time. For each pair, a total number of PV-positive cells were counted from matched sections of each genotype.

5.3.3 Optogenetic stimulation of lOFC in *Sapap3* mutants enhances feed-forward inhibition in striatal circuitry

In the light of clinical evidence[274,276], we asked whether we could restore the striatal inhibition by optogenetically altering lOFC input to the striatum. We injected the lOFC bilaterally with adeno-associated virus (AAV5) to express a fusion protein of channelrhodopsin-2 and enhanced yellow fluorescent protein (ChR2- EYFP) under the calcium- and calmodulin- dependent protein kinase II (CaMKII) promoter to target cortical pyramidal neurons of *Sapap3* mutant mice (Fig. 5.13). We delivered pulses of blue light (473 nm, 5mW, 10Hz pulses) through two independently movable optical fibers and simultaneously recorded neural activity in the lOFC and striatum (Fig.5.12, A and D, and Fig. 5.14)[279]. We confirmed expression of ChR2 and spike and LFP modulation at the stimulation frequency (Fig.5.12, B and C, and Figs. 5.13 and 5.14). Control experiments with noneffective laser stimulation and with control virus were negative (Fig. 5.15). We stimulated the ChR2-containing lOFC axon terminals within the striatum while we recorded from ensembles of striatal neurons (Fig.5.12 D). To assess specifically the direct effect of lOFC stimulation on FSIs and MSNs in the *Sapap3* mutants, we isolated 10 FSI-MSN pairs in which both members of the pair were recorded on the same tetrode (Fig.5.12 E and Figs. 5.9 B and 5.16). In these recordings, MSN spiking was inhibited after FSI spikes, and this inhibition was greatly increased during optogenetic stimulation of lOFC terminals in the striatum (unpaired t test, $P<0.01$). This effect could also be seen at the population level (Fig.5.12, F and G). These dynamics suggest that activation of the lOFC-striatal pathway in the *Sapap3* mutants compensated for their abnormally high MSN activity at the end of the training by eliciting a powerful feed-forward inhibition of MSNs driven by the cortical activation of FSIs[170]. We applied this lOFC-striatal optogenetic stimulation at the end of training and showed that it could restore MSN tone-response inhibition in the *Sapap3* mutants (Fig.5.12 H).

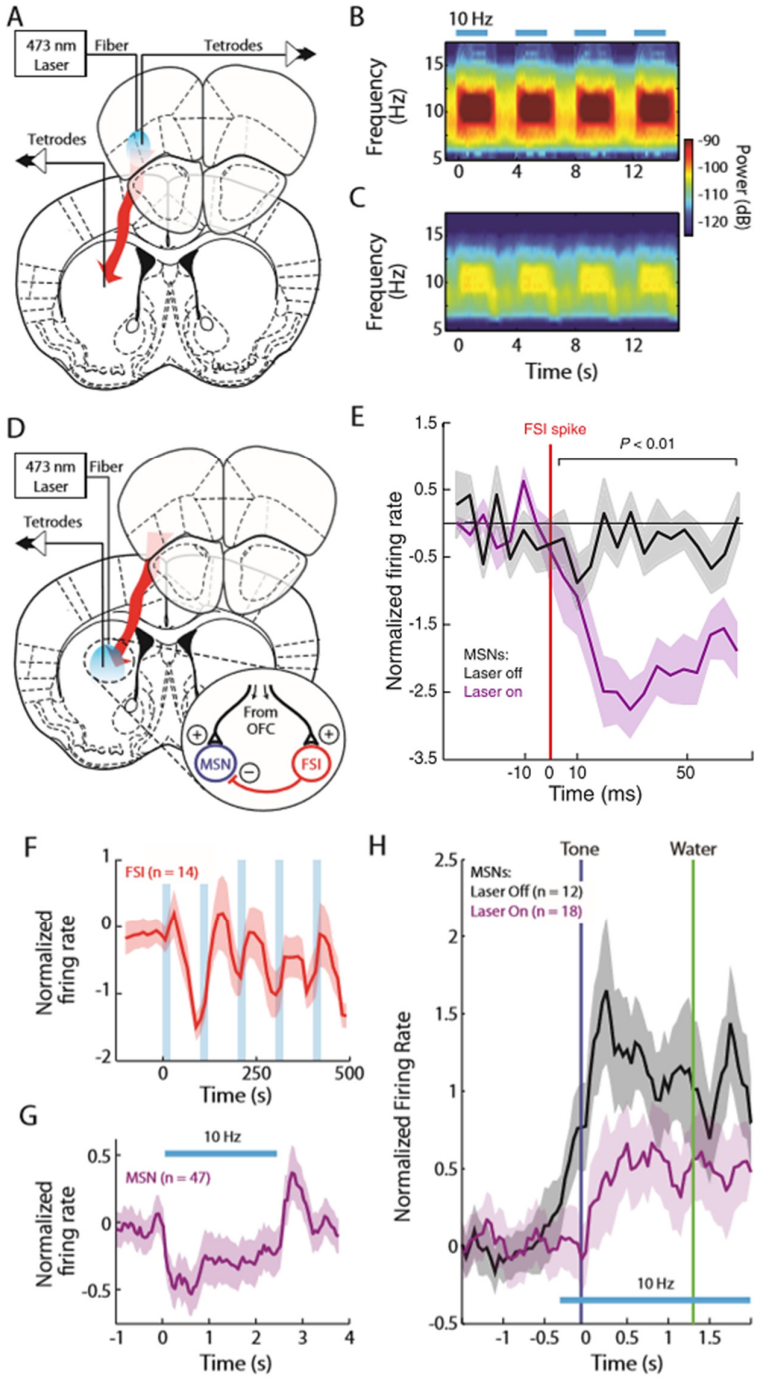

Figure 5.12 | Optogenetic stimulation of lOFC in *Sapap3* mutants enhances feed-forward inhibition in striatal circuitry.

Simultaneous chronic recording and optogenetic stimulation in lOFC (A) and striatum (D) of mutants. LFP activity in lOFC (B) and striatum (C) at lOFC stimulation frequency (10 Hz, 5 mW, 5-ms pulse for 2.5 s, blue bars). E) MSN spiking relative to FSI spikes (red line) during 2.5-s stimulation (purple) or no stimulation (black) of lOFC terminals in striatum (n= 10 FSI-MSN pairs recorded on the same tetrode, three mutants; stimulation

effect P<0.01, unpaired t test). Light stimulation (blue bars) induces synchrony of FSI population firing at stimulation frequency F) (n= 14 units, three mutants) and long-lasting inhibition of MSNs during stimulation (G) (n= 47 units, three mutants). H) Same stimulation protocol applied at the end of the training significantly decreased MSNs firing (purple) relative to no-stimulation condition (black). Shading, SEM.

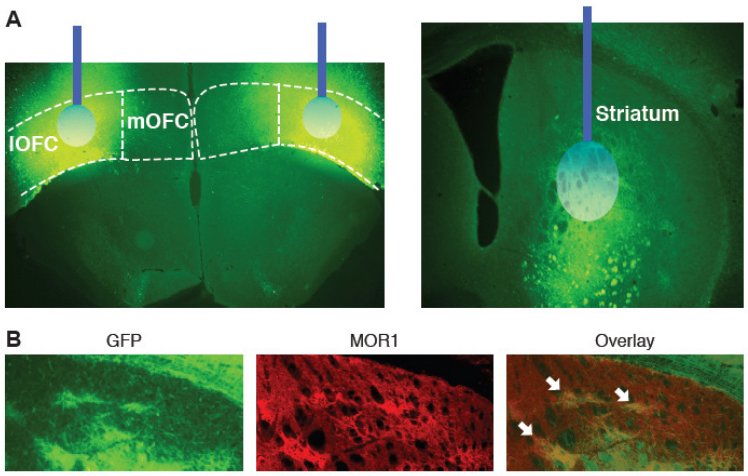

Figure 5.13 | Expression of ChR2-EYFP protein in pyramidal cells in the orbitofrontal cortex and their projection terminals in the striatum.

A) ChR2-EYFP was expressed in the lOFC (left) and striatum (right) after bilateral injection of the virus in the lOFC. Optical fibers (blue bars) and the estimated region of effective stimulation with 5 mW power (ellipses) are schematically shown. mOFC: medial orbitofrontal cortex. **B**) Staining of GFP (left) and MOR1 (middle) in the dorsal part of the striatum. Overlay (right) show a partial striosomal projection from lOFC (white arrows).

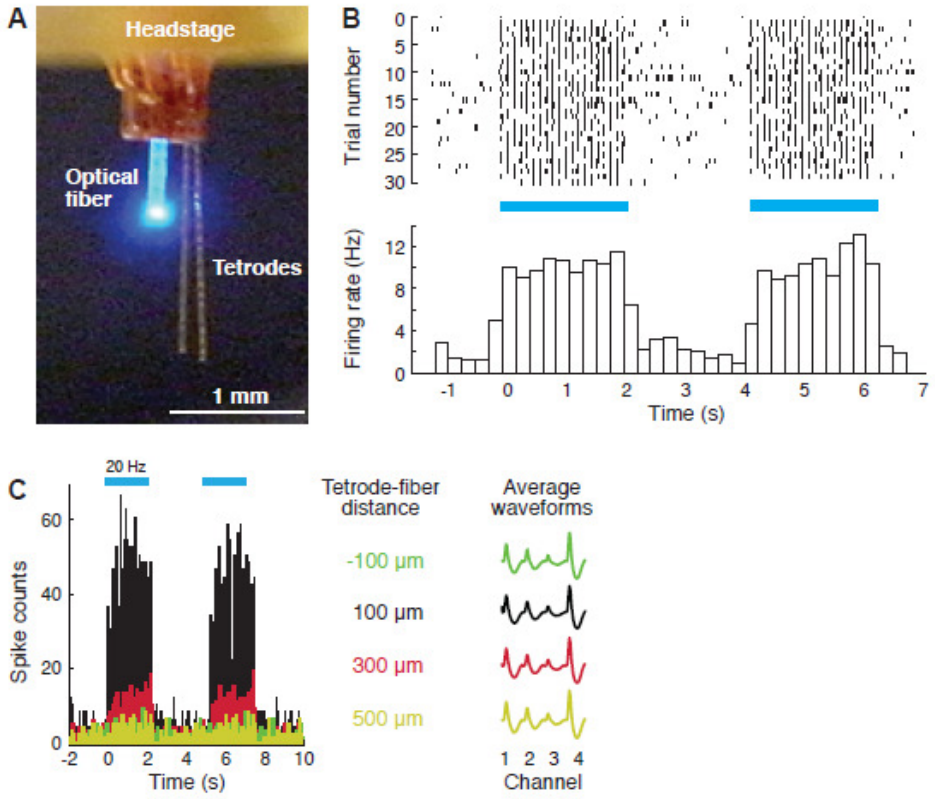

Figure 5.14 | Neuronal responses to optogenetic stimulation.

A) Close view of the tip of our custom-built headstage with eight independently mobile microdrives. **B**) Optical stimulation in the lOFC (10 Hz, 5 mW, 10-ms light pulse, represented by blue bars) elicited reliable neuronal spiking (top, raster plot of 30 trials with each spike represented by a black dot) with an average firing rate nearly identical to the stimulation frequency (bottom, spike histogram with 200-ms bins). **C**) Spiking activity of lOFC units during light stimulation (blue bars), recorded as an optical fiber was lowered in 200-µm steps relative to the tip of a tetrode recording activity of a single unit. The optical stimulation (5 mW) elicited spike activity at a restricted distance from the fiber (~500 µm).

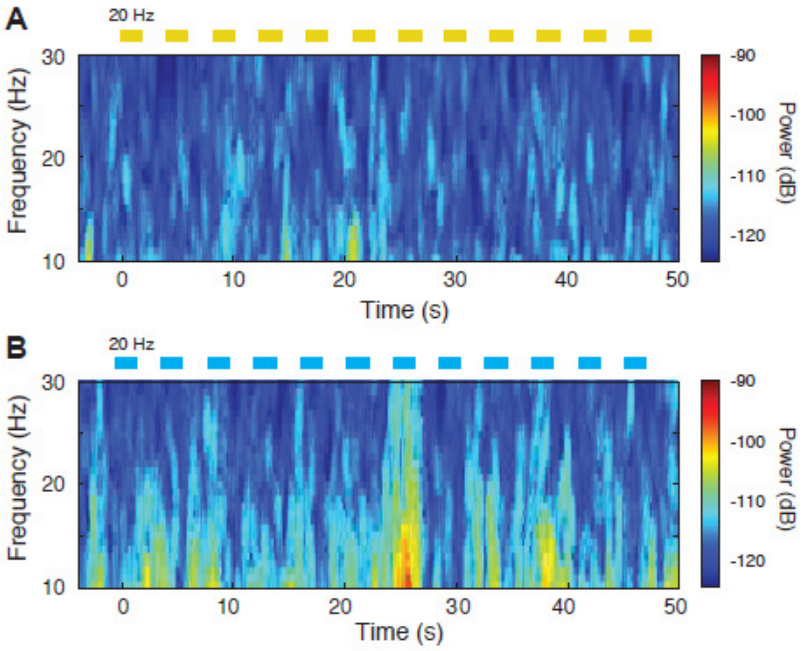

Figure 5.15 | Lack of local field potential responses in optogenetic stimulation control protocols.

A) In contrast to the robust local field potential responses observed with blue light stimulation in *Sapap3* mutants mice injected with the AAV-CaMKII-ChR2 virus (Fig. 5.12B), delivery of yellow light (593 nm) did not affect local field potential activity in the lOFC, confirming the absence of possible electromagnetic artifact by light stimulation in the electrical recordings that we made for the main experiments. **B**) Similarly, we did not observe any consistent change in local field potential activity during appropriate blue light stimulation in *Sapap3* mutant mice injected with a control virus AAV-CaMKII, confirming that blue light alone did not generate oscillatory activity in the absence of the expression of ChR2.

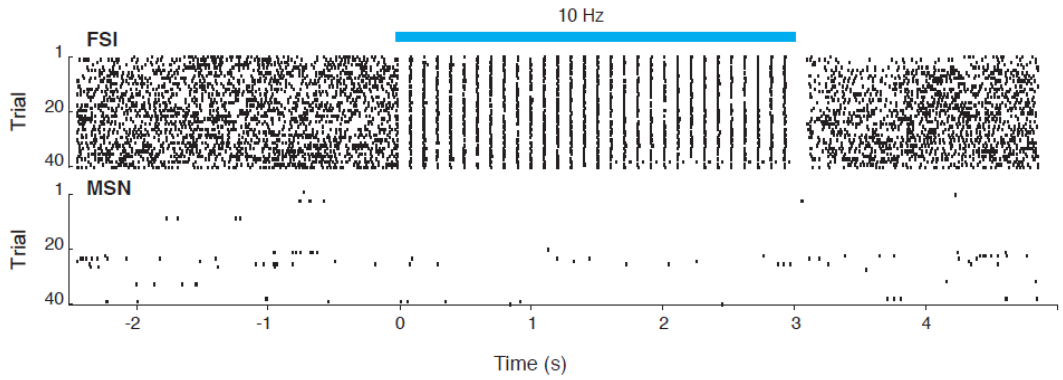

Figure 5.16 | Spike raster plots of a putative FSI and a putative MSN.

Spike raster plots of a putative FSI and a putative MSN simultaneously recorded on the same tetrode during 40 trials with optical stimulation of the lOFC terminals in the striatum (10 Hz, 5 mW, 5-ms light pulse, represented by blue bar). The lOFC stimulation elicited reliable neuronal spiking of the FSI (top) and an inhibition of the MSN activity.

5.3.4 Optogenetic stimulation of lOFC alleviates compulsive grooming of *Sapap3* mutant mice

We then asked whether such stimulation could also ameliorate the behavior of the *Sapap3* mutant mice (Fig.5.17, A to D). At the end of the training, we excited either projection neurons in the lOFC or their terminals in the striatum in different experiments, triggering the laser at tone onset and continuing it for 2.5s at 10Hz. When the *Sapap3* mutants were under optical stimulation, their early grooming responses to the tones were almost completely abolished, both by lOFC stimulation (n= 4) (Fig. 5.17, A, B, and E) and by striatal stimulation (n= 3) (Fig. 5.17, C to E). Yet the mutants groomed normally as soon as the water drop was delivered. The abnormal stimulus-evoked compulsive behavior in the *Sapap3* mutants thus could have resulted from a deficit of behavioral inhibition that was restored by optogenetically stimulating the lOFC-striatal pathway. We next tested whether we could also rescue the spontaneous compulsive phenotype of the *Sapap3* mutants by optogenetically stimulating in lOFC (n= 6) or striatum (n= 4) during their unconditioned, natural behavior, which is typified by excessive grooming, but for which the triggers impelling the grooming behavior are unknown (Fig.5.17 F)[279]. Stimulation (5 Hz, 5 mW, 5ms pulse for 3 minutes) almost fully alleviated their compulsive grooming (Fig.5.17 F), leaving intact other out-of-task behaviors requiring fine motor coordination and motivation (n= 5) (Fig.5.17 G). Wild types expressing CaMKII-ChR2 (n= 3) and *Sapap3* mutants expressing control virus (n= 3) showed no difference in grooming with the laser on or off (Fig.5.17 F).

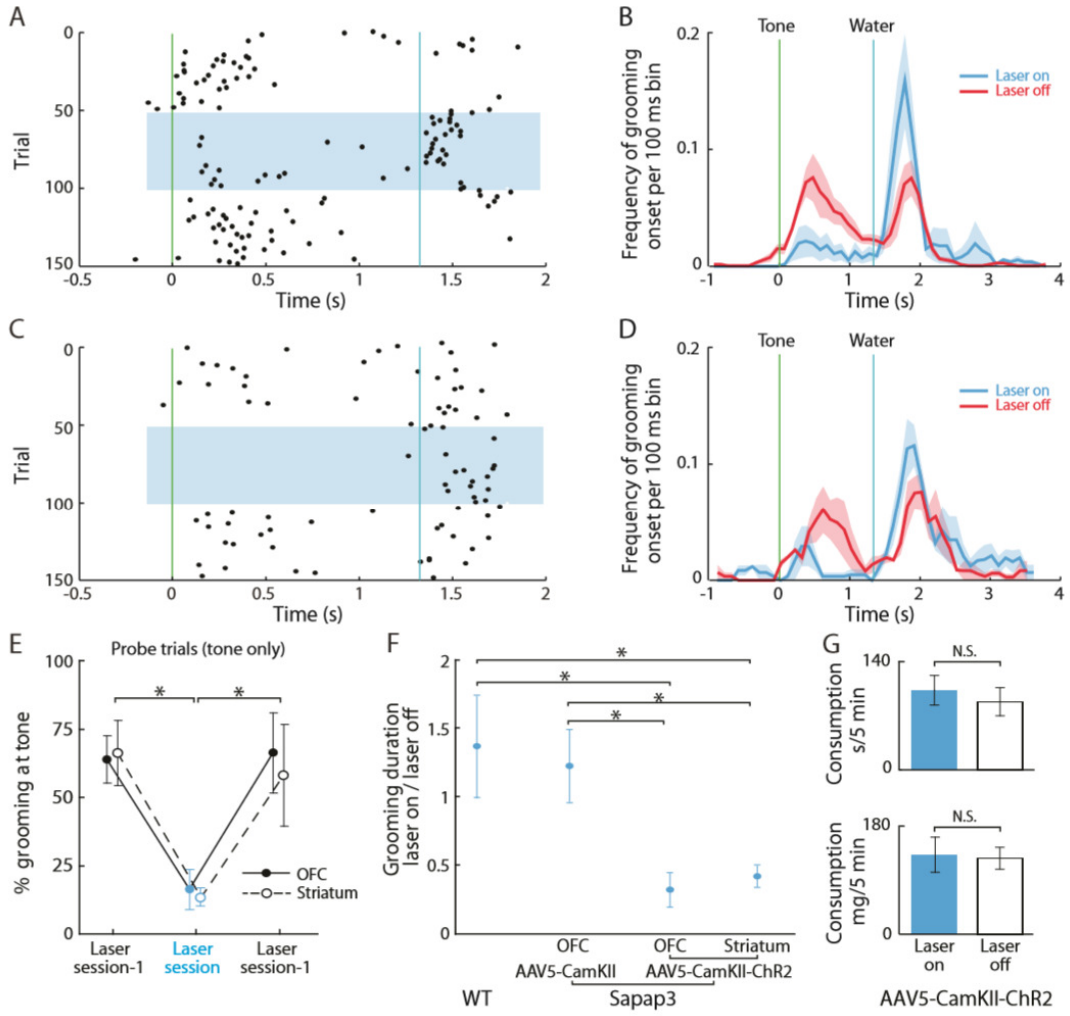

Figure 5.17 | Optogenetic stimulation of lOFC alleviates compulsive grooming of *Sapap3* mutant mice.

Rasters of grooming onsets before, during (blue shading), and after bilateral lOFC (**A**) or striatal (**C**) stimulation (10 Hz, 5 mW, 5-ms light pulses) in a *Sapap3* mutant, late in training. Grooming onsets for the *Sapap3* population during session with laser stimulation (blue) in lOFC (**B**) (n= 4) or striatum (**D**) (n= 3) compared with preceding laser-off session (red). Shading, SEM. **E**) Suppression of tone-evoked grooming by lOFC or striatal stimulation during probe trials (P<0.01, unpaired t test). **F**) Alleviation of compulsive grooming in *Sapap3* mutants (n= 4) by lOFC or striatal stimulation (5 Hz, 5 mW, 5-ms light pulses) during 3-minutes free-movement periods, and control virus (n= 3) and wild-type (n= 3) comparisons (P<0.05, unpaired t test). **G**) Lack of effect of same out-of-task lOFC stimulation in mutants (n= 4) on time spent eating (top) or food consumed (bottom) during 5-minutes free-feeding periods. Error bars in (E to G), SEM.

5.4 Discussion

Our findings demonstrate that selective stimulation of the lOFC-striatal pathway can restore a behavioral inhibition signal in an animal model expressing pathological repetitive behaviors and can prevent overexpression of both conditioned and spontaneous repetitive grooming. Optogenetic stimulation increased inhibition of striatal MSNs in the mutants, and it specifically activated striatal FSIs and affected FSI-MSN striatal microcircuitry. The abnormally elevated MSN baseline firing rates in the *Sapap3* mutant striatum and reduced numbers of PV-immunostained striatal interneurons, likely corresponding to physiologically identified FSIs, suggest that the microcircuit necessary for inhibiting MSN responses through FSI excitation may not have been fully functional (supplementary text)[277,278]. A pathologic decrease of PV-containing striatal neurons has been observed in Tourette's syndrome, and FSI microcircuits have been implicated in other extrapyramidal disorders[283,284]. Our findings suggest that a key role of the lOFC in underpinning response inhibition could include specific effects on FSI-MSN microcircuitry by which the lOFC controls striatal neurons (supplementary text). Our finding that optogenetic control of this lOFC-striatal pathway can alleviate repetitive behaviors in a genetic model of compulsive behavior raises important questions for future work (supplementary text). Are subsystems of striatal MSNs (e.g., D1 and D2 dopamine receptor–expressing neurons or striosome and matrix neurons) differentially affected[284–287]? Can this targeted optogenetic therapy alleviate repetitive behaviors in other models? What microcircuits underlie the normal orbitofronto-striatal pathway neuroplasticity and behavioral adaptation evident in the wild types? Our findings should provide a platform for exploring these differential influences and for developing new potential therapeutic targets to alleviate conditions characterized by abnormally repetitive behavior.

5.5 Methods

Animals: Forty-two mice (24 *Sapap3* mutants and 18 wildtype littermates, male, 3-9 months old, C57BL6/J background) were maintained under a 12 hours light/dark cycle with *ad libitum* food and water. Each *Sapap3* mouse in the grooming conditioning task was intentionally chosen as not having a facial skin lesion prior to the experiment (despite having excessive grooming behavior) so that lesion-induced skin sensitivity would not be a confounding variable influencing reactions to water drops.

Tetrodes, optical fibers and headstage: Custom-built headstages with 8 independently mobile microdrives weighed ~3 g and were made of plastic and brass[288]. Microdrives were designed to hold either a tetrode (twisted 12-µm Ni/Cr wires) or an optical fiber (100 µm diameter) inserted in a zirconia ferrule. A spout was fixed at the front of the headstage to permit delivery of water drops onto the animal's forehead.

Surgical procedures: Each mouse was deeply anesthetized (1-2 % isoflurane) and was mounted in a stereotaxic frame with non-puncturing ear bars. Small openings (2 mm wide) were made over the left central caudoputamen (AP= +0.2 mm, ML= +1.5 mm) and lateral orbitofrontal cortex (AP= +2.8 mm, ML= +1.5 mm), and AAV virus (0.2 µl) was injected with graduated pipettes at a rate of 0.02 µl/minute. Several small burr holes (0.6 mm) were drilled around the perimeter of the exposed skull surface to accept brass anchor screws. The headstage was then fixed to the skull and screws with dental acrylic. Tetrodes were advanced individually over 5-7 post-operative days and were carefully put into position in the striatum (DV= 2.2-2.8 mm) and orbitofrontal cortex (DV= 1.5-2 mm), with an attempt to maximize the number of recorded units per site prior to the first training session. The tetrodes then were left in place throughout training, except for rare small adjustments (movements of less than 25 µm) to maintain multiple-unit recording at the same location over training. Throughout the entire training, we moved 7 of the 98 total tetrodes, each by an estimated distance of 25-50 µm.

Opsin delivery and optical stimulation in neural tissue: The adeno-associated viruses AAV-CaMKIIa-ChR2-EYFP and AAV-CaMKIIa-EYFP were packaged as AAV5 by the University of North Carolina vector core facility. These

viral vectors have been shown to be expressed selectively in excitatory neurons (but not in neurons expressing GABA) when injected into the neocortex, with a level of transduction efficacy and expression of ChR2 of about 90 %[289,290]. In all experiments, a minimum of 4 weeks elapsed before optical stimulation. Chronic optical fiber implants (Doric) were connected to optical patch cables coupled to 473-nm laser equipped with a collimator. Optical stimulation was controlled by a stimulus pulse generator and by signal pulses generated by digital input/output board.

The grooming conditioning task: Mice were allowed to recover for at least 7 days after surgery before any behavioral experimentation. The conditioning task was performed in a rectangular enclosure (15x25x15cm) composed of anti-static plastic walls and a transparent Plexiglas floor (Fig. 5.1 A). Mice were first habituated to the experimental box for several days. Each daily conditioning session consisted of 40 paired trials and 10 probe trials. In the paired trial, an 8 kHz tone was presented 1.3 s before the delivery of a water drop to the forehead of the mouse through the spout connected to a computer-controlled pump (Fig. 5.1 B). The tone terminated simultaneously with the water drop. In the 10 probe trials randomly inserted within the 40 paired trials, the 8 kHz tone sounded for 1.3s without water-drop delivery. Mice were allowed to groom freely in response to the tone and water. The inter-trial intervals began when the mice stopped grooming and were randomized in length (30-60 s). Each training session was conducted in dim light and lasted approximately 1h. Grooming behavior was recorded with a video camera placed under the experimental box. Grooming onset events were assigned at the time when the mouse' front paws reached its nose to engage in phase 1 of grooming as defined in [291,292]. At the end of the training lasting at least 16 consecutive days, a subset of the *Sapap3* mutant mice (n= 7) were exposed to an extra session with laser stimulation delivered from 0.2 s before to 2.5 s after the tone onset (5 mW, 5 ms pulses, 10 Hz).

Out-of-task optogenetic stimulation: We delivered steady optical stimulation (5 mW, 5 ms pulses, 5 Hz) to mice placed in the experimental box without applying the conditioning protocol. Three-minute periods with and without continuous light stimulation were alternated consecutively 5 times.

Free-feeding behavioral task: Mice were food deprived for 3 days prior to this control experiment. The durations of feeding and food consumption were

measured for each 5-minutes period with or without light stimulation. The light on/off periods were alternated twice for a 20-minutes total duration.

Data acquisition and analysis: Stimulus events (tone onset, water drop delivery, laser stimulation) were recorded during all training sessions, along with behavior (video) and neuronal activity. Neuronal recording of MSN and FSI activity with laser stimulation were performed after the training. Unit activity (gain: 200-10,000, filter: 600-6,000 Hz) was recorded with a Data Acquisition System. Spikes exceeding a preset voltage threshold were sampled at 32 kHz and were stored with time-stamps. For local field potential recording, neural signals were amplified (gain: 1,000), filtered (1-475 Hz) and sampled at 1 kHz. The spectral content of the local field potential signals was analyzed using open-source Chronux algorithms (http://chronux.org), in-house software, and the Matlab Signal Processing Toolkit. Spectrograms were constructed by the multitaper method, with three tapers, time bandwidth product of 2, and window width of 0.75 s. Unit activity containing spikes of multiple neurons was sorted manually off-line into putative single units according to multiple spike parameters (e.g., peak height, valley depth, peak time) on the 4 channels of each tetrode. The accuracy of spike-sorting and the quality of the single units were then evaluated by the use of spike waveform overlays to confirm uniform waveforms for a given unit and autocorrelograms to detect the presence of an absolute refractory period. Based on these tests, “clusters” judged as being noise were excluded from the analysis. We classified as putative excitatory pyramidal cells neurons in which the baseline firing rate averaged over 50 trials did not exceed 10 Hz, with a spike width (at half-peak amplitude) within a range of 110-220µs. With this criterion, we selected 79.1 % (480/607) of the total units recorded in the lOFC (Fig. 5.9 A). For the striatal units, a unit with the average baseline firing rate of 5 Hz or below and with a spike width (at half-peak amplitude) within a range of 130-250 µs was classified as a putative MSN (Fig. 5.9 B). With this criterion, we identified 81.5 % (495/608) of the units recorded in the striatum as putative MSNs. We classified as putative FSIs recorded units with the average baseline firing rate exceeding 10 Hz and with a spike width within a range of 70-120 µs (Fig. 5.9 B). We identified 4.3 % (26/608) of the striatal units as putative FSIs. Units that did not meet these criteria (putative tonically active neurons, other types or noisy units) were excluded from the analysis. A unit (either putative MSN or putative pyramidal neuron) was further classified as ‘‘task-related” unit if its firing rate between the tone and water-drop events was greater than 2 standard deviations above its pretrial

baseline firing rate (2 s before the tone event) for at least three consecutive 50ms bins. For statistical analyses, statistical significance was assessed using repeated measures analysis of variance (ANOVA) on the entire training period, unpaired t-tests (with Bonferroni test for multiple comparisons) and chi-square tests. Data were analyzed using Statview and SPSS software.

Histology: At the end of training, mice were deeply anesthetized (Nembutal, 50-100 mg/kg), and lesions were made to mark the final recording sites (25 µA, 10 s). Mice were then perfused with 4 % paraformaldehyde (PFA) in 0.1 M sodium-potassium phosphate buffered saline (PBS), and 30 µm thick transverse frozen sections were stained for Nissl substance to identify lesion sites and by immunohistochemistry for GFP protein to confirm viral expression.

Immunostaining and cell count: Eight *Sapap3* mutant mice and eight age-matched wildtype mice (3-10 months) were compared for this study. Mice were anesthetized by isoflurane inhalation and transcardially perfused with cold PBS solution followed by 4 % PFA fixative solution. Brains were coded in order to blind the experimenter and kept in 4 % PFA ON at 4 °C. Brains were then transferred to PBS and sectioned at 50 µm on a Vibratome. Two to six matched coronal sections (every 50 µm from 0.05-0.30 mm relative to Bregma point) containing the striatum from each animal were selected according to the mouse brain atlas. Sections were washed 3 times in PBS and incubated in 1.2 % Triton-X 100 for 15 minutes, followed by another PBS wash (3 times). Blocking was performed for 1 hour in PBS containing 2 % BSA and 0.2 % Triton-X. Mouse anti-parvalbumin antibody (Swant, PV235, 1:5000) was incubated overnight at 4 °C. Next day, sections were washed 3 times in PBS, followed by 2 hours room temperature incubation in biotinylated goat anti-mouse antibody (Jackson ImmunoResearch, 115-065-003). Sections were then washed and processed using the Vectastain ABC kit (Vector Laboratories, PK-4000) and DAB substrate kit for peroxidase (Vector Laboratories, SK4100). Sections were mounted in Krystalon and imaged at the highest focal plane (to control for potential differences in labeling due to focal depth changes) using a microscope, 20x objective. Cells were counted from a 500 x 500 µm region defined according to the area of recording for both hemispheres in each section (Fig. 5.8 B; ML: 1.0-1.5 mm, DV: 2.0-2.5 mm). Statistical analysis was performed using a chi-square test on the total number of cells counted in both genotypes.

PART III

GENERAL DISCUSSION

Chapter 6

Discussion and future directions

The studies described in this thesis summarize my work in the Feng Lab. The goal of these studies was to deepen the current knowledge on synaptic and circuitry mechanisms of basal ganglia dysfunction in compulsive and repetitive behavior. Two synaptic genes were studied to achieve this goal: *Sapap3* and *Shank3*. Different KO/KI mice lines were generated and used throughout the experimental work, helping us to identify both overlapping and distinct phenotypes between these two genes and their associations to OCD and ASD – two distinct neuropsychiatric disorders that share some behavioral commonalities and can be often comorbid with one another.

Several fundamental findings emerging from this work are discussed below as well as future experimental work that can be derived from those findings.

Obsessive-Compulsive Disorder (OCD) and *Sapap3*

In order to understand striatal function (and dysfunction) is crucial to illuminate the neuronal players underlying specific behavioral responses. Diminished behavioral flexibility (i.e., behavioral changes according to contextual cues) and disrupted balance between goal-directed control and habit learning (with overreliance on habits) have been described in OCD patients[294,295].

One theory in the basal ganglia field is that the dynamics between MSNs and FSis might be important for the striatum to maintain a general structure of the task while concomitantly processing changes in task details (and thus adjusting task performance). Work done by Kubota *et al.* in 2009 shows that both MSNs and FSi in DLS express task-bracketing activity pattern[288]. When task changes occur, MSNs pattern is unaffected. Remarkably this pattern suffers changes in simultaneously recorded FSi. The FSis novel response to the new cue fades with further training, suggesting that striatal interneurons may promote behavioral flexibility and help to shape behavioral performance.

First, our experimental studies described on chapter 2 demonstrate that parvalbumin fast-spiking interneurons in DMS are required for habit learning. These results pose a model where after extensive training, FSi activity in DMS will help habit formation (by possibly helping to dampen MSNs activity in DMS and allowing activity in DLS to emerge). In a scenario where a novel task change occurs (such as the cue change described by Kubota *et al.*), FSi in DLS would then suffer a change in their activity pattern, hypothetically dampening DLS activity at the same time that DMS

activation occurs. Once learning as occurred for the novel cue, FSi activity in DLS would faden (as well as DMS activity) and a new habit would be formed. Future experiments can be made to address this hypothesis by simultaneously recording striatal FSi activity in DMS and DLS territories *in vivo*, during goal-directed and habitual learning and upon task changes.

Second, experimental evidence from our lab in collaboration with Dr. Ann Graybiel's lab[257] (described on chapter 5) shows that lack of proper striatal FSi inhibition might contribute to the etiology of compulsive grooming and lack of behavioral adaptation observed in the *Sapap3* OCD-mouse model. Although this published work focused on centromedial striatum region, it would be interesting to address what changes are simultaneously occurring in DLS territory. Unpublished data from our lab shows that the decreased PV interneuron numbers observed in dorsomedial striatum of *Sapap3* mice, are accompanied by a reduced PV number in dorsolateral region as well. This suggests that DLS baseline firing activity may also be increased in these mice, adding to the existing increased baseline activity already reported for their centromedial striatum region. Given that a dynamic competition between DMS and DLS activity seems to guide the expression of habits, we hypothesize that a disruption in this balance could be underlying the pathological behavior. It would be important to clarify which striatum subregion (DLS or DMS) is guiding behavioral expression in these mice. Unpublished data from my graduate work using *Sapap3*-KO in the operant chamber task, shows enhanced habit formation (DLS overactivation?). Future experimental work should directly test whether the beneficial effect on grooming behavior observed upon lOFC-striatal pathway activation in *Sapap3* mice is accompanied by parallel changes in other striatum territories (DLS and even ventral striatum) that are known to coordinate their activity with DMS.

These two experimental studies suggest that striatum interneuron pathology might be associated with increased striatal activity in OCD. Striatum overactivation might result in increased motor routines such as the self-injurious overgrooming that is observed in the *Sapap3*-KO mice.

Autism-Spectrum Disorders (ASD) and *Shank3*

Further experimental work described on this thesis deepens our knowledge on the neural (and genetic) basis of compulsive behavior and anxiety (two behavioral phenotypes shared by the OCD- and ASD-mouse models - the *Sapap3* and *Shank3* KO mice respectively).

First, our experimental study using the *Shank3*-cKI mouse (described on chapter 3) allowed us to study neurodevelopmental behavior phenotypes that can be reversed in

adulthood upon normal gene expression. The results from this study not only demonstrate that it is possible to reverse pathological grooming and social interaction deficits in adult mice, but surprisingly reveal that anxiety cannot be reversed by this strategy. This finding brings tremendous implications for ASD, indicating that although both symptoms are present in this ASD model, they are independent of one another. This suggests that the same gene can play a different role in distinct brain circuits and can differentially affect their activity at distinct developmental periods. Future experimental work can take advantage of the conditional strategy present in this mice to address which brain regions/cell types are responsible for the various behavioral deficits, by crossing them with *cre*-specific lines.

Second, our experimental work (chapter 4) using two mouse lines carrying different human SHANK3 mutations associated with two distinct clinical diagnosis (ASD and schizophrenia) further adds that within the same gene, specific mutations can lead to different phenotypes contributing to a great complexity level. Mice carrying InsG3680 mutation (ASD associated) show full deletion of SHANK3 protein expression and have more pronounced striatal synaptic deficits and increased repetitive overgrooming behavior. On the other hand, mice carrying R117X mutation (schizophrenia associated) show a truncated SHANK3 protein band and pronounced synaptic defects in prefrontal cortex that are not seen in InsG3680 mice. This work specifically uses 2 point mutations identified in humans, portraying the importance of establishing close animal models of human conditions that may allow us to isolate specific endophenotypes. Patients carrying different mutations within the *Shank3* gene (and even within the same *Shank3* exon) might present differential benefit from the same therapeutic approaches and hence should be accounted for differently in clinical trials. It is thus important to determine first whether those mutations result in lost (or gain) of function of the *Shank3* gene and how they affect brain circuits. Results from this study bring tremendous implications for the rationale design of successful clinical trials and to understand data from human genetic screenings. Current data from large scale genomic studies, suggests overlapping genes and pathways for different neuropsychiatric disorders. Taking advantage of emerging scientific approaches such as iPSC-derived neurons from human patients, one can envision the emergence of personalized tretament for neuropsychiatric disorders, in line with what is currently done in the oncology field. Identifying how specific mutations can lead to cell type and disease specific disregulations will significantly improve the neuroscience field. Future experimental work using these mutant mice lines can address if it is possible to genetically correct these human insertions and reverse the behavioral phenotypes specifically elicited by those. These hypotheses can be explored through *in vivo* genome editing using modern tools such as TALEN or CRISPR-Cas9 system.

Those results will certainly be highly translational and informative in terms of how efficiently can we access those locus and modify them for future gene therapy approaches in human patients.

PART IV

REFERENCE LIST

References

1. Steiner H, Tseng KY, eds. *Handbook of Basal Ganglia Structure and Function*. Academic Press; 2010.
2. Vesalius A. *De Humani Corporis Fabrica Libri Septem*. School of medicine, Padua; 1543.
3. Parent A. The History of the Basal Ganglia: The Contribution of Karl Friedrich Burdach. *Neuroscience & Medicine*. 2012; 3:374-379.
4. Wilson S. Progressive lenticular degeneration: a familial nervous disease associated with cirrhosis of the liver. *Brain*. 1912;34. http://brain.oxfordjournals.org/content/34/4/295.full.pdf.
5. Parent A. *Comparative Neurobiology of the Basal Ganglia*. 99th ed. New York: Wiley-Interscience; 1986.
6. Krack P, Hariz MI, Baunez C, Guridi J, Obeso J a. Deep brain stimulation: from neurology to psychiatry? *Trends Neurosci*. 2010;33(10):474-484. doi:10.1016/j.tins.2010.07.002.
7. Graybiel a M, Rauch SL. Toward a neurobiology of obsessive-compulsive disorder. *Neuron*. 2000;28(2):343-347. http://www.ncbi.nlm.nih.gov/pubmed/11144344.
8. Dalley JW, Cardinal RN, Robbins TW. Prefrontal executive and cognitive functions in rodents: neural and neurochemical substrates. *Neurosci Biobehav Rev*. 2004;28(7):771-784. doi:10.1016/j.neubiorev.2004.09.006.
9. Yin HH, Knowlton BJ. The role of the basal ganglia in habit formation. *Nat Rev Neurosci*. 2006;7(6):464-476. doi:10.1038/nrn1919.
10. Hilário MRF, Costa RM. High on habits. *Front Neurosci*. 2008;2(2):208-217. doi:10.3389/neuro.01.030.2008.
11. Fuster J. The prefrontal cortex-An update-Time is of the essence. *Neuron*. 2001;30(C):319-333.
12. Euston DR, Gruber AJ, McNaughton BL. The role of medial prefrontal cortex in memory and decision making. *Neuron*. 2012;76(6):1057-1070. doi:10.1016/j.neuron.2012.12.002.
13. Voorn P, Vanderschuren LJMJ, Groenewegen HJ, Robbins TW, Pennartz CM a. Putting a spin on the dorsal-ventral divide of the striatum. *Trends Neurosci*. 2004;27(8):468-474. doi:10.1016/j.tins.2004.06.006.
14. Yin HH, Ostlund SB, Knowlton BJ, Balleine BW. The role of the dorsomedial striatum in instrumental conditioning. *Eur J Neurosci*. 2005;22(2):513-523. doi:10.1111/j.1460-9568.2005.04218.x.
15. Alexander G, DeLong MR, Strick P. Parallel organization of functionally segregated circuits linking basal ganglia and cortex. *Annu Rev Neurosci.* 1986; 9:357-81. doi:10.1146/annurev.ne.09.030186.002041.

16. Hilario M, Holloway T, Jin X, Costa RM. Different dorsal striatum circuits mediate action discrimination and action generalization. *Eur J Neurosci*. 2012;35(7):1105-1114. doi:10.1111/j.1460-9568.2012.08073.x.

17. Yin HH, Knowlton BJ, Balleine BW. Lesions of dorsolateral striatum preserve outcome expectancy but disrupt habit formation in instrumental learning. *Eur J Neurosci*. 2004;19(1):181-9. doi:10.1046/j.1460-9568.2003.03095.x.

18. Yin HH, Knowlton BJ, Balleine BW. Blockade of NMDA receptors in the dorsomedial striatum prevents action-outcome learning in instrumental conditioning. *Eur J Neurosci*. 2005;22(2):505-512. doi:10.1111/j.1460-9568.2005.04219.x.

19. Yin HH, Knowlton BJ, Balleine BW. Inactivation of dorsolateral striatum enhances sensitivity to changes in the action-outcome contingency in instrumental conditioning. *Behav Brain Res*. 2006;166(2):189-196. doi:10.1016/j.bbr.2005.07.012.

20. Yin HH, Knowlton BJ. Contributions of striatal subregions to place and response learning. *Learn Mem*. 2004;11(4):459-463. doi:10.1101/lm.81004.

21. Gremel CM, Costa RM. Orbitofrontal and striatal circuits dynamically encode the shift between goal-directed and habitual actions. *Nat Commun*. 2013;4(May):2264. doi:10.1038/ncomms3264.

22. Smith KS, Graybiel AM. A dual operator view of habitual behavior reflecting cortical and striatal dynamics. *Neuron*. 2013;79(2):361-374. doi:10.1016/j.neuron.2013.05.038.

23. Thorn CA, Atallah H, Howe M, Graybiel AM. Differential Dynamics of Activity Changes in Dorsolateral and Dorsomedial Striatal Loops during Learning. *Neuron*. 2010;66(5):781-795. doi:10.1016/j.neuron.2010.04.036.

24. Grabli D, McCairn K, Hirsch EC, et al. Behavioural disorders induced by external globus pallidus dysfunction in primates: I. Behavioural study. *Brain*. 2004;127(Pt 9):2039-2054. doi:10.1093/brain/awh220.

25. Mink JW. The basal ganglia: Focused selection and inhibition of competing motor programs. *Prog Neurobiol*. 1996;50:381-425. doi:10.1016/S0301-0082(96)00042-1.

26. Albin R, Young A, Penney J. The functional anatomy of basal ganglia disorders. *Trends Neurosci*. 1989;12(10):366-75. doi:10.1016/0166-2236(89)90074-X.

27. DeLong MR, Wichmann T. Circuits and circuit disorders of the basal ganglia. *Arch Neurol*. 2007;64(1):20-24. doi:10.1001/archneur.64.1.20.

28. Kreitzer AC, Malenka RC. Striatal plasticity and basal ganglia circuit function. *Neuron*. 2008;60(4):543-554. doi:10.1016/j.neuron.2008.11.005.

29. Smith Y, Raju D, Pare J, Sidibe M. The thalamostriatal system: a highly specific network of the basal ganglia circuitry. *Trends Neurosci*. 2004;27(9):520-7. http://www.sciencedirect.com/science/article/pii/S0166223604002322.

30. Bevan MD, Booth PA, Eaton SA, Bolam JP. Selective innervation of neostriatal interneurons by a subclass of neuron in the globus pallidus of the rat. *J Neurosci*. 1998;18:9438-9452.

31. Kita H, Kitai ST. The morphology of globus pallidus projection neurons in the rat: An intracellular staining study. *Brain Res*. 1994;636:308-319. doi:10.1016/0006-8993(94)91030-8.

32. Tepper JM, Abercrombie ED, Bolam JP. Basal ganglia macrocircuits. *Prog Brain Res*. 2007;160:3-7. doi:10.1016/S0079-6123(06)60001-0.

33. Koós T, Tepper JM. Inhibitory control of neostriatal projection neurons by GABAergic interneurons. *Nat Neurosci*. 1999;2(5):467-472. doi:10.1038/8138.

34. Nambu A, Tokuno H, Hamada I, et al. Excitatory cortical inputs to pallidal neurons via the subthalamic nucleus in the monkey. *J Neurophysiol*. 2000;84:289-300. doi:10.1016/S0168-0102(98)82646-1.

35. Wichmann T, Delong MR, Guridi J, Obeso JA. Milestones in research on the pathophysiology of Parkinson's disease. *Mov Disord*. 2011;26:1032-1041. doi:10.1002/mds.23695.

36. Kita H. *The Basal Ganglia IV*. (Percheron G, ed.). New York: Plenum Press; 1994.

37. Kreitzer AC. Physiology and pharmacology of striatal neurons. *Annu Rev Neurosci*. 2009;32:127-147. doi:10.1146/annurev.neuro.051508.135422.

38. Gittis AH, Nelson AB, Thwin MT, Palop JJ, Kreitzer AC. Distinct roles of GABAergic interneurons in the regulation of striatal output pathways. *J Neurosci*. 2010;30(6):2223-2234. doi:10.1523/JNEUROSCI.4870-09.2010.

39. Bennett BD, Callaway JC, Wilson CJ. Intrinsic Membrane Properties Underlying Spontaneous Tonic Firing in Neostriatal Cholinergic Interneurons. *J Neurosci*. 2000;20(22):8493-8503.

40. DeLong MR. Primate models of movement disorders of basal ganglia origin. *Trends Neurosci*. 1990;13(7):281-285. http://www.ncbi.nlm.nih.gov/pubmed/1695404.

41. Alexander GE, Crutcher MD. Functional architecture of basal ganglia circuits: neural substrates of parallel processing. *Trends Neurosci*. 1990;13(7):266-271. http://www.ncbi.nlm.nih.gov/pubmed/1695401.

42. Kravitz A V, Freeze BS, Parker PRL, et al. Regulation of parkinsonian motor behaviours by optogenetic control of basal ganglia circuitry. *Nature*. 2010;466(7306):622-626. doi:10.1038/nature09159.

43. Cui G, Jun SB, Jin X, et al. Concurrent activation of striatal direct and indirect pathways during action initiation. *Nature*. 2013;494(7436):238-242. doi:10.1038/nature11846.

44. Calabresi P, Picconi B, Tozzi A, Ghiglieri V, Di Filippo M. Direct and indirect pathways of basal ganglia: a critical reappraisal. *Nat Neurosci*. 2014;17(8):1022-1030. doi:10.1038/nn.3743.

45. Freeze BS, Kravitz A V, Hammack N, Berke JD, Kreitzer AC. Control of basal ganglia output by direct and indirect pathway projection neurons. *J Neurosci*. 2013;33(47):18531-18539. doi:10.1523/JNEUROSCI.1278-13.2013.

46. Ramanathan S, Hanley JJ, Deniau J-M, Bolam JP. Synaptic convergence of motor and somatosensory cortical afferents onto GABAergic interneurons in the rat striatum. *J Neurosci*. 2002;22(18):8158-8169. http://www.ncbi.nlm.nih.gov/pubmed/12223570.

47. Berke JD. Functional properties of striatal fast-spiking interneurons. *Front Syst Neurosci*. 2011;5(June):45. doi:10.3389/fnsys.2011.00045.

48. Bennett B, Bolam J. Synaptic input and output of parvalbumin-immunoreactive neurons in the neostriatum of the rat. *Neuroscience*. 1994;62(3):707-719. http://www.sciencedirect.com/science/article/pii/0306452294904715.

49. Wilson CJ. GABAergic inhibition in the neostriatum. *Prog Brain Res*. 2007;160:91-110. doi:10.1016/S0079-6123(06)60006-X.

50. Izzo PN, Bolam JP. Cholinergic synaptic input to different parts of spiny striatonigral neurons in the rat. *J Comp Neurol*. 1988;269:219-234. doi:10.1002/cne.902690207.

51. Koós T, Tepper JM. Dual cholinergic control of fast-spiking interneurons in the neostriatum. *J Neurosci*. 2002;22(2):529-535. http://www.ncbi.nlm.nih.gov/pubmed/11784799.

52. Tepper JM, Wilson CJ, Koós T. Feedforward and feedback inhibition in neostriatal GABAergic spiny neurons. *Brain Res Rev*. 2008;58(2):272-281. doi:10.1016/j.brainresrev.2007.10.008.

53. Gertler TS, Chan CS, Surmeier DJ. Dichotomous anatomical properties of adult striatal medium spiny neurons. *J Neurosci*. 2008;28(43):10814-10824. doi:10.1523/JNEUROSCI.2660-08.2008.

54. Sheng M, Hoogenraad CC. The postsynaptic architecture of excitatory synapses: a more quantitative view. *Annu Rev Biochem*. 2007;76:823-847. doi:10.1146/annurev.biochem.76.060805.160029.

55. Okabe S. Molecular anatomy of the postsynaptic density. *Mol Cell Neurosci*. 2007;34:503-518. doi:10.1016/j.mcn.2007.01.006.

56. Boeckers TM. The postsynaptic density. *Cell Tissue Res*. 2006;326(2):409-422. doi:10.1007/s00441-006-0274-5.

57. Peça J, Ting J, Feng G. SnapShot: autism and the synapse. *Cell*. 2011;147(3):706-706.e1. doi:10.1016/j.cell.2011.10.015.

58. Welch JM, Lu J, Rodriguiz RM, et al. Cortico-striatal synaptic defects and OCD-like behaviours in Sapap3-mutant mice. *Nature*. 2007;448(7156):894-900. doi:10.1038/nature06104.

59. Peça J, Feliciano C, Ting JT, et al. Shank3 mutant mice display autistic-like behaviours and striatal dysfunction. *Nature*. 2011;472(7344):437-442. doi:10.1038/nature09965.

60. Fontenelle LF, Mendlowicz M V, Versiani M. The descriptive epidemiology of obsessive-compulsive disorder. *Prog Neuropsychopharmacol Biol Psychiatry*. 2006;30:327-337. doi:10.1016/j.pnpbp.2005.11.001.

61. Ruscio A, Stein D, Chiu W, Kessler R. The epidemiology of obsessive-compulsive disorder in the National Comorbidity Survey Replication. *Mol Psychiatry*. 2010;15:53-63. doi:10.1038/mp.2008.94.

62. Fineberg N a, Gale TM. Evidence-based pharmacotherapy of obsessive-compulsive disorder. *Int J Neuropsychopharmacol*. 2005;8(1):107-129. doi:10.1017/S1461145704004675.

63. Pallanti S, Hollander E. Pharmacological, experimental therapeutic, and transcranial magnetic stimulation treatments for compulsivity and impulsivity. *CNS Spectr*. 2014;19(1):50-61. doi:10.1017/S1092852913000618.

64. Goodman WK, Foote KD, Greenberg BD, et al. Deep brain stimulation for intractable obsessive compulsive disorder: pilot study using a blinded, staggered-onset design. *Biol Psychiatry*. 2010;67:535-542. doi:10.1016/j.biopsych.2009.11.028.

65. Greenberg BD, Gabriels LA, Malone DA, et al. Deep Brain Stimulation of the Ventral Internal Capsule/ventral Striatum for Obsessive-Compulsive Disorder: Worldwide Experience.; *Mol Psychiatry*. 2010;15(1):64-79. doi:10.1038/mp.2008.55.

66. Sturm V, Lenartz D, Koulousakis A, et al. The nucleus accumbens: A target for deep brain stimulation in obsessive-compulsive- and anxiety-disorders. *Journal of Chemical Neuroanatomy*. 2003;26(4):293-9. doi:10.1016/j.jchemneu.2003.09.003.

67. Pittenger C, Bloch MH, Williams K. Glutamate abnormalities in obsessive compulsive disorder: neurobiology, pathophysiology, and treatment. *Pharmacol Ther*. 2011;132(3):314-332. doi:10.1016/j.pharmthera.2011.09.006.

68. Saxena S, Rauch SL. Functional neuroimaging and the neuroanatomy of obsessive-compulsive disorder. *Psychiatr Clin North Am*. 2000;23:563-586. doi:10.1016/S0193-953X(05)70181-7.

69. Ting JT, Feng G. Neurobiology of obsessive-compulsive disorder: Insights into neural circuitry dysfunction through mouse genetics. *Curr Opin Neurobiol*. 2011;21:842-848. doi:10.1016/j.conb.2011.04.010.

70. Saxena S, Brody AL, Schwartz JM, Baxter LR. Neuroimaging and frontal-subcortical circuitry in obsessive-compulsive disorder. *Br J Psychiatry*. 1998;173:26-37.

71. Tye KM, Deisseroth K. Optogenetic investigation of neural circuits underlying brain disease in animal models. *Nat Rev Neurosci*. 2012;13(4):251-266. doi:10.1038/nrn3171.

72. Zhang F, Wang L, Boyden ES, Deisseroth K. Channelrhodopsin-2 and Optical Control of Excitable Cells. *Nat Methods*. 2006;3(10):785-92. doi:10.1038/NMETH936.

73. Ahmari SE, Spellman T, Douglass NL, et al. Repeated cortico-striatal stimulation generates persistent OCD-like behavior. *Science*. 2013;340(6137):1234-1239. doi:10.1126/science.1234733.

74. Nestler EJ, Barrot M, Self DW. DeltaFosB: a sustained molecular switch for addiction. *Proc Natl Acad Sci USA*. 2001;98(20):11042-11046. doi:10.1073/pnas.191352698.

75. Insel TR, Winslow JT. Neurobiology of obsessive compulsive disorder. *Psychiatr Clin North Am*. 1992;15(4):813-824.

76. Rothwell PE, Fuccillo M V., Maxeiner S, et al. Autism-associated neuroligin-3 mutations commonly impair striatal circuits to boost repetitive behaviors. *Cell*. 2014;158:198-212. doi:10.1016/j.cell.2014.04.045.

77. Pauls DL, Abramovitch A, Rauch SL, Geller D a. Obsessive-compulsive disorder: an integrative genetic and neurobiological perspective. *Nat Rev Neurosci*. 2014;15(6):410-424. doi:10.1038/nrn3746.

78. Stein DJ, Fineberg NA, Bienvenu OJ, et al. Should ocd be classified as an anxiety disorder in DSM-V? *Depress Anxiety*. 2010;27:495-506. doi:10.1002/da.20699.

79. Fineberg NA, Potenza MN, Chamberlain SR, et al. Probing compulsive and impulsive behaviors, from animal models to endophenotypes: a narrative review. *Neuropsychopharmacology*. 2010;35:591-604. doi:10.1038/npp.2009.185.

80. Aruga J, Mikoshiba K. Identification and characterization of Slitrk, a novel neuronal transmembrane protein family controlling neurite outgrowth. *Mol Cell Neurosci*. 2003;24:117-129. doi:10.1016/S1044-7431(03)00129-5.

81. Shmelkov S V, Hormigo A, Jing D, et al. Slitrk5 deficiency impairs corticostriatal circuitry and leads to obsessive-compulsive-like behaviors in mice. *Nat Med*. 2010;16(5):598-602, 1p following 602. doi:10.1038/nm.2125.

82. Clifford CA, Murray RM, Fulker DW. Genetic and environmental influences on obsessional traits and symptoms. *Psychol Med*. 1984;14:791-800. doi:10.1017/S0033291700019760.

83. Hollander E, Kim S, Khanna S, Pallanti S. Obsessive-compulsive disorder and obsessive-compulsive spectrum disorders: diagnostic and dimensional issues. *CNS Spectr*. 2007:1-10. http://europepmc.org/abstract/med/17277719.

84. Grootheest D van. Twin studies on obsessive–compulsive disorder: a review. *Twin Res Hum Genet.* 2005;8(5):450-458.

85. Hanna GL, Veenstra-VanderWeele J, Cox NJ, et al. Genome-wide linkage analysis of families with obsessive-compulsive disorder ascertained through pediatric probands. *Am J Med Genet - Neuropsychiatr Genet*. 2002;114:541-552. doi:10.1002/ajmg.10519.

86. Arnold PD, Sicard T, Burroughs E, Richter MA, Kennedy JL. Glutamate transporter gene SLC1A1 associated with obsessive-compulsive disorder. *Arch Gen Psychiatry*. 2006;63:769-776. doi:10.1001/archpsyc.63.7.769.

87. Wendland JR, Moya PR, Timpano KR, et al. A haplotype containing quantitative trait loci for SLC1A1 gene expression and its association with obsessive-

compulsive disorder. *Arch Gen Psychiatry*. 2009;66:408-416. doi:10.1001/archgenpsychiatry.2009.6.

88. Wang Y, Adamczyk A, Shugart YY, et al. A screen of SLC1A1 for OCD-related alleles. *Am J Med Genet Part B Neuropsychiatr Genet*. 2010;153:675-679. doi:10.1002/ajmg.b.31001.

89. Peghini P, Janzen J, Stoffel W. Glutamate transporter EAAC-1-deficient mice develop dicarboxylic aminoaciduria and behavioral abnormalities but no neurodegeneration. *EMBO J*. 1997;16:3822-3832. doi:10.1093/emboj/16.13.3822.

90. Wu H, Wang X, Xiao Z, et al. Association between SLC1A1 gene and early-onset OCD in the han chinese population: A case-control study. *J Mol Neurosci*. 2013;50:353-359. doi:10.1007/s12031-013-9995-6.

91. Stewart SE, Yu D, Scharf JM, et al. Genome-wide association study of obsessive-compulsive disorder. *Mol Psychiatry*. 2013;18(7):788-798. doi:10.1038/mp.2012.85.

92. Mattheisen M, Samuels JF, Wang Y, et al. Genome-wide association study in obsessive-compulsive disorder: results from the OCGAS. *Mol Psychiatry*. 2014;(October 2013):1-8. doi:10.1038/mp.2014.43.

93. Proenca C, Gao K, Shmelkov S. Slitrks as emerging candidate genes involved in neuropsychiatric disorders. *Trends Neurosci.* 2011 Mar;34(3):143-53. doi: 10.1016/j.tins.2011.01.001.

94. Abelson JF, Kwan KY, O'Roak BJ, et al. Sequence Variants in SLITRK1 Are Associated with Tourette's Syndrome. *Science.* 2005 Oct 14;310(5746):317-20. doi:10.1126/science.1116502.

95. Leckman JF. Tourette's syndrome. *Lancet*. 2002;360(9345):1577-1586. doi:10.1016/S0140-6736(02)11526-1.

96. Aruga J, Yokota N, Mikoshiba K. Human SLITRK family genes: genomic organization and expression profiling in normal brain and brain tumor tissue. *Gene*. 2003;315:87-94. doi:10.1016/S0378-1119(03)00715-7.

97. Greer JM, Capecchi MR. Hoxb8 is required for normal grooming behavior in mice. *Neuron*. 2002;33(1):23-34. http://www.ncbi.nlm.nih.gov/pubmed/11779477.

98. Chen S-K, Tvrdik P, Peden E, et al. Hematopoietic origin of pathological grooming in Hoxb8 mutant mice. *Cell*. 2010;141(5):775-785. doi:10.1016/j.cell.2010.03.055.

99. Murphy TK, Kurlan R, Leckman J. The immunobiology of Tourette's disorder, pediatric autoimmune neuropsychiatric disorders associated with Streptococcus, and related disorders: a way forward. *J Child Adolesc Psychopharmacol*. 2010;20(4):317-331. doi:10.1089/cap.2010.0043.

100. Goddard AW, Shekhar A, Whiteman AF, McDougle CJ. Serotoninergic mechanisms in the treatment of obsessive-compulsive disorder. *Drug Discov Today*. 2008;13(7-8):325-332. doi:10.1016/j.drudis.2007.12.009.

101. Chou-Green JM, Holscher TD, Dallman MF, Akana SF. Compulsive behavior in the 5-HT2C receptor knockout mouse. *Physiol Behav*. 2003;78(4-5):641-649. doi:10.1016/S0031-9384(03)00047-7.

102. Abdallah L, Bonasera SJ, Hopf FW, et al. Impact of serotonin 2C receptor null mutation on physiology and behavior associated with nigrostriatal dopamine pathway function. *J Neurosci*. 2009;29:8156-8165. doi:10.1523/JNEUROSCI.3905-08.2009.

103. Giorgetti M, Tecott LH. Contributions of 5-HT2C receptors to multiple actions of central serotonin systems. *Eur J Pharmacol*. 2004;488:1-9. doi:10.1016/j.ejphar.2004.01.036.

104. Heisler LK, Zhou L, Bajwa P, Hsu J, Tecott LH. Serotonin 5-HT(2C) receptors regulate anxiety-like behavior. *Genes Brain Behav*. 2007;6(5):491-496. doi:10.1111/j.1601-183X.2007.00316.x.

105. Tang R, Noh H, Wang D, et al. Candidate genes and functional noncoding variants identified in a canine model of obsessive-compulsive disorder. *Genome Biol*. 2014;15(3):R25. doi:10.1186/gb-2014-15-3-r25.

106. Langen M, Schnack HG, Nederveen H, et al. Changes in the Developmental Trajectories of Striatum in Autism. *Biol Psychiatry*. 2009;66:327-333. doi:10.1016/j.biopsych.2009.03.017.

107. Kanner L. Autistic Disturbances of Affective Contact. *Nerv Child*. 1943;(2):217-250.

108. Centers for Disease Control and Prevention. Prevalence of autism spectrum disorders - Autism and Developmental Disabilities Monitoring Network, 14 sites, United States, 2008. *Morb Mortal Wkly Rep*. 2012;61:1-19. http://www.ncbi.nlm.nih.gov/pubmed/22456193.

109. Lai MC, Lombardo M V., Ruigrok AN V, et al. Cognition in Males and Females with Autism: Similarities and Differences. *PLoS One*. 2012;7. doi:10.1371/journal.pone.0047198.

110. Lord C, Cook EH, Leventhal BL, Amaral DG. Autism spectrum disorders. *Neuron*. 2000;28:355-363. doi:10.1002/9780470682340.

111. Frith CD. The social brain? *Philos Trans R Soc Lond B Biol Sci*. 2007;362:671-678. doi:10.1098/rstb.2006.2003.

112. Dalton KM, Nacewicz BM, Johnstone T, et al. Gaze fixation and the neural circuitry of face processing in autism. *Nat Neurosci*. 2005;8:519-526. doi:10.1038/nn1421.

113. Schumann CM, Hamstra J, Goodlin-Jones BL, et al. The amygdala is enlarged in children but not adolescents with autism; the hippocampus is enlarged at all ages. *J Neurosci*. 2004;24:6392-6401. doi:10.1523/JNEUROSCI.1297-04.2004.

114. Chevallier C, Kohls G, Troiani V, Brodkin ES, Schultz RT. The social motivation theory of autism. *Trends Cogn Sci*. 2012;16:231-238. doi:10.1016/j.tics.2012.02.007.

115. Bachevalier J, Loveland KA. The orbitofrontal-amygdala circuit and self-regulation of social-emotional behavior in autism. *Neurosci Biobehav Rev*. 2006;30:97-117. doi:10.1016/j.neubiorev.2005.07.002.

116. Heinrichs M, von Dawans B, Domes G. Oxytocin, vasopressin, and human social behavior. *Front Neuroendocrinol*. 2009;30:548-557. doi:10.1016/j.yfrne.2009.05.005.

117. Dölen G, Darvishzadeh A, Huang KW, Malenka RC. Social reward requires coordinated activity of nucleus accumbens oxytocin and serotonin. *Nature*. 2013;501:179-184. doi:10.1038/nature12518.

118. Gunaydin LA, Grosenick L, Finkelstein JC, et al. Natural neural projection dynamics underlying social behavior. *Cell*. 2014;157:1535-1551. doi:10.1016/j.cell.2014.05.017.

119. Tachibana M, Kagitani-Shimono K, Mohri I, et al. Long-term administration of intranasal oxytocin is a safe and promising therapy for early adolescent boys with autism spectrum disorders. *J Child Adolesc Psychopharmacol*. 2013;23:123-127. doi:10.1089/cap.2012.0048.

120. Hollander E, Bartz J, Chaplin W, et al. Oxytocin Increases Retention of Social Cognition in Autism. *Biol Psychiatry*. 2007;61:498-503. doi:10.1016/j.biopsych.2006.05.030.

121. Nayate A, Bradshaw JL, Rinehart NJ. Autism and Asperger's disorder: Are they movement disorders involving the cerebellum and/or basal ganglia? *Brain Res Bull*. 2005;67:327-334. doi:10.1016/j.brainresbull.2005.07.011.

122. Jeste SS. The neurology of autism spectrum disorders. *Curr Opin Neurol*. 2011;24:132-139. doi:10.1097/WCO.0b013e3283446450.

123. Bradshaw JL, Sheppard DM. The neurodevelopmental frontostriatal disorders: evolutionary adaptiveness and anomalous lateralization. *Brain Lang*. 2000;73:297-320. doi:10.1006/brln.2000.2308.

124. Ridley RM. The psychology of perserverative and stereotyped behaviour. *Prog Neurobiol*. 1994;44:221-231.

125. Leyfer OT, Folstein SE, Bacalman S, et al. Comorbid psychiatric disorders in children with autism: Interview development and rates of disorders. *J Autism Dev Disord*. 2006;36:849-861. doi:10.1007/s10803-006-0123-0.

126. Sears LL, Vest C, Mohamed S, Bailey J, Ranson BJ, Piven J. An MRI study of the basal ganglia in autism. *Prog Neuro-Psychopharmacology Biol Psychiatry*. 1999;23:613-624. doi:10.1016/S0278-5846(99)00020-2.

127. Siegel Jr. B V, Asarnow R, Tanguay P, et al. Regional cerebral glucose metabolism and attention in adults with a history of childhood autism. *J Neuropsychiatry Clin Neurosci*. 1992;4:406-414.

128. Qiu A, Adler M, Crocetti D, Miller MI, Mostofsky SH. Basal ganglia shapes predict social, communication, and motor dysfunctions in boys with autism spectrum disorder. *J Am Acad Child Adolesc Psychiatry*. 2010;49:539-551, 551.e1-e4. doi:10.1016/j.ypsy.2010.09.023.

129. Wang X, McCoy PA, Rodriguiz RM, et al. Synaptic dysfunction and abnormal behaviors in mice lacking major isoforms of Shank3. *Hum Mol Genet*. 2011;20:3093-3108. doi:10.1093/hmg/ddr212.

130. Bozdagi O, Sakurai T, Papapetrou D, et al. Haploinsufficiency of the autism-associated Shank3 gene leads to deficits in synaptic function, social interaction, and social communication. *Mol Autism*. 2010;1:15. doi:10.1186/2040-2392-1-15.

131. Schmeisser MJ, Ey E, Wegener S, et al. Autistic-like behaviours and hyperactivity in mice lacking ProSAP1/Shank2. *Nature*. 2012;486(7402):256-260. doi:10.1038/nature11015.

132. Yang M, Bozdagi O, Scattoni ML, et al. Reduced Excitatory Neurotransmission and Mild Autism-Relevant Phenotypes in Adolescent Shank3 Null Mutant Mice. *J Neurosci*. 2012;32:6525-6541. doi:10.1523/JNEUROSCI.6107-11.2012.

133. Kouser M, Speed HE, Dewey CM, et al. Loss of Predominant Shank3 Isoforms Results in Hippocampus-Dependent Impairments in Behavior and Synaptic Transmission. *J Neurosci*. 2013;33(47):18448-18468. doi:10.1523/JNEUROSCI.3017-13.2013.

134. Rosenberg RE, Law JK, Yenokyan G, McGready J, Kaufmann WE, Law PA. Characteristics and concordance of autism spectrum disorders among 277 twin pairs. *Arch Pediatr Adolesc Med*. 2009;163:907-914. doi:10.1001/archpediatrics.2009.98.

135. Geschwind DH. Advances in autism. *Annu Rev Med*. 2009;60:367-380. doi:10.1146/annurev.med.60.053107.121225.

136. Huguet G, Ey E, Bourgeron T. The genetic landscapes of autism spectrum disorders. *Annu Rev Genomics Hum Genet*. 2013;14:191-213. doi:10.1146/annurev-genom-091212-153431.

137. Betancur C. Etiological heterogeneity in autism spectrum disorders: More than 100 genetic and genomic disorders and still counting. *Brain Res*. 2011;1380:42-77. doi:10.1016/j.brainres.2010.11.078.

138. Toro R, Konyukh M, Delorme R, et al. Key role for gene dosage and synaptic homeostasis in autism spectrum disorders. *Trends Genet*. 2010;26:363-372. doi:10.1016/j.tig.2010.05.007.

139. Südhof TC. Neuroligins and neurexins link synaptic function to cognitive disease. *Nature*. 2008;455:903-911. doi:10.1038/nature07456.

140. Levy D, Ronemus M, Yamrom B, et al. Rare De Novo and Transmitted Copy-Number Variation in Autistic Spectrum Disorders. *Neuron*. 2011;70:886-897. doi:10.1016/j.neuron.2011.05.015.

141. Tabuchi K, Blundell J, Etherton MR, et al. A neuroligin-3 mutation implicated in autism increases inhibitory synaptic transmission in mice. *Science*. 2007;318:71-76. doi:10.1126/science.1146221.

142. Jamain S, Radyushkin K, Hammerschmidt K, et al. Reduced social interaction and ultrasonic communication in a mouse model of monogenic heritable autism. *Proc Natl Acad Sci U S A*. 2008;105:1710-1715. doi:10.1073/pnas.0711555105.

143. Sheng M, Kim E. The Shank family of scaffold proteins. *J Cell Sci*. 2000;113 (Pt 11):1851-6. http://www.ncbi.nlm.nih.gov/pubmed/10806096.

144. Wang X, Xu Q, Bey AL, Lee Y, Jiang Y. Transcriptional and functional complexity of Shank3 provides a molecular framework to understand the phenotypic heterogeneity of SHANK3 causing autism and Shank3 mutant mice. *Mol Autism*. 2014;5:30. doi:10.1186/2040-2392-5-30.

145. Lim S, Sala C, Yoon J, et al. Sharpin, a novel postsynaptic density protein that directly interacts with the shank family of proteins. *Mol Cell Neurosci*. 2001;17:385-397. doi:10.1006/mcne.2000.0940.

146. Böckers TM, Mameza MG, Kreutz MR, et al. Synaptic scaffolding proteins in rat brain: Ankyrin repeats of the multidomain Shank protein family interact with the cytoskeletal protein α-fodrin. *J Biol Chem*. 2001;276:40104-40112. doi:10.1074/jbc.M102454200.

147. Naisbitt S, Kim E, Tu JC, et al. Shank , a Novel Family of Postsynaptic Density Proteins that Binds to the NMDA Receptor / PSD-95 / GKAP Complex and Cortactin. *Neuron*. 1999 Jul;23(3):569-82.

148. Tu JC, Xiao B, Naisbitt S, et al. Coupling of mGluR/Homer and PSD-95 complexes by the Shank family of postsynaptic density proteins. *Neuron*. 1999;23(3):583-592. http://www.ncbi.nlm.nih.gov/pubmed/10433269.

149. Hayashi MK, Tang C, Verpelli C, et al. The Postsynaptic Density Proteins Homer and Shank Form a Polymeric Network Structure. *Cell*. 2009;137:159-171. doi:10.1016/j.cell.2009.01.050.

150. Baron MK, Boeckers TM, Vaida B, et al. An architectural framework that may lie at the core of the postsynaptic density. *Science*. 2006;311:531-535. doi:10.1126/science.1118995.

151. Boeckers TM, Liedtke T, Spilker C, et al. C-terminal synaptic targeting elements for postsynaptic density proteins ProSAP1/Shank2 and ProSAP2/Shank3. *J Neurochem*. 2005;92:519-524. doi:10.1111/j.1471-4159.2004.02910.x.

152. Phelan K, McDermid HE. The 22q13.3 deletion syndrome (Phelan-McDermid syndrome). *Mol Syndromol*. 2012;2:186-201. doi:10.1159/000334260.

153. Bonaglia MC, Giorda R, Beri S, et al. Molecular mechanisms generating and stabilizing terminal 22q13 deletions in 44 subjects with phelan/mcdermid syndrome. *PLoS Genet*. 2011;7. doi:10.1371/journal.pgen.1002173.

154. Leblond CS, Nava C, Polge A, et al. Meta-analysis of SHANK Mutations in Autism Spectrum Disorders: A Gradient of Severity in Cognitive Impairments. *PLoS Genet*. 2014;10(9):e1004580. doi:10.1371/journal.pgen.1004580.

155. Gauthier J, Spiegelman D, Piton A, et al. Novel de novo SHANK3 mutation in autistic patients. *Am J Med Genet Part B Neuropsychiatr Genet*. 2009;150:421-424. doi:10.1002/ajmg.b.30822.

156. Moessner R, Marshall CR, Sutcliffe JS, et al. Contribution of SHANK3 mutations to autism spectrum disorder. *Am J Hum Genet*. 2007;81:1289-1297. doi:10.1086/522590.

157. Durand CM, Betancur C, Boeckers TM, et al. Mutations in the gene encoding the synaptic scaffolding protein SHANK3 are associated with autism spectrum disorders. *Nat Genet*. 2007;39:25-27. doi:10.1038/ng1933.

158. Boccuto L, Lauri M, Sarasua SM, et al. Prevalence of SHANK3 variants in patients with different subtypes of autism spectrum disorders. *Eur J Hum Genet*. 2012. doi:10.1038/ejhg.2012.175.

159. Jiang Y hui, Ehlers MD. Modeling Autism by SHANK Gene Mutations in Mice. *Neuron*. 2013;78:8-27. doi:10.1016/j.neuron.2013.03.016.

160. Jamain S, Quach H, Betancur C, et al. Mutations of the X-linked genes encoding neuroligins NLGN3 and NLGN4 are associated with autism. *Nat Genet*. 2003;34:27-29. doi:10.1038/ng1136.

161. Haber SN, Fudge JL, McFarland NR. Striatonigrostriatal pathways in primates form an ascending spiral from the shell to the dorsolateral striatum. *J Neurosci*. 2000;20(6):2369-2382. http://www.ncbi.nlm.nih.gov/pubmed/10704511.

162. Reep RL, Cheatwood JL, Corwin J V. The associative striatum: organization of cortical projections to the dorsocentral striatum in rats. *J Comp Neurol*. 2003;467(3):271-292. doi:10.1002/cne.10868.

163. Smith KS, Graybiel AM. Investigating habits: strategies, technologies and models. *Front Behav Neurosci*. 2014;8:39. doi:10.3389/fnbeh.2014.00039.

164. Yin HH, Mulcare SP, Hilário MRF, et al. Dynamic reorganization of striatal circuits during the acquisition and consolidation of a skill. *Nat Neurosci*. 2009;12(3):333-341. doi:10.1038/nn.2261.

165. Balleine BW, Liljeholm M, Ostlund SB. The integrative function of the basal ganglia in instrumental conditioning. *Behav Brain Res*. 2009;199(1):43-52. doi:10.1016/j.bbr.2008.10.034.

166. Berke JD, Okatan M, Skurski J, Eichenbaum HB. Oscillatory entrainment of striatal neurons in freely moving rats. *Neuron*. 2004;43(6):883-896. doi:10.1016/j.neuron.2004.08.035.

167. Kvitsiani D, Ranade S, Hangya B, Taniguchi H, Huang JZ, Kepecs a. Distinct behavioural and network correlates of two interneuron types in prefrontal cortex. *Nature*. 2013;498(7454):363-366. doi:10.1038/nature12176.

168. Todtenkopf MS, Stellar JR, Williams E a, Zahm DS. Differential distribution of parvalbumin immunoreactive neurons in the striatum of cocaine sensitized rats. *Neuroscience*. 2004;127(1):35-42. doi:10.1016/j.neuroscience.2004.04.054.

169. Kita H, Kosaka T, Heizmann CW. Parvalbumin-immunoreactive neurons in the rat neostriatum: a light and electron microscopic study. *Brain Res*. 1990;536(1-2):1-15.

170. Mallet N, Le Moine C, Charpier S, Gonon F. Feedforward inhibition of projection neurons by fast-spiking GABA interneurons in the rat striatum in vivo. *J Neurosci*. 2005;25(15):3857-3869. doi:10.1523/JNEUROSCI.5027-04.2005.

171. Gittis A, Leventhal D. Selective inhibition of striatal fast-spiking interneurons causes dyskinesias. *J Neurosci.* 2011;31(44):15727-31. doi: 10.1523/JNEUROSCI.3875-11.2011.

172. Murray AJ, Sauer J-F, Riedel G, et al. Parvalbumin-positive CA1 interneurons are required for spatial working but not for reference memory. *Nat Neurosci*. 2011;14(3):297-299. doi:10.1038/nn.2751.

173. Südhof TC. The synaptic vesicle cycle: a cascade of protein-protein interactions. *Nature*. 1995;375(6533):645-653. doi:10.1038/375645a0.

174. Yu CR, Power J, Barnea G, et al. Spontaneous neural activity is required for the establishment and maintenance of the olfactory sensory map. *Neuron*. 2004;42:553-566. doi:10.1016/S0896-6273(04)00224-7.

175. Schnütgen F, Doerflinger N, Calléja C, Wendling O, Chambon P, Ghyselinck NB. A Directional Strategy for Monitoring Cre-Mediated Recombination at the Cellular Level in the Mouse. *Nat Biotechnol*. 2003;21(5):562-5. doi:10.1038/nbt811.

176. Dickinson a, Nicholas DJ, Adams CD. The effect of the instrumental training contingency on susceptibility to reinforcer devaluation. *Q J Exp Psychol*. 1983;35B(March 2015):35-51. doi:10.1080/14640748308400912.

177. Ragozzino ME. The contribution of the medial prefrontal cortex, orbitofrontal cortex, and dorsomedial striatum to behavioral flexibility. *Ann N Y Acad Sci*. 2007;1121:355-75. doi:10.1196/annals.1401.013.

178. Weilburg JB, Mesulam M-M, Weintraub S, Buonanno F, Jenike M, Stakes JW. Focal Striatal Abnormalities in a Patient With Obsessive-Compulsive Disorder. *Arch Neurol*. 1989;46(2):233-235. doi:10.1001/archneur.1989.00520380139028.

179. Baxter LR, Phelps ME, Mazziotta JC, Guze BH, Schwartz JM, Selin CE. Local cerebral glucose metabolic rates in obsessive-compulsive disorder. A comparison with rates in unipolar depression and in normal controls. *Arch Gen Psychiatry*. 1987;44(3):211-218. doi:10.1001/archpsyc.1987.01800150017003.

180. Hippenmeyer S, Vrieseling E, Sigrist M, et al. A developmental switch in the response of DRG neurons to ETS transcription factor signaling. *PLoS Biol*. 2005;3(5):e159. doi:10.1371/journal.pbio.0030159.

181. Arenkiel BR, Hasegawa H, Yi JJ, et al. Activity-induced remodeling of olfactory bulb microcircuits revealed by monosynaptic tracing. *PLoS One*. 2011;6. doi:10.1371/journal.pone.0029423.

182. Kohara K, Pignatelli M, Rivest AJ, et al. Cell type-specific genetic and optogenetic tools reveal hippocampal CA2 circuits. *Nat Neurosci*. 2014;17(2):269-279. doi:10.1038/nn.3614.

183. Hilario M, Clouse E, Yin HH, Costa RM. Endocannabinoid signaling is critical for habit formation. *Front Integr Neurosci*. 2007;1:6. doi: 10.3389/neuro.07.006.2007.

184. Rossi M a., Yin HH. Methods for studying habitual behavior in mice. *Curr Protoc Neurosci*. 2012;1(SUPPL.60):1-13. doi:10.1002/0471142301.ns0829s60.

185. Baio J. Prevalence of autism spectrum disorder among children aged 8 years - autism and developmental disabilities monitoring network, 11 sites, United States, 2010. *Morb Mortal Wkly report*. 2014;63:1-21.

186. Rogers SJ. What are infant siblings teaching us about Autism in infancy? *Autism Res*. 2009;2:125-137. doi:10.1002/aur.81.

187. Guy J, Gan J, Selfridge J, Cobb S, Bird A. Reversal of neurological defects in a mouse model of Rett syndrome. *Science*. 2007;315:1143-1147. doi:10.1126/science.1138389.

188. Clement JP, Aceti M, Creson TK, et al. Pathogenic SYNGAP1 mutations impair cognitive development by disrupting maturation of dendritic spine synapses. *Cell*. 2012;151:709-723. doi:10.1016/j.cell.2012.08.045.

189. Amaral D, Geschwind D, Dawson G, eds. *Autism Spectrum Disorders*. 1st ed. Oxford University Press; 2011.

190. El-Fishawy P, State MW. The genetics of autism: key issues, recent findings, and clinical implications. *Psychiatr Clin North Am*. 2010;33:83-105. doi:10.1016/j.psc.2009.12.002.

191. Ebert DH, Greenberg ME. Activity-dependent neuronal signalling and autism spectrum disorder. *Nature*. 2013;493:327-337. doi:10.1038/nature11860.

192. Kim E, Naisbitt S, Hsueh YP, et al. GKAP, a novel synaptic protein that interacts with the guanylate kinase- like domain of the PSD-95/SAP90 family of channel clustering molecules. *J Cell Biol*. 1997;136:669-678. doi:10.1083/jcb.136.3.669.

193. Takeuchi M, Hata Y, Hirao K, Toyoda A, Irie M, Takai Y. SAPAPs. A family of PSD-95/SAP90-associated proteins localized at postsynaptic density. *J Biol Chem*. 1997;272:11943-11951. doi:10.1074/jbc.272.18.11943.

194. Boeckers TM, Winter C, Smalla KH, et al. Proline-rich synapse-associated proteins ProSAP1 and ProSAP2 interact with synaptic proteins of the SAPAP/GKAP family. *Biochem Biophys Res Commun*. 1999;264:247-252. doi:10.1006/bbrc.1999.1489.

195. Han K, Holder JL, Schaaf CP, et al. SHANK3 overexpression causes manic-like behaviour with unique pharmacogenetic properties. *Nature*. 2013;503:72-77. doi:10.1038/nature12630.

196. Chandler KJ, Chandler RL, Broeckelmann EM, Hou Y, Southard-Smith EM, Mortlock DP. Relevance of BAC transgene copy number in mice: Transgene copy number variation across multiple transgenic lines and correlations with transgene integrity and expression. *Mamm Genome*. 2007;18:693-708. doi:10.1007/s00335-007-9056-y.

197. Waehler R, Russell SJ, Curiel DT. Engineering targeted viral vectors for gene therapy. *Nat Rev Genet*. 2007;8:573-587. doi:10.1038/nrg2141.

198. Karayannis T, Au E, Patel JC, et al. Cntnap4 differentially contributes to GABAergic and dopaminergic synaptic transmission. *Nature*. 2014;511(7508):236-40. doi:10.1038/nature13248.

199. Guo C, Yang W, Lobe CG. A Cre recombinase transgene with mosaic, widespread tamoxifen-inducible action. *Genesis*. 2002;32:8-18. doi:10.1002/gene.10021.

200. Niwa H, Yamamura K, Miyazaki J. Efficient selection for high-expression transfectants with a novel eukaryotic vector. *Gene*. 1991;108:193-199. doi:10.1016/0378-1119(91)90434-D.

201. Chao H-T, Chen H, Samaco RC, et al. Dysfunction in GABA signalling mediates autism-like stereotypies and Rett syndrome phenotypes. *Nature*. 2010;468:263-269. doi:10.1038/nature09582.

202. Gross C, Zhuang X, Stark K, et al. Serotonin1A receptor acts during development to establish normal anxiety-like behaviour in the adult. *Nature*. 2002;416:396-400. doi:10.1038/416396a.

203. Eon JP, Sun X, Nichol P, Saijoh Y, Martin JF, Moon AM. System for tamoxifen-inducible expression of Cre-recombinase from the Foxa2 locus in mice. *Dev Dyn*. 2008;237:447-453. doi:10.1002/dvdy.21415.

204. De Lacy N, King BH. Revisiting the relationship between autism and schizophrenia: toward an integrated neurobiology. *Annu Rev Clin Psychol*. 2013;9:555-587. doi:10.1146/annurev-clinpsy-050212-185627.

205. Courchesne E, Pierce K, Schumann CM, et al. Mapping early brain development in autism. *Neuron*. 2007;56(2):399-413. doi:10.1016/j.neuron.2007.10.016.

206. Insel TR. Rethinking schizophrenia. *Nature*. 2010;468(7321):187-193. doi:10.1038/nature09552.

207. Lewis DA, Lieberman JA. Catching up on schizophrenia: natural history and neurobiology. *Neuron*. 2000;28(2):325-334. doi:S0896-6273(00)00111-2 [pii].

208. Mitchell KJ, Porteous DJ. Rethinking the genetic architecture of schizophrenia. *Psychol Med*. 2011;41(1):19-32. doi:10.1017/S003329171000070X.

209. Walsh CA, Morrow EM, Rubenstein JLR. Autism and Brain Development. *Cell*. 2008;135(3):396-400. doi:10.1016/j.cell.2008.10.015.

210. Akil H, Brenner S, Kandel E, et al. Medicine. The future of psychiatric research: genomes and neural circuits. *Science*. 2010;327(5973):1580-1581. doi:10.1126/science.1188654.

211. Bernier R, Golzio C, Xiong B, et al. Disruptive CHD8 mutations define a subtype of autism early in development. *Cell*. 2014;158(2):263-276. doi:10.1016/j.cell.2014.06.017.

212. De Rubeis S, He X, Goldberg AP, et al. Synaptic, transcriptional and chromatin genes disrupted in autism. *Nature*. 2014. doi:10.1038/nature13772.

213. Burbach JPH, van der Zwaag B. Contact in the genetics of autism and schizophrenia. *Trends Neurosci*. 2009;32(2):69-72. doi:10.1016/j.tins.2008.11.002.

214. Guilmatre A, Dubourg C, Mosca A-L, et al. Recurrent rearrangements in synaptic and neurodevelopmental genes and shared biologic pathways in schizophrenia, autism, and mental retardation. *Arch Gen Psychiatry*. 2009;66(9):947-956. doi:10.1001/archgenpsychiatry.2009.80.

215. Kenny EM, Cormican P, Furlong S, et al. Excess of rare novel loss-of-function variants in synaptic genes in schizophrenia and autism spectrum disorders. *Mol Psychiatry*. 2013;19(8):872-879. doi:10.1038/mp.2013.127.

216. Reichelt AC, Rodgers RJ, Clapcote SJ. The role of neurexins in schizophrenia and autistic spectrum disorder. *Neuropharmacology*. 2012;62(3):1519-1526. doi:10.1016/j.neuropharm.2011.01.024.

217. Fromer M, Pocklington AJ, Kavanagh DH, et al. De novo mutations in schizophrenia implicate synaptic networks. *Nature*. 2014;506(7487):179-184. doi:10.1038/nature12929.

218. Peñagarikano O, Abrahams BS, Herman EI, et al. Absence of CNTNAP2 leads to epilepsy, neuronal migration abnormalities, and core autism-related deficits. *Cell*. 2011;147(1):235-246. doi:10.1016/j.cell.2011.08.040.

219. Zoghbi HY, Bear MF. Synaptic dysfunction in neurodevelopmental disorders associated with autism and intellectual disabilities. *Cold Spring Harb Perspect Biol*. 2012;4(3). doi:10.1101/cshperspect.a009886.

220. Group C, Consortium PG. Identification of risk loci with shared effects on five major psychiatric disorders: a genome-wide analysis. *Lancet*. 2013;381(9875):1371-1379. doi:10.1016/S0140-6736(12)62129-1.

221. Fernandez T V., Sanders SJ, Yurkiewicz IR, et al. Rare copy number variants in tourette syndrome disrupt genes in histaminergic pathways and overlap with autism. *Biol Psychiatry*. 2012;71(5):392-402. doi:10.1016/j.biopsych.2011.09.034.

222. Guilmatre A, Huguet G, Delorme R, Bourgeron T. The emerging role of SHANK genes in neuropsychiatric disorders. *Dev Neurobiol*. 2014;74(2):113-122. doi:10.1002/dneu.22128.

223. McCarthy SE, Gillis J, Kramer M, et al. De novo mutations in schizophrenia implicate chromatin remodeling and support a genetic overlap with autism and intellectual disability. *Mol Psychiatry*. 2014;19(6):652-658. doi:10.1038/mp.2014.29.

224. Rodenas-Cuadrado P, Ho J, Vernes SC. Shining a light on CNTNAP2: complex functions to complex disorders. *Eur J Hum Genet*. 2014;22(2):171-178. doi:10.1038/ejhg.2013.100.

225. Kim E, Sheng M. PDZ domain proteins of synapses. *Nat Rev Neurosci*. 2004;5(10):771-781. doi:10.1038/nrn1517.

226. Montgomery JM, Zamorano PL, Garner CC. MAGUKs in synapse assembly and function: An emerging view. *Cell Mol Life Sci*. 2004;61(7-8):911-929. doi:10.1007/s00018-003-3364-5.

227. McAllister AK. Dynamic aspects of CNS synapse formation. *Annu Rev Neurosci*. 2007;30:425-450. doi:10.1146/annurev.neuro.29.051605.112830.

228. Tu JC, Xiao B, Naisbitt S, et al. Coupling of mGluR/Homer and PSD-95 complexes by the Shank family of postsynaptic density proteins. *Neuron*. 1999;23:583-592. doi:10.1016/S0896-6273(00)80810-7.

229. Hung AY, Futai K, Sala C, et al. Smaller dendritic spines, weaker synaptic transmission, but enhanced spatial learning in mice lacking Shank1. *J Neurosci*. 2008;28(7):1697-1708. doi:10.1523/JNEUROSCI.3032-07.2008.

230. Roussignol G, Ango F, Romorini S, et al. Shank expression is sufficient to induce functional dendritic spine synapses in aspiny neurons. *J Neurosci*. 2005;25(14):3560-3570. doi:10.1523/JNEUROSCI.4354-04.2005.

231. Sala C, Piëch V, Wilson NR, Passafaro M, Liu G, Sheng M. Regulation of dendritic spine morphology and synaptic function by Shank and Homer. *Neuron*. 2001;31(1):115-130. doi:10.1016/S0896-6273(01)00339-7.

232. Arons MH, Thynne CJ, Grabrucker AM, et al. Autism-Associated Mutations in ProSAP2/Shank3 Impair Synaptic Transmission and Neurexin-Neuroligin-Mediated Transsynaptic Signaling. *J Neurosci*. 2012;32(43):14966-14978. doi:10.1523/JNEUROSCI.2215-12.2012.

233. Durand CM, Perroy J, Loll F, et al. SHANK3 mutations identified in autism lead to modification of dendritic spine morphology via an actin-dependent mechanism. *Mol Psychiatry*. 2012;17(1):71-84. doi:10.1038/mp.2011.57.

234. Valtschanoff JG, Weinberg RJ. Laminar organization of the NMDA receptor complex within the postsynaptic density. *J Neurosci*. 2001;21(4):1211-1217. doi:21/4/1211 [pii].

235. Kreienkamp HJ. Scaffolding Proteins at the Postsynaptic Density: Shank as the Architectural Framework. *Handb Exp Pharmacol*. 2008;186:365-380. doi:10.1007/978-3-540-72843-6-15.

236. Jeffries AR, Curran S, Elmslie F, et al. Molecular and phenotypic characterization of ring chromosome 22. *Am J Med Genet A*. 2005;137(2):139-147. doi:10.1002/ajmg.a.30780.

237. Manning MA, Cassidy SB, Clericuzio C, et al. Terminal 22q deletion syndrome: a newly recognized cause of speech and language disability in the autism spectrum. *Pediatrics*. 2004;114(2):451-457. doi:10.1542/peds.114.2.451.

238. Prasad C, Prasad AN, Chodirker BN, et al. Genetic Evaluation of Pervasive Developmental Disorders: The Terminal 22q13 Deletion Syndrome May Represent a Recognizable Phenotype. *Clinical genetics*. 2000;57(2):103-9. doi:10.1034/j.1399-0004.2000.570203.x.

239. Precht KS, Lese CM, Spiro RP, et al. Two 22q Telomere Deletions Serendipitously Detected by FISH. *Journal of medical genetics*. 1998;35(11):939-42. doi:10.1136/jmg.35.11.939.

240. Wilson HL, Wong ACC, Shaw SR, et al. Molecular characterisation of the 22q13 deletion syndrome supports the role of haploinsufficiency of SHANK3/PROSAP2 in the major neurological symptoms. *J Med Genet*. 2003;40(8):575-584. doi:10.1136/jmg.40.8.575.

241. Gauthier J, Champagne N, Lafrenière RG, et al. De novo mutations in the gene encoding the synaptic scaffolding protein SHANK3 in patients ascertained for schizophrenia. *Proc Natl Acad Sci U S A*. 2010;107(17):7863-7868. doi:10.1073/pnas.0906232107.

242. Frischmeyer PA, Dietz HC. Nonsense-mediated mRNA decay in health and disease. *Hum Mol Genet*. 1999;8(10):1893-1900. doi:ddc211 [pii].

243. Anderson SW, Bechara A, Damasio H, Tranel D, Damasio AR. Impairment of Social and Moral Behavior Related to Early Damage in Human Prefrontal Cortex. *Nature neuroscience*. 1999;2(11):1032-7. doi:10.1038/14833.

244. Seamans JK, Lapish CC, Durstewitz D. Comparing the prefrontal cortex of rats and primates: Insights from electrophysiology. *Neurotox Res*. 2008;14(2-3):249-262. doi:10.1007/BF03033814.

245. Wang F, Zhu J, Zhu H, Zhang Q, Lin Z, Hu H. Bidirectional control of social hierarchy by synaptic efficacy in medial prefrontal cortex. *Science*. 2011;334(6056):693-697. doi:10.1126/science.1209951.

246. Adhikari A, Topiwala MA, Gordon JA. Synchronized Activity between the Ventral Hippocampus and the Medial Prefrontal Cortex during Anxiety. *Neuron*. 2010;65(2):257-269. doi:10.1016/j.neuron.2009.12.002.

247. Amodio DM, Frith CD. Meeting of minds: the medial frontal cortex and social cognition. *Nat Rev Neurosci*. 2006;7(4):268-277. doi:10.1038/nrn1884.

248. Glantz LA, Lewis DA. Decreased dendritic spine density on prefrontal cortical pyramidal neurons in schizophrenia. *Arch Gen Psychiatry*. 2000;57(1):65-73. doi:10.1001/archpsyc.57.1.65.

249. Lim S, Naisbitt S, Yoon J, et al. Characterization of the Shank family of synaptic proteins. Multiple genes, alternative splicing, and differential expression in brain and development. *J Biol Chem*. 1999;274(41):29510-29518. doi:10.1074/jbc.274.41.29510.

250. Böckers TM, Segger-Junius M, Iglauer P, et al. Differential expression and dendritic transcript localization of Shank family members: Identification of a dendritic targeting element in the 3′ untranslated region of Shank1 mRNA. *Mol Cell Neurosci*. 2004;26(1):182-190. doi:10.1016/j.mcn.2004.01.009.

251. Coba MP, Pocklington AJ, Collins MO, et al. Neurotransmitters drive combinatorial multistate postsynaptic density networks. *Sci Signal*. 2009;2(68):ra19. doi:10.1126/scisignal.2000102.

252. Sheng M, Kim E. The postsynaptic organization of synapses. *Cold Spring Harb Perspect Biol*. 2011;3(12). doi:10.1101/cshperspect.a005678.

253. Tu JC, Xiao B, Yuan JP, et al. Homer binds a novel proline-rich motif and links group 1 metabotropic glutamate receptors with IP3 receptors. *Neuron*. 1998;21(4):717-726. http://www.ncbi.nlm.nih.gov/pubmed/9808459.

254. Weickert CS, Fung SJ, Catts VS, et al. Molecular evidence of N-methyl-D-aspartate receptor hypofunction in schizophrenia. *Mol Psychiatry*. 2012. doi:10.1038/mp.2012.137.

255. Funk AJ, Rumbaugh G, Harotunian V, McCullumsmith RE, Meador-Woodruff JH. Decreased expression of NMDA receptor-associated proteins in frontal cortex of elderly patients with schizophrenia. *Neuroreport*. 2009;20(11):1019-1022. doi:10.1097/WNR.0b013e32832d30d9.

256. Silverman JL, Yang M, Lord C, Crawley JN. Behavioural phenotyping assays for mouse models of autism. *Nat Rev Neurosci*. 2010;11(7):490-502. doi:10.1038/nrn2851.

257. Burguière E, Monteiro P, Feng G, Graybiel AM. Optogenetic Stimulation of Lateral Orbitofronto-Striatal Pathway Suppresses Compulsive Behaviors. *Science.* 2013;340(6137):1243-6. doi:10.1126/science.1232380.

258. Burguière E, Monteiro P, Mallet L, Feng G, Graybiel AM. Striatal circuits, habits, and implications for obsessive-compulsive disorder. *Curr Opin Neurobiol*. 2014;30C:59-65. doi:10.1016/j.conb.2014.08.008.

259. King BH, Lord C. Is schizophrenia on the autism spectrum? *Brain Res*. 2011;1380:34-41. doi:10.1016/j.brainres.2010.11.031.

260. Meyer U, Feldon J, Dammann O. Schizophrenia and autism: Both shared and disorder-specific pathogenesis via perinatal inflammation? *Pediatr Res*. 2011;69(5 PART 2). doi:10.1203/PDR.0b013e318212c196.

261. Rapoport J, Chavez A, Greenstein D, Addington A, Gogtay N. Autism spectrum disorders and childhood-onset schizophrenia: clinical and biological contributions to a relation revisited. *J Am Acad Child Adolesc Psychiatry*. 2009;48(1):10-18. doi:10.1097/CHI.0b013e31818b1c63.

262. Unenge Hallerbäck M, Lugnegård T, Gillberg C. Is autism spectrum disorder common in schizophrenia? *Psychiatry Res*. 2012;198(1):12-17. doi:10.1016/j.psychres.2012.01.016.

263. Krystal JH, State MW. Psychiatric disorders: Diagnosis to therapy. *Cell*. 2014;157(1):201-214. doi:10.1016/j.cell.2014.02.042.

264. Lin D, Boyle MP, Dollar P, et al. Functional identification of an aggression locus in the mouse hypothalamus. *Nature*. 2011;470(7333):221-226. doi:10.1038/nature09736.

265. Nelson RJ, Trainor BC. Neural mechanisms of aggression. *Nat Rev Neurosci*. 2007;8(7):536-546. doi:10.1038/nrn2174.

266. Baker SA, Chen L, Wilkins AD, Yu P, Lichtarge O, Zoghbi HY. An AT-hook domain in MeCP2 determines the clinical course of Rett syndrome and related disorders. *Cell*. 2013;152(5):984-996. doi:10.1016/j.cell.2013.01.038.

267. Sanjana NE, Cong L, Zhou Y, Cunniff MM, Feng G, Zhang F. A transcription activator-like effector toolbox for genome engineering. *Nat Protoc*. 2012;7(1):171-192. doi:10.1038/nprot.2011.431.

268. Spencer CM, Alekseyenko O, Serysheva E, Yuva-Paylor LA, Paylor R. Altered anxiety-related and social behaviors in the Fmr1 knockout mouse model of fragile X syndrome. *Genes, Brain Behav*. 2005;4(7):420-430. doi:10.1111/j.1601-183X.2005.00123.x.

269. Wan Y, Feng G, Calakos N. Sapap3 deletion causes mGluR5-dependent silencing of AMPAR synapses. *J Neurosci*. 2011;31(46):16685-16691. doi:10.1523/JNEUROSCI.2533-11.2011.

270. Franklin ME, Foa EB. Treatment of obsessive compulsive disorder. *Annu Rev Clin Psychol*. 2011;7:229-243. doi:10.1146/annurev-clinpsy-032210-104533.

271. Otte C. Cognitive behavioral therapy in anxiety disorders: Current state of the evidence. *Dialogues Clin Neurosci*. 2011;13(4):413-421.

272. Goodman WK, Lydiard RB. Recognition and treatment of obsessive-compulsive disorder. *J Clin Psychiatry*. 2007;68(12):e30. doi:10.4088/JCP.1207e30.

273. Milad MR, Rauch SL. Obsessive-compulsive disorder: beyond segregated cortico-striatal pathways. *Trends Cogn Sci*. 2012;16(1):43-51. doi:10.1016/j.tics.2011.11.003.

274. Chamberlain SR, Menzies L, Hampshire A, et al. Orbitofrontal dysfunction in patients with obsessive-compulsive disorder and their unaffected relatives. *Science*. 2008;321(5887):421-422. doi:10.1126/science.1154433.

275. Eagle DM, Baunez C. Is there an inhibitory-response-control system in the rat? Evidence from anatomical and pharmacological studies of behavioral inhibition. *Neurosci Biobehav Rev*. 2010;34(1):50-72. doi:10.1016/j.neubiorev.2009.07.003.

276. Mar AC, Walker ALJ, Theobald DE, Eagle DM, Robbins TW. Dissociable effects of lesions to orbitofrontal cortex subregions on impulsive choice in the rat. *J Neurosci*. 2011;31(17):6398-6404. doi:10.1523/JNEUROSCI.6620-10.2011.

277. Chen M, Wan Y, Ade K, Ting J, Feng G, Calakos N. Sapap3 deletion anomalously activates short-term endocannabinoid-mediated synaptic plasticity. *J Neurosci*. 2011;31(26):9563-9573. doi:10.1523/JNEUROSCI.1701-11.2011.

278. Züchner S, Wendland JR, Ashley-Koch AE, et al. Multiple rare SAPAP3 missense variants in trichotillomania and OCD. *Mol Psychiatry*. 2009;14(1):6-9. doi:10.1038/mp.2008.83.

279. Materials and methods are available in supplementary.

280. Morein-Zamir S, Fineberg NA, Robbins TW, Sahakian BJ. Inhibition of thoughts and actions in obsessive-compulsive disorder: extending the endophenotype? *Psychol Med*. 2010;40(2):263-272. doi:10.1017/S003329170999033X.

281. Steinmetz JE, Tracy JA, Green JT. Classical eyeblink conditioning: clinical models and applications. *Integr Physiol Behav Sci*. 36(3):220-238. doi:10.1007/BF02734095.

282. Gage GJ, Stoetzner CR, Wiltschko AB, Berke JD. Selective Activation of Striatal Fast-Spiking Interneurons during Choice Execution. *Neuron*. 2010;67(3):466-479. doi:10.1016/j.neuron.2010.06.034.

283. Kalanithi PS a, Zheng W, Kataoka Y, et al. Altered parvalbumin-positive neuron distribution in basal ganglia of individuals with Tourette syndrome. *Proc Natl Acad Sci U S A*. 2005;102(37):13307-13312. doi:10.1073/pnas.0502624102.

284. Crittenden JR, Graybiel AM. Basal Ganglia disorders associated with imbalances in the striatal striosome and matrix compartments. *Front Neuroanat*. 2011;5(September):59. doi:10.3389/fnana.2011.00059.

285. Canales JJ, Graybiel AM. A measure of striatal function predicts motor stereotypy. *Nat Neurosci*. 2000;3(4):377-383. doi:10.1038/73949.

286. Saka E, Goodrich C, Harlan P, Madras BK, Graybiel AM. Repetitive behaviors in monkeys are linked to specific striatal activation patterns. *J Neurosci*. 2004;24(34):7557-7565. doi:10.1523/JNEUROSCI.1072-04.2004.

287. Eagle DM, Wong JCK, Allan ME, Mar AC, Theobald DE, Robbins TW. Contrasting roles for dopamine D1 and D2 receptor subtypes in the dorsomedial striatum but not the nucleus accumbens core during behavioral inhibition in the stop-signal task in rats. *J Neurosci*. 2011;31(20):7349-7356. doi:10.1523/JNEUROSCI.6182-10.2011.

288. Kubota Y, Liu J, Hu D, et al. Stable encoding of task structure coexists with flexible coding of task events in sensorimotor striatum. *J Neurophysiol*. 2009;102(4):2142-2160. doi:10.1152/jn.00522.2009.

289. Lee JH, Durand R, Gradinaru V, et al. Global and local fMRI signals driven by neurons defined optogenetically by type and wiring. *Nature*. 2010;465(7299):788-792. doi:10.1038/nature09108.

290. Tye KM, Prakash R, Kim S-Y, et al. Amygdala circuitry mediating reversible and bidirectional control of anxiety. *Nature*. 2011;471(7338):358-362. doi:10.1038/nature09820.

291. Aldridge JW, Berridge KC. Coding of serial order by neostriatal neurons: a “natural action” approach to movement sequence. *J Neurosci*. 1998;18:2777-2787.

292. Fentress JC. Development and patterning of movement sequences in inbred mice. *Biol Behav*. 1972:83-132.

293. Wan Y, Ade KK, Caffall Z, et al. Circuit-selective striatal synaptic dysfunction in the Sapap3 knockout mouse model of obsessive-compulsive disorder. *Biol Psychiatry*. 2014;75(8):623-630. doi:10.1016/j.biopsych.2013.01.008.

294. Gillan C. Disruption in the balance between goal-directed behavior and habit learning in obsessive-compulsive disorder. *Am J Psychiatry*. 2011;168(7):718-26. doi: 10.1176/appi.ajp.2011.10071062.

295. Remijnse PL, Nielen MMA, van Balkom AJLM, et al. Reduced orbitofrontal-striatal activity on a reversal learning task in obsessive-compulsive disorder. *Arch Gen Psychiatry*. 2006;63(11):1225-1236. doi:10.1001/archpsyc.63.11.1225.

PART V

APPENDIX

Appendix A

Striatal circuits, habits, and implications for obsessive-compulsive disorder

Striatal circuits, habits, and implications for obsessive–compulsive disorder

Abstract

Increasing evidence implicates abnormalities in corticostriatal circuits in the pathophysiology of obsessive–compulsive disorder (OCD) and OC-spectrum disorders. Parallels between the emergence of repetitive, compulsive behaviors and the acquisition of automated behaviors suggest that the expression of compulsions could in part involve loss of control of such habitual behaviors. The view that striatal circuit dysfunction is involved in OC-spectrum disorders is strengthened by imaging and other evidence in humans, by discovery of genes related to OCD syndromes, and by functional studies in animal models of these disorders. We highlight this growing concordance of work in genetics and neurobiology suggesting that frontostriatal circuits, and their links with basal ganglia, thalamus and brainstem, are promising candidates for therapeutic intervention in OCD.

Introduction

OCD is a neuropsychiatric disorder characterized by obsessions (intrusive thoughts) and compulsions (physical or mental rituals such as washing or checking), often associated with high levels of anxiety. OCD has an estimated lifetime prevalence of 2–3 % worldwide. In recognition of the core clustering of symptoms in OCD, and in the light of neurological findings, OCD has newly been separated from the class of anxiety disorders in the revised Diagnostic and Statistical Manual of Mental Disorders [1]. Among the heterogeneous symptoms observed in OCD patients, four clusters have been identified in this new classification: symmetry/ordering, hoarding, contamination/cleaning, and obsessions/checking. These symptom-clusters all have features of repetitive thought and action, expressed in relation to external and internal stimuli, and often appear in ritualized form. Here we emphasize emerging evidence that the striatum is critical to the establishment of such ritualized sequences of actions [2–5], and that the striatal connections of anterior cingulate and orbitofrontal cortical regions are linked to OCD and OC-spectrum disorders, based on physiological, genetic and neuroimaging evidence. We point to remaining challenges to characterize the endophenotypes of OCD in relation to a reconsideration of the central role of the striatum in the emergence of this complex neuropsychiatric pathophysiology.

Striatum-based circuitry and the pathophysiology of OCD: insights from studies in human

New neuroimaging studies are helping to characterize both the circuits implicated in OCD and the potential circuit functions that might contribute, when disturbed, to the symptoms of OCD and related disorders. These studies highlight a special relationship between the caudate nucleus, the orbitofrontal cortex (OFC) and anterior cingulate cortex (ACC). At a morphological level, differences in volumes between OCD patients and healthy controls have been reported for the putamen [6,7] and, especially, for the caudate nucleus [8], but the results reported have not been consistent. Meta-analyses have not yet indicated clear volumetric differences in striatal grey matter in the striatum of OCD patients [9]. By contrast, there is concordance in work estimating coordinate activities of the striatum relative to those of the OFC and ACC. Studies done with functional magnetic resonance imaging (fMRI) indicate that activities in the striatum and these two cortical regions are altered during resting-state and during expression of symptoms [10,11]. fMRI has been employed extensively to study functional relationships across these regions as indicated by correlations of spontaneous metabolic fluctuations during cognitive tasks or symptom provocation in frontostriatal circuits. These studies have consistently shown altered functional connectivity between striatum and prefrontal regions in OCD patients [12–15]. These results have been supported by the use of diffusion tensor imaging tractography in studies that report abnormalities in white matter (e.g., fiber tracts) in the caudate nucleus and its associated frontal regions [16,17].

Clinical work early on suggested that dysfunction of the striatum might be important in the emergence of OCD symptoms. Comorbid OCD symptoms were identified in neurodegenerative disorders such as Parkinson's disease and Huntington's disease [18–20], and in the wake of focal lesions in the caudate nucleus produced by infarcts [21]. New clinical evidence supports this connection between striatum-related circuits and OCD symptoms. For example, the most widely applied treatments for OCD patients are pharmacologic therapy with selective serotonin-reuptake inhibitors (SSRI) and cognitive behavioral therapy (CBT). Neuroimaging studies reported differentially decreased activity in the striatum and associated cortical regions including the OFC after these treatments [21,22].

Further evidence implicating striatal circuitry in OCD is being obtained with the therapeutic use of deep brain stimulation (DBS) targeting subcortical structures to treat

severely ill OCD patients for whom conventional treatments have proved ineffective. About a quarter (20–30 %) of OCD patients are resistant to conventional treatments, but some receive benefit from the DBS [23]. To date, the main DBS targets include the anterior limb of the internal capsule, also referred to as the ventral capsule/ventral striatum region [24–26], the nucleus accumbens and anterior caudate nucleus [27,28], and the anterior ventral part of the subthalamic nucleus, a nucleus embedded in striatopallidal output pathways [29].

Despite encouraging results of DBS therapy in these different targets (at least half of the patients showed a diminution of symptoms from 25 % to total remission [23]), the physiological mechanisms through which therapeutic effects are achieved remain unclear, given that electrical DBS can have varying effects depending on local cell and fiber types. However, neuronal single-unit recording can be performed during surgery, prior to the insertion of the stimulating electrode, to verify the electrophysiological signature of the targeted structures. Abnormally high firing rates and variability in firing of putative medium spiny neurons (the main population of projection neurons in the striatum, MSNs) have been reported for the caudate nucleus of OCD patients during the expression of symptoms compared to features of firing recorded during resting-state conditions [30].

This finding is notable in light of evidence in the related disorder of Tourette syndrome. In two studies of post- mortem striatal tissue from patients who suffered from Tourette syndrome, characterized by tics and overexpression of ritualized motor and/or vocal behaviors, the authors observed a significant decrease of parvalbumin (PV)-immunoreactive interneurons and cholinergic interneurons relative to their incidence in normal striatum [31*,32]. Each of these neuronal types has been found in animal studies to exert powerful effects on striatal circuitry, and the PV interneurons, which are GABAergic and thought to be striatal fast-spiking or ‘high-firing’ interneurons, have been shown capable of inhibiting up to $100 nearby MSNs apiece. They can be broadly activated by microstimulation of small regions of the motor cortex, and so could be suited to control corticostriatal flow [33] through fast feed-forward inhibition. Work on an animal model of OCD, summarized below, reports both increased firing rates of MSNs and lowered counts of PV interneurons in the striatum, suggesting potential bridges between findings related to Tourette and OCD syndromes.

Genetic evidence for the involvement of striatal circuitry in OCD

Genetically engineered mice that exhibit both corticostriatal dysfunction and OCD-like behaviors support a function for candidate OCD-related genes in the pathogenesis of OCD and point toward a common dysfunction in glutamatergic signaling, including dysfunction within the striatum, as a major contributor to the OCD-like behaviors. These mouse models include the transgenic D1CT-7 model (over-activation of glutamatergic input to the striatum produced by chronic potentiation of dopamine D1-receptor expressing neurons); the Sapap3/Dlgap3 deletion model (defective corticostriatal glutamatergic transmission) and the Slitrk5 deletion model (increased OFC activity, reduced striatal volume and defective corticostriatal transmission), among others [34–38].

A recently published genome-wide association study (GWAS) in dogs further identified genomic loci associated with OCD, with four genes having the most case- only variation: neuronal cadherin (CDH2), catenin alpha2 (CTNNA2), ataxin-1 (ATXN1), and plasma glutamate carboxypeptidase (PGCP)—all of which have functions at synapses [39*]. In human studies using magnetic resonance spectroscopy (1H-MRS), strong associations be- tween genes involved in glutamate signaling and pediatric OCD have been found [40]. However, despite this consensus between basic research and human stu- dies, a comprehensive understanding of the genetics of OCD has remained elusive.

The first GWAS study of OCD in human patients, involving more than 20 research groups, has provided new data that support the central involvement of glutamate signaling in OCD [41*]. In this case-control analysis, the top two single-nucleotide polymorphisms (SNPs) were located within DLGAP1, a gene that influences glutamate signaling and encodes SAPAP1, a protein from the same super-family as SAPAP3 that is not striatum- enriched, but is strongly expressed in cerebellum, hippo-campus and neocortex. Another study led by the OCD Collaborative Genetics Association Study (OCGAS) observed significance of a marker on chromosome 9, near PTPRD. This protein promotes the pre-synaptic differentiation of glutamatergic synapses and interacts with SLITRK3 to regulate the development of inhibitory GABAergic synapses [42**]. These results from genetic studies pointed toward genes implicated in glutamatergic synaptic transmission, suggesting that imbalances in excitation/inhibition signaling within frontostriatal circuitry could be one of the etiologic factors leading to OCD and OC-spectrum disorders.

Striatum-based circuitry and the pathophysiology of OCD: insights from studies in animals

Major advances are coming from the use of genetically engineered models of OCD and OCD-like disorders together with the use of new methods now available to neuroscientists, such as optogenetic. Animal models of OC-spectrum symptoms were originally generated by employing either behavioral conditioning, pharmacological treatment or physical manipulation, and these studies suggested that corticostriatal circuitry contributed to OCD-like symptoms, in keeping with the growing clinical literature (for review see [43,44]). With the new engineered mouse models of OCD-like disorders, it is possible for the first time to link genes implicated in OCD and related disorders to behavioral phenotypes [35,36,45,46].

Several of these mouse models have phenotypes related to excessive grooming behavior, which might be interpreted as a proxy for compulsive behavior in mice. These grooming bouts are expressions of abnormal ritualistic behavior that occur despite their negative consequences (e.g., the production of skin lesions). The validation of these mutant animals as models of OCD and OC-related disorders has depended on their genetic linkage with candidate OCD genes discovered in patient populations (e.g., SAPAP3 variants in trichotillomania [47] and SLITRK1 in Tourette syndrome [48]), and the rescue of the pathological behavior in these animal models with SSRI treatment (fluoxetine, administered to OCD patients) [35,36].

The study of these mouse models has proved striking confirmation of earlier conclusions that the striatum and corticostriatal pathways are related to OCD. Introduction of gene mutations related to OCD and Tourette syndrome have resulted in decreased striatal volume [36] and in dysfunctional corticostriatal synaptic transmission following deletion of genes coding for Sapap3, Slitrk5, and EAAC1, proteins located post-synaptically in striatal neurons [35,36,46]. In the Sapap3 deletion mutants, chronic electrophysiological recording has demonstrated abnormally high spontaneous activity of MSNs in the dorsomedial striatum, considered as the mouse equivalent of part of the caudate nucleus in primates [49**]. In the Slitrk5-KO mouse model, elevated early-gene activation in MSNs has been found by measuring levels of expression of FosB [36]. Yet another study, done in normal mice, demonstrated that chronic optogenetic stimulation of the medial OFC, activating the orbito- fronto-striatal pathway, could lead to the emergence of compulsive behavior accompanied by sustained increases in the activity of MSNs [50**]. All of these studies indicate overactive striatal activity as a key component of the model phenotypes of OCD and Tourette syndrome.

Notably, study of the Sapap3 deletion model also showed that these mice, compared to control animals, have reduced numbers of PV-immunoreactive interneurons in the dorsomedial striatum. This decrease was accompanied by decreased feed-forward inhibition of MSNs by fast-spiking interneurons (FSIs), putative PV neurons, as shown by paired FSI-MSN spike recordings [49**]. This finding supports the idea that a lack of inhibitory drive in striatal microcircuitry could lead to enhanced MSN spiking in this compulsive mouse model (Figure 1).

Causal evidence for the importance of this interneuron- projection neuron circuitry for compulsive, OCD-like behavioral symptoms was obtained by optogenetically stimulating the OFC corticostriatal pathway in the Sapap3 deletion mutants [49**]. This treatment blocked compulsive grooming, leaving other motor behaviors unaffected. The treatment also produced inhibition of striatal MSNs by increasing excitation of local inter-neurons. The involvement of the corticostriatal glutamatergic pathway in behavioral inhibition thus likely includes not only direct effects on corticostriatal (or other glutamatergic) synapses, but also local intrastriatal effects on microcircuits that can modulate the efficacy of corticostriatal glutamatergic drive (Figure 1).

This conclusion is bolstered by recent evidence that selective ablation of striatal PV interneurons in mice can lead to increased stereotypical grooming after stress [51]. Moreover, pharmacologic interference with striatal PV interneurons can lead to behavioral abnormalities as shown in a study in which selective blockade of synaptic excitation of PV interneurons produced dyskinesia-like movement abnormalities [52*].

In search of relevant corticostriatal- dependent behavioral and neurophysiological endophenotypes of OCD

The evidence that we have reviewed points to new opportunities to refine our understanding of both the neural correlates of OCD and the endophenotypes of OCD and OC-spectrum disorders. Many lines of evidence point to the caudate nucleus-anterior putamen and their connected cortical regions, the OFC and the ACC, as important to the disorder (Figure 1). A major current challenge is to identify core functions supported by these corticostriatal loops, circuits likely affected in patients.

The ‘habit hypothesis’ of OCD suggests that OCD and related disorders reflects dysregulation of neural processes favoring the expression of routinized, habitual sequence of actions triggered by environmental stimuli ([2,53**] and reference therein).

Evidence from neural recording experiments in animals suggests that such behavioral routines can be encapsulated in 'chunks' marked by action boundary signals both in the striatum [3,54,55] and in the prefrontal cortex [56**,57]. Such neural beginning-and-end signals, if relevant to the behaviors repeatedly released in compulsive behavior, could be central to the OCD and related disorders. Within the striatum, such signals are dynamically regulated as habits are acquired, and they can be strikingly marked by specific patterns of oscillatory activity as well as specific patterns of spiking activity [58*]. The ventromedial striatum has strong task-end signals involving local field oscillatory activity that entrains the striatal neurons [58*], and in OCD patients, DBS aimed at the ventral striatal region can powerfully ameliorate symptoms [59*]. A recent study involving 70 OCD patients suggests that a dysfunction related to the termination of action could provoke the patients' symptoms [60]. Signals related to successful completion of action sequences are a promising target for further study, as noted below.

New evidence obtained by studying OCD patients favors the habit hypothesis of OCD and related disorders. Gillan et al. introduced, for the first time, the reward devaluation procedure commonly accepted as distinguishing habits (independent of forthcoming reward) from other behaviors for which acquisition of rewarding outcomes drive the behavior [53**]. Critically, their study focused on avoidance behaviors, the behaviors that are the hallmark of individuals with OCD. Their evidence suggests that individuals with OCD, relative to controls, tend to perseverate in making avoidance responses to external stimuli signaling negative outcomes even after they are informed that the outcome will no longer depend on their action.

In related work, rigid ritualistic behaviors observed in OCD patients have been proposed to be the consequence of diminished behavioral flexibility (i.e., ability to change one's behavior according to contextual cues). Behavioral flexibility can be challenged in experimental tasks such as reversal learning paradigms, which test the ability to adapt behavior in response to a reversal of reinforcement contingencies. Such behavioral flexibility tasks, and reversal learning, in particular, appear to engage differentially frontostriatal circuits including the caudate nucleus, OFC and ACC. In a study of OCD patients, Remijinse *et al*. showed that OCD was associated with reduced response in an OFC-striatal network during adaptive switching to the new stimulus-reinforcement association [61*]. With a different type of behavioral flexibility task, Chamberlain *et al*. have demonstrated that OCD patients, as well as their relatives, exhibit diminished OFC responses to behavioral adaptation triggered by the task, pointing toward the identification of an OCD endophenotype [62*]. Similar results have

been obtained in animal studies implicating the medial striatum [63] and the OFC in reversal learning [64].

Compulsive checking represents another core symptom of OCD. It is characterized by the urge to verify repeatedly that an action, usually aimed at preventing a possible harm, has been properly completed beyond doubt [65]. One possibility to account for these problems is, as noted above, defective neural end-signals. The clinical phenomenology of compulsive checking illustrates two further, and potentially related, hypotheses regarding possible psychopathological mechanisms in OCD: compulsive checking may proceed from maladaptive goal-directed behavior toward uncertainty reduction or, in the context of habit-driven behavior, it may result from a failure to control impulses to check.

These two alternatives fit nicely with two lines of research on the behavioral functions of the corticostriatal circuits [66]. Investigations of repetitive checking in human have employed 'verification task' paradigms based on a working memory protocol in which, on each trial, participants could review the stimuli before proceeding to the feed-back. This strategy allowed provocation and assessment of compulsive checking in OCD patients in behavioral studies [67,68] and also the reproduction of this pathological behavior during DBS surgery, in which the patient is awake and can behave [69*]. Despite challenges in designing such tasks for animals, new behavioral paradigms have been developed to assess uncertainty monitoring in animals. These demonstrate that, when given the opportunity, rats can adaptively 'opt-out' and move on to the next, possibly easier, trial of the task [70,71*]. In these tasks, varying uncertainty about stimulus identity (hence decision difficulty) leads the animal to discard trials in which the answer is most uncertain. Simultaneous electrophysiological recordings demonstrated that stimulus-related uncertainty is encoded in the spike rate of OFC neurons. Whether such uncertainty-monitoring signals reach the striatum and participate in the regulation of goal-directed behavior, either to opt-out from a trial or to check back at the stimulus, is a matter of great interest.

Conclusions and perspectives

Converging findings from clinical and experimental work, across anatomical, physiological, genetic and behavioral levels, point to the importance of the striatum and corticostriatal pathways in the pathophysiology of OCD and related OC-spectrum disorders. The strength of these studies comes both from their diversity of approaches and from the increasing specificity with which underlying genetic and neural circuit level

mechanisms can be identified. The challenge presented by these studies is to discover which dysfunctional executive functions are embedded within these circuits, and to characterize the behavioral and neurophysiological endophenotypes of OCD and related disorders. This integrative approach could lead to more appropriate treatments for such psychiatric diseases and is supported by a growing number of clinicians [72,73]. To meet this challenge, new methodologies based on circuit neuromodulation in humans and in animal models will offer great support. The examples that we have reviewed here hint at a new era in which dynamic interactions between studies of large genomic data sets, research on genetically engineered animal models and improved study of patient endophenotypes can help to define and to target therapeutically the neural circuits disordered in OCD and related conditions.

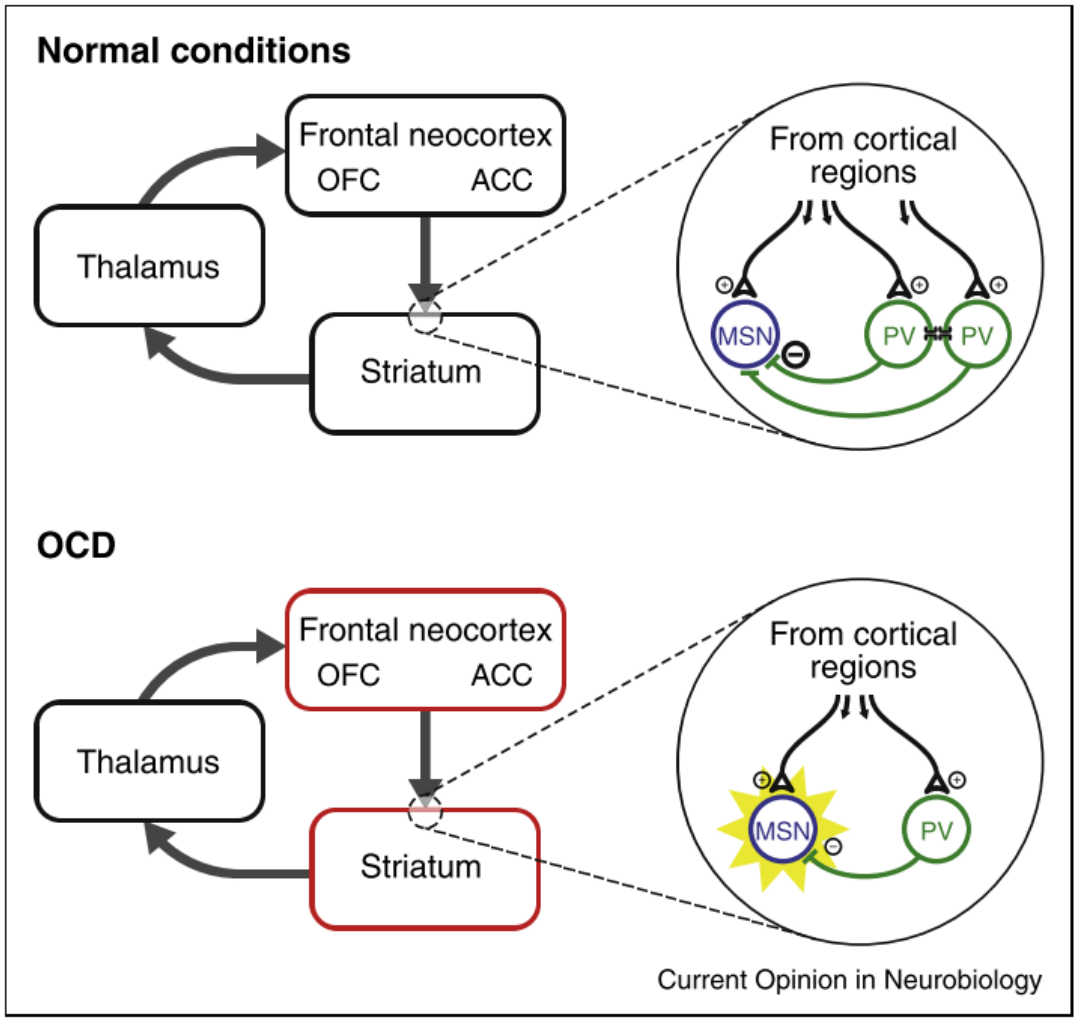

Appendix A, Figure 1 | Hypothetical dysfunctional corticostriatal circuity in OCD.

In normal conditions (top), the excitatory corticostriatal projections modulate striatal activity through a balance between excitation and inhibition. Medium spiny neurons (MSNs) are maintained under tonic inhibition by a network of parvalbumin (PV)-positive interneurons (and possibly other interneuron's not shown here), with the PV interneurons tightly interconnected through gap-junctions. In pathological OCD conditions (bottom), both cortical and striatal regions are hyperactive, possibly due to a decrease in the number and/or function of striatal PV interneurons that could lead to enhancement of MSN excitation by corticostriatal inputs and eventually to an increased activity throughout the affected corticostriatal loops.

Appendix A - References

Papers of particular interest, published within the period of review, have been highlighted as: *of special interest **of outstanding interest

[1] American Psychiatric Association: Diagnostic and statistical manual of mental disorders (DSM-V). Arlington, VA: American Psychiatric Publishing; 2013.

[2] Graybiel AM: Habits, rituals, and the evaluative brain. Annu Rev Neurosci 2008, 31:359-387.

[3] Barnes TD, Kubota Y, Hu D, Jin DZ, Graybiel AM: Activity of striatal neurons reflects dynamic encoding and recoding of procedural memories. Nature 2005, 437:1158-1161.

[4] Yin HH, Mulcare SP, Hila´ rio MRF, Clouse E, Holloway T, Davis MI, Hansson AC, Lovinger DM, Costa RM: Dynamic reorganization of striatal circuits during the acquisition and consolidation of a skill. Nat Neurosci 2009, 12:333-341.

[5] Tricomi E, Balleine BW, O'Doherty JP: A specific role for posterior dorsolateral striatum in human habit learning. Eur J Neurosci 2009, 29:2225-2232.

[6] Pujol J, Soriano-Mas C, Alonso P, Cardoner N, Mencho´ n JM, Deus J, Vallejo J: Mapping structural brain alterations in obsessive–compulsive disorder. Arch Gen Psychiatry 2004, 61:720-730.

[7] Atmaca M, Yildirim H, Ozdemir H, Tezcan E, Poyraz AK: Volumetric MRI study of key brain regions implicated in obsessive–compulsive disorder. Prog Neuropsychopharmacol Biol Psychiatry 2007, 31:46-52.

[8] Van den Heuvel OA, Remijnse PL, Mataix-Cols D, Vrenken H, Groenewegen HJ, Uylings HBM, van Balkom AJLM, Veltman DJ: The major symptom dimensions of obsessive–compulsive disorder are mediated by partially distinct neural systems. Brain J Neurol 2009, 132:853-868.

[9] Rotge JY, Guehl D, Dilharreguy B, Tignol J, Bioulac B, Allard M, Burbaud P, Aouizerate B: Meta-analysis of brain volume changes in obsessive–compulsive disorder. Biol Psychiatry 2009, 65:75-83.

[10] Whiteside SP, Port JD, Abramowitz JS: A meta-analysis of functional neuroimaging in obsessive–compulsive disorder. Psychiatry Res 2004, 132:69-79.

[11] Harrison BJ, Pujol J, Cardoner N, Deus J, Alonso P, Lo´ pez-Sola` M, Contreras-Rodrı´guez O, Real E, Segala` s C, Blanco-Hinojo L et al.: Brain corticostriatal systems and the major clinical symptom dimensions of obsessive–compulsive disorder. Biol Psychiatry 2013, 73:321-328.

[12] Hou J-M, Zhao M, Zhang W, Song L-H, Wu W-J, Wang J, Zhou D- Q, Xie B, He M, Guo J-W et al.: Resting-state functional connectivity abnormalities in patients with obsessive–compulsive disorder and their healthy first-degree relatives. J Psychiatry Neurosci JPN 2014, 39:130220.

[13] Anticevic A, Hu S, Zhang S, Savic A, Billingslea E, Wasylink S, Repovs G, Cole MW, Bednarski S, Krystal JH et al.: Global resting-state functional magnetic resonance imaging

analysis identifies frontal cortex, striatal, and cerebellar dysconnectivity in obsessive–compulsive disorder. Biol Psychiatry 2014, 75:595-605.

[14] Sakai Y, Narumoto J, Nishida S, Nakamae T, Yamada K, Nishimura T, Fukui K: Corticostriatal functional connectivity in non-medicated patients with obsessive–compulsive disorder. Eur Psychiatry J Assoc Eur Psychiatr 2011, 26:463-469.

[15] Beucke JC, Sepulcre J, Talukdar T, Linnman C, Zschenderlein K, Endrass T, Kaufmann C, Kathmann N: Abnormally high degree connectivity of the orbitofrontal cortex in obsessive– compulsive disorder. JAMA Psychiatry 2013, 70:619-629.

[16] Zhong Z, Zhao T, Luo J, Guo Z, Guo M, Li P, Sun J, He Y, Li Z: Abnormal topological organization in white matter structural networks revealed by diffusion tensor tractography in unmedicated patients with obsessive–compulsive disorder. Prog Neuropsychopharmacol Biol Psychiatry 2014, 51:39-50.

[17] Fan Q, Yan X, Wang J, Chen Y, Wang X, Li C, Tan L, You C, Zhang T, Zuo S et al.: Abnormalities of white matter microstructure in unmedicated obsessive–compulsive disorder and changes after medication. PLoS ONE 2012, 7:e35889.

[18] Alegret M, Junque´ C, Valldeoriola F, Vendrell P, Martı´ MJ, Tolosa E: Obsessive–compulsive symptoms in Parkinson's disease. J Neurol Neurosurg Psychiatry 2001, 70:394-396.

[19] Mallet L, Mesnage V, Houeto J-L, Pelissolo A, Yelnik J, Behar C, Gargiulo M, Welter M-L, Bonnet A-M, et al.: Compulsions, Parkinson's disease, and stimulation. Lancet 2002, 360:1302-1304.

[20] Cummings JL, Cunningham K: Obsessive–compulsive disorder in Huntington's disease. Biol Psychiatry 1992, 31:263-270.

[21] Carmin CN, Wiegartz PS, Yunus U, Gillock KL: Treatment of late- onset OCD following basal ganglia infarct. Depress Anxiety 2002, 15:87-90.

[22] Abramowitz JS, Taylor S, McKay D: Obsessive–compulsive disorder. Lancet 2009, 374:491-499.

[23] Haynes WIA, Mallet L: High-frequency stimulation of deep brain structures in obsessive–compulsive disorder: the search for a valid circuit. Eur J Neurosci 2010, 32:1118-1127.

[24] Greenberg BD, Gabriels LA, Malone DA Jr, Rezai AR, Friehs GM, Okun MS, Shapira NA, Foote KD, Cosyns PR, Kubu CS et al.: Deep brain stimulation of the ventral internal capsule/ventral striatum for obsessive–compulsive disorder: worldwide experience. Mol Psychiatry 2010, 15:64-79.

[25] Nuttin BJ, Gabrie¨ ls LA, Cosyns PR, Meyerson BA, Andre´ ewitch S, Sunaert SG, Maes AF, Dupont PJ, Gybels JM, Gielen F et al.: Long-term electrical capsular stimulation in patients with obsessive–compulsive disorder. Neurosurgery 2008, 62:966-977.

[26] Goodman WK, Foote KD, Greenberg BD, Ricciuti N, Bauer R, Ward H, Shapira NA, Wu SS, Hill CL, Rasmussen SA et al.: Deep brain stimulation for intractable obsessive compulsive disorder: pilot study using a blinded, staggered-onset design. Biol Psychiatry 2010, 67:535-542.

[27] Sturm V, Lenartz D, Koulousakis A, Treuer H, Herholz K, Klein JC, Klosterko¨ tter J: The nucleus accumbens: a target for deep brain stimulation in obsessive–compulsive- and anxiety-disorders. J Chem Neuroanat 2003, 26:293-299.

[28] Huff W, Lenartz D, Schormann M, Lee S-H, Kuhn J, Koulousakis A, Mai J, Daumann J, Maarouf M, Klosterko¨ tter J et al.: Unilateral deep brain stimulation of the nucleus accumbens in patients with treatment-resistant obsessive–compulsive disorder: outcomes after one year. Clin Neurol Neurosurg 2010, 112:137-143.

[29] Mallet L, Polosan M, Jaafari N, Baup N, Welter M-L, Fontaine D, du Montcel ST, Yelnik J, Chereau I, Arbus C et al.: Subthalamic nucleus stimulation in severe obsessive–compulsive disorder. N Engl J Med 2008, 359:2121-2134.

[30] Guehl D, Benazzouz A, Aouizerate B, Cuny E, Rotge JY, Rougier A, Tignol J, et al: Neuronal correlates of obsessions in the caudate nucleus. Biol Psychiatry 2008, 63:557-562.

*[31] Kalanithi PSA, Zheng W, Kataoka Y, DiFiglia M, Grantz H, Saper CB, Schwartz ML, Leckman JF, Vaccarino FM: Altered parvalbumin-positive neuron distribution in basal ganglia of individuals with Tourette syndrome. Proc Natl Acad Sci U S A 2005, 102:13307-13312.

This unbiased stereological study with postmortem basal ganglia tissue from individuals with Tourette syndrome and normal controls was the first one to report a deficiency in PV interneurons in the caudate nucleus of patients with severe Tourette syndrome.

[32] Kataoka Y, Kalanithi PSA, Grantz H, Schwartz ML, Saper C, Leckman JF, Vaccarino FM: Decreased number of parvalbumin and cholinergic interneurons in the striatum of individuals with Tourette syndrome. J Comp Neurol 2010, 518:277-291.

[33] Parthasarathy HB, Graybiel AM: Cortically driven immediate- early gene expression reflects modular influence of sensorimotor cortex on identified striatal neurons in the squirrel monkey. J Neurosci 1997, 17:2477-2491.

[34] Greer JM, Capecchi MR: Hoxb8 is required for normal grooming behavior in mice. Neuron 2002, 33:23-34.

[35] Welch JM, Lu J, Rodriguiz RM, Trotta NC, Peca J, Ding J-D, Feliciano C, Chen M, et al.: Cortico-striatal synaptic defects and OCD-like behaviours in Sapap3-mutant mice. Nature 2007, 448:894-900.

[36] Shmelkov SV, Hormigo A, Jing D, Proenca CC, Bath KG, Milde T, Shmelkov E, Kushner JS, Baljevic M, Dincheva I et al.: Slitrk5 deficiency impairs corticostriatal circuitry and leads to obsessive–compulsive-like behaviors in mice. Nat Med 2010, 16:598-602.

[37] Ting JT, Feng G: Neurobiology of obsessive–compulsive disorder: insights into neural circuitry dysfunction through mouse genetics. Curr Opin Neurobiol 2011, 21:842-848.

[38] Nordstrom EJ, Burton FH: A transgenic model of comorbid Tourette's syndrome and obsessive–compulsive disorder circuitry. Mol Psychiatry 2002, 7:617-625 524.

*[39] Tang R, Noh H, Wang D, Sigurdsson S, Swofford R, Perloski M, Duxbury M, Patterson EE, Albright J, Castelhano M et al.: Candidate genes and functional noncoding variants identified in a canine model of obsessive–compulsive disorder. Genome Biol 2014, 15:R25.

This study used dogs as a naturally occurring animal model of OCD. Of particular interest, 4 genes, all with synaptic function, were found to be associated with canine OCD.

[40] Wu K, Hanna GL, Rosenberg DR, Arnold PD: The role of glutamate signaling in the pathogenesis and treatment of obsessive–compulsive disorder. Pharmacol Biochem Behav 2012, 100:726-735.

*[41] Stewart SE, Yu D, Scharf JM, Neale BM, Fagerness JA, Mathews CA, Arnold PD, Evans PD, Gamazon ER, Davis LK et al.: Genome-wide association study of obsessive–compulsive disorder. Mol Psychiatry 2013, 18:788-798. This paper describes the results of the first GWAS for human OCD.

**[42] Mattheisen M, Samuels JF, Wang Y, Greenberg BD, Fyer AJ, McCracken JT, Geller DA, Murphy DL, Knowles JA, Grados MA et al.: Genome-wide association study in obsessive– compulsive disorder: results from the OCGAS. Mol Psychiatry 2014 http://dx.doi.org/10.1038/mp.2014.43.

This study is the most recent GWAS study of human OCD and involves association testing at both SNP and gene levels.

[43] Albelda N, Joel D: Animal models of obsessive–compulsive disorder: exploring pharmacology and neural substrates. Neurosci Biobehav Rev 2012, 36:47-63.

[44] Boulougouris V, Chamberlain SR, Robbins TW: Cross-species models of OCD spectrum disorders. Psychiatry Res 2009, 170:15-21.

[45] Chen S-K, Tvrdik P, Peden E, Cho S, Wu S, Spangrude G, Capecchi MR: Hematopoietic origin of pathological grooming in Hoxb8 mutant mice. Cell 2010, 141:775-785.

[46] Aoyama K, Suh SW, Hamby AM, Liu J, Chan WY, Chen Y, Swanson RA: Neuronal glutathione deficiency and age- dependent neurodegeneration in the EAAC1 deficient mouse. Nat Neurosci 2006, 9:119-126.

[47] Bienvenu OJ, Wang Y, Shugart YY, Welch JM, Grados MA, Fyer AJ, Rauch SL, McCracken JT, Rasmussen SA, Murphy DL et al.: Sapap3 and pathological grooming in humans: results from the OCD collaborative genetics study. Am J Med Genet B: Neuropsychiatr Genet 2009, 150B:710-720.

[48] Karagiannidis I, Rizzo R, Tarnok Z, Wolanczyk T, Hebebrand J, No¨ then MM, Lehmkuhl G, Farkas L, Nagy P, Barta C et al.: Replication of association between a SLITRK1 haplotype and Tourette Syndrome in a large sample of families. Mol Psychiatry 2012, 17:665-668.

**[49] Burguiere E, Monteiro P, Feng G, Graybiel AM: Optogenetic stimulation of lateral orbitofronto-striatal pathway suppresses compulsive behaviors. Science 2013, 340:1243-1246.

This work demonstrated that optogenetic excitation of the pathway from the lateral OFC to striatum could prevent repetitive grooming in the Sapap3 knockout mouse model. Importantly, it also highlighted the crucial role of striatal PV inhibitory interneurons that could underlie behavioral inhibition.

**[50] Ahmari SE, Spellman T, Douglass NL, Kheirbek MA, Simpson HB, Deisseroth K, Gordon JA, Hen R: Repeated cortico-striatal stimulation generates persistent OCD-like behavior. Science 2013, 340:1234-1239.

This study also confirmed the role of the OFC-striatal pathway in the emergence of compulsive behavior. Authors demonstrated that chronic optogenetic stimulation of this pathway could modify permanently corti- costriatal plasticity and induce excessive compulsive behaviors in wild- type mice.

[51] Xu M, Pogorelov V, Li LPC: Selective removal of parvalbumin interneurons from striatal networks to model the pathophysiology of Tourette syndrome. Neuropsychopharmacology 2013, 38:S273-S434 Poster T46.

*[52] Gittis AH, Leventhal DK, Fensterheim BA, Pettibone JR, Berke JD, Kreitzer AC: Selective inhibition of striatal fast- spiking interneurons causes dyskinesias. J Neurosci 2011, 31:15727-15731.

In this study, authors used a pharmacological approach to specifically inhibit firing of FSIs in the sensorimotor striatum. This FSI inhibition had strong behavioral effects characterized by abnormal hyperkinetic movements.

**[53] Gillan CM, Morein-Zamir S, Urcelay GP, Sule A, Voon V, Apergis- Schoute AM, Fineberg NA, Sahakian BJ, Robbins TW: Enhanced avoidance habits in obsessive–compulsive disorder. Biol Psychiatry 2014, 75:631-638.

This study was the first to use a shock avoidance task designed to induce habits through overtraining in humans. The authors reported that OCD patients made more avoidance responses than control subjects, suggesting that OCD patients have a tendency to develop excessive habits to avoid negative outcomes.

[54]. Jog MS, Kubota Y, Connolly CI, Hillegaart V, Graybiel AM: Building neural representations of habits. Science 1999, 286:1745-1749.

[55] Jin X, Costa RM: Start/stop signals emerge in nigrostriatal circuits during sequence learning. Nature 2010, 466:457-462.

**[56] Smith KS, Graybiel AM: A dual operator view of habitual behavior reflecting cortical and striatal dynamics. Neuron 2013, 79:361-374.

This was the first study to show that optogenetic inhibition of the medial prefrontal cortex could prevent the development of habits in rodent.

[57] Fujii N, Graybiel AM: Representation of action sequence boundaries by macaque prefrontal cortical neurons. Science 2003, 301:1246-1249.

*[58] Howe MW, Atallah HE, McCool A, Gibson DJ, Graybiel AM: Habit learning is associated with major shifts in frequencies of oscillatory activity and synchronized spike firing in striatum. Proc Natl Acad Sci U S A 2011, 108:16801-16806.

This study demonstrated that task-end-related signals in local field potentials evolve from strong gamma-band activity early during habit learning to strong beta-band activity after learning, with the spike activity of interneurons and projection neurons synchronizing differentially to first gamma and then beta oscillations in accord with this switch.

*[59] Figee M, Luigjes J, Smolders R, Valencia-Alfonso C-E, van Wingen G, de Kwaasteniet B, Mantione M, Ooms P, de Koning P, Vulink N et al.: Deep brain stimulation

restores frontostriatal network activity in obsessive–compulsive disorder. Nat Neurosci 2013, 16:386-387.

This study using neuroimaging with implanted OCD patients showed that chronic DBS of nucleus accumbens could restore normal corticostriatal activity and connectivity between cortical and striatal regions.

[60] Hinds AL, Woody EZ, Van Ameringen M, Schmidt LA, Szechtman H: When too much is not enough: obsessive– compulsive disorder as a pathology of stopping, rather than starting. PLoS ONE 2012, 7:e30586.

*[61] Remijnse PL, Nielen MMA, van Balkom AJLM, Cath DC, van Oppen P, Uylings HBM, Veltman DJ: Reduced orbitofrontal- striatal activity on a reversal learning task in obsessive–compulsive disorder. Arch Gen Psychiatry 2006, 63:1225-1236.

In this study, the authors designed a reversal task for OCD patients and healthy subject. OCD patients exhibited a reduced number of correct responses relative to control subjects during this task and aberrant OFC- striatal activity.

*[62] Chamberlain SR, Menzies L, Hampshire A, Suckling J, Fineberg NA, del Campo N, Aitken M, Craig K, Owen AM, Bullmore ET et al.: Orbitofrontal dysfunction in patients with obsessive–compulsive disorder and their unaffected relatives. Science 2008, 321:421-422.

This neuroimaging work proposes that dysfunctional lateral orbitofrontal cortex and altered behavioral flexibility could be a relevant endophenotype of OCD.

[63] Kimchi EY, Laubach M: Dynamic encoding of action selection by the medial striatum. J Neurosci 2009, 29:3148-3159.

[64] Schoenbaum G, Roesch MR, Stalnaker TA, Takahashi YK: A new perspective on the role of the orbitofrontal cortex in adaptive behaviour. Nat Rev Neurosci 2009, 10:885-892.

[65] Rachman S: A cognitive theory of compulsive checking. Behav Res Ther 2002, 40:625-639.

[66] Dolan RJ, Dayan P: Goals and habits in the brain. Neuron 2013, 80:312-325.

[67] Rotge JY, Clair AH, Jaafari N, Hantouche EG, Pelissolo A, Goillandeau M, Pochon JB, Guehl D, Bioulac B, Burbaud P et al.: A challenging task for assessment of checking behaviors in obsessive–compulsive disorder. Acta Psychiatr Scand 2008, 117:465-473.

[68] Clair AH, N'diaye K, Baroukh T, Pochon JB, Morgie` ve M, Hantouche E, Falissard B, Pelissolo A, Mallet L: Excessive checking for non-anxiogenic stimuli in obsessive–compulsive disorder. Eur Psychiatry 2013, 28:507-513.

*[69] Burbaud P, Clair A-H, Langbour N, Fernandez-Vidal S, Goillandeau M, Michelet T, Bardinet E, Che´ reau I, Durif F, Polosan M et al.: Neuronal activity correlated with checking behaviour in the subthalamic nucleus of patients with obsessive–compulsive disorder. Brain 2013, 136:304-317.

In this study the authors recorded single cell activity in OCD patients who were performing a decision-making task during surgery to implant devices for DBS treatment. Authors showed that the subthalamic nucleus, a structure in the cortico-basal ganglia loop, exhibited increased activity during checking behavior relative to resting state.

[70] Foote AL, Crystal JD: Metacognition in the rat. Curr Biol 2007, 17:551-555.

*[71] Kepecs A, Uchida N, Zariwala HA, Mainen ZF: Neural correlates, computation and behavioural impact of decision confidence. Nature 2008, 455:227-231.

This work focused on how the brain computes confidence estimates about decisions in rats by using behavioral analysis, neuronal recording and computational modelling. They showed that the firing rates of single neurons in the OFC match closely to the predictions of confidence models, suggesting that rodents, as humans, could have a conscious awareness on their choice, a process known as 'metacognition'.

[72] Casey BJ, Craddock N, Cuthbert BN, Hyman SE, Lee FS, Ressler KJ: DSM-5 and RDoC: progress in psychiatry research? Nat Rev Neurosci 2013, 14:810-814.

[73] Craske MG: The R-DoC initiative: science and practice. Depress Anxiety 2012, 29:253-256.

Appendix B

Supplementary materials

Chapter 4 supplementary materials

Table S4.1 – List of antibodies and their working condition

Protein	Antibody	Species	Vendor	Dilution	Blocking Buffer
SynGAP	D88G1	Rabbit mAb	CST	1 to 1000	5 % BSA
GluR1	#MAB2263	Mouse	Millipore	1 to 1000	5 % milk
GluR2	32-0300	Mouse (IgG2a)	Invitrogen	1 to 500	5 % milk
PSD95	ab18258	Rabbit	Abcam	1 to 1000	5 % milk
Homer	AB5875	Rat	Chemicon	1 to 1000	5 % milk
NR2A	07-632	Rabbit	Millipore	1 to 1000	5 % milk
NR2B	N59/36	Mouse	NeuroMAB	1 to 1000	5 % milk
NR1	556308	Mouse (IgG2a)	BD Pharmingen	1 to 1000	5 % milk
Synaptotagmin1	105 103	Rabbit	Synaptic Systems	1 to 1000	5 % BSA
Shank1	162 002	Rabbit	Synaptic Systems	1 to 1000	5 % BSA
Shank2	#12218	Rabbit	CST	1 to 500	5 % BSA
Shank3N	N367/62	Mouse (IgG2a)	NeuroMab	1 to 100	5 % milk
Shank3C	SC-30193	Rabbit	Santa Cruz	1 to 1000	5 % milk
SAPAP3	homemade	Rabbit	Feng lab	1 to 1000	5 % milk
PSD93	ABR-01252	Rabbit	Dianova	1 to 1000	Odyssey blocking buffer
mGluR5	ab76316	Rabbit	Abcam	1 to 5000 (unboiled sample)	5 % milk

Chapter 5 supplementary materials

Supplementary Tables

Table S5.1 – P-values for difference between wildtype mice and *Sapap3* mutant mice tested by unpaired t-tests with Bonferroni correction.

	Sessions															
	1	2	3	4	5	6	7	8	9	10	11	12	13	14	15	16
Mean grooming onset time	0.784	0.774	0.585	0.747	0.535	0.104	0.342	0.823	0.793	0.075	**0.005**	**0.025**	0.118	**0.037**	**0.007**	**0.001**
% grooming in probe trials	0.771	1.000	0.876	0.982	1.000	0.996	0.997	0.982	1.000	0.869	0.645	0.310	0.564	**0.048**	**0.012**	**0.023**

Red bold face indicates statistically significant differences ($P < 0.05$).

Table S5.2 – Proportions of task-related units among all putative pyramidal neurons recorded in the lOFC and all putative MSNs recorded in the striatum.

	Training phase		
	Early training	Mid-training	Late Training
Lateral orbitofrontal cortex			
Wildtypes	31/152 (19.5%)	48/159 (30.2%)	43/154 (27.9%)
Sapap3 mutants	36/154 (23.4%)	35/129 (27.1%)	25/88 (28.4%)
Centromedial striatum			
Wildtypes	56/105 (53.3%)	42/87 (48.3%)	36/76 (47.4%)
Sapap3 mutants	26/78 (33.3%)	37/94 (39.4%)	27/86 (31.4%)

Supplementary Text

Conditioning in the grooming task: In our conditioning task, the wildtype animals exhibited progressively increased grooming in response to the conditioning tone, followed by a progressive sharpening of their responses and alignment of these responses to immediately after the water-drop delivery. The final latencies (154 ± 75 ms) at the end of the training were nearly optimal responses, given the sensorimotor reaction time constraints of the mice. Thus in the wildtype mice, the short-latency responses to the tone, initially acquired, were decreased while the near-optimally timed responses were increased. These mice did not groom at the drop-time if no water had been released (probe trials, Fig. 5.1 F). Detailed analysis of the dynamics of their performance indicated that they adapted their behavior through a continuous learning process. First, they all showed a reliable conditioning for several consecutive days at mid-training (approximately from day 5 to day 12, Fig. 5.3). Second, their grooming onset distributions early in training differed substantially from those late in training: early on, the averaged distribution is spread over 2-3 s after the water-drop delivery, but at the end of the training their responses occurred consistently at short latencies (154 ± 75 ms) after the water-drop delivery (Fig. 5.1 D, unpaired t-test between beginning and end of training, $P<0.05$). These results do not favor the possibility that there was a deficit in conditioning or an extinction process, but rather, favor an adaptive learning process in the wildtypes. This adaptive process was not present in the *Sapap3* mutant animals.

Deficit in striatal inhibition in the *Sapap3* mutant mice: In our conditioning task, late in training there was a significant decrease in MSN firing in the wildtypes relative to the firing of MSNs in the mutants. This decrease in the wildtypes could be a neural pattern related to the behavioral adaptation shown by the wildtypes during training, one not shown in the mutants. Therefore, in this mouse model, what could be the cause of the abnormal increase of task-dependent MSNs firing? Numerous mechanisms could be considered, but we discuss here a small number that appear relevant in regard to our findings.

With respect to whether the lack of decline of the MSN firing in the mutants was due to over-excitation or to lack of inhibition, the literature on the *Sapap3* mutant mice published so far tends not to favor the possibility that *Sapap3* mutant mice exhibit an abnormal increase in excitatory inputs in the

striatum. First, in their original paper, Welch *et al*.[58] reported that the *Sapap3* mutant mice showed a decrease of NMDA-dependent corticostriatal excitatory neurotransmission to the MSNs and a deficit in evoked field post-synaptic potentials recorded in slice preparations, suggesting that this excitatory NMDA-dependent pathway was deficient. Later, a study demonstrated that *Sapap3* deletion reduces AMPAR-mediated excitatory synaptic transmission in MSNs through postsynaptic endocytosis of AMPARs and excessive synapse silencing[269]. In a following study, the same group found that in the absence of SAPAP3 protein, MSN excitatory synapses exhibit endocannobinoid-mediated synaptic depression under conditions that do not normally activate this process[277]. And finally, very recently, they demonstrate that another major excitatory input pathway, the thalamostriatal pathway, was not affected by *Sapap3* deletion[293]. All together, these results suggest that the excitatory inputs to the MSNs in the striatum are not modified in a major way that could increase the striatal excitatory tone; if anything they would suggest the opposite. By contrast, our electrophysiological results demonstrating abnormally elevated MSN firing in the mutants relative to levels in wildtypes, and our finding of a significant decrease in numbers of PV-containing neuron in the *Sapap3* mutant mice, suggest that a deficit of the PV-neuron-dependent inhibitory micro-circuitry could account for the abnormal task-dependent MSNs excitation that we observed. We emphasize that other deficits could occur in the *Sapap3* mutants. For example, corticostriatal FSIs neurotransmission properties could also be modified in the *Sapap3* mutant mice, in addition to the corticostriatal input to the MSNs. We did not monitor electrotonic transmission in the FSIs, we did not study the LFP oscillatory activity in the mutants and their wildtype controls, and we did not study properties of other inhibitory elements in striatal circuitry, all of which might be abnormal. What our findings do show is that in the mutants, the inhibition of MSN spikes relative to FSI spikes of neighboring FSIs could be greatly augmented by stimulation of the lOFC-striatal pathway to the centromedial striatum, the region in which we observed the deficit in numbers of FSIs. One possible implication of this set of findings is that the lOFC-striatal pathway stimulation affected MSN inhibition via increasing FSI-MSN inhibitory efficacy.